STUDIES IN NUCLEATE BOILING

Thesis submitted for the Degree of

Doctor of Philosophy

at the University of Edinburgh

by

M. M. AL-BADRY, M.Sc.

September, 1969

ACKNOWLEDGMENTS

The author wishes to express his deep regards to Professor T. D. Patten, without his guidance, encouragement and discussion this work could not have been conducted.

Thanks are due to the Heriot-Watt University authorities for the use of their laboratory and work shop facilities.

The financial support for the project throughout the period of study by the C.E.G.B. is also gratefully acknowledged.

ABSTRACT

This work is mainly concerned with the region of isolated bubbles in boiling heat transfer. Horizontal surfaces in the form of 2 x ½ in. nickel-chrome strips heated electrically from a D.C. supply were used, with distilled deionized water as a boiling medium. Individual cavities with radii ranging from 0.0002 in. to 0.025 in. were created on a set of test surfaces, approximately ten cavities to each surface. Tests were carried out at pressures in the range from atmospheric up to 415 psi. Experimental values of initiation superheat temperature difference were found to be larger than those predicted theoretically by the Gibbs and the Clapeyron equations but in better agreement with predictions by Howell and Seigel based on a thermal layer thickness of 0.001 in. At higher pressures superheat values required were still higher than theoretical predictions and the suggestion of a critical cavity radius varying with pressure was introduced. Contrary to findings by Han and Griffith a limit to the size of active sites depending on the thermal layer thickness was not found.

A large number of cavities, approximately 120, was created on each of a second set of test surfaces either in rows or randomly distributed. Again the superheat temperature differences were larger than theoretical predictions but the discrepancy was not as great as for the first series of surfaces already referred to.

The cavity size distribution on the second set of test surfaces was approximated by a sine function and this, coupled with Gibbs-Clapeyron equation gave a relationship between the number of active sites and the applied superheat. Experimental data was found to be in agreement with the theoretical predictions. The variation of number of active sites with heat flux was also studied both visually and photographically up to a maximum heat flux of 22,000 Btu/ft^{2}hr.

The construction is described of a capacitor probe capable of detecting individual bubbles leaving the surface and, after development, of detecting bubbles at any part of the surface or measuring the total population. A theory for the capacitor probe was proposed which relates the height of the output pulse, to the size of the departing bubble. For a probe capable of measuring a large number of bubbles, a proposal for a correction based on the dead time was introduced.

The frequency of bubble emission from single cavities with sizes ranging from 0.0096 in. to 0.016 in. was studied experimentally as the heat flux increased from 0 to 30,000 Btu/ft^{2}hr. at atmospheric pressure and pressures of 30, 45, 60 and 75 psi. The total frequency from a general surface was also studied for the flux and pressure ranges mentioned above.

The variation of bubble frequency with cavity radius was also investigated for single cavities with radii varying between 0.0002 in. and 0.017 in. and at constant heat fluxes of 7,000 Btu/ft^{2}hr. and 10,000 Btu/ft^{2}hr. A theoretical expression for the waiting time, tw, was obtained and, defining the frequency as 1/tw at atmospheric pressure, reasonable agreement was obtained with the experimental variation of frequency with heat flux and cavity radius. At pressures above atmospheric the theoretical waiting time was coupled with the relationship for the growth time, tg, proposed by Plesset and Zwick and when the frequency was re-defined as $\frac{1}{tg + tw}$ good agreement was obtained between theoretical and experimental data.

To obtain experimentally the bubble departure size the detecting probe was calibrated using photographic records of bubbles generated from nozzles of different dimensions and measuring the simultaneous signal heights obtained on a

U.V recorder. The size of bubbles, departing from a test surface, obtained from the calibration agreed with experimental values. The possibility of measuring the velocity of a rising bubble is also considered.

An equation to predict heat flux based on the enthalpy of superheat liquid removed from the surface with each individual bubble is introduced. The frequency and number of active sites are obtained from theoretical considerations presented here while the thermal layer thickness is obtained from an empirical relation by Jakob and the departure radius from a first order approximation by Patten. At atmospheric pressure theoretical predictions were found to be higher than experimental values. As the pressure increased the discrepancy was reversed and probable explanations for divergence were forwarded. Experimental values of the product of the number of active sites, N, and frequency, f, were substituted in one set of calculations and gave better agreement. Excellent agreement was obtained when experimental values of N, f, bubble radius R and an assumed value of thermal layer thickness δ = 0.035 in. were substituted.

CONTENTS

CONTENTS (Contd.)

CONTENTS (Contd.)

CONTENTS (Contd.)

CONTENTS (Contd.)

LIST OF FIGURES

LIST OF FIGURES (Contd.)

LIST OF FIGURES (Contd.)

LIST OF FIGURES (Contd.)

LIST OF FIGURES (Contd.)

LIST OF FIGURES (Contd.)

CHAPTER 1

INTRODUCTION

Modern industrial developments in, for example, power stations, whether nuclear or conventional, space and rocketry research as well as in electronics, have, in the last two decades, demanded extensive research into the mechanism of boiling heat transfer. In very many applications boiling heat transfer is an ideal mechanism for extracting an enormous amount of heat from a surface thereby keeping the temperature of that surface reasonably constant. The alternative is often a forced convection technique which may require a very high rate of liquid circulation and which may not be able to maintain a fairly uniform surface temperature.

The phenomenon of boiling is a very complicated one as it comprises not only a heat transfer problem but also problems of mass transfer, phase change and a combination of liquid-solid property characteristics, furthermore, there may be at least three different classes of boiling, nucleate, transition and film boiling as described by Zuber (1), and each region is marked by different thermal and hydraulic conditions.

The nucleation regime to which this investigation is confined is recognised by the existence of discrete bubbles on the surface. To understand better the mechanism of heat removal in this region, the initiation superheat temperature difference required for each individual bubble and its relation to the surface condition, the frequency of bubble emission and the number of active sites at each applied heat flux must be considered.

The temperature at which bubbles start forming is rather important not only in the heat flux correlation but also in approximate estimations of the working surface temperature in the nucleate boiling region. Corty and Foust (2) found

that rougher surfaces initiate at a lower superheat temperature difference than smooth surfaces. In preliminary research carried out in this programme, Grant (3), found that the Clausius - Clapeyron equation coupled with Gibbs' bubble equilibrium equation gave a good guide to the conditions of bubble formation on a horizontal surface immersed in distilled deionized water. The findings were limited since only one type of cavity distribution with an average size of 0.00036 in. was investigated.

In the investigation planned here it was decided to study the bubble formation in detail and to eliminate the possible influence of neighbouring bubbles, by investigating cavities with exact radii ranged from 0.0002 in. to 0.025 in. placed on eight different polished test surfaces. Studies were to be made at atmospheric pressure and at pressures up to 415 psi. Later this was taken a step further and surfaces with a relatively large population of cavities, approximately 120/in^2 arranged either in rows or randomly distributed, with average sizes ranging from 0.00176 in. to 0.0038 in. were studied in the above pressure range. Chapters (3) and (4) show the procedure adopted in polishing and producing cavities. Experimental results concerned with initiation were discussed and compared with other existing initiation criteria and further suggestions are proposed in Chapter (9).

The number of active sites on a surface increases as the applied heat flux increases, Jakob (4) expressed this relation in a linear form. Gaertner (5) Bushell (6), and Grant (3) approximated the cavity size distribution to a specific function and, from a criterion for initiation, related the active sites to the superheat temperature difference. The particular cavity distribution examined in this work was approximated to a sine function and an equation

relating the number of active sites to superheat temperature is proposed in Chapter (5). Discussion and comparison of experimental and theoretical data is given in Chapter (9). The frequency of bubble emission is a fundamental factor in heat flux correlation. The existing data in the literature, however, is very limited and refers mostly to tests carried out at atmospheric pressure using photographic techniques, Hsu and Graham (7), Yatabe and Westwater (8), Han and Griffith (9) and Ivey (10). One aim of this work was, therefore, to develop a refined experimental technique to determine the bubble population and allow bubble detection at working pressures higher than atmospheric. The arrangement finally adopted was a bubble capacitor probe capable of detecting single bubbles and thence frequency on any section of the test surface area or over the whole area and working at atmospheric and higher pressures, furthermore it offered the possibility of bubble size and velocity determination. Chapters (6) and (8) describe the probe technique, its development, proposed theory for prediction of signal heights, correction due to bubble interference based on the measured value of dead time and bubble sizing.

With the development of the detecting probe the frequency variation with heat flux, cavity size and pressure for individual cavities and general surfaces was studied and data is presented and discussed in Chapter (7). A theoretical expression for the frequency is proposed and a comparison of theoretical data and experimental results is made and discussed in Chapter (7).

The final aim in a study of boiling heat transfer is to give the designer a means whereby the heat flux may be predicted easily from measured values of superheat temperature difference or vice versa. Empirical relations are proposed in the literature, for example, McAdams et al (11), Gaertner and Westwater (12),

Gaertner (13) Yamagata et al (14) but with wide disagreement. Dimensional and analytical approaches are also proposed by Rohsenow (15) and Zuber (16). An approach based on enthalpy removal by departing bubbles is proposed here. Predicted results are compared with experimental data and also with the data of Zuber and Rohsenow in Chapter (9).

The boiling medium was distilled dionized water at saturation conditions.

CHAPTER 2

HISTORICAL BACKGROUND AND CRITICAL REVIEW

2.1 INTRODUCTION

Since the amount of boiling literature published in past years is so vast, it has been necessary to restrict the coverage and to emphasise certain aspects such as the superheat temperature required for initiation, the frequency of bubble emission and heat transfer correlation.

When considering initiation, only those theories concerned with the boiling of a liquid from a solid surface, as opposed to boiling within a liquid, have been covered. Although the rate of bubble growth has been discussed the rate of collapse has not, nor have the effects of subcooling since most of the work of this particular investigation was carried out at saturated conditions at a specified pressure. For similar reasons, the experiments having been restricted to weak nucleate boiling, no aspect of film boiling is reviewed. Discussion of heat transfer correlations has been limited to those based on an analytical approach and empirical formulae have not been included, since most of these formulae are obtained for a specific surface under certain conditions which may have no relation to industrial or other applications.

2.2 BUBBLE INITIATION

The idea of bubble initiation from a solid surface in contact with a liquid was discussed by Fisher (17) and then by Bankoff (18) who extended the Volmer and Fisher theory to a superheated liquid either in contact with a solid or not. Bankoff concluded that homogeneous nucleation within liquids or in the presence of flat or projecting solid surfaces, requires a superheat vapour pressure of a

magnitude several hundred times that observed and hence is impossible. Finally he concluded that the most preferable site for nucleation was a non wetted cavity, since only a small amount of work is required to tear the liquid away from the cavity apex. In the presence of an energy excess the cavity then spontaneously fills with vapour the superheat being determined by the cavity radius.

Clark, Strenge and Westwater (19) verified the above conclusions by photographing pentane vapour bubbles forming at atmospheric pressure from active sites on aluminium and zinc surfaces. They found that initiation occured from circular cavities with radii varying from 0.003 in. to 0.0033 in.

Westwater (20) classified cavities into four types according to their geometry. The groups were wide shallow cavities which fill with liquid, cavities with rounded bottoms which can either fill with liquid or trap gas depending upon the liquid contact angle and on the cavity angle, cavities which are deep and narrow and have a contact angle significantly greater than zero and lastly re-entrant cavities with narrow mouths regarded as excellent gas traps.

The relation of initiation superheat to the surface condition was reported by Corty and Foust (2) who, by carefully polishing copper and nickel surfaces succeeded in reducing but not completely eliminating the number of cavities on the surface and found that a much higher degree of superheat was required for initiation, for example, for a surface of 2.2μin.r.m.s., ΔT_{int} was 41^{o}F and for a surface of 23μ in.r.m.s., ΔT_{int} was 22^{o}F.

Griffith and Wallis (21) considered an ideal conical cavity illustrated in Fig. (1), with a bubble already present. They assumed the contact angle to be 90^{o}, Fig. (1), and from considerations of the growing bubble radius concluded

that the cavity mouth radius is equal to the critical radius of the bubble and hence determines the initiation superheat temperature. Gibbs equation was used to relate the cavity radius to the pressure inside and outside the bubble in the form

$$\Delta P = \frac{2\sigma}{r} \qquad (2.2.1)$$

When the bubble is at equilibrium, the vapour must be at the saturation temperature corresponding to the bubble pressure and the surrounding liquid must be at the same temperature. The liquid is therefore superheated. Clausius-Clapyron equation was used to relate the excess temperature in the liquid to the excess pressure in the bubble in the form

$$\frac{\Delta P}{(T_w - T_{sat})} = \frac{h_{fg}\rho_v}{T_w} \qquad (2.2.2)$$

By combining Equations (2.2.1) and (2.2.2) Griffith and Wallis obtained the following equation

$$T_w - T_{sat} = \frac{2\sigma T_w}{r_c h_{fg}\rho_v} \qquad (2.2.3)$$

Although this equation gives the minimum ΔT needed to initiate bubble growth from a cavity of radius r_c, it does not indicate the maximum or minimum cavity radius corresponding to that initiation superheat.

Griffith and Wallis found a difference between the predicted ΔT_{int} of 3^oF and the observed ΔT_{int} of 20^oF and suggested that this may be due to the fact that the surface temperature was not a true representation of the cavity temperature. They concluded nevertheless that Equation (2.2.3) is substantially correct and that specification of a single characteristic dimension for a nucleation site is

sufficient.

Hsu and Graham's (7) criterion for initiation was based on the proposal that heat must be conducted to the bubble from the thermal layer to provide the latent heat of vapourization and hence that the temperature of the thermal layer surrounding the bubble must be equal to or greater than that inside the bubble. Combining the Gibbs and Clapeyron equations they obtained an expression similar to that of Griffith and Wallis but in terms of bubble radius i.e.

$$T_w - T_{sat} = \frac{2\sigma T_{sat}}{R \rho_v h_{fg}} \qquad (2.2.4)$$

The bubble radius was related to the cavity radius from geometrical considerations and with an average contact angle of 53.2^0 in the form

$$R = 1.25\, r_c$$

Han and Griffith (9) introduced a model in which the temperature of the vapour inside a hemispherical bubble, with the same centre and radius as the cavity mouth, was obtained from the Gibbs and Clapeyron relations.

From potential flow considerations they proposed that the isothermal line passing through the top of a bubble is at $\frac{3}{2} r_c$ from the heating surface, where the temperature distribution across the thermal layer is assumed to be linear. By equating the temperature obtained from the Gibbs-Clapeyron equations to that at $\frac{3}{2} r_c$ from the surface they obtained the following equation

$$r_{c\,max,min} = \frac{\delta_{NC}\,(T_w - T_{sat})}{3\,(T_w - T_\infty)} \left\{ 1 \mp \sqrt{1 - \frac{6(T_w - T_\infty)\,B}{(T_w - T_{sat})^2\,\delta_{NC}}} \right\} \qquad (2.2.5)$$

The transient conduction equation is used in the calculation of the re-establishment of the thermal layer after the departure of the bubble. Fig. (3) shows the development of the thermal layer at successive times up to a maximum width δ_{NC} . The temperature of the vapour inside the bubble is also shown in Fig. (3), the points of intersection represent the size range of active cavities.

Hsu (22) proposed a model similar to that of Han and Griffith equating the bubble vapour temperature to the temperature in the liquid at a height of $2\ r_c$, rather than the $\frac{3}{2}\ r_c$ of Han and Griffith. To relate the bubble nucleus radius to the cavity radius Hsu introduced a factor based on geometry and the contact angle in a similar manner to Hsu and Graham (7) and obtained

$$r_{c\,max,min} = \frac{\delta}{2C_1}\left\{ 1 - \frac{(T_{sat} - T_\infty)}{(T_w - T_\infty)} \mp \sqrt{\left(1 - \frac{T_{sat} - T_\infty}{T_w - T_\infty}\right)^2 - \frac{4B\,C_3}{(T_w - T_\infty)}} \right\} \qquad (2.2.6)$$

The transient conduction equation with different boundary conditions was used to calculate the re-establishment of the thermal layer for the case of constant wall temperature and constant heat flux. Hsu found that the experimental results from (21) fit Equation (2.2.6) very well assuming δ to be 0.003 in. and C_3 and C_1 to be 1.

Grant (3) adopted a similar approach to Griffith and Wallis (21) in relating the vapour temperature inside the nucleus to that of the surrounding liquid using the Gibbs and Clapeyron equations. Furthermore, experimental considerations showed the thermal layer thickness to be much greater than the cavity radius and it was possible to equate the temperature of the surrounding liquid to that of the surface, and thereby obtain equation (2.2.3), similar to (21). Grant found that predicted results agreed with experimental data at

atmospheric pressure and at 30 psi. for a cavity radius of 360 x 10^{-6} inch.

Hatton and Hall (23) considered the same basic model as Ref (9), (22) in addition assuming there to be a linear temperature gradient across a thermal layer of constant thickness and a uniform temperature distribution within the solid surface of infinite thermal conductivity. They proposed that the applied heat energy is partially stored in the test surface and partially conducted to the bulk liquid. Their results can be written as

$$r_{c\ max,\ min} = \frac{\delta}{2C} \frac{(Tw - Tsat)}{(Tw - T\infty)} \left\{ 1 \mp \sqrt{1 - \frac{4\ BC\ (Tw - T\infty)}{(tw - T_{sat})^2\ \delta}} \right\} \qquad (2.2.7)$$

where C is a constant introduced to allow for some distortion of the isothermal surface in the vicinity of the bubble.

Howell and Siegel (24) carried the work further and differentiated between the two cases:-

i) a bubble completely immersed in the thermal layer and

ii) a bubble projecting into the bulk liquid.

The temperature in the thermal layer was assumed to be linear and the net heat added to the bubble was given as

$$Q = h_c\, 2\pi r_c \int_0^{\delta} \left\{ (Tw - T_{sat})\left(1 - \frac{x}{\delta}\right) - \frac{B}{r_c} \right\} dx - h_c\, 2\pi r_c \int_{\delta}^{r_c} \frac{B}{r_c}\, dx$$

In the case of $\delta < r_c$ the initiation criterion was given as

$$(Tw - T_{sat}) > \frac{2B}{\delta} \qquad (2.2.8)$$

and for bubbles completely immersed in the thermal layer as

$$(T_w - T_{sat}) = \frac{B}{r_c} \qquad \frac{1}{(1 - \frac{r_c}{2\delta})} \qquad (2.2.9)$$

Howell and Siegel found that the theoretical predictions of equation (2.2.8.,2.2.9) gave smaller values of superheat temperature difference than the experimental data.

2.3 BUBBLE GROWTH

Through time the problem of bubble growth has been classified in the literature into two categories:-

i) bubble growth in a uniform temperature field and

ii) bubble growth in a non-uniform temperature field

2.3 -1 Bubble Growth in a Uniform Temperature Field

According to Bosnjakovic (25), the growth of a bubble in a superheated liquid of uniform temperature distribution is due to evaporation of liquid into the bubble as a result of heat flow from the bulk liquid. He also postulated that as the evaporation proceeds there is a temperature drop across a thin thermal layer according to the equation

$$h\,(T_{sup} - T_{sat}) = h_{fg}\rho_v \frac{dR}{dt} \qquad (2.3.1)$$

Fritz and Ende (26) took this further and proposed that the transient conduction equation could be used to find the energy absorbed by the bubble and obtained an expression of the form

$$h_{fg}\rho_v \frac{dR}{dt} = K \frac{(T_{sup} - T_{sat})}{\sqrt{(\pi\alpha t)}} \qquad (2.3.2)$$

The dynamic problem represented by the Raleigh equation coupled with the equation of heat diffusion was used by Plesset and Zwick ($_{27}$) to study the effects of inertia, surface tension, sphericity and a moving boundary on the problem.

A spherical bubble in an incompressible inviscous fluid was assumed, and it was found that the effects of liquid inertia and surface tension are unimportant so that the growth of the vapour bubble is governed by the heat transfer process. They obtained the expression

$$h_{fg} \rho_v \frac{dR}{dt} = \sqrt{3}K \frac{(T_{sup} - T_{sat})}{\sqrt{\pi \alpha t}} \qquad (2.3.3)$$

Similar conclusions were reached by Forster and Zuber ($_{28}$) though they suggested that at the initial stages, when the radius is microscopic, growth is controlled by the hydrodynamic forces. Only when the bubble radius reaches a higher order of magnitude will the heat transfer process become controlling.

2.3 - 2 Bubble growth in a non-uniform temperature field

Although the basic mechanism of bubble growth in a non-uniform field is similar to that in a uniform field, there are two apparent differences. For a non-uniform field there is an additional heat loss from the thermal layer to the bulk liquid and the temperature drop across the thermal layer is not constant but decreasing.

Zuber (1) using Bosnjakovic's Equation (2.3.1) introduced a term Q_{out} to account for the amount of heat conducted to the bulk liquid

$$h_{fg} \rho_v \frac{dR}{dt} = K \frac{(T_{sup} - T_{sat})}{\sqrt{\pi \alpha t}} - Q_{out} \qquad (2.3.4)$$

The model used is shown in Figure (5). It can be seen that direct heat flow to the base of the bubble is excluded and that the flux Q_{out} is equal to that conducted from solid to liquid.

Hsu and Graham (7) concluded that Zuber's assumption may be valid for the case of constant wall temperature but not for that of constant flux. They in turn proposed a system where the heat flux from the base Q_w is included and where the value of Q_{in}, the heat conducted from the thermal layer to the bubble, was calculated and not assumed equal to Q_w. They used the transient conduction equation to obtain a final expression of the form

$$R-\delta = \frac{c}{h_{fg}\rho_v}\left[\left(\frac{0.5Q_w}{c} - K\frac{(T_{sat}-T_\infty)}{\delta}\right)t + 2\left(Q_w - K\frac{(T_w-T_\infty)}{\delta}\right)\frac{\delta^2}{\alpha\pi^2}\left(\frac{\pi^2}{6} - \sum_1^\infty \frac{e^{\frac{\alpha\pi^2N^2t}{\delta^2}}}{N^2}\right)\right] \quad (2.3.5a)$$

and for $R > R_* = 0.1$ cm.

$$R - 0.1 = \frac{c}{h_{fg}\rho_v}\left[\left(\frac{0.25Q_w}{c} - K\frac{(T_{sat}-T_\infty)}{\delta}\right)(t-t_*) + 2\left(Q_w - K\frac{(T_{sat}-T_\infty)}{\delta}\right)\frac{\delta^2}{\alpha\pi^2}\sum\frac{1}{N^2}\left(e^{\frac{\alpha\pi^2N^2t_*}{\delta^2}} - e^{-\frac{\alpha\pi^2N^2t}{\delta^2}}\right)\right] \quad (2.3.5b)$$

When bubble radius is plotted as a function of time Zuber's equation seems initially to fit some available practical results but predictions fall below experimental data in later stages of growth. In comparison, the above Equations (2.3.5.a,b) have a flatter initial slope but provide better agreement in the later stages.

Han and Griffith (9), introducing a theory similar to that of Ref (1), included the convection process to account for the heat transfer to the bubble

base. They included geometric factors such as curvature, surface, base, volume and contact angle and by equating the rate at which the bubble absorbs heat to the sum of heat conducted across the thermal layer and heat convected from the surface to the bubble derived an equation of the form

$$\rho_v\left(4\pi R^2 \frac{dR}{dt}\right) Q_v h_{fg} = Q_c \rho_s \quad (4\pi R^2) \quad C_p \rho_L d \frac{(T - T_{sat})}{dx}\Big)_{x=0} + Q_b (4\pi R^2) \times h_e (T_w - T_{sat}). \tag{2.3.6}$$

It should be noted that Han and Griffith ignored the initial stages of growth where hydrodynamic forces control the process and considered only thermodynamic forces. Their final equation was of the form

$$R - r_c = \frac{Q_s Q_c}{Q_v} \quad \frac{C_p \rho_v}{\rho_v h_{fg}} \left[\frac{2(T_w - T_{sat})\sqrt{t}}{\sqrt{\pi \alpha}} - \frac{(T_w - T_\infty)}{\delta} \cdot \delta^2 \left(\frac{4t}{\delta^2} \operatorname{erf} \frac{\delta}{\sqrt{4t}} + \frac{2}{\sqrt{\pi}} \frac{\sqrt{4t}}{\delta} e^{-\frac{\delta^2}{4t}} - 2 \operatorname{erfc} \frac{\delta}{\sqrt{4t}} \right) \right]$$

Excellent agreement was claimed by Han and Griffith when Equation (2.3.6) was compared with experimental data at atmospheric pressure.

2.4 BUBBLE DEPARTURE DIAMETER

The forces acting on a bubble at the moment of departure have been included in many correlations to determine the departure radius. Y. P. Chang [29] gave the forces as the gravitational force, surface tension force, pressure gradient force, inertia forces of the vapour and liquid, forces due to the circulation inside the bubble and finally the resistances due to molecular and eddy viscosities.

Fritz [30] considered the gravitational, surface tension and pressure gradient forces acting on a bubble in static equilibrium on a horizontal surface and obtained the expression

$$D_d = 0.021 \ \beta \sqrt{\frac{g_c \sigma}{g(\rho_L - \rho_v)}} \qquad (2.4.1)$$

Jakob (4) cited the disturbance of equilibrium conditions in experimental work as a reason for the variation between predicted values and practical results.

By extending Bosnjakavic's (25) theory for bubble growth to take into account the heat transfer from the thermal layer to the bulk liquid Zuber (1) obtained an expression for the maximum bubble diameter as

$$D_{max} = C \ \frac{\Delta T C_p \rho_L}{h_{fg} \rho_v} \ \frac{K \Delta T}{Q/A} \qquad (2.4.2)$$

He also considered a gas bubble formed at an orifice and by equating the buoyancy and surface tension forces derived the relation

$$D_d = \left(\frac{12 r_o g_c \sigma}{g(\rho_L - \rho_v)} \right)^{1/3} \qquad (2.4.3)$$

This was the first case in which r_o, the radius of the orifice or cavity was included in the correlation.

Staniszewski (31) noted that rapidly growing bubbles leave the surface with a relatively larger radius and suggested that an empirical dynamic growth factor of the form ($\propto \frac{dD}{dt}$) should be added to Fritz correlation. His final expression was of the form

$$D_d = 0.0071 \beta \left(\frac{2 g_c \sigma}{g(\rho_L - \rho_v)} \right)^{1/2} \left(1 + 0.435 \frac{dD}{dt} \right) \qquad (2.4.4)$$

Units
$\frac{dD}{dt}$ = in/s
D_d = ft ?

The effect of pressure on bubble departure is to decrease the departure radius as the pressure is increased. Semeria ($_{32}$) correlated his results for pressures ranging from atmospheric to 300 psi. and suggested the relationship

$$D_d = 0.242\ P^{-0.5} \qquad (2.4.5)$$

where P is in psi.

This was found to give agreement with practical data for higher pressures but not when extended to cover pressure below atmospheric. For these pressures Nishikawa and Urakawa ($_{33}$) introduced the correlation

$$D_d = 0.72\ \bar{P}^{0.575} \qquad (2.4.6)$$

The effect of pressure was also studied by Patten ($_{34}$) using distilled deionized water boiling from 0.018 in. diameter nickel chromium wire at pressures ranging from atmospheric to 0.935 psi. He equated the energy in the superheated layer available for vapour formation to the latent energy of the vapour in the spherical bubble and obtained the expression

$$R_{max} = (3/2\ R'\ N_j\ Y)^{\frac{1}{2}} \qquad (2.4.7)$$

Where R' is the radius of heating surface and N_j is Jakob number.

He also gave a relationship for a flat surface of the form

$$R_{max} = 3/8\ N_j\ Y$$

which is similar to an earlier relation by Zuber ($_1$).

More recently Cole and Shulman ($_{35}$) in their studies of bubble departure

diameter from electrically heated zirconium ribbon immersed in acetone, carbon tetrachloride, pentane and methane at pressures below atmospheric suggested a relationship of the form

$$D_d \sim \left(\frac{g_c \sigma}{g(\rho_L - \rho_V)}\right)^{\frac{1}{2}} P^{-1} \qquad (2.4.8)$$

When the term $D_d \Big/ \left(\frac{g_c \sigma}{g(\rho_L - \rho_V)}\right)^{\frac{1}{2}}$ was plotted against P it was found to be consistent with the data of Patten and Semeria.

2.5 BUBBLE FREQUENCY

The frequency with which bubbles form and leave the surface is generally defined as

$$F = \frac{1}{t_g + t_w} \qquad (2.5.1)$$

where t_g is the time required for the bubble to grow until it leaves the surface and t_w is the time which elapses before the next bubble starts to form from the same site.

Cole (36) generalised this expression by taking F_s as the frequency at a specific site and n as the number of bubbles formed at that site to obtain

$$F = \frac{1}{(t_g + t_w)_s} = \frac{n}{\sum_i^n 1/F_i} \qquad (2.5.2)$$

Zuber (1) suggested, from practical data obtained in boiling water on a horizontal surface, that as the heat flux is increased there are two observable regions in the frequency of bubble emission

(i) the region of isolated bubbles

(ii) the region of interference.

Yatabe and Westwater (8) using isoproponal-ethanel mixture found that a departing bubble coalesced with one or more small bubbles from neighbouring

sites and the bubble so formed then departed and another began to grow. Accordingly they suggested the existence of two frequencies, one based only on major bubbles, which was in the range 38 - 57 bubbles/sec for a heat flux giving $\Delta T_{sup} = 3.8°C$ and one based on all bubbles, this ranged from 38 - 179 bubbles/sec for the same heat flux.

Yamagata et al (14) were among the first people to discuss the terms t_g and t_w. They suggested that when a bubble originates at a spot on the heating surface and grows adhering to the surface, the liquid temperature especially in the neighbourhood of the bubble, decreases gradually, since latent heat is absorbed continuously by the vapour evaporating into the bubble. This they called the generation period or t_g. They suggested further that when a bubble has left the surface the temperature again rises without phase change in the liquid. This they called the pausing period which is synomonous with the waiting time t_w.

Hsu and Graham (7) defined the waiting period t_w as the time required for re-establishment of the thermal layer after a bubble has left the site. They measured its magnitude using a photographic technique and found it to be variable, although in general longer than the bubble growth period t_g.

Strenge and Westwater (37) used a cinemicrophotographic technique to study the frequency of bubbles in liquid pentane and found it to vary by a factor of 5. They gave as a possible explanation the convection current which moves past a cavity and carries eddies of various temperatures over it.

Marcus (38) obtained the frequency by measuring the fluctuations in the voltage of a wire immersed in water and recording these on a Dynagraph. He concluded that even in a single isolated nucleation site, the frequency is not

constant at constant heat flux, but varies according to some statistical distribution and suggested that a turbulent transient convection process in the thermal layer should be considered.

From the suggestion that cool liquid will fill the place of a departing bubble and the subsequent thermal layer develop by conduction, Ivey (10) approximated the temperature change in the liquid by a sine function of frequency ($1/t_b$). According to Eckert (39) the temperature oscillations in the liquid reach negligible proportions at a liquid depth b, given by

$$b = 1.6 \left(\pi \alpha t_b \right)^{\frac{1}{2}} \qquad (2.5.3)$$

This equation is used by Ivey to obtain an expression for the frequency of the form

$$f = \frac{1}{t_b} = \frac{\pi \alpha}{\left(b/1.6 \right)^2} \qquad (2.5.4)$$

where b is the thermal layer thickness.

Hatton and Hall (23) in their photographic study of the boiling on a prepared surface obtained an expression for min. waiting time t_w (see Section 2.2) of the form

$$tw = \frac{c_w \rho_w \delta}{K} \log \left(\frac{1}{1 - \frac{2}{(T_w - T_\infty)} \left(\frac{2\beta c}{\delta} + (T_{sat} - T_\infty) \right)} \right) \qquad (2.5.5)$$

It can be seen that at a given pressure, the above equation predicts longer waiting times for smaller cavities while that of Han and Griffith (9) shows the opposite trend.

Hatton and Hall found that for pressures of 14.6 psi. and 9.6 psi. the growth time is large compared to the waiting time and from an equation for t_g

given by Plesset and Zwick (27) obtained an expression for the frequency of the form

$$f = \frac{3}{\pi\alpha} \left(\frac{46\,K\ T_{sat}}{(h_{fg}\rho_v)^2\ R\ r_c} \right)^2 \qquad (2.5.6)$$

For pressures below 9.6 psi. t_g was assumed to be small when compared to the waiting time and the frequency was taken as the reciprocal of t_w. This was substantiated by Rallis and Jawurek (53) who found that the waiting time became larger as the pressure decreased and that nucleation became unstable and ceased completely at 0.136 atm. A complete absence of nucleation at low pressures was also reported by Von Stralen (41), Lienhard and Schrock(42).

Frequency considerations in the literature also appear in the form of a product of frequency with either bubble diameter or bubble volume. McFadden and Grassman (43) assumed fD to be a function of $\rho, \sigma, \Delta\rho$ and D and used a dimensional analysis approach to obtain Equation (2.5.7). This was modified by Ivey by the introduction of the factor g.

$$fD^2 \left(\frac{\rho_L}{g_c \sigma D} \right)^{1/2} = \phi\left(\frac{g \Delta\rho D^2}{g_c \sigma} \right) \qquad (2.5.7)$$

Perkins and Westwater (44) suggested that the product fD is constant for medium and high fluxes, up to 80% of the peak flux value.

Jakob and Linke (4) noted that the product fv was constant at a particular pressure. A similar relation was also reported by Yamagata et al (14).

2.6 NUMBER OF ACTIVE SITES AND ITS RELATION TO HEAT FLUX AND SUPERHEAT TEMPERATURE DIFFERENCE

In the heat flux literature the number of active sites is related either to the applied heat flux or to the superheat temperature difference.

An electroplating technique, to deposit a thin nickel layer on a flat copper surface, 2 ins. in diameter in a solution of nickel salts was used by Gaertner and Westwater (12) to obtain the number of active sites at fluxes varying from 7,680 to 535,000 Btu/ft^{2}hr. and at atmospheric pressure. They proposed the relationship

$$Q/A = 1400 \left(N/A \right)^{0.47} \qquad (2.6.1)$$

Recently Gaertner (13) carried out a photographic study of boiling from 4/0 polished copper and 2/0 polished platinum surfaces and proposed a similar relationship

$$Q/A = 181 \left(N/A \right)^{\frac{2}{3}} \qquad (2.6.2)$$

He referred the change in indices to the variation in surface conditions.

To relate the number of active sites to the superheat temperature difference Bushell (6) suggested that if the cavity size distribution can be approximated to a specific form then the cavity size may be related to ΔT using either the Gibb - Clapeyron or Han and Griffith equations. Gaertner (5) found that the experimental distribution of active sites for boiling water containing dissolved nickel salts at high heat flux, fits a Poisson distribution quite well. Grant (3) approximated the distribution of artificially produced cavities on a 2 x ½ in. nickel-chrome flat surface to a normal distribution. By introducing the Gibbs - Clapeyron initiation equation he obtained the relation

$$N = -BC_5 \int_0^{\Delta T_{sup}} \frac{1}{\Delta T_{sup}} \, e^{-1/2 \left(\frac{B}{\Delta T_{sup}} - \eta \right)^2} \, d(\Delta T_{sup}) \qquad (2.6.3)$$

which predicts the number of cavities active from the assumed cavity distribution at a superheat temperature difference ΔT_{sup}. When predicted values were compared with experimental visual counts of active sites for pressures of 14.6 and 30 psi. it was found necessary to reduce the predicted values by a factor of 10^{-4} to obtain approximate agreement.

It was later suggested by Grant, Carrie? and Patten (45) that this factor is influenced by the probability of a cavity being able to trap vapour and the probability of bubble growth from a cavity being prevented by earlier initiation at a neighbouring site. Although Grant assumed the area of influence to be approximately twice the area covered by the bubble, this area was reduced as the pressure increased and Grant, Carrie? and Patten suggested that the factor should vary with the pressure.

2.7 CORRELATION OF HEAT TRANSFER DATA

The analytical analysis of heat flux correlation may be classified into three main categories

i) Those based on turbulent forced convection, Rohsenow (15)

ii) Those based on enthalpy transport, Han and Griffith (9) Han (46) Grant (3)

iii) Those based on natural convection, Zuber (16)

From the assumption that the heat transfer rate in nucleate boiling is related to the turbulence created by the bubble growing, departing or collapsing, Rohsenow (15) employed the theory of turbulent forced convection in the dimensionless relation

$$N_{Nu} = \emptyset \ (N_{Re}, N_{Pr}) \qquad (2.7.1)$$

where the bubble Reynolds number, which in this case measures the magnitude of agitation caused by the bubble motion, was defined as

$$N_{Re} = \frac{G_b D_d}{\mu} \qquad (2.7.2)$$

and G_b, the mass velocity of the bubbles as they leave the surface

$$G_b = \pi/6 \frac{Nf}{A} \rho_v D_d^3 \qquad (2.7.3)$$

D_d, the bubble departure diameter, is obtained from Equation (2.4) and the relation between the frequency of bubble formation and the bubble diameter may be approximately represented by Jakob's Equation

$$fD = C \qquad (2.7.4)$$

According to Rohsenow and Clark (47) the rate of heat transfer by bubbles attached to the surface is given by

$$(Q/A)_b = \frac{\pi}{6} \frac{Nf}{A} h_{fg} \rho_v D_d^3 \qquad (2.7.5)$$

and if it is assumed that the suggestion, given by Jakob, that the number of active sites (emitting bubbles) is proportional to the heat flux at a given pressure i.e. that (Q/A) is proportional to $(Q/A)_b$ is valid, then

$$(Q/A) = C_g \frac{\pi}{6} \frac{Nf}{A} h_{fg} \rho_v D_d^3 \qquad (2.7.6)$$

C_g is a constant depending upon pressure

From Equations (2.7.3, 2.7.6 and 2.4.1) Reynolds number may be expressed as

$$N_{Re} = \sqrt{2} \frac{C_d}{C_g} \beta \frac{Q/A}{\mu h_{fg}} \sqrt{\frac{g_c \sigma}{g(\rho_L - \rho_v)}} \qquad (2.7.7)$$

and Nusselt number as

$$N_{Nu} = \frac{h}{k} D = \sqrt{2}\, C_d\, \beta \frac{h}{K} \sqrt{\frac{g_c \sigma}{g(\rho_L - \rho_v)}} \qquad (2.7.8)$$

where the value of h is

$$h = \frac{Q/A}{T_{sup} - T_{sat}}$$

By establishing the ratio

$$\frac{N_{Re} \times N_{Pr}}{N_{Nu}} = \frac{\frac{G_b D}{\mu} \frac{C\mu}{K}}{\frac{hD}{K}} = \frac{C_p (T_W - T_{sat})}{C_g h_{fg}}$$

the rules of dimensional analysis permit Equation (2.7.1) to be written as

$$\frac{C_p (T_W - T_{sat})}{h_{fg}} = \phi (N_{Re}, N_{Pr}) \qquad (2.7.9)$$

If Equation (2.7.9) is expressed as a power series and only the first term is retained, then

$$\frac{C_p (T_W - T_{sat})}{h_{fg}} = C_{sf} \left(\frac{Q/A}{\mu h_{fg}} \sqrt{\frac{g_c \sigma}{g(\rho_L - \rho_v)}} \right)^{r'} \left(\frac{C_p \mu}{K} \right)^{m'} \qquad (2.7.10)$$

where C_{sf} is equal to constant $(\beta)^{r'}$ and hence should be a function of the particular fluid-heating surface combination only. From Adams data Rohsenow proposed the values of $r' = 0.33$ and $m' = 1.7$ which correlate results of Cichelli-Bonilla (48) for different liquids quite successfully. Recently Vachon et al proposed the value of $m' = 1$ and correlated their results (49) also successfully. Further discussion and the application of Equation (2.7.10) to experimental data are given in Chapter (9).

A second approach in predicting the heat flux was introduced by Zuber (16). He showed that the equation used in obtaining the heat transfer coefficient for the natural turbulent convection from a horizontal surface in a single phase flow problem can also be used in the region of isolated bubbles, a two-phase flow problem, if the vapour void fraction is taken into account in obtaining the density of the fluid.

From an experimental and analytical study of the problem of natural convection from a horizontal surface Malkas (50), [illegible] suggested, at high Rayleigh Number, the relation

$$\frac{hd}{k} = \text{Constant} \left\{ \frac{Q/A}{K\alpha} \beta' \Delta T d^3 \right\}^{1/3} \qquad (2.7.11)$$

where

$$\Delta T \beta' = \frac{\rho_{L\infty} - \rho_{Lw}}{\rho_{L\infty}} \qquad (2.7.12)$$

In the case of nucleate boiling the density of the two-phase mixture adjacent to the heating surface may be expressed as

$$\rho_{mw} = (1 - \alpha_w)\rho_{Lw} + \alpha_w \rho_v \qquad (2.7.13)$$

then from Equation (2.7.12)

$$\frac{\rho_{L\infty} - \rho_{mw}}{\rho_{L\infty}} = \beta'\Delta T + \alpha_w \frac{\Delta\rho}{\rho_{L\infty}} \qquad (2.7.14)$$

and substituting from Equation (2.7.14) into Equation (2.7.11) gives

$$\frac{hd}{k} = \text{Constant} \left\{ \frac{gd^3}{\nu\alpha} \left(\beta'\Delta T + \alpha \frac{\Delta\rho}{\rho_{L\infty}} \right) \right\}^{1/3} \qquad (2.7.15)$$

To obtain the value of the void fraction α_w a system with bubble population density N/A, bubble rise velocity U_v and frequency of bubble emission f may be assumed, then

$$\alpha_w = \frac{\text{volume of bubble}}{\text{volume of space available to one bubble}} \qquad (2.7.16)$$

$$\alpha_w = \frac{\pi}{6} D^3 \frac{N}{A} \frac{f}{Uv}$$

In the case where N/A is small Ref. (16), then α_w for both laminar and turbulent flow can be approximated to

$$\alpha_w = \frac{N}{A} \frac{\pi D^3}{6 U_t}$$

where, according to Peebles(51) U_t can be expressed as

$$Ut = 1.18 \left[\frac{\sigma g (\rho_L - \rho_v)}{\rho_L^2} \right]^{1/4} \qquad (2.7.17)$$

then substituting Equation (2.7.17,16) in Equation (2.7.11) gives approximately

$$\frac{hd}{K} = \text{Const.} \left[\frac{g d^3}{\nu^2 \alpha} \left(\beta \Delta T + \frac{N \pi D^2}{A 6} \frac{\Delta \rho}{\rho_{L\infty}} \right) \right]^{1/3} \qquad (2.7.18)$$

It may be mentioned here that the above approach is applicable only in the region of isolated bubbles. With the increase of applied heat flux i.e. in the region of interference it was indicated by Moore and Mesler (52) and also by Zuber (16) that the mechanism of heat transport is changing from a stirring effect of bubbles to that of latent heat. In Zuber's analysis (16) however, it was possible to estimate the limit of the isolated bubble region, using the

upper limit of the void fraction.

The application of Equation (2.7.18) to the experimental data and further discussion are given in Chapter (9)

The final analytical approach to the process of heat transfer is that of enthalpy transport. The heat removed is usually obtained by calculating the product of the enthalpy transported by one bubble with the frequency of emission and the bubble population density.

Grant (3) used the above technique and evaluated the heat energy carried away by each bubble as superheated enthalpy associated with a liquid cylinder of diameter $2D$, based on observations of Hsu and Graham (7), and height equal to the thermal layer thickness δ . A linear temperature distribution across the thermal layer was also assumed and the average value of ΔT_{sup} was used. Grant obtained the expression

$$Q/A = \frac{4\pi D^2}{4} \delta \frac{(T_w - T_\infty)}{2} Nf \qquad (2.7.19)$$

For the area which is not affected by the existence of bubbles, the natural convection process, for example Jakob's equation, was used in Ref. (4) to obtain $(q/A)_{NC}$ and hence the total heat carried away may be finally formulated as

$$Q/A = (Q/A)_{NC} + Nf \frac{4\pi D^2}{4} \delta \frac{(T_w - T_\infty)}{2} \qquad (2.7.20)$$

Grant (3) found that Equation (2.7.20) predicted results in good agreement with experimental data. The same kind of agreement was also reported by Han (46).

In contrast to Rallis and Jawurek (53) the above approach neglects the

latent heat carried in the bubble. This may be permissible at low heat fluxes, for example in the region of isolated bubbles, where analytical calculations based on the mass of vapour and liquid showed that Φ_{LH} is small and may be neglected.

CHAPTER 3

EXPERIMENTAL APPARATUS

3.1 Introduction

The experimental apparatus used was originally designed and built by Grant (3). A general description is given below but full details will be found in Ref. (3).

During the course of this work it was found necessary to modify some parts of the system to provide the optimum working conditions under a particular set of circumstances. Some new equipment, mainly instrumentation, was also introduced to allow further data to be obtained and to increase the rate at which results were taken.

3.2 General Description

The heart of the apparatus was a pressure vessel, or boiler, containing the test surface and auxiliary equipment concerned with temperature, pressure and heat flux measurement. The boiler, of Austenitic stainless steel, was constructed in the form of a cross, each arm being of circular cross-section of 5.8 in. inside diameter. Circular flanges of 1¼ in. thickness bolted to the end of each arm, could be easily removed allowing access for modification and cleaning. The flange on each of the side arms was fitted with a specially designed window of ¾ in. diameter so that the test surface could be viewed. The assembly was built to withstand temperaturesup to 550^{0}F and pressures up to 1000 psi. although a working pressure of 500 psi. was never exceeded in this work. Further details of design and construction are available in Ref (3).

The test surface nickel-chrome alloy strip, of length 2 in. width ½ in. and thickness of either 0.003 in., 0.006 in. or 0.01 in. was mounted on a block

of p.t.f.e. material with adhesive, whose choice is discussed in Section (4.7). Two nickel-plated brass channel supports fixed, through an insulator, to the bottom flange held the p.t.f.e. block and a feather spring attached to the channel supported the block from beneath. Electrical flux used to heat the test surface was supplied through the two supports, Fig. (7).

Two 500 watt heater coils fitted in U-shaped pyrex glass tubes fixed to the side flanges of the boiler served as a bulk liquid heater. The amount of electrical energy supplied to the coils was controlled through a Variac type 100R/2B-M.

To eliminate any heat loss from the boiler to the atmosphere, a 3,000 watt Hotfoil Type G heater 16 ft. in length, was wrapped round the outer surface of the boiler and covered with a thick layer of insulation in the form of glass wool and asbestos. The flux through the heater was controlled by feed-back temperature control using a sensing thermocouple fitted to the boiler wall. Manual control was also available through a fine Variac which was adjusted according to the observation of the wall temperature thermocouple readings. This form of control was used in most cases.

The test surface temperature was measured with a 0.002 in. diameter chromel-alumel thermocouple welded to the lower face of the strip, the welding technique will be discussed in Section (4.6.3). A 0.076 in. diameter chromel-alumel thermocouple, held in a channel cut in the p.t.f.e. block and bent so that the junction was ½ in. above the test surface and ½ in. to one side, was used to measure the bulk liquid temperature. Four more chromel-alumel thermocouples of diameter 0.076 in. fitted to the four arms of the boiler in direct contact with the outside surface were used to measure the wall temperature.

All e.m.f.'s generated by the above thermocouples were measured on a digital voltmeter.

The electrical flux supplied to the test strip was obtained from two high current cells connected in series to give a maximum strip current of 50 amps., maximum strip voltage of 1.2 volts, and hence maximum heat flux of approximately 30,000 Btu/ft^{2}hr. During the course of the experimental work a third cell was connected in series with the first two to raise the maximum heat flux to 40,000 Btu/ft^{2}hr. The voltage was applied through a fuse and a knife switch which enabled the current direction to be reversed and was finely controlled through a variable resistance (0.07Ω to 1.4Ω). The strip current and voltage were measured on the digital voltmeter.

Pressures above atmospheric were obtained by means of a high-pressure nitrogen cylinder connected to the boiler through a control valve. Pressure values were indicated on a pressure gauge reading up to 500 psi. in steps of 2 psi., see Fig. (107). A cooling coil fitted to the outside of the boiler neck and acting as a condenser controlled the pressure of steam in the boiler and was used in conjunction with the nitrogen cylinder to obtain the desired pressure. Pressures below atmospheric were obtained with the aid of a water jet vacuum pump connected to the boiler through a fine valve. Vacuum was measured on a vacuum gauge, see Fig. (107).

3.3 Modifications made to the System

In the original apparatus design, the test surface was on the same level as the side viewing windows which made it impossible to see the actual active sites or to differentiate between bubbles from cavities on the strip and those arising from the contact area with the p.t.f.e. block. In order to overcome

this difficulty the block holder was lowered so that the surface was viewed at an angle. This also facilitated lighting of the strip for photographic purposes. A second modification, made in order to reduce the number of bubbles arising from the area of contact of the strip edges and the p.t.f.e. block, was to reduce the width of the block to 0.490 in. This, together with the use of a new adhesive material which will be discussed later eliminated the problem of bubble formation from the strip sides.

Possible turbulent effects from the bulk liquid heater were eliminated by shortening the heater tube approximately 2 inches while retaining the original power of 500 watts. Care was taken in wrapping the wall heater round the boiler outer surface since overlapping could produce localized heating resulting in either local boiling on the inside surface of the boiler or a burnt out heater.

3.4 New Equipment Introduced

The strip temperature, bulk liquid temperature and wall temperature were originally measured using a two channel precision potentiometer type P2 , where the required variable was selected with a set of switches. The strip voltage and current were also measured on the potentiometer after introducing a standard resistance and resistance box into the circuit to bring the voltage and current into the potentiometer range. With this arrangement a considerable time was involved in taking a set of readings, particularly if adjustments were necessary between individual measurements.

A Solartron Data logger was introduced and programmed to measure not only the above temperatures but also the strip voltage and current directly. The voltmeter was capable of scanning the results manually or automatically in the

latter case the scan lasted one minute and results were punched on a paper tape. The potentiometer was retained in the system as a check to the voltmeter at intervals during the experimental work.

During most of the experimental work the digital voltmeter was used manually. This mode of operation was chosen for three reasons. Firstly, the measurements of temperature and electrical flux were taken when the system was in an equilibrium state. This meant that each time the heat flux was changed the system had to be left for at least five minutes to attain equilibrium and it would be necessary to stop and restart the voltmeter scan each time. Secondly, certain variables, for example the surface temperature of the strip, were continually varying slightly about a mean value which could be better judged from a direct observation than by means of an automatic scan. Finally most results obtained were calculated manually so that direct readings were a more convenient form of output.

A Honeywell constant temperature controller with a range of 0-300 $^{\circ}$C was introduced to provide a specific wall temperature. Other items of equipment such as power units, counter, UV recorder, oscilloscope, AC amplifier and Polaroid camera are used in conjunction with the frequency measurement, see Fig. (107).

3.5 Choice of Testing Surface

The original choice of a test surface was a plane strip, with a surface area 2 x ½ in. and thickness 0.003 in. The strip material chosen was 80 - 20 Nickel-chrome alloy since its resistance is high enough to generate heat flux from a low voltage battery supply of 2 volts, and because it has a good

resistance to corrosion. It was decided, since this was the continuation of previous work, to continue using this surface so that results could be compared with those obtained in that work.

During the course of the work strips with thicknesses of 0.006 in. and 0.01 in. were introduced so that larger cavities could be either drilled or made by one of the methods discussed in Chapter (4).

CHAPTER 4

PREPARATION OF TEST SURFACES AND EXPERIMENTAL PROCEDURE

4.1 TEST SURFACE POLISHING

The commercial test strips were found to contain many natural scratches and cavities when examined under an ordinary microscope and in order to eliminate these several techniques were used.

4.1 - 1 Polishing with Emery Paper

An initial attempt to obtain an adequate surface polish was made using emery paper of grades 4/0, 2/0, 1/0. The strip was mounted on a horizontal surface and polished in the direction of its length for ten minutes and then perpendicular to its length for a further ten minutes, three times. It was then thoroughly washed in distilled water, dried and the same procedure followed with the next grade of emery paper.

When, after this procedure, the strip was examined under a microscope of a magnification of 50 times, it was found that there were still a number of scratches on the surface. Since, however, Westwater (20), has suggested that a surface scratch should not give rise to boiling initiation in water, because of the ability of water to wet the scratch, it was decided to perform a preliminary experiment.

A number of artificial cavities were made on the strip using methods discussed in section (4.2), and the strip inserted in the boiler with distilled deionized water as the boiling medium. A number of bubbles were seen coming from the strip apart from those formed on the artificial cavities indicating that there were still natural active cavities.

Natural cavities were found to remain on the strip after the above procedure had been repeated several times and therefore this procedure was discarded.

4.1 - 2 Polishing with Durmax Alumina Liquid

It was suggested by Howie (54) that Durmax alumina liquid could be used to improve the finish.

The strip was again mounted horizontally and first polished for an hour with wet silicon carbide paper, grade A600, changing the polishing direction each ten minutes as before. Course grade Durmax alumina liquid was applied to the strip with chamois leather for twenty minutes and the strip then rinsed successively in hot water, distilled water and acetone and allowed to dry after each rinsing. Medium and fine grades of the liquid were used in a similar manner. On microscopic examination natural cavities could still be distinguished on the surface and the polishing procedure, from the use of silicon carbide paper to the fine grade alumina liquid, was therefore repeated. When a trial run was carried out on this strip bubbles still formed in natural cavities as well as on the artificial cavities and this procedure was also rejected.

4.1 - 3 Polishing with Dialop Compound (Diamond dust)

The third attempt to obtain an adequate surface involved the use of diamond dust (Dialop compound), produced by Metallurgical Services Lab. Ltd., of grades 6/3, 1/1 and ¼/1.

The strip was mounted horizontally and again given an initial polishing with wet silicon carbide paper and then cleaned and dried. The coarsest grade of Dialop compound, 6/3, was applied to the strip for forty minutes with a specially

manufactured polishing cloth, type B.101/2 Metron B, the polishing direction being changed every ten minutes. The strip was rinsed in water many times, carefully wiped with clean tissue and washed in distilled water to remove any of the Dialop compound particles left before changing to a finer grade. The procedure was repeated with the two finer grades 1/1 and ½/1 of the Dialop compound and the strip given a final polish with very fine alumina powder when the surface was seen to have a mirror finish.

Microscopic examination revealed that this was the best surface finish achieved and a test experiment showed that by far the greater number of bubbles arose from artificial cavities with only one or two individual bubbles coming from natural cavities. After repeating the Dialop compound polishing all initiation from natural cavities was eliminated and the surface was acceptable.

This procedure using the Dialop compound was adopted for all test surfaces throughout the experimental work.

4.2 METHODS OF PRODUCING ARTIFICIAL CAVITIES

Once a flawless surface finish had been achieved on the test surface, artificial cavities of known properties could be made and boiling from these cavities studied. The cavity size, shape and depth must all be taken into account when considering methods of cavity production and the resulting cavities must be active, i.e. they must be capable of trapping gas or vapour or they will not give rise to bubbles Bankoff (18).

A large range of cavity radii was required for this investigation which was eventually decided as 0.0002 to 0.025 in.

4.2 -1 Production of small cavities

Initially a pyramid-shaped diamond of apex angle 135° fitted into a micro hardness tester was tried. When the same diamond was used with two values of constant applied pressure two sets of cavities of average size 0.0074 in. and 0.00038 in. were produced. However eighteen cavities made in this manner were found to be completely inert when the strip was tested in the boiler. This was attributed to the fact that they were shallow and inefficient in trapping air or vapour. It was decided therefore that the method was unsuitable.

It was thought that sharper cavities might result if a needle was used in place of the diamond. Accordingly a gramaphone needle was fixed in a holder and again used with a micro hardness tester. A set of cavities was produced using the same needle and a constant pressure. Examination of the set, however, revealed that the ratio of their surface area to the depth was very large, they were not of a constant size and not of uniform shape. The latter was thought to be due to the fact that the needle quickly lost its initial sharpness. Attempts to use a needle of smaller diameter were unsuccessful as the needle could withstand only small pressures.

Ordinary sewing needles proved initially to be too brittle to make a cavity and although a heat treatment, whereby the needles were raised to a high temperature and then quenched, improved their strength, fine smooth cavities could not be produced. Surgical needles of varying radii were also found to be too weak to produce a proper cavity.

Finally a silver steel needle ground to a very fine point was tried. The needle was mounted in a holder, Fig. (4) fitted with a screw and spring so that varying pressures could be applied gradually. The holder was clamped in a heavy

block of steel, 3 in. deep 2 in. x 2 in. cross section, and the strip fixed beneath it. Cavities were produced by screwing the needle into the test surface, the size of cavity being proportional to the number of turns of the screw.

Cavities produced in this manner were found upon examination to be generally satisfactory, especially in the sense that they were circular and of constant size. When the test surface was installed in the boiler the cavities were found to be active and the strip behaviour satisfactory, apart from bubbles generated from the strip edges, a problem to be discussed in Section (4.10.) Smaller cavities in the size range 0.0002 in. to 0.006 in. were produced in this manner on two test surfaces used in the experimental work.

4.2 - 2 Production of Large Cavities

Larger cavities, with radii in the approximate range 0.007 in. to 0.025 in. were formed using fine drills of various radii on an ordinary high speed drilling machine. The cavities obtained were cylindrical Fig. (94) in shape and accurate in size. Three strips were produced using this method, two of them each containing ten cavities of varying sizes evenly spread along a horizontal line in the surface. The strips when tested in the boiler proved to be satisfactory and were used for further experimental work.

4.2 - 3 Simultaneous Production of Large Numbers of Cavities

Attempts were made to devise a method for making quickly a large number of evenly-spaced uniform size cavities on a strip. As a first attempt a set of pyramids was machined onto a steel roller which was hardened and then rolled over the strip, using a milling machine with an adjustable bed to exert suitable pressure. Five strips were made using this method.

Microscopic examination however revealed that the cavities were not even approximately square as had been expected but of varying shapes which made cavity sizing so difficult that other production methods were sought.

An alternative method was devised using a silver steel needle holder precision ground to a very fine point. The test surface was placed on a milling machine bed and the holder clamped into the machine so that it just touched the surface. The bed of the machine could then be raised a fixed amount to maintain a constant pressure and the horizontal traverse of the bed used to space the cavities.

When cavities produced in this way were examined they were found to be of an approximately constant circular shape and were quite satisfactory. Two strips with average cavity sizes of 0.00176 in. and.0036 in. respectively were produced by this method, each containing approximately 120 cavities. These strips later proved satisfactory in experiments.

A third strip with a random distribution of cavity sizes and placement was also made.

4.3 MEASUREMENT OF CAVITY SIZES

The diameters of artificial cavities placed on a test surface were measured using an ordinary microscope. The microscope was fitted with a graticule of ten divisions of 0.1mm, each division capable of being measured to a hundredth part using a vernier fixed to the eyepiece so that its accuracy was $\mp$ 0.001 mm.

The diameters of single cavities on a strip were measured in two perpendicular directions and the average value obtained.

Surfaces containing rows of cavities of approximately constant size were traversed row by row measuring the diameter in one direction. Any cavities with

obviously non-circular cross section were measured in two perpendicular directions.

Measurement of cavities in a normal distribution on a strip was more complicated since the cavity formation was not regular. The problem was solved by dividing the strip into small sections and masking out all but the section under consideration. For that section the microscope was traversed across the width of the strip, measuring the diameters of all cavities encountered, moved along the length of the strip a distance of the largest cavity radius found and retraversed across the width so that all cavities in that section were measured. Cavities directly on the line of traverse and those on the side of this line towards the start of the section were measured in one scan so that no cavity was measured twice.

4.4 MINIMISING POSSIBLE EFFECTS OF FACTORS ON REPRODUCIBILITY OF RESULTS

The existence of a large number of factors which may affect boiling makes the reproducibility of results rather difficult. These factors include contamination of boiling liquid from the boiler, the type of liquid and its purity, dissolved gases in the liquid and corrosion of the boiler. The following procedures were adopted in minimising the possible effects.

4.4 - 1 Cleaning the Boiler and Test Surface

The boiler was cleaned internally by removing the boiler flanges and washing the inside thoroughly with detergent and hot water to remove all dust and traces of any type of grease, rinsing twice with hot water then distilled water and drying with a clean tissue. The surface was given a final wipe with a tissue soaked in acetone and the acetone left to evaporate. The flanges were similarly treated and the boiler reassembled.

Once the test surface had been fixed to the p.t.f.e. block and placed in the holder the surface was cleaned with carbon tetrachloride, rinsed with distilled water and dried with a clean tissue. After a final wipe with a tissue soaked in acetone, the acetone was left to evaporate.

4.4 - 2 The Choice and Treatment of Boiling Liquid

Since this work was planned as the continuation of the previous work carried out in the same programme the boiling liquid was retained as distilled deionized water. This also eliminated possible contamination from organic or inorganic material, which could affect the behaviour of the liquid either chemically or by providing possible potential sites or by forming a deposit on the test surface which may act as an insulating layer. The distilled water was obtained from a constant source and was passed through a Griffith-Raleigh deionizer several times until its resistance measured on the deionizer fixed meter was $>10^6 \Omega/cm$. This value was checked during the experimental work.

4.4 - 3 Degassing Procedure

The effect of dissolved gas in the boiling liquid on the experimental data has long been recognized McAdams et al (11). In order to minimise this factor a standard degassing procedure was introduced and used throughout the work.

2000 ml of distilled deionized water were added to the boiler, which brought the water level to three inches above the top of the test surface. The bulk liquid heater was used to bring the water to boiling temperature at which point the heat flux was applied to the test surface and vigorous boiling from the surface carried out for 20 minutes. The top boiler flange was then replaced, the pressure increased to 10 psi. gauge and the bulk liquid heater used to reach the near saturation temperature. Vigorous boiling from the surface was then

continued for a further twenty minutes. At this point the pressure was dropped suddenly to atmospheric, care being taken to reduce the test strip heat flux gradually so that the surface was not overheated. The flux was then increased to the specified maximum value of 40,000 Btu/ft^{2}hr. and boiling continued for a further 20 minutes.

The above procedure was found to be satisfactory and to give reasonably reproducible results when measurements of the heat flux and corresponding superheat temperature difference were plotted. It compared favourably with a procedure based on reducing the boiler pressure to sub-atmospheric and then increasing it suddenly to atmospheric.

4.4 _4 Corrosion in the Boiler

During the early stages of this work it was noticed that the water became dull and yellowish in colour after approximately seven hours in the boiler and was extremely discoloured if allowed to remain in the boiler overnight. This phenomenon was also reported by Grant ([3]). This effect was referred to the corrosion in the boiler. Corrosion introduces an uncontrollable parameter which may affect the nucleation characteristics and hence the reproducibility of the results. Elord et al (55) related the corrosion in a stainless steel boiler to the oxidation of the surface when exposed to high temperature fluid. With the thermal expansion and contraction the so formed oxide broke and dissolved into the liquid. As the level of this solid material increases some may be deposited on the test surface and hence affect the data. It was also reported in the literature, Even (56), that the use of an alkali such as ammonia either to neutralise the water or to make it slightly alkaline prevents corrosion in the boiler.

Accordingly five mls of ammonia were added to the boiler after degassing. This amount, which represents less than 0.5% of the liquid volume, was found to be sufficient to give protection for at least ten hours.

Grant (3) found that the experimental data before and after adding the ammonia were in excellent agreement, this was also substantiated in this work.

4.5 PROCEDURE USED IN INCREASING AND DECREASING THE PRESSURE

The following procedure was adopted, after the initial degassing, when an experimental run was to be conducted at a pressure higher than atmospheric.

The top flange was bolted to the boiler and the connections from the boiler to the pressurizing nitrogen cylinder and to the pressure gauge made. Pressure was applied to the boiler by opening the cylinder valve and the pressure read from the main pressure gauge as shown in Fig. (10).

The saturation temperature at the required pressure was achieved and maintained by controlling the bulk liquid heater, wall heater and cold water flow through the outside condenser.

Sub-cooled conditions at any pressure were achieved by controlling the coolant flow and the bulk liquid heater power.

It was necessary to keep the wall temperature at a value slightly higher than the working bulk liquid temperature by means of either the thermocouple feedback controller Fig. (10), or manual control. This was to provide for any heat losses to the surroundings so that the boiler may be considered an adiabatic system.

Pressures below atmospheric were obtained by connecting a water ejector vacuum pump to the boiler through a control valve. The pressure was indicated on a vacuum gauge.

4.6 THERMOCOUPLES AND THEIR CALIBRATIONS

4.6 - 1 Bulk Liquid Thermocouple

The bulk liquid thermocouple was constructed from 0.076 in. diameter chromel-alumel wire, electrically insulated throughout, except for the junction. This was formed using a Spembly discharge welder, type WPL4, the appropriate values of voltage and capacitance for suitable weld strength having been determined by trial and error. The thermocouple was fixed to the p.t.f.e. block in the holder so that the junction was 0.5 in. from the strip and 0.5 in. above the surface. This position was chosen to minimize the effect of convection currents from the strip and from the bulk liquid heater.

4.6 - 2 Calibration of the Bulk Liquid Thermocouple

The thermocouple leads were each placed into a glass tube and the tubes clamped so that the junction was rigid. The arrangement was immersed in an oil bath to a minimum depth of 3 in. so that errors in temperature measurement due to natural convection from the free oil surface were eliminated. The oil was heated by an electrical heater at the bottom of the bath and a uniform temperature assured by stirring the oil. The leads were each soldered to a copper wire and each junction formed, fitted into a test tube filled with paraffin to give uniform temperature distribution. The tubes were immersed in an ice bath.

The e.m.f. generated in the above arrangement was measured to an accuracy of $\pm$ 0.001 mvolts using a precision potentiometer and the corresponding temperature obtained from B.S.T. 1827 152 table. This was compared with the oil temperature in the range $80^{o}F$ - $300^{o}F$, which was measured by a mercury thermometer to an accuracy of $\pm$ $0.1^{o}F$. Any thermocouple with a discrepancy greater than $\pm$ 0.5% was rejected.

As a further check to the calibration of the bulk liquid thermocouple, steam point was chosen because of the simplicity and accuracy of obtaining a corrected constant temperature.

The thermocouple was placed in a flask, half-full of distilled water and located 3 in. above the water level in the path of the outflowing vapour. The e.m.f. generated from the thermocouple was recorded and boiling temperature was corrected to atmospheric pressure. The accuracy of this system was estimated to be $\pm$ 0.5°F.

4.6-3 Test Surface Thermocouple

To obtain the temperature of the test surface, a thermocouple was attached to the lower surface of the strip and from this reading the upper surface temperature was estimated.

The thermocouple was constructed from 0.002 in. diameter chromel-alumel wires and the junction electrically welded to the centre of the strip with the wire in a horizontal plane perpendicular to the strip length. Since there is a D.C. voltage gradient along the strip length the thermocouple will acquire a pick-up voltage which can be minimized by ensuring that the area of contact of the strip and thermocouple is as small as possible. This led to the choice of fine diameter wire and care was taken to ensure for the thermocouples selected that the junction size was never greater than the wire diameter. The pick-up is also minimized by arranging for the wires to lie on the surface perpendicular to the strip length i.e. a plane of constant voltage. By this means also the loss of heat by conduction along the thermocouple wires was reduced since the leads lay in an isothermal plane.

Grant (3) found that the pick-up was negligible provided care was taken to

put the thermocouple in a plane perpendicular to the current direction and with minimum contact area. It was also reported that the pick-up may be estimated as half the difference in the measured values of the generated e.m.f. when the current direction is reversed.

The value of the pick-up was determined in this work by placing the test surface in cold water and applying a fixed voltage in both a positive and negative direction. The pick-up was then estimated as half the difference in the measured values of e.m.f. Test surfaces with a pick-up greater than $\pm$ 0.05 mV were rejected.

The test surface thermocouple was calibrated using the steam point as a hot junction and an ice bath as a cold junction and the calibration was checked against that of the bulk liquid thermocouple.

4.7 ELIMINATION OF BUBBLES FROM THE CONTACT AREA OF THE STRIP EDGE and p.t.f.e. BLOCK

The test strip was fitted into a groove, of the exact dimensions of the strip, cut in the p.t.f.e. block and fixed there with an I.C.I. adhesive type (PA79). When this arrangement was tried in the boiler, it was found that a large number of bubbles were coming from the contact area of the strip edge and the p.t.f.e. This made it impossible to observe throught the side windows the initiation of boiling from cavities on the strip. It also made it difficult to ascertain the exact number of active sites at a particular heat flux. It was thought that the phenomenon might be due to imperfections in the edge of the groove which formed cavities larger than those on the strip surface. The effect might also be attributed to air trapped in the contact area, although the effect was present after degassing.

An attempt to solve the problem was made by introducing a different adhesive material. An I.C.I. Silicoset type 151 was chosen since this leaves a very smooth surface when dry, forms a strong bond and stands up well to operating temperatures. The lower surface of the strip and the face of the p.t.f.e. block were thoroughly cleaned with acetone and allowed to dry. A few drops of the Silicoset were spread over the p.t.f.e. surface and left for five minutes to partially dry and form a strong bond. The strip was than placed carefully on the block surface and even pressure applied by means of a small weight, covered with cloth to prevent scratching, and the adhesive allowed to dry. This procedure made a strong bond which was unaffected by water and heat.

When the Silicoset-fixed strip was tried in the boiler it was found that the number of the bubbles was reduced but the improvement was unsatisfactory. Another suggestion was that a thin film of a metal be deposited over the strip and the face of the p.t.f.e. but this was discounted after discussion, mainly because of the probability of changing strip properties such as thermal conductivity and resistance.

Since all the bubbles arose from the contact area of the strip and p.t.f.e. the problem would be solved if this area could be dispensed with. Accordingly, the block width was reduced to that of the strip and the above procedure repeated in fixing the strip to the block, care being taken to smear the adhesive along the edges of the strip to give a completely smooth joint.

When this configuration was tried in the boiler it was found to be very satisfactory. A further improvement was that of reducing the width of the block by a further 0.004 in. and covering the area of the strip overlap with adhesive. This gave a very smooth surface which proved satisfactory.

CHAPTER 5

THEORY OF NUCLEATE BOILING

5.1 Introduction

Many attempts have been made to establish the criteria of bubble initiation and two approaches seem to have emerged. Firstly a simple correlation using Gibb's Equation for the equilibrium of a bubble coupled with the Clausius-Clapeyron equation and secondly an equation proposed by Han and Griffith (9) and also by Hsu (22), which considers the temperature inside the bubble and refers to the height of the thermal layer and the transient conduction across it. Recently there have been attempts to modify the formulae thus obtained and to combine them to some degree, Hsu and Graham (7) Grant (3). In this Chapter the first approach is discussed and explanations proposed where divergence from experimental data is found. Pressure effects are similarly considered.

The frequency of bubble emission is predicted by separate consideration of waiting time, t_w, and growth time, t_g, A first order approximation for the prediction of t_w is proposed and compared with that of Hsu (22). The equations for t_g of Golovin et al (57) and Zuber (1), are compared to those of Plesset and Zwick (27), and the latter used to evaluate the growth time.

Although empirical formulae for the number of active sites have been proposed an analytical approach based on the cavity size distribution coupled with an equation for initiation is introduced and adopted here.

A formula for predicting heat flux in the weak nucleate region is proposed in which the energy carried by each individual bubble and the effects of natural convection are considered.

5.2 Bubble Initiation

The existence of a cavity containing trapped gas or vapour, surrounded by a liquid, superheated with respect to the saturation temperature at that pressure, is a normal requirement for the initiation of a bubble, Bankoff ($_{18}$).

For a spherical vapour bubble the relation between the vapour bubble radius at equilibrium and the pressure is given by Gibb's Equation:

$$P_v - P_L = \frac{2\sigma}{r} \qquad (5.2.1)$$

where r_b is the bubble radius. In the case of a vapour-filled cavity this can be expressed in terms of r_c, the cavity mouth radius where the liquid vapour boundary contacts the cavity wall, θ the cavity cone angle and β the contact angle, Fig. (2), as

$$P = P_v - P_L = \frac{2\sigma}{r_c} \cos(\theta/2 - \beta) \qquad (5.2.2)$$

According to Griffith & Wallis (21) the contact angle for water with a clean metal surface at atmospheric pressure and saturated temperature is 40^o, if it is assumed that $\theta/2$ has this value then Equation (5.2.2) can be written as:

$$\Delta P = \frac{2\sigma}{r_c} \qquad (5.2.3)$$

and the Clausius-Clapeyron Equation may then be used to relate the excess pressure in the bubble to the excess temperature, in the form

$$\frac{\Delta P}{T_w - T_{sat}} = \frac{h_{fg}\, J}{T\,(V_v - V_L)} \qquad (5.2.4)$$

For pressures below 1000 psi. the specific volume V_v is much greater than V_l so that Equations (5.2.3) and (5.2.4) can be combined to give:

$$Tw - Tsat = \frac{2 \sigma Tw}{h_{fg} J \rho_v r_c} \qquad (5.2.5)$$

This can be further simplified by the assumption that the vapour behaves as a perfect gas, so that the relation:

$$1/\rho_v = \frac{R' Tsat}{P} \qquad (5.2.6)$$

may be used. Equation (5.2.5) can then be written in the form:

$$Tw - Tsat = \frac{2 \sigma Tw \; Tsat \; R'}{h_{fg} J P_l r_c} \qquad (5.2.7)$$

Which may be approximated to give:

$$\Delta T_{int} = Tw - Tsat = \frac{2 \sigma Tsat^2}{r_c h_{fg} J P_l} \qquad (5.2.8)$$

Equation (5.2.8) predicts the minimum temperature difference needed to initiate a bubble from a cavity of radius r_c. It can be seen from Fig. (45) that predicted values of Equation (5.2.8) are less then those obtained practically for the eight test surfaces, in particular the discrepancy is most obvious for values of r_c greater than 0.005 in. This effect is discussed fully in Chapter (9) but it may be mentioned here that two ideas are forwarded. Firstly it is postulated that there exists within a large cavity one of a smaller

radius and that the initiation is from that sub-cavity, substitution of a smaller r_c value, r_c^*, in Equation (5.2.8) makes the predicted values more comparable with practical results. Secondly it is thought possible that a cavity becomes partially filled with liquid and that the effective cavity radius is less than the radius at the mouth.

5.3 The Effect of Pressure on Superheat Temperature Difference

As the pressure increases the superheat temperature required for initiation appears to decrease.

If it is assumed that Equation (5.2.8) is applicable, then the variation of each of the individual properties with pressure may be considered. Since σ and r_c are assumed to be independent of pressure the variation in ΔT_{int} is approximately $(T_{sat}/\rho_v h_{fg})$. When this is plotted as a function of pressure Fig. (8) the following expression is obtained from the fitted curve:

$$\Delta T_{int} = \frac{2\sigma}{r_c} \left(\frac{160}{778}\right) P_L^{-0.78} \qquad (5.3.1)$$

where ΔT in ^{o}F, r_c in ft. and P_L in lb/in^2

When predictions from this equation were compared with practical data, see Chapter (9), it was found necessary to introduce the concept of r_c as a function of pressure. This is justifiable if it is considered that with higher pressure the liquid is pushed deeper into the cavity. The new radius may then be expressed as a function of pressure and physical cavity radius as:

$$r_{new} = \phi (r_c, P_l) \qquad (5.3.2)$$

Then Equation (5.3.1) may be written in the form:

$$\Delta T_{int} = \frac{320}{778} \sigma \frac{P_l^{-.786}}{r_{new}} \qquad (5.3.3)$$

The predicted values of Equation (5.3.3) are discussed and compared with the experimental data in Section (9 -2).

5.4 Bubble Frequency

Bubble emission frequency in the weak nucleate boiling region is usually defined as $f = \frac{1}{t_g + t_w}$. To predict the frequency, expressions for t_w and t_g in terms of all the factors on which f is dependent, e.g. cavity size, heat flux, pressure, must be obtained.

5.4 - 1 Waiting Time

Consider a cavity in a liquid-solid boundary heated to such a temperature as to give rise to a thermal layer thickness δ Fig. (9). If δ and the rate of heat conduction through the thermal layer are constant then the temperature at the thermal layer top surface is also constant. The temperature distribution within the thermal layer may then be taken as linear, and the temperature T at distance (x) from the test surface is

$$T = T_{\infty} + \frac{x}{\delta} (T_w - T_{\infty}) \qquad (5.4.1)$$

excess

The amount of energy ΔQ in a thin layer of thickness d_x and area equal to πD_x^2, where D_x is proportional to the bubble departure radius may be expressed as

$$\Delta Q = \frac{x}{\delta} (T_w - T_{\infty}) (\pi D_x^2) d_x \rho_l c_p \qquad (5.4.2)$$

The total heat Q in that portion of the thermal layer which covers the area is then given by:

$$Q = (\pi D_x^2)\ \rho_1\ c_p \int_0^{\delta} \frac{x}{\delta}\ (T_w - T_\infty)\ d_x$$

which may be written in the form:

$$Q = \pi D_x^2\ c_p\ \rho_1\ \frac{\delta}{2}\ (T_w - T_\infty) \qquad (5.4.3)$$

This amount of heat is removed by the bubble partly as latent heat conducted through the thermal layer to the growing bubble and partly as thermal layer carried with the departing bubble.

As the bubble leaves, relatively cold liquid will rush to occupy the space vacated so that heat will be conducted from the surface and the thermal layer will be re-established. The conduction takes a time t_w and can be represented by the expression:

$$Q = \int_0^{t_w} \left(\frac{dQ}{dt}\right) dt \qquad (5.4.4)$$

where $\left(\frac{dQ}{dt}\right)$ is the rate of heat conduction to the liquid through the influenced area.

Since the above approach is very simple one may assume that the relation:

$$\frac{dQ}{dt} = - KA \frac{dT}{dx} \qquad (5.4.5)$$

is valid. From Equation (5.4.5.) this may be expressed in the form:

$$dQ = - KA\ \frac{(T_w - T_\infty)\ dt}{\delta}$$

Equations (5.4.3) and (5.4.4) give:

$$\pi D_x^2 C_p \rho_1 \frac{\delta}{2} (Tw - T\infty) = \frac{KA}{\delta} (Tw - T\infty) tw$$

from which we obtain

$$tw = \frac{\pi D_x^2}{A} \frac{C_p \rho}{K} \frac{\delta^2}{2} \qquad (5.4.6)$$

The area ratio $\frac{\pi D_x^2}{A}$ may be taken as 1, hence

$$tw = 0.5 \frac{\delta^2}{\alpha} \qquad (5.4.7)$$

According to Zuber's analysis (1) δ may be put as $\frac{K\Delta T}{Q/A} = \delta$ and hence Equation (5.4.7) becomes:

$$tw = \frac{0.5}{\alpha} \left(\frac{K\Delta T}{Q/A}\right)^2 \qquad (5.4.8)$$

Equation (5.4.8) shows clearly the effect of the heat flux or superheat temperature on the waiting time, but, in contrast to Han and Griffith's Equation (App B), the effect of cavity size is not explicit. Since, however, the relation ($Q \vee \Delta T$) is affected by the surface condition and hence by cavity size, the effect is inherent in the ($\frac{K\Delta T}{Q/A}$) term. This can be seen from Fig. (32) and (33).

For pressures higher than atmospheric, the effect is again found in the ($Q \vee \Delta T$) relation and can be seen in Fig. (75) and (77).
This is discussed in Chapter (9).

Hsu (22) proposed a model in which the transient conduction equation was used to calculate the heat conducted through a constant width thermal layer, Fig. (10) assuming the heat flux to be constant and, for $x = \delta$ i.e. $t = t_w$,

obtained the final equation:

$$Tw - Tsat = \frac{2\,Q/A}{K} (\alpha tw)^{1/2} \sum_{n=0}^{\infty} (-1)^n \left\{ ierfc \frac{(2n+1)\delta - \delta}{2(\alpha tw)^{1/2}} - ierfc \frac{(2n+1)\delta + \delta}{2(\alpha tw)^{1/2}} \right\} \qquad (5.4.9)$$

But for all possible values of δ only the first term in the summation is significant and Carrie and Patten (63) found that the equation reduces to

$$\Delta T_{sup} = Tw - Tsat = \frac{2\,Q/A}{K} (\alpha tw)^{1/2} ierfc(0) \qquad (5.4.10$$

which can be written as:

$$tw = 0.78 \frac{1}{\alpha} \left(\frac{K\Delta T}{Q/A} \right)^2 \qquad (5.4.11)$$

The similarity between Equations (5.4.11) and (5.4.8) is obvious, the only difference occuring in the constant. In the derivation of Equation (5.4.8) the assumption that πD_x^2 the area of the thermal layer section, is equal to that of the cavity mouth may be revised and the constant modified accordingly.

5.4 – 2 Growth Time

The growth time is the time required for the bubble to grow from the instant of initiation to the moment of departure from the surface. It is again a quantity affected by many factors for example, ΔT, rc, σ, P.

Among the expressions for growth time put forward is that of Plesset and Zwick (27), see also Chapter (2), who proposed the equation:

$$tg = \frac{\pi\alpha}{3} \left(\frac{Dd\, h_{fg}\, \rho_v}{4\, K\Delta T} \right)^2 \qquad (5.4.12)$$

Although the above equation is subject to several limitations, Zuber (1) reported that it was a good approximation at high Jakob number $N_J \gg 1$. When experimental values of superheat temperature difference, bubble departure

diameter etc, were substituted in the equation the resulting value of t_g was comparable with that obtained experimentally by Han and Griffith (9) and Hsu and Graham (7) and also with results from an empirical relation derived by Golovin et al (57) from their results for water, benzene and alcohol.

Zuber's Equation (1), which is a modification of that of Bosnjakovic (25) was computed and Fig. (11) obtained which shows the results for different heat fluxes. The results were comparable with those predicted by Equation (5.4.12). Equation (5.4.12) was used throughout this work to calculate t_g.

The value of D, the bubble departure diameter, was obtained experimentally at atmospheric pressure, Fig. (78), and Semeria' (32) Equation:

$$D = 0.242 \; P^{-0.5} \qquad (5.4.14)$$

was used to obtain D, at higher pressures. It was necessary to introduce a factor of 1.5 to correlate experimental results with those obtained from equation (5.4.14), at atmospheric pressure, this factor was used also for higher pressures.

From table (7.2.1), it can be seen that at atmospheric pressure the waiting time t_w is much longer than the growth time t_g expecially at low heat flux. Hsu and Graham (7) found experimentally that $t_g/t_w \sim 1/9$ and on this basis one may define frequency as $f = \frac{1}{t_w}$ at atmospheric pressure, which gives:

$$f = 2 \; \frac{\alpha}{\delta^2} \qquad (5.4.15)$$

Ivey (10), working with Eckert's expression for the temperature fluctuations on the test surface as a bubble leaves, obtained the relation: (See Chapter 2)

$$f = 8.0 \; \frac{\alpha}{\delta^2} \qquad (5.4.16)$$

Again the similarity between Equations (5.4.15) and (5.4.16) apart from the constant factor is notable.

For the pressures higher than atmospheric, Tables (3a, b), the growth time is comparable with or larger than the waiting time, and the growth time t_g may no longer be neglected in estimations of bubble frequency.

The above theory is applicable to individual bubbles, When a test surface with a large number of cavities is considered, the effect of neighbouring sites on a particular bubble must be taken into consideration. This will be discussed in Chapter (7).

5.5 Number of Active Sites

Attempts have been made by Gaertner (5), Bushell (6) and Grant (3), to relate the number of active sites and superheat temperature difference.

If the cavity size distribution of the heating surface is used in conjunction with an equation predicting ΔT_{int} for initiation, for example $\Delta T_{int} = \frac{B}{\epsilon}$, the number of cavities which should initiate when a superheat ΔT is applied can be predicted.

Figs. (12) and (13) and (14) show the cavity size distributions for test surfaces NG1, NG2 and NG3. It can be seen from the continous line drawn that the distributions can be approximated to a sine wave of the form

$$y = \frac{\Delta N}{\Delta r} = a \sin \left(\frac{\pi}{4\epsilon} rc - \frac{\pi}{4\epsilon} (r_m - 2\epsilon) \right) \qquad (5.5.1)$$

with a maximum distribution of 2ϵ from the mean radius r_m.

If the total number of cavities is assumed to be N_o, then

$$N_O = \int_{r_m-2\epsilon}^{r_m+2\epsilon} ydr = \int_{r_m-2\epsilon}^{r_m+2\epsilon} a \sin\left(\frac{\pi r}{4\epsilon} - \frac{\pi}{4\epsilon}(r_m-2\epsilon)\right) dr \qquad (5.5.2)$$

which can be integrated to give

$$a = \frac{N_o \pi}{8\epsilon} \qquad (5.5.3)$$

To relate the cavity radius to the superheat required for initiation Equation (5.2.8) is used to give

$$dr = \frac{-B}{\Delta T^2} d(\Delta T)$$

and combining Equations (5.2.8) and (5.5.3) with (5.5.1) gives

$$\Delta N = \frac{N_o \pi}{8\epsilon} \sin\left(\frac{\pi r_c}{4\epsilon} - \frac{\pi}{4\epsilon}(r_m-2\epsilon)\right) \times \frac{-B}{\Delta T^2} d(\Delta T) \qquad (5.5.4)$$

If the superheat temperature is increased from T_1, to T_2, then the corresponding increase in the number of active sites will be:

$$N_2 - N_1 = \int_{\Delta T_1}^{\Delta T_2} \frac{\pi N_o}{8\epsilon} \sin\left\{\frac{\pi}{4\epsilon}\frac{B}{\Delta T} - \frac{\pi}{4\epsilon}(rm-2\epsilon)\right\} \times \frac{-B}{\Delta T^2} d(\Delta T)$$

which can be integrated to give

$$N_2-N_1 = \frac{No}{2}\left\{\cos\left(\frac{\pi}{4\epsilon}\frac{B}{\Delta T_2} - \frac{\pi}{4\epsilon}(r_m-2E)\right) - \cos\left(\frac{\pi}{4\epsilon}\frac{B}{\Delta T_1} - \frac{\pi}{4\epsilon}(r_m-2E)\right)\right\} \qquad (5.5.5)$$

Equation (5.5.5) is quite simple and can be directly applied to experimental data, in contrast with that of Grant ([3]). Predicted results from Equation (5.5.5) are compared with the experimental data and discussed in Section (9.3).

An alternative approach using a linear distribution is also proposed in Appendix (A), where a rough estimation of the number of active sites may be obtained.

5.6 Prediction of Weak Nucleate Boiling Heat Flux

Throughout the nucleate boiling literature it is accepted that high heat flux densities may be attributed to bubbles which induce strong local agitations of the liquid near the heating surface. When each bubble leaves the surface a certain amount of enthalpy will be carried away with it and relatively cold liquid will fill its place. This cycle is repeated each $1/f$ sec.

To evaluate the heat flux associated with an individual bubble it is assumed here that superheated liquid, in the form of a portion of the thermal layer characterised by height δ and area πD_x^2 is removed with each bubble. The thermal layer thickness was obtained from Jakob's natural convection Equation:

$$N_{Nu} = 0.16 \ (N_{Gr} \cdot N_{pr})^{\frac{1}{3}} \qquad (5.6.1)$$

since only the region of weak heat flux, i.e. that of isolated bubbles, is corrolated in this approach. The departure bubble diameter is estimated from an equation obtained by Patten (34).

$$R_{max} = \lambda (N_j \delta) \qquad (5.6.2)$$

It may be noticed that this equation is similar to Zuber's Equation (2.4.2) when λ is taken as unity. Hsu and Graham (7) suggested that the radius of bubble influence may be taken as 2 x R_b. This correction factor and other possibilities will be discussed in Section (9.4). From Equations (5.6.1) and (5.6.2) the heat removed may then be expressed as:

$$\Delta Q = \delta (C_p \times \rho) \left(\frac{T_w - T_\infty}{2} \right) \times 4\pi (N_j \delta)^2 \qquad (5.6.3)$$

where ($T_w - T_\infty$) is the temperature superheat across the thermal layer assuming a linear temperature distribution.

For N active sites, each with a frequency of f, the total heat energy removed is given by:

$$Q/A = \delta (C_p \times \rho) \left(\frac{T_w - T_\infty}{2} \right) 4\pi (N_j \delta)^2 \; Nf \qquad (5.6.4)$$

The frequency of bubble emission may be taken as $f = \frac{1}{t_w}$ or $f = \frac{2\alpha}{\delta^2}$ as shown in Section (5.4.2). The number of active sites on a surface with a general distribution of cavities may be obtained from Sections (5.4) or from Appendix (A) where a linear distribution is used.

In either case the number of active sites may be represented in terms of ΔT .

Combining Equations (5.6.4) with (5.5.5) and (5.4.7) gives the equation:

$$Q/A = \delta (C_p \times \rho) \left(\frac{\Delta T}{2} \right) 4\pi (N_j \delta)^2 \frac{No}{2} \left\{ \cos \left(\frac{\pi}{4\epsilon} \frac{B}{\Delta T} - \frac{\pi}{4\epsilon} (r_m - 2\epsilon) \right) - \cos \left(\frac{\pi}{4\epsilon} \frac{B}{\Delta T} - \frac{\pi}{4\epsilon} (r_m - 2\epsilon) \right) \right\} \frac{2\alpha}{\delta^2} \qquad (5.6.5)$$

For areas not affected by bubble formation, it is assumed that the mechanism of heat removed is that of natural convection . When Qnc is included the final equation obtained is of the form:

$$(Q/A)_{ToT} = (Q/A)_{Nc} + Q/A \qquad (5.6.6)$$

Qnc is obtained from Jakob's Equation (5.6.1) for natural convection, not only because it gives good agreement with the data obtained by Jakob but is also omits the effects of surface dimensions. The final equation may then be expressed as

$$(Q/A)_{ToT} = \frac{0.16\ K\Delta T}{d} (N_{Gr}\, N_{Pr})^{\frac{1}{3}} + S(\pi D^2) \left(\frac{\Delta T}{2}\right) \beta_1\, C_p\, \frac{No}{2} \left\{ \cos\left(\frac{\pi}{4\epsilon} \frac{B}{\Delta T} - \frac{\pi}{4\epsilon} (r_m - 2\epsilon) \right) - \cos\left(\frac{\pi}{4\epsilon} \frac{B}{\Delta T} - \frac{\pi}{4\epsilon} (r_m - 2\epsilon) \right) \right\} \frac{2\alpha}{S^2} \qquad (5.6.7)$$

The application of Equation (5.6.7) to experimental data either directly or with some modifications is discussed in Sections (9.4) where it is also compared with results from a correlation suggested by Rohesnow (15) and Zuber (16).

CHAPTER 6

BUBBLE-DETECTING PROBES AND THEIR DEVELOPMENT

6.1 Introduction

A basic characteristic of the nucleate boiling process is f, the frequency with which bubbles are formed and leave a site. Expressions for the frequency have been proposed by many research workers, see Section (2.5). It was defined by Hsu and Graham (7)

$$f = \frac{1}{tw + tg}$$

where t_w is the waiting time, or the time before bubble development begins, and t_g is the time for bubble growth until the bubble departs. Equation (2.5.1) was generalised by Cole (35) to obtain

$$f = \frac{n}{\sum_{i=1}^{n} (t_g + t_w)_i} = \frac{n}{\sum_{i=1}^{n} 1/f_i} \qquad (6.1.1)$$

where n refers to the total of individual bubbles formed at a specific site and f is the frequency at that site. A theoretical prediction of t_w, the waiting time, was proposed by Hsu (22) using the transient conduction equation. In this work an expression for t_w was obtained, see Section (5.4.1), based on the amount of heat energy removed with each departing bubble. Plesset and Zwick (27) obtained an expression for t_g, the growth time, in terms of superheat temperature difference, while Golovin et al (57) obtained an empirical formula for t_g based on their results.

Most of the experimental work done to verify such predictions has used

photographic techniques. While photography is a satisfactory method it is subject to certain limitations, for example, photography at pressures higher than atmospheric may be difficult with some apparatus. Photographing large populations from a plane surface introduces the problems of interference and coalesence between bubbles from different sites, and in addition the cost can be high.

Several detecting methods other than photography were considered. It was suggested that a photoelectric cell placed across the test strip would be suitable, but again this was complicated by interference between, for example, bubbles from sites in the same line. Similarly a pressure transducer, while suitable for single bubbles cannot be used successfully for large populations because of the interaction of pressure waves in the system. A third possibility considered was a sound detector. A metal bar immersed in the system will transmit a longitudinal wave generated on the formation of a bubble. An accelerometer fixed at the other end of the rod will in turn generate a signal which can be counted. Again the problems of noise and interference between waves from large numbers of bubbles make it difficult to obtain good results.

6.2 Frequency Probe

In his work, Lackme (59) referred to the use of a probe for measurement of void fraction in two-phase flow. It was decided to investigate this technique and in the first configuration the probe used, see Fig. (15), was simply a five inch long stainless steel tube of ⅛ in. diameter containing an insulated wire with a constant potential difference maintained between the tube and wire. When a bubble approached, or made contact with the stem of the probe a voltage pulse was generated in the probe circuit which was measured across a resistance, R.

Although no reason for the pulse generation was given in Lackmé's paper, it must be due to a change in impedance of the circuit in the area of the stem of the probe, a sudden alteration of the dielectric characteristic in that area for example could result in a voltage change.

Lackmé obtained his results in an air-water medium and a preliminary experiment was performed to test the probe in water-vapour surroundings.

A circuit of the form shown in Fig. (17) was used with the applied voltage raised to 25 V. Bubbles were generated on the floor of a beaker of water in which the probe was placed and voltage pulses obtained across the resistance were fed simultaneously to an oscilloscope and a counter. Visual counting at very low frequency agreed completely with results obtained from the probe over various periods and in general the method proved very satisfactory.

The system was next tried in the boiler with the probe fixed above a specific site on a test strip. A sample of the signals obtained is shown in Fig. (104). The induced voltage seems to increase sharply with time to reach a peak value. This value may correspond to the maximum displacement of dielectric, i.e. to a bubble position in the centre of the probe. As the bubble leaves this position the value of the voltage starts to decrease probably at the same rate as the increase since at that height the speed of the departing bubble may be assumed to be constant.

The simplicity of the probe and the ease with which it could be manouvered to any required part of the test strip made it a very satisfactory device with which to detect bubble formation and to measure bubble frequency, not only at atmospheric pressure but at those higher and lower. The results obtained in sets of experiments using this method will be discussed in subsequent Chapters.

6.3 Development of the Frequency Probe

Since the probe is assumed to operate by virtue of a sudden impedance change between the tube and the stem maintained at a constant potential difference there is no reason why its configuration should be limited to that of Fig. (15). A circular probe Fig. (16) and one of two parallel strips Fig. (18) were built and tested in distilled deionised water and all were found to be effective.

The circular probe was developed further to provde a system capable of detecting bubbles from any specific section of the test surface - in this case a plane surface in which artificial cavities are formed. At an intermediate stage the system evolved isshown in Fig. (19) where areas 1-10 cover all the required surface. The probe was made from 0.1 in. diameter wires with araldite to insulate the intersections. A selection board connected to the system allowed a potential difference to be maintained between pairs of the terminals a-h, if, for example, readings were required from area 6, terminals c and f would be used. With this arrangement bubble frequencies from specified areas could be determined.

Prediction of the total bubble population per unit area from a test surface is a problem which has proved basic in all analysis of the nucleate boiling heat flux. It follows from the experimental work already described that the capacitor probe could provide a method of determining experimentally the total population per unit time.

The probe developed for this purpose Fig. (18) covered the test area completely and all bubbles leaving the strip passed through it. It was made initially from $\frac{1}{8}$ in. silver plated steel strips with the intersections insulated by araldite. The length of each strip was 2 in. and the distance between them $\frac{1}{8}$ in.

When it was tested in the boiler a large pulse was obtained as a bubble passed between the strips. It was found however that the duration of a signal from a single bubble, i.e. the time taken for the bubble to pass through the detector, was comparatively long, in the range of 15-20 ms., and this increased the likelihood of signals overlapping as bubbles passed through, in time introducing an error in the count rate. To try to reduce this effect the strip thickness was reduced to $^1/_{16}$ in. and the pulses produced with different strip separations of $\frac{1}{8}$ in., $^1/_{16}$ in., and $^1/_{32}$ in. examined. Finally the strips were replaced by fine wire diameter 0.0136 in., with $\frac{1}{8}$ in. separation. This reduced the time constant of the pulse to approximately 5ms. but did not eliminate the error completely.

6.4 Theory for the Frequency Probe

Consider the bubble detecting circuit Fig. (17). Since the resistance of distilled deionized water is extremely high and since all the probe junctions are insulated, the probe itself constitutes an open circuit and can be considered as a capacitor with distilled deionized water as the dielectric medium. As a bubble passes through the probe the dielectric medium is disturbed which results in a change of potential, detected as a pulse across the circuit resistance.

Shalton [59] has shown that a sphere of radius R and dielectric constant ϵ_1, placed in a medium of dielectric constant ϵ_2 and subject to an external field E_0 will induce a field outside itself as if it were a dipole of moment,

$$P = 4\pi\epsilon_2 \frac{(\epsilon_1 - \epsilon_2)}{\epsilon_1 + 2\epsilon_2} R^3 E_0 \qquad (6.4.1)$$

The potential, V, induced by such a dipole at a point distant a_1 from the dipole centre and on a line at an angle Θ_1 to the dipole axis, Kip (60), is from Fig. (21),

$$V = \frac{P' \cos\Theta_1}{4\pi\epsilon_2 a_1^2} \qquad (6.4.2)$$

Consider such a dipole placed between the plates of a capacitor. In order to obtain an estimate of the potential induced across the capacitor consider the dipole to be at the centre of the dielectric medium, Fig. (21).

If 2d is the separation of the capacitor plates then in general

$$\cos\theta_1 = \frac{d}{a_1} \qquad (6.4.3)$$

and V may be expressed as

$$V = \frac{P'}{4\pi\epsilon_2} \frac{\cos\theta_1}{d^2} \cdot \cos^2\theta_1$$

or

$$V = \frac{P' \cos^3\theta_1}{4\pi\epsilon_2 d^2} \qquad (6.4.4)$$

The average potential induced at the capacitor plate can be expressed as I where

$$I = \frac{K_1}{2\alpha} \int_{-\alpha'}^{\alpha'} \cos^3\theta_1 \, d\theta_1 \qquad (6.4.5)$$

and where

$$\alpha' = \sin^{-1}\left(\frac{L}{\sqrt{d^2+L^2}}\right)$$

and

$$K_1 = \frac{P'}{4\pi\epsilon_2 d^2}$$

then

$$I = \frac{K_1}{2\alpha'} \int_{-\alpha'}^{\alpha'} \cos\theta_1 (1 - \sin^2\theta_1)\, d\theta_1$$

This can be integrated to give

$$I = \frac{K_1}{2\alpha'} \left(\sin\theta_1\right)_{-\alpha'}^{\alpha'} - \frac{K_1}{2\alpha'^3} \left(\sin^3\theta_1\right)_{-\alpha'}^{\alpha'}$$

which can be written as

$$I = \frac{P'}{4\pi\epsilon_2 d^2} \sin^{-1}\left(\frac{L}{\sqrt{d^2+L^2}}\right) \left\{ \frac{L}{\sqrt{d^2+L^2}} - \frac{L^3}{3\left(\sqrt{d^2+L^2}\right)^3} \right\} \qquad (6.4.6)$$

Equations (6.4.1) and (6.4.6) can be combined to give an expression for the induced potential difference V between the plates of the form

$$V = 2I$$

$$\text{or } V = \frac{2E_0(\epsilon_1 - \epsilon_2)}{\epsilon_1 + 2\epsilon_2} \quad \frac{R^3}{\sin^{-1}\left(\frac{L}{\sqrt{d^2+L^2}}\right)} \left\{ \frac{L}{\sqrt{d^2+L^2}} - \frac{L^3}{3\left(\sqrt{d^2+L^2}\right)^3} \right\} \qquad (6.4.7)$$

Since ϵ_1, ϵ_2, L, d and E_0 are constant for a given configuration the potential difference produced is proportional to the cube of the bubble radius i.e. proportional to the bubble volume.

An estimate of the potential difference which could result from a bubble of a certain size can be obtained from Equation (6.4.7) and a sample calculation is given below

V = 30 volts $\alpha' = \pi/2$

d = 0.15 in R = 0.05 in L = 1 in

Then $V = \frac{2 \times 30}{0.15} \left(\frac{1.60}{1+120} \right) \frac{1}{\pi/2} (4/3)(0.05)^3$

$= 23.8$ mV.

The value of bubble radius used is approximately the same as the average bubble departure radius obtained from photographing test surfaces.

In order to compare this prediction with results obtained experimentally the detecting system Fig. (15) must be calibrated. In the system a pulse from the probe circuit is amplified and in some cases passed through a differentiating circuit before it reaches the counter and oscilloscope. To enable the calibration to be made a Farnell pulse generator type L.F.M. was used to apply pulses of a recorded voltage to the system. The resulting pulses were measured using a storage oscilloscope and the calibration made. A low heat flux was used to generate single bubbles from a test strip which were detected by the probe system. The resulting pulses were photographed using a storage oscilloscope and U.V. recorder. The average pulse height was found to correspond with an imput voltage of 22 mV which shows agreement with the theoretically predicted value within the experimental error of 10%.

6.5 Correction to the Total Frequency Measurement

The counter used in the detecting system records individual voltage pulses only. When two bubbles pass through the probe simultaneously or when two pulses overlap the counting rate recorded is not the true one. The probability of this occuring increases as the heat flux rises. See Fig. (106).

An electric differentiating circuit was designed to sharpen the voltage pulses from the probe and a more realistic counting rate was obtained when this was used. The effect of the circuit is represented diagramatically in Fig. (23) and its design is shown in Fig. (22).

It was suggested that this problem was analogous to that of finding the true counting rate in γ ray detection when there is a possibility of more than one γ entering the counter at one time. An example of the effect is given by Hole (61). Fig. (20) shows events A,B,C,D,E occuring naturally at times t_1, t_2, t_3, t_4, and t_5. If the duration of each event is τ then only A, C and D can be detected. τ is the time when the counter is ineffective and is known as the counter dead time. If n_o is the true rate of occurrence of events and n the measured rate, then

$$\frac{n}{n_o} = \frac{1}{1 + n_o \tau} \qquad (6.5.1)$$

which gives the true counting rate as

$$n_o = \frac{n}{1 + n\tau}$$

In order to enable this correction to be applied the time τ was

determined by photographing pulses from a storage oscilloscope. The results will be discussed in subsequent Chapters.

6.6 Bubble Sizing Using Frequency Probe

It has been shown that the magnitude of the pulse generated when a bubble passes through the probe is dependent on the bubble volume. This suggests the possibility of developing a technique for determining the size of a bubble from the voltage pulse it produces if a calibration can be made. This was tested by generating bubbles of a constant size from a nozzle, photographing the bubbles to find their diameter and recording the pulse height from the bubbles on a U.V. recorder. The procedure was repeated for several different nozzles. The experiments are described and discussed in Chapter (8).

6.7 Bubble Velocity Using Frequency Probe

The time t which it takes for a bubble to pass through the probe is related to the length of the probe l , the diameter of the bubble D and its velocity by the equation:

$$U_t = \frac{l + D}{t}$$

For one probe l is a constant and the bubble diameter can be determined from the pulse so that measuring the pulse duration allows the bubble velocity to be determined. This method is straightforward when applied to a probe of the form shown in Fig. (15) but the field associated with the probes shown in Fig. (16) is fringed so that detection of a bubble will start before the bubble has actually reached the probe. An experimental constant may be introduced to account for this. Further discussion is given in Chapter (8).

6.8 Conclusion

The simplicity of this detecting system gives it a great advantage over more complicated procedures. The probe itself can be produced quite easily and quickly and the auxiliary equipment of oscilloscope and counter is readily available. Amplification is needed only when the total frequency of a bubble population is to be measured and even in this case it may be no more than 10 times. Signals can be photographed or recorded on a U.V. recorder and statistical measurements of pulse height and duration can be made.

The mobility of the system is unique as the probe can be easily moved to study any cavity on the test surface at atmospheric pressure and pressures higher and lower. The total frequency probe, Fig. (18), need not be moved if it is located to cover the test surface as the voltage can be applied separately to any section.

Another advantage of the system is that several factors can be determined from one set of recordings. As the bubble is detected its diameter can be determined from the magnitude of the pulse and its velocity from the signal duration. The cost of the system is small compared to photographic techniques and has the additional advantage of providing the desired information almost immediately.

CHAPTER 7

DISCUSSION OF BUBBLE EMISSION FREQUENCY

7.1 Frequency of Departing Bubbles

The development of the bubble detecting capacitor probe Fig. (16) made it possible to study the frequency of bubble emission and the factors, such as heat flux, cavity size and pressure, which could possibly affect it. The aim was to study first an individual cavity and then to go a step further and study the total frequency from a general surface.

7.2 Frequency of Bubble Emission from a Single Cavity

7.2-1 Frequency Variation with Applied Heat Flux

Individual cavities of size ranging from 0.0092 in. to 0.0168 in. on different test surfaces were studied with the applied heat flux varying from 0.to 30,000 Btu/ft^{2}hr. When the system was at equilibrium at a certain applied heat flux, the frequency was recorded over a period of a minute, in some cases as many as eleven times.

Figs. (24), (25), (26), (27), (28) show the results obtained at atmospheric pressure and at saturation temperature conditions. The theoretical predictions of frequency from Equation (5.4.15), using the experimental values of superheat temperature difference, ΔT_{sup} , and heat flux Q/A , are also plotted on the above figures.

It can be seen that the general trend of the theoretical curve is similar to that of the experimental one but that there is a difference in the absolute values of frequency, especially at heat fluxes above 10,000 Btu/ft^{2}hr. Fig. (28) is an exception and shows excellent agreement with Equation (5.4.15) when the growth time obtained from Plesset and Zwick's Equation (2.4.12) is incorporated in the expression for frequency

The discrepancy at high heat flux may be explained by the choice of the value of the area constant $\frac{\pi D_X^2}{A} = 1$ in obtaining Equation (5.4.7), See Chapter (5), an assumption in line with the simple approach used in the analysis. If for example the area ratio value was chosen as 0.75 the predicted curve would be in better agreement with experimental results.

It can also be seen from the Figures that, for low heat fluxes, up to 6,000 Btu/ft^{2}hr. the predicted frequency is larger than the experimental value. This may be attributed to the fact that the frequency at atmospheric pressure, was taken as $1/tw^*$, a definition based on the conclusions of Hsu and Graham (7) and on theoretical calculations of Plesset and Zwick (27) and Zuber (1) as well as an empirical relation of Golovin et al (57). The Table on the subsequent page (7.2.1) shows t_g to be much smaller than t_w.

* Some doubt has been cast on the certainty of this assertion as a result of reference to the work of Siegel and Keshock (71) and Hatton, Jones and Liew (62).

Heat Flux Q/A Btu/ft^{2}hr.	Waiting Time Equa (5.4.7) tw sec	Growth Time Plesset and Zwick Equa. (2.4,12) sec	Growth Time (tg) Golovin et al Equa. (57) sec	Growth Time (tg) Zuber's Equa. (2.34) sec	Ratio of tg/tw	Test Surface	Pressure psi.
2000	0.30	0.0383	0.0225	See Fig. (11) where computed results are plotted.	0.127	D	14.6
5000	0.178	0.00825	0.0117		0.0469	D	14.6
10000	0.0775	0.00482	0.0085		0.0622	D	14.6
15000	0.0425	0.00385	0.00805		0.0908	D	14.6
20000	0.0271	0.00340	0.00759		0.1255	D	14.6
25000	0.0189	0.00304	0.00725		0.160	D	14.6

Table (7.2.1)

The general definition of frequency, $f = \frac{1}{t_g + t_w}$, may be written in the form, $f = \frac{1}{t_w\left(1 + \frac{t_g}{t_w}\right)}$.

It can be seen from the table that the ratio t_g/t_w, decreases, from a value of 0.1265 at 2,000 Btu/ft^{2}hr, as the flux increases then increases again as the flux increases further.

The inclusion of t_g will reduce the frequency and give closer agreement with the experimental results at low heat flux but increase the discrepancy at higher fluxes.

Hsu's Equation (5.4.11) was also applied firstly using the superheat temperature difference required for initiation and was found to give a curve with a trend different from that of the experimental data Figs.(24),(25),(26)(27) When, however, the superheat temperature difference corresponding to each heat flux was substituted in Equation (5.4.11) a trend similar to that of experimental results was obtained although the absolute values were much smaller. Ivey's Equation (5.4.16) seems to predict much higher frequency values, they are, in actual fact, four times greater than those of Equation (5.4.15).

To explain the trend of the curve, the possible limits of t_w and t_g must b e considered. If t_g is obtained from Plesset and Zwick's Equation (2.4.12) it can be seen that for an increase in applied heat flux the superheat temperature difference will increase and hence t_g will decrease until a stage will be reached, depending on the condition of the test surface where ΔT_{sup} will be independent of Q, and if it is assumed that bubble departure diameter remains constant then from Equation (2.4.12) t_g is also constant.

When Equation (5.4.7) is considered it can be seen that t_w decreases as Q/A

increases, but the term $\frac{K\Delta T}{Q/A}$ represents δ the thermal layer thickness, see Chapter (5), and a stage will be reached when this tends to a constant. This may sound contrary to the procedure used in the calculation of δ, but it may be pointed out that the calculations were done for the weak nucleate boiling region i.e. for low heat flux. It may be then concluded that if δ and t_w tend to constant values then f itself tends to a constant value which is shown in Figs. (24),(25),(26) and (27).

The value of the constant depends, of course, on the liquid properties and surface conditions and it is therefore possible that it will be different for each surface. It is also possible that at such high heat flux the bubble interacts and frequently coalesces with its predecessor, this region is referred to as the region of bubble interference, Zuber (63), when this stage is reached the above definition of frequency is not applicable.

7.2 - 2 Frequency Variation with Cavity Radius

The frequency variation with cavity radius was studied at two fixed values of heat flux, 7,000 Btu/ft^{2}hr. and 10,000 Btu/ft^{2}hr, for cavity radii ranged between 0.0024 in. and 0.017 in. on different test surfaces. The frequency was recorded for one minute at each site and the recording repeated many times to check the reproducibility of results. The experimental data obtained is plotted in Figs. (32) and (33).

It was shown in Section (7.2.1) that the frequency may be taken as the reciprocal of waiting time, t_w, whose value may be obtained from either Equation (47) or Hsu's Equation (5.4.11). At a constant applied heat flux, the superheat temperature difference, ΔT_{sup}, and hence the frequency, f, will be constant. The effect of cavity radius enters into this consideration in that the heat

flux-temperature difference relation, at a constant pressure and under saturated conditions, is dependent on the surface condition of the test strip so that for different surfaces different values of the ratio $\frac{\Delta T}{Q/A}$ and hence of f are obtained from the above equations. Results from Equations (5.4.15) and (5.4.11) are plotted in Fig. (32) and are in fairly good agreement with experimental values.

The direct influence of cavity size can be seen from Han & Griffith's Equation (App B). The calculated value of frequency, f, from this equation using a fixed heat flux of 7,000 Btu/ft^{2}hr. is also shown in Fig. (32). It can be seen that the waiting time increases with cavity size, which to some extent is evident from the experimental results. The explanation for this is that as a bubble departs from a large cavity a larger amount of relatively cold water will rush to the surface than for a smaller cavity and hence a longer time is required to attain the superheat temperature difference required for initiation.

Hatton and Hall (23) adopted an alternative approach and defined the frequency as the reciprocal of the growth time t_g, for pressures at atmospheric and below. They used Plesset and Zwick's Equation (5.4.12) coupled with Equation (2.2.4) to obtain the expression for the frequency,

$$f = \frac{3}{\pi\alpha}\left(\frac{45\,K\,T_{sat}}{(h_{fg}\rho_v)^2\,R_c}\right)^2$$

This clearly demonstrates that f is inversely proportional to the square of cavity diameter and is plotted in Fig. (33). The results obtained by Hatton

and Hall for small cavity radii are in good agreement with those obtained in this work, Fig. (33).

Hatton and Hall proposed a model in which, contrary to that of Han and Griffith, a smaller cavity requires a greater superheat temperature to initiate and a correspondingly larger waiting time to re-establish the thermal layer. In support of Han and Griffith's proposals it may be noted that

(i) The initiation theories of Hsu, Equation (2.2.6) and Han and Griffith (2.2.5) seem to predict the same superheat temperature, independent of the thermal layer thickness for small cavity radii, up to 0.001 in.

(ii) When the subcooling effect is considered only larger cavities of radii above 0.001 in. are affected which substantiates the suggestion that cold liquid rushing to the surface affects these cavities and increases the waiting time. More recently Hatton and Liew (62) modified the above approach by introducing the effect of δ and reached the same conclusions as Han and Griffith (9).

In general we may conclude that the waiting time increases but rather gradually, with the increase of cavity size.

7.2. - 3 Frequency Variation with Pressure

Pressure effects on frequency were studied by recording frequency variation with heat flux at a particular site for fluxes up to 30,000 Btu/ft^{2}hr. and for pressures of 14.8, 29.8, 44.8 and 59.8 psi. Figs. (28, 29, 30 and 31) show the experimental results obtained. Predictions of waiting time, t_w, from Equation (5.4.7) and of growth time, t_g, from either Plesset and Zwick's Equation (5.4.12) or that of Golovin et al (57), indicate that t_w decreases as the pressure increases whereas t_g increases with pressure. For a constant heat flux and cavity radius of 0.02805in t_w is 0.144 sec. at atmospheric pressure and 0.0496 sec.

at 60 psi. while t_g is 0.0328 sec. at atmospheric pressure and 0.343 sec. at 60 psi. The frequency was accordingly defined as

$$f = \frac{1}{tg + tw}$$

The net variation of frequency with heat flux at different pressures is shown in Figs.(28, 29, 30 and 31) and it may be concluded from the theoretical approach and from the experimental results that the change in the frequency is not significant.

The agreement of theoretical values of frequency, f, with experimental results is excellent for values of applied heat flux up to 20,000 Btu/ft^{2}hr at which divergence occurs and the experimental data tends to a limit (see above figures). This effect seems to occur at a lower value of heat flux as the pressure increases, for example at 60 psi. this effect begins at a heat flux of 16,000 Btu/ft^{2}hr. while at atmospheric pressure it is not apparent until the heat flux is 19,000 Btu/ft^{2}hr. This provides further support for the suggestion forwarded in Section (7.2), that a stage will be reached where the superheat temperature difference becomes independent of the applied heat flux. This occurs at a lower heat flux as the pressure increases, Fig. (31).

7.3 The Frequency From a General Surface with a Large Number of Active Sites

So far, the behaviour of the frequency at an individual cavity has been examined, Section (7.2). The factors which may affect the frequency from a surface with a large number of sites and how far properties can be generalized from those found in the single cavity study, will be investigated in this section.

Three surfaces NG1, NG2 and NG3 each containing approximately 120 cavities see Section (4.2.3) were studied. Experiments were performed with pressures up to 75 psi. and heat fluxes up to 35,000 Btu/ft^{2}hr. and were repeated at separate times to check their reproducibility.

7.3.– 1 Variation of Total Frequency with Heat Flux

Figs. (34), (35) and (36) show the experimental results obtained for variation of frequency with applied heat flux as the latter was increased to 35,000 Btu/ft^{2}hr. at atmospheric pressure. It may be noted initially that the reproducibility of the results is quite good and within the scatter of a single experiment.

The capacitor probe used in measuring the total frequency, f_{tot} , required a correction for dead time i.e. the time interval when the probe is detecting one bubble and is therefore insensitive to others, Chapter (6). The correction was evaluated from the signal obtained from individual bubbles detected by probe Fig. (15). Fig. (104) shows a typical pulse. Signals were obtained on a storage oscilloscope and subsequently photographed. The average value of f from both sources was estimated to be 0.005 sec. This value was used in the correction of total frequency and all values referred to are corrected values, Tables (2a),(2b) and (2c) * . Further discussion of the dead time will take place later in this section.

The general trend of Figs. (34), (35) and (36) is that the total frequency increases sharply for heat fluxes up to approximately 10,000 Btu/ft^{2}hr. and then tends to a constant value for fluxes from 10,000 Btu/ft^{2}hr. to 25,000 Btu/ft^{2}hr. When the heat flux was increased further f_{tot} was found to decline. The general trend is similar to that found by Kirby and Westwater (68)

* The total frequency values plotted in Figures (34,35,36,38,39,40,41) are not corrected. This, however, does not affect the shape of the curve on the application of the above discussion and comment.

Fig. (37).

The following qualitative explanation for the trend is offered. At low heat flux only a certain number of sites is active, for example, surface (NG3) at a flux of 5,000 Btu/ft^{2}hr. has approximately 17 active sites. As the heat flux increases up to approximately 15,000 Btu/ft^{2}hr. the number of active sites increases to about 46 and probably the frequency from sites already active increases so that the total frequency tends towards the peak value. A further increase in the applied heat flux does not seem to produce any further increase in the total frequency, although the number of active sites keeps increasing, Fig. (55), which of course indicates a reduction in the frequency at a particular site. This may be explained by the fact that at high heat flux, bubbles which initiate independently on the surface begin to coalesce as they grow. The idea of coalescence is substantiated by photographs of surfaces (NG1 and NG3) Figs.(78 to 93) at different fluxes (2,660 to 26,550 Btu/ft^{2}hr.) and at atmospheric pressure. It was found that at a flux of approximately 15,000 Btu/ft^{2}hr. the bubbles on both surfaces appear to be coalescing, and that for higher values of heat flux the extent of the coalescence seems to increase and a reduction in the frequency follows. This is the type of interaction referred to by Zuber (53) as horizontal interaction as opposed to vertical interaction which usually occurs at a higher heat flux when bubbles from the same site interact.

It can also be seen from Table 7.3.1 that the average individual site frequency $f = \frac{f_{tot}}{N}$ for this type of surface is smaller than that obtained for an individual site at all fluxes considered, even at low heat fluxes (0-10,000 Btu/ft^{2}hr) where the problem of interaction does not arise.

It is also much smaller than the theoretical prediction of Equation (5.4.15) and of Hsu's Equation (5.4.11). Table (7.3.1) below for surface (NG3) demonstrates the above point clearly.

Heat Flux Q/A Btu/ft^{2}hr	Exp. Frequency sec^{-1}	Frequency from Equa. (5.4.15) sec^{-1}	Frequency from Equa. (5.4.11) sec^{-1}	Exp. Frequency indivdual Cavity sec^{-1}	Test Surface	Press. psi.
5000	2.5	8.64	5.54	2.9	NG3	14.6
10000	2.05	13.9	8.80	10	NG3	14.6
15000	1.57	19.5	12.5	21	NG3	14.6
20000	1.2	25.5	16.35	25.5	NG3	14.6
25000	1.11	33.9	21.7	26.8	NG3	14.6

Table (7.3.1)

The following proposals for the difference are forwarded.

The total frequency, f_{tot} is evaluated as the product of number of active sites and the frequency of an individual cavity obtained from Equation (5.4.15), although this equation predicted a lower frequency than the experimental value at high heat flux for all cavities considered. This value of f_{tot} substituted in Equation (5.6.7) predicted a heat flux greater than the actual heat flux applied, See Table (7.3.2) below.

Table 7.3.2

Test Surface	Applied Heat flux Q/A Btu/ft^{2}hr.	Heat flux Predicted from Equ. (5.6.7) using f_{tot} from Equ (5.4.15)
NG1	15000	30500
NG2	21000	22500
NG3	13500	20500

The above heat flux values are obviously not in agreement and since the number of active sites was visually observed to remain almost constant there must be a reduction in the frequency of an individual site which implies an increase in t_w, t_g or both. As isolated bubbles leave the surface a source and wake flow which increases liquid circulation may occur, Zuber (63). According to Jakob hot liquid will rise and cold will rush to the surface, an idea substantiated by Gaertner (13) using a shadowgraph technique. The circulation will be larger for a greater number of active sites and provide a more efficient

mechanism for the removal of heat from the surface so that a reduction in surface temperature and hence a drop in frequency will occur until an equilibrium stage is reached.

It was mentioned earlier that the dead time correction for the frequency was evaluated as 0.005 sec., a value based on measurements of the pulses of individual bubbles. At higher heat fluxes, however, a larger number of bubbles are being detected and two things may occur. Firstly bubbles may coalesce on the surface and the resulting larger bubbles which are detected will be associated with a larger value of $\mathcal{F}$, Fig. (105), or alternatively two or more consecutive bubbles may pass through the probe almost simultaneously and again produce a larger value of $\mathcal{F}$, Fig. (106) so that one single bubble is detected. If the value of $\mathcal{F}$ is increased, then a larger correction is necessary and consequently a higher corrected frequency is obtained.

7.3 - 2 Frequency Variation with Pressure

Figs.(36,38,39,40,41) show the total frequency versus heat flux curves for surface NG3 at pressures of 15, 30, 45, 60 and 75 psi. Each experiment was repeated once and results obtained for increasing and decreasing heat flux. The reproducibility of the results seems to be excellent and within the experimental scatter. The dead time correction to the frequency was taken as 0.005 sec.

It can be seen that the variation of frequency with pressure is not significant which agrees with results already presented for a single cavity, Section (7.2.3). Certain trends are observed which are contrary to the results at atmospheric pressure, for example, in the flux region 25,000 - 35,000 Btu/ft^{2}hr. the frequency at higher pressure does not decline, but increases as is seen

clearly in Fig. (40) and (41). This may be attributed to the fact that the bubble size is reduced as pressure increases, Semeria (32) and more single bubbles leave the surface. It is also noticeable that the net frequency reaches a maximum value at a lower heat flux as the pressure increases. This is due to the fact that the initiation superheat temperature difference is much less at higher pressures, Section (9.2), and hence there is earlier initiation from a larger number of active sites.

Again in general the frequency is smaller than that from individual cavities and the suggestions forwarded in Section (7.3.1) may also be applicable here.

7.3.-3 Variation of Total Frequency with Average Cavity Size

The average cavity size of test surfaces used here, 0.00176 in. to 0.0038 in. did not provide a particularly good representative range. It was found however, that the variation of frequency with cavity size at all heat fluxes considered was not significant, for example:

Heat flux Btu/ft^{2}hr	Frequency = $\frac{f_{tot}}{N}$ sec^{-1}	Average Cavity radius in.
10000	3.3	0.00176
10000	2.02	0.002805
10000	2.0	0.0378

This, to a certain extent, is in agreement with findings for the frequency variation with cavity radius at constant heat flux and at atmospheric pressure,

Section (7.3.3).

The gradual decrease of frequency with the increase of cavity radius substantiates to a certain extent the prediction of Han and Griffith Equation (App. B).

CHAPTER 8

APPLICATION OF THE FREQUENCY PROBE TO BUBBLE SIZE - VELOCITY DETERMINATION

8.1 Introduction

The volume of a bubble leaving the heating surface is a factor included in the majority of heat flux correlations since it is a measure of the energy which is removed from the surface, namely the latent heat and energy associated with the thermal layer.

It was found that the shape of the departing bubble could be of different forms, Yamagata et al ([14]), Johnson et al ([64]). The effects of cavity size, pressure and heat flux were also investigated using photographic techniques, Semeria ([32]), Cole ([36]), Patten ([34]), Han and Griffith ([9]), Hsu and Graham ([7]).

At the present time, so far as the author is aware photography is the sole technique used to size a bubble. In this Chapter we propose to describe a new method in ascertaining the bubble size employing the capacitor probe detector and to discuss experiments performed, the results and future developments. The use of the method in the determination of the rise velocity of a bubble is also discussed.

8.2 The Calibration of the Capacitor Probe

It was seen in Chapter (6) that the height of pulse generated by the probe is dependent on the bubble size. To obtain bubbles of different sizes, steam, from an evaporator, was fed to a set of surgical needles, with radii varying from 0.018 in. to 0.050 in. placed in a specially adapted beaker of distilled water. The energy input to the evaporator was kept constant and a receiver,

Fig. (42), in the form of an aluminium box with dimensions 1' x 1' x ½' acted as a steam reservoir and damped small pressure variations. A valve controlled the steam flow so that individual bubbles at a low frequency were obtained. A bunsen burner was used to supply a small amount of heat to the beaker base to maintain the water temperature at saturation value. The temperature was measured on an ordinary mercury thermometer.

The steam flow was started and the system left for ten minutes to reach equilibrium. An Exacta camera, using HP4 film and fitted with a telephoto lens plus two extensions rings, was used to photograph the bubble leaving the needle, Fig. (102), and simultaneously the probe signals were recorded on the U.V. recorder. A sample recording is shown in Fig. (103). The procedure was repeated for each of seven needles of varying radius.

A stroboscope was used with the above arrangement to give a velocity calibration of the probe. Since the stroboscope frequency is known, the absolute velocity, U_t , can be found from the distance between the positions of adjacent images on the photograph.

If the probe length is ℓ , the bubble diameter D and the duration of the signal t then

$$U_t = \frac{\ell + D}{t} \qquad (8.2.1)$$

t, can be obtained from the time base of the U.V. record of the signal.

The procedure, however, was not successful because of the difficulty encountered in obtaining suitable photographs, and an alternative arrangement was devised to demonstrate that the signal width is proportional to the probe

length, i.e. to the time taken by the bubble to travel along the probe stem and thus to the bubble velocity.

In the experimental arrangement of Fig. (42) the probe stem was shortened in successive stages and at each stage a U.V. recording was obtained. The same needle was used throughout this part of the experiment.

8.3 Discussion

The average height, H, of up to one hundred signals from the U.V. recording for each needle was evaluated with an accuracy of 0.005 in. giving a possible error of approximately 10%. The corresponding bubble size was determined from the photograph, measuring the diameters of eight bubbles to an average accuracy of 5% using a specially adapted microscope. Fig. (43) shows a plot of the relation D^3 versus H drawn using the least squares method. It must be mentioned here that for bubbles which are not spherical the horizontal diameter was used rather than the average of two perpendicular diameters. This is justified by considering that the probe signal depends on the volume change in dielectric materials and from Fig. (102) it can be seen that the horizontal dimension is the controlling factor in that respect. The calibration can be used to determine bubble size from the signal height if it is assumed that the bubbles are spherical. It can be seen that there is an amount of scatter in the results which is thought to be mainly due to the fact that the bubbles appear to grow non-uniformly after leaving the needle. A cine photograph or photographs of a larger number of bubbles would be needed to give an exact calibration. The spiralling movement of the bubbles also affects the results since a bubble may only partially contact the probe and give rise to a reduced size signal. This effect would be eliminated by using a probe of

Fig. (16b), which was developed later, where the bubble passes through the probe and gives a true signal.

To estimate bubble size using the calibrated capacitor probe a U.V. recording was made of a signal from a specific site on a test surface at saturation temperature condition and atmospheric pressure and the average height of the signal was evaluated. The corresponding bubble volume was obtained from Fig. (43) and when compared with experimental values obtained from previously taken photographs agreed to within 10%.

The stroboscope technique was not successful in obtaining bubble velocity since difficulties were encountered with the lighting and limitations were imposed by the equipment available. However, Fig. (44) of probe length versus signal width demonstrates quite clearly that there exists a linear relationship between these two quantities. This may be considered in greater detail using the equation

$$U_t = \frac{\ell + D}{t}$$

It may be assumed that the velocity of all bubbles leaving the surgical needle is constant, since the system is kept at the same temperature and pressure. This implies that a change in ℓ, the probe length, produces a corresponding change in t. Fig. (44) represents this relation as ℓ is varied and the corresponding t is obtained from the U.V. recording. For a fixed value of ℓ, U_t can be obtained from the above expression using the values of D and t from the signal. The scatter in the results is thought to be due to the fact that, for a long stem in particular, some of the bubbles move away from the probe after the initial contact. It is recommended that in practice

the probe stem be short to avoid possible error. Again a probe of Fig.(16) well positioned above the test site will minimize this error.

8.4 Conclusion

A record from a calibrated probe allows the bubble diameter and possibly velocity to be obtained directly and gives the average of these quantities to a reasonable degree of accuracy if a large number of signals are obtained. It was seen in Section (8.3) that the bubble size could be predicted to within 10%.

The probe might be used to give information about boiling from surfaces, such as those in high pressure vessels, which would be otherwise inaccessible. In preliminary experimental work bubbles from a general surface were detected at a pressure of 350 psi. However accurate experimental data was obtained only up to pressures of 75 psi.

Unfortunately the probe must be recalibrated for use with different liquids although an approximate value for the bubble size can be obtained using the theoretical equation presented in Chapter (6), with the appropriate dielectric constant.

The probe has a possible medical application in the detection of very small oxygen bubbles present in the blood flow through a heart-lung machine. If such bubbles remain in the flow they may cause brain damage to the patient. They are at present detected by a microwave system which is complex and apace consuming in relation to a simple detecting system employing the probe, Fig. (16).

Much experimental investigation would of course be necessary to thoroughly test the method.

CHAPTER 9

DISCUSSION OF THE RESULTS

9.1 Bubble Initiation

The phenomenum of bubble initiation is controlled by a large number of factors including liquid properties, cavity size, superheat temperature difference, thermal layer thickness, pressure, the effect of neighbouring bubbles, surface material and dissolved gases and solids.

The initial selection of strips with single cavities widely spaced on the surface was made to eliminate the effects of neighbouring bubbles. Distilled deionized water was taken from a constant source and the same procedure of degassing was adopted to eliminate possible effects of dissolved gases or any impurities so that the effects of cavity radius, pressure and initiation superheat could be studied in a controlled environment and free from such variables. The knowledge gained from the study of a simple cavity arrangement was then applied to a surface with a large number of cavities.

Before there is further discussion, incipience of boiling must be defined. In the present study incipience point is taken as the superheat temperature difference required for the bubble nucleus to start growing so that the bubble is just about to leave the surface. This definition meets the requirements raised by Howell and Siegel (24), that the bubble can sit on the surface without leaving since, as the bubble grows, a stage must be reached when the buoyancy force becomes the controlling factor in bubble departure.

9.1 – 1 Initiation from an Individual Site

Eight test surfaces were prepared and an average of ten cavities as widely spaced as possible formed in a straight line down the centre of each strip.

A large cavity size range, from 0.0002 in. to 0.025 in. was produced, with some cavities of the same size on different test surfaces to check the reproducibility of the results.

Figs. (45) and (46) show the initiation superheat temperature difference as a function of cavity mouth radius for the above eight test surfaces. The incipience was observed visually for each cavity and the corresponding superheat temperature difference and heat flux recorded. Equation (5.2.8), giving the initiation superheat for a certain radius, was applied to each test surface at atmospheric pressure and predicted values plotted. Although great care was taken in every aspect of the experimental work, for example in cleaning the apparatus, and taking steps to prevent corrosion, degassing the liquid, calibrating the thermocouples and in measurement of power, it can be seen that there is scatter in the results. The scatter increases with cavity radius and seems to be greater for cavities in the region 0.002 in. to 0.02 in. while in the lower region 0.0002 in. to 0.002 in. the scatter is less obvious.

In general it seems that the experimental superheat temperature difference ΔT_{int}, is much larger than that predicted by Equation (5.2.8), When, however, Howell and Siegel's Equation (2.2.8) was plotted with thermal layer thickness equal to 0.001 in. better agreement was obtained, Figs. (45) and (46).

The scatter in the results at larger cavity radii is so great that those theoretical equations such as Han and Griffith's (9) and Hsu's (22) see Chapter (2), which predict a limit to the active cavity size depending on the thermal layer thickness, must be examined. Fig. (46) shows plots of Han and

Griffith ( ) Equation (2.2.5) with δ taken as 0.01 in. 0.02 in. 0.03 in. and 0.003 in. Consideration of results shows that even with a fairly large thermal layer thickness of 0.03 in. when it is predicted that no cavity with radius greater than 0.0195 in. will be active, certain cavities with the largest radius studied, 0.025 in. do initiate. This value of thermal layer thickness is ten times greater than the value chosen by Hsu (22) and five times greater than that of Howell and Seigel but approximately the same as that of Marcus and Dropken (65). When a value of δ = 0.035 in. which is the value assumed in predicting the heat flux from Equation (5.6.7), was substituted in Han and Griffith equation (2.2.5) it predicted a size limit to the active sites of 0.0235 in. Again larger size cavities were found to be active.

In attempting to explain the discrepancy in the results the following suggestions are proposed:

(i) It is possible that within an artificial cavity there exists a smaller cavity which may initiate and, which because of its size, requires a larger superheat than the mother cavity. Before this suggestion is examined in greater detail it may be remembered that when Equation (5.2.8) was obtained it was assumed that θ , the cavity cone angle, was equal to twice the liquid-solid contact angle β . The validity of this assumption cannot be investigated practically because of the difficulty in measuring θ , and this may be a possible source of error. However, since the scatter of the results increases with cavity radius additional factors must be considered. This raises the possibility of a small cavity existing within a larger one. To find practical evidence for this proposal the test surfaces used in this study, expecially surfaces (C), (D)

and (F) which have large cavity sizes, were examined under a travelling microscope with magnification X150 where small cavities or grooves within cavities were seen. A very fine film of an orange-coloured deposit was observed in the vicinity of these small cavities, within the larger ones, a type of film also observed on small active, artificial, cavities after a prolonged period of boiling.

The investigation was taken a step further by selecting from Fig. (46) three cavities on three different test surfaces which showed obvious discrepancy and studying them under a powerful Stereoscon electron microscope, Figs. (94 to 99) show the cavity walls taken under different magnification. It can be seen clearly that there are sub-cavities or scratches in the walls. What is perhaps more noticeable is the existence of dust in the cavities, which because of electron charges is seen as white on the photographs, which may act as potential nucleation sites. Attempts to clear the cavity using compressed air were not successful. Only sub-cavities or scratches on the bottom of a cavity can be measured directly, for those on the cavity sides only a projection can be obtained which could give rise to misleading data. In Fig. (95) a possible longitudinal cavity or scratch approximately one tenth of the size of the mother cavity can be seen. It is possible that this sub-cavity initiates in which case the discrepancy would be reduced by a factor of ten. When the points on Fig. (46) representing the remainder of cavities found to contain smaller cavities were referred to they were found to have the largest amount of scatter. To explain the existence of these sub-cavities the cavity production methods must be examined. The larger cavities were produced with either a fine drill

or a sharp needle, neither of which was perfectly smooth, so that imperfections of the inner cavity surface are possible.

(ii) The critical bubble radius used in the application of Equation (5.2.8) is that of the cavity mouth, it is feasible however that some of the cavities, particularly the larger ones, will be partially filled with liquid and a smaller effective cavity radius may be relevant. The superheat required for initiation will thus be greater than expected and would give rise to scatter in the results.

Experimental tests were carried out to investigate the proposition that water may pattially fill a cavity for the test surfaces used. The strip was covered with distilled deionized water and the liquid drained slowly away until the surface was exposed to the air. Any excess water was blown off smoothly and the surface observed under a microscope. It was found that water existed in most cavities observed even for radii as low as 0.005 in. To check the observation a surgical needle was dipped in ink and the needle tip placed at the cavity mouth while the strip was under observation. The ink was seen to diffuse inside the cavity which indicates the presence of water there. It was not possible to assess here how far the water penetrated. Wei and Preckshot (66), using a glass capillary tube of radius 0.02 in. demonstrated that a residual pocket of vapour remains in the cavity after a bubble has departed. Kosky (67) used the same arrangement and found that the liquid penetrated the cavity to various depths. It was suggested that this penetration may be related to condensation on the incoming relatively cold liquid in the wake of the departing bubble, an effect which would be intensified in the case of a sub-cooled liquid, and also to other factors such as the effect of pressure waves generated by departing or collapsing bubbles. The fact that liquid is able to

penetrate the cavity makes the suggestion that a radius different to that of the cavity mouth be used in Equation (2.5.8), more viable.

9.1 - 2 Initiation from surfaces with a large number of active sites

Seven test surfaces each containing an average of 120 cavities were used in this part of the study. Most of the experimental work was concentrated on three of the surfaces and each experiment was repeated at three different times to check the reproducibility of results.

Fig. (47) shows a plot of the average cavity radius against superheat temperature difference ΔT_{int} . Incipience was recorded when approximately ten sites were active, this was because in most cases approximately ten sites initiated simultaneously, although in some cases the number was greater than this since each test surface was designed to have several cavities of the same size.

A comparison of the results with Equation (5.2.8) and with Howell and Siegel's Equation (2.2.8) with $\delta = 0.001$ is also shown in Fig. (47). It is seen that a better fit isagain obtained with Howell and Seigel's Equation.

For a particular cavity size the initiation superheat required for this type of surface is slightly less than that for the test surfaces with a small number of cavities, although it is still greater than the value predicted by Equation (5.2.8). The following three reasons are suggested for the difference.

(i) A bubble, in the process of growing or departing causes a localized disturbance in the thermal layer which may provide optimum thermal layer thickness at a neighbouring site and this may encourage growth provided that the heat capacity of the surface is not greatly affected by the first bubble. The disturbance will be damped and will probably be effective over an area two to

three times that of the departing bubble size so that for widely spaced cavities the effect is negligible.

(ii) The existence of a temperature gradient across the thermal layer surrounding a growing bubble gives rise to Q_{out} Figure (6) a weak heat energy which passes to the bulk of the liquid.

Therefore in the vicinity of active sites a temporarily higher superheat temperature will exist which may start or encourage the growth of other bubbles again provided that the surface heat capacity is not greatly affected.

(iii) The growth, departure or collapse of a bubble may induce a pressure wave in the liquid, with a large number of active sites it is possible that a compression or refraction wave formed from neighbouring sites will produce a temporary local reduction in pressure thus facilitating initiation.

9.2 Initiation at Pressures Higher than Atmospheric

The effects of pressures ranging from atmospheric to 415 psi. were studied. The superheat temperature and heat flux at the saturation condition were recorded for five different surfaces Figs. (48), (49), (50), (51), (52) chosen to give a wide range and distribution of cavity sizes. See Table (1a,b).

At pressures above 415 psi. it was found difficult to bring the system to equilibrium at the corresponding saturation condition without using the full power of the bulk liquid heater, which, beside producing a stream of bubbles

making the observation of the test surface difficult, could give rise to a strong convection current and thus affect the measurement of the bulk liquid temperature and hence the superheat ΔT_{int}. For pressures above 415 psi. ΔT_{int} is considerably less than $1\,^{0}F$ so that the accuracy of the bulk liquid thermocouple, $\mp 0.5^{\circ}F$ is considered to invalidate the measurements.

Figs.(49) (50)(51) (52) &(53)show the experimental results. The theoretical predictions of Equation (5.2.8) for each surface and those of Howell and Seigel (2.2.8) with $S = 0.001$ are also shown in the above figures.

It can be seen that the values of ΔT_{int} obtained experimentally are higher than those from Equation (2.5.8). Furthermore the superheat temperature difference, ΔT_{int}, for test surfaces with individual cavities Figs. (48) (49) & (50)is larger than that for surfaces with a large number of cavities Fig. (51) and (52), even when the individual cavity sizes are larger than the average cavity size on the general surface.

When Equation (5.2.8) is considered in greater detail the assumption that σ and r_c are pressure independent gives Equation

$$\frac{T_{sat}}{h_{fg}\rho} = \frac{160}{778} P^{-.786} \qquad (9.2.1)$$

Substitution of Equation (9.2.1) in Equation (5.2.8) yields

$$\Delta T_{int} = \frac{15.4\ 10^{-4}}{r_c} P^{-.786} \qquad (9.2.2)$$

where r_c is measured in ft., P in psi. From a curve fitted to the experimental results Figs.(48 to 52) a ΔT - P relationship was obtained for example

that for surface NG2 gives a relation

$$\Delta T_{int} = 12.8\ \bar{p}^{\,0.466} \qquad (9.2.3)$$

A comparison of Equation (9.2.2) & (9.2.3) shows that for the theorectical equation to predict the experimental superheat, ΔT_{int}, the cavity radius, must be a function of pressure. Equating Equations (9.2.2) and (9.2.3) gives

$$r_{new} = \frac{15.4}{12.8}\ 10^{-4}\ \bar{p}^{.786\ +\ .466}$$

$$r_{new} = \frac{15.4}{12.8}\ 10^{-4}\ \bar{p}^{0.320}$$

A general expression may be written in the form

$$r_{new} = \frac{c_1}{c}\ \bar{p}^{0.786\ +\ n}$$

where $c_1 = 14.4\ 10^{-4}$ and C and n are constants obtained from each experimental curve. This of course implies that the cavity radius will decrease as the pressure increases which may appear unrealistic but physically this may be explained by the fact that as the pressure increases the liquid will be pushed deeper inside the cavity to an extent dependent on the cavity geometry and size. Table (9.2.1) gives the calculated results of r_{new} as the pressure increases for each test surface.

It can be seen from the table that good agreement is obtained for r_{new}, between surfaces NG2 and NG3 this is probably due to the fact that both test surfaces were produced in the same way, see Chapter (4) so that

Test Surface	Cavity radius in	Equation Obtained for r_{new}	Press. atm.	50 psi. r_{new}	100 psi. r_{new}	200 psi. r_{new}	300 psi. r_{new}	400 psi. r_{new}
NG2	0.00176	$r_{new} = 0.001475\ \bar{P}^{-.32}$	.0062	.000422	.000338	0.000261	0.000237	.000217
NG3	0.00285	$r_{new} = 0.00225\ \bar{P}^{.346}$	.000883	.00058	.000458	.000360	.000312	.000282
B′	0.0058	$r_{new} = 0.00228\ \bar{P}^{.557}$	0.00055	.000257	.000176	000119	0.000955	0000815
A′	0.00285	$r_{new} = 0.00287\ \bar{P}^{.621}$	.000534	.000259	.000164	0001065	0000825	0000687
D	0.0170	$r_{new} = 0.00258\ \bar{P}^{.562}$	00078	000398	.000267	0001828	000145	.000123

Table (9.2.1)

Calculated values of r_{new} as the pressure increases

the cavity geometry of each will be similar. Furthermore, for a large average cavity size, test surface NG3 , the reduction in the cavity mouth radius is greater than that for test surface NG2 , which implies that there is greater penetration of the liquid at atmospheric pressure for a large cavity than for a smaller one.

The same trend of behaviour is observed for surfaces A B and D which were produced in a different manner to NG2 and NG3

The conclusion that the cavity radius must change to obtain the experimental results from Equation (5.2.8) with the reservation discussed in Section (5.2), emphasizes the proposals forwarded in Section (9.1.1) particularly that of a partially liquid filled cavity.

The fact that no experimental results are available for the thermal layer thickness, δ , at pressures higher than atmospheric, led to the choice of a value of 0.001 Figs. (48,49,50,51 and 52) to give the best possible fit with the experimental results and thus caused the emphasis to be placed on the application of Equation (5.2.8).

9.3 Number of Active Sites

9.3 - 1 Introduction

As the applied heat flux is increased a number of the potentially active sites initiate. The number of sites which become active depends on three factors:-

(i) The applied heat flux

(ii) The surface condition, that is cavity size and distribution

(iii) The pressure and other liquid properties.

The primary aim of this study is to be able to predict the population at any applied heat flux when the condition of the surface is known, for example in a general distribution with cavities of known average size.

The investigation comprised three test surfaces, reference numbers NG1, NG2 and NG3 each with approximately 120 cavities of average size ranging from 0.00176 in. to 0.00381 in. respectively and of distributions shown in Figs. (12), (13) and (14). At each heat flux studied the system was allowed to reach equilibrium and then, for increasing and decreasing heat flux, the number of active sites was counted visually several times and then finally recorded. The experiment was repeated to check the reproducibility of the results. It was found that at high heat flux it was much easier to count the inactive sites, especially for surfaces NG1 and NG2 where the cavities are distributed evenly in five rows.

The limitations of the boiler's design, Fig. (7), are such that it is impossible to count visually the number of active sites at pressures above atmospheric. However, the bubble flux, f_N , was obtained for these surfaces using the frequency probe Fig. (18) referred to in Section (6.3).

Surfaces with approximately ten individual cavities were also studied at pressures ranging from atmospheric up to 145 psi.

9.3-2 The variation of Number of Active Sites with Applied Heat Flux

The variation of the number of active sites with increasing heat flux at atmospheric pressure is shown for surfaces with a large number of cavities in Figs. (53), (54) and (55) and for those with approximately ten cavities in Fig. (56). Curves were fitted to the above results using a least squares fit and corresponding equations of the form

$$Q/A = C_1 (N/A)^C$$

were obtained, see Table (9.3.2).

Test Surface	Runs	Equation obtained from fitted curve.
NG1	1	$Q = 0.00013N^{2.0165}$
	2	$Q = 0.0084N^{1.52098}$
NG2	1	$Q = 8.2N^{0.936}$
	2	$Q = 145N^{0.5434}$
NG3	1	$Q = 0.416N^{1.16674}$
	2	$Q = 8.15N^{0.85464}$

Table (9.3.2)

As the heat flux increases more potentially active sites initiate. The increase in active sites depends on the cavity sizes and their distribution and

more precisely on the geometry of an individual cavity, which may explain the variation in constants for different test surfaces in the above equations, Figs. (53), (54) and (55). Scatter in the experimental results for two different experiments with the same surface is also obvious in the above figures. This discrepancy, however, may well be due to a combination of factors, not least the human error in counting the active sites. Any such error becomes exaggerated since N/ft^2 is obtained from the measured value of N/in^2. A more direct and obvious explanation is not apparent.

If the curve for surface NG3, Fig. (55), is examined, it is seen that there is a discontinuity in the slope. This surface is one which has a large range of cavity sizes, i.e. the standard deviation of the cavity size distributions is large. A similar effect was reported by Hatton and Hall (23) for 0.031 in. I.D. tubes with C.L.A. of 30 μin and 165 μin. The change in slope was not apparent for surfaces NG1 and NG2, Figs. (53) and (54). These surfaces were produced with the intention that all the cavities should be of approximately the same size, which is reflected in the small value of the standard deviation of the cavity size distributions.

In agreement with the initiation equation (5.2.8), a larger value of heat flux is required to activate a particular number of sites on a small cavity surface, Fig. (54), than for the surface of Fig. (53) containing larger cavities.

The experimental estimation of the number of active sites, N, is limited to the region of isolated bubbles, beyond which interference between neighbouring bubbles occurs. The onset of interference is seen clearly from photographing the number of active sites on surfaces NG1 and NG3, Figs. (78) to

(93), as the heat flux increases from 2660 Btu/ft^{2}hr to 26550 Btu/ft^{2}hr. Interference occurs at 16900 Btu/ft^{2}hr. and 15620 Btu/ft^{2}hr. respectively.

9.3 - 3 Variation of Number of Active Sites, N, with Superheat Temperature Difference, ΔT_{sup}.

The variation of number of active sites, N, with superheat temperature difference ΔT_{sup} is shown in Figs. (58), (59) and (60). Equation (5.5.5), proposed in Section (5.5), is also shown in the above figures.

It can be seen that the theoretical prediction of number of active sites is substantially higher than the experimental data for all the surfaces studied. There are however two considerations to be made in the application of Equation (5.5.5) which may explain the discrepancies.

(i) The derivation of Equation (5.2.8), which is combined with a particular cavity distribution to give Equation (5.5.5), assumes that each cavity is an ideal one. It was seen in Section (9.1.1) that Equation (5.2.8) predicts much smaller values of superheat temperature difference than experimental data, a result also found by Grant (3) and Griffith and Wallis (21). It may be expected therefore that Equation (5.5.5) would predict a certain number of active sites for a much lower superheat value than the experimental one which is in fact the case. Improved agreement was obtained by introducing into Equation (5.5.5) the experimental value of initiation superheat temperature for each test surface rather than that obtained from Equation (5.2.8) but there was still some discrepancy.

(ii) The initiation of each individual cavity is controlled by the geometry of that cavity which may give rise to scatter in the number of active sites and

cause discrepancy between experimental and theoretical values. It can be seen that at high superheat temperature difference i.e. for small cavities, the discrepancy is much less than for low superheat values. This is in agreement with the experimental results for initiation, Fig. (45).

It can be seen from Figs. (12), (13) and (14) that the cavity distributions may be approximated by a sine function which justifies the use of this function in Equation (5.5.5). The distribution could, alternatively, have been approximated by a Gaussian or Poisson function, Grant (3), Gaertner (5), however the simplicity of the sine function facilitates direct application.

The table below shows a set of factors introduced to Equation (5.2.8) to give the closest agreement with the experimental results. It may be observed that the factor decreases as the average cavity size decreases, which emphasises the point already discussed in Section (9.1.1) that the scatter in initiation is less for small size cavities.

Cavity Radius	Factor	Test Surface
0.00176	12	NG2
0.002825	16	NG3
0.003805	21	NG1

Table (9.3.3)

It was thought more appropriate to introduce the correction factor into Equation (5.2.8) than as a direct reduction of the number of active sites, predicted by Equation (5.5.5) since it was seen in the earlier discussion of

initiation that Equation (5.2.8) predicts a low value of superheat temperature especially for large cavity sizes.

It was not necessary to introduce here the factor of 10^{-4} referred to by Grant (3) and it is possible that the assumption there that all cavities on the surface are potentially active was incorrect.

The variation of the number of active sites, superheat temperature difference relation with pressure is also shown in Fig. (60). No experimental data was obtained to verify the predictions.

The experimental variation of the number of active sites with pressure for a surface with ten cavities at a fixed heat flux is also shown in Fig. (61). The trend agrees with reports in the literature.

9.4 Heat Flux Correlation

9.4 – 1 Introduction

Many empirical heat flux correlations have been proposed either in the form, $Q = \text{Const } \Delta T^m$ Cichelli & Bonilla(48) McAdams (11) and Grant (3), or, alternatively, in terms of the number of active sites as, $Q = \text{Const } N^n$ Gaertner (13), Kirby and Westwater (68). More recent approaches have incorporated both variables in the form $Q = \text{Const } \Delta T^m N^n$.

Only analytical and semi-empirical solutions to the problem will be discussed fully in this section. These include the transport of enthalpy proposed in Chapter (5), Rohsenow's correlation based on forced convection and Zuber's turbulent natural convection correlation. Predictions are compared with experimental results obtained for three surfaces with an applied heat flux up to 40,000 Btu/ft^{2}hr. Results were taken with heat flux increasing and decreasing

and were repeated twice to check reproducibility. The effect of pressure up to 75 psi. and the application of the above approaches at these pressures was also investigated.

9.4 – 2 Heat Flux variation with superheat temperature difference at atmospheric pressure.

Figures (62), (64) and (66) show the heat flux v superheat temperature difference curves at atmospheric pressure for the three general surfaces (NG1), (NG2) and (NG3) plots of Equation (5.6.7) are also shown.

The equation is first shown as it is obtained from purely theoretical considerations of frequency, number of active sites, thermal layer thickness and bubble size. Chapter (5). At low heat flux, up to 10,000 Btu/ft^{2}hr. there is agreement with experimental data to within about 20% but at higher fluxes, predicted flux values are considerably greater than experimental ones for all surfaces tested.

In discussing the discrepancy it must be remembered that the heat transfer mechanism employed in deriving Equation (5.6.7) is one of superheated liquid enthalpy carried away by individual bubbles.

As the heat flux is increased and a greater number of cavities initiate the chance of partial horizontal bubble interference occuring also increases. The onset of such interference marks the end of the isolated bubble region, to which Equation (5.6.7) is limited since it does not take into account any interference effects. Zuber (16) predicted that the minimum heat flux density in the transition region was 50,300 Btu/ft^{2}hr. which may be compared with the value of 10,000 Btu/ft^{2}hr. where the divergence in theoretical and experimental data widens. The large number of active sites on the test surface increases the

likelihood of interference which may occur for lower flux values.

One effect of interference is to reduce the heat energy removed from the surface since the almost continuous vapour layer on the surface causes a reduction in the direct heat conduction to the liquid. According to Zuber (63) the vapour layer disturbs the liquid circulation near the surface, which in the region of isolated bubbles is maintained by a constant displacement and entrainment of liquid by the rising bubbles, and produces a reduction in heat flux. In this case the mechanism of heat removal is different from the superheat liquid enthalpy removed by individual bubbles of Equation (5.6.7).

The area of influence may be another factor contributing to the reduction in heat flux. Under normal circumstances the area is taken as πD^2 . Hsu and Graham (7) observed the diameter of influence to be twice the bubble diameter, Zuber (16) predicted the existence of an area of influence πD^2 around an active site and other experiments on gas bubbles passing through a fluidized bed confirmed these conclusions. Hsu and Graham (7) postulated, however, that once the areas of influence begin to overlap any further increase in heat flux results in a decrease in the size of the departing bubbles and, since the mass of fluid removed decreases with bubble radius the agitation affect caused by bubble departure may decline. This may result in a reduction of heat energy removed from the surface even though the frequency may increase.

The occurrence of interference also means that the size of an individual bubble and therefore the quantity of thermal layer removed is not clearly defined which brings uncertainties into the application of Equation (5.6.7). It may be remarked here that there is uncertainty about the theoretical estimation of bubble departure size in general. Fritz (30), proposed an equation,

substantiated more recently by Gaertner (13), where the bubble departure radius remains constant, while, according to the Equation of Patten (34) which is used here, and also that of Zuber (1) the radius is proportional to Jakob's number. It would seem therefore that the determination of bubble departure size and the bubble influence area and hence of the amount of superheat liquid removed must be considered a weak point in the proposed theory and indeed in all correlations employing an enthalpy transport mechanism.

Because of the difficulties encountered in purely theoretical heat flux predictions, experimental values of Nf the frequency number of active sites product, were substituted in Equation (5.6.7). Although flux values closer to the experimental results are predicted in this way, predicted values for higher fluxes were again greater than experimental data. This may be attributable to the fact that neither the value of bubble departure radius nor thermal layer thickness were evaluated at high heat fluxes. The fact that closer agreement was obtained implies that theoretical values of either N or f or both are larger than experimental ones - it was found in Section (9.3) that the predicted number of active sites is larger than the experimental value.

In the final heat flux correlation made, experimental values of R, Nf and ΔT_{sup} and an assumed value of S are substituted in Equation (5.6.7) and the results are shown in Figs. (62), (64) and (66). A value of $D = 0.108$ in was obtained from a large number of still photographs of bubbles departing from the test surface. This may be compared to that of Fritz, 0.132 inch Cole, 0.120 in and with the average experimental data of Gaertner (13) 0.120 in . An area of influence proportional to $2D$, as discussed earlier, was used. Jakob's Equation for natural convection (5.6.1), predicts a thermal

layer thickness of 0.0342 in. at an applied superheat of $\Delta T_{sup} = 5\ ^{o}F$. Hsu (22) used a value of 0.006 in to give the best correlation while Grant and Patten (70) found δ to be 0.03 in. using a direct probe technique and shadowgraph methods at atmospheric pressure and also at 30 psi. According to Gaertner (13) the thermal layer thickness changes little in the region of isolated bubbles, he found th measured value to be 0.059 in. while McNeill (69) found δ to vary from 0.011 in to 0.0195 in. In this study a value of δ = 0.035 in. is used not only because it represents a reasonable mean value but because it is very near to the value obtained from the natural convection equation and this is the equation relevant to the weak nucleate boiling region. Values of N_f and ΔT_{sup} are those obtained experimentally.

It can be seen from Figs. (62), (64) and (66) that there is very good agreement with experimental results up to 15,000 Btu/ft^{2}hr, the limit, found photographically to the isolated bubble region. For fluxes above this value it was necessary to incorporate a factor of the form

$$E = \frac{0.5Q/A}{10,000} + 0.25$$

into Equation (5.6.7) to account for the effects of interference. The predicted values after the introduction of E are shown in Figs. (62), (64) and (66) and it can be seen that the agreement is excellent. Uncorrected values for fluxes greater than 15,000 Btu/ft^{2}hr. are shown in Table (4a,b,c). To justify the introduction of the factor E it is necessary to consider again the measured value of N_f. At high heat fluxes bubbles coalesce so that bubbles leaving the surface are larger than individual ones formed. The frequency correction factor however is based on single bubbles so that an appropriate

constant may be introduced to predict a larger value of f and provide better agreement.

In all the above calculations $(Q/A)_{NC}$ was obtained from Jakob's equation for natural convection (5.6.). This term, however, is significant only at low heat flux where there is a relatively large area not influenced by bubble formation.

9.4 - 3 Application of Rohsenow Equations

Equation (2.7.10) which was proposed by Rohsenow, and is probably the most widely used type of heat flux correlation is applied to the experimental results as shown in Figs. (63), (65) and (67) . To apply the above equation the value of the constant C_{sf} and indices r' and m' must be considered. A value of $r' = 0.33$ was suggested initially by Rohsenow (15) and this value has been used in most correlations subsequently including the more recent work of Vachon et al (49). Although Equation (2.7.10) is applicable to only a clean surface, Rohsenow reported that even when the surface is contaminated the value of r' does not seem to vary.

The value of the constant m' was taken to be 1.7 originally but more recently in colaboration with Rohsenow, Vachon et al (49) proposed a value of unity. In contrast to the value of r', m' was found to vary between 0.8 and 2 when the surface was contaminated.

Values of $r' = 0.33$ and $m' = 1$ are used in this calculation.

The constant C_{sf} which is a function of contact angle i.e. $C_{sf} = f(\beta)$ is obviously related to the particular fluid-heating surface combination and will thence vary accordingly. Vachon et al (49) obtained an average value of $C_{sf} = 0.132$

for a cleaned mechanically polished surface of stainless steel with water as the boiling liquid. When, however, one measured value of Q/A was used in calculating C_{sf}, the following values were obtained.

General Test Surface	C_{sf}	Pressure
NG1	0.0155	Atmospheric
NG2	0.0124	"
NG3	0.0166	"

For each test surface the appropriate calculated value of the constant C_{sf} see above table, was used for one set of calculations, and the average value of $C_{sf} = 0.0132$ used for a second set, Figs (63) (65) & (67). From the Figures it is seen that Rohsenow Equation is in good agreement with experimental results, even at high heat fluxes up to 40,000 Btu/ft^{2}hr. Although an experimental value of heat flux, q/A, is required to obtain the value of C_{sf} which may in some industrial projects prove to be difficult, it may be concluded that Rohsenow Equation gives good agreement with experimental data for all the surfaces used at atmospheric pressures.

9.4-4 The Application of Zuber Equation

Zuber Equation (2.7.18) which is based on natural turbulent convection was also used to calculate the heat flux and is compared with experimental values

in Figs. (63) (65) and (67).

Consideration of Equation (2.7.18) in more detail shows that experimental values of ΔT_{sup} and N, the number of active sites must be obtained. The experimental value of N for the test surfaces was used in one set of calculations and a second set was obtained using the value of N predicted by Equation (5.5.5). The need to establish the value of N may make Zuber's equation rather difficult to apply in some practical applications, the use of Equation (5.5.5) however, removes this difficulty since only the superheat temperature difference is then required. Zuber (16) suggested that his equation is valid only in the region of isolated bubbles. Figs. (63), (65) and (67) show clearly that the agreement is good up to approximately 10,000 Btu/ft^{2}hr. in all three cases. When the equation is applied in the combined form Equation (C3) requiring only the experimental superheat, ΔT_{sup}, the agreement is maintained to a higher heat flux, approximately 15,000 Btu/ft^{2}hr. Although more experimental data on different types of cavity distributions is probably required to verify the combined equation, it may be concluded that in this work, the predicted fluxes agreed with those obtained experimentally in the region 0 - 15,000 Btu/ft^{2}hr.

9.4 - 5 Heat Flux Variation with Superheat Temperature Difference at Pressure Above Atmospheric

Figs. (68), (70), (72) and (73) show the heat flux variation with superheat temperature at pressures of 30, 45, 60 and 75 psi. The trend of the curve is similar to that reported in the literature (3) and (48). With an increase of pressure the initiation temperature difference is reduced and at any

applied superheat the number of active sites increases and more agitation is introduced to the system so that a greater amount of heat energy is removed from the surface. This shows in Fig. (72) and (73) where the curvature of the graph is clearly reduced. To demonstrate that this effect is due to an increase in the number of active sites and hence to an increase in the agitation, experimental heat flux versus ΔT_{sup} curves for a special surface (D) with only a small number of sites, were obtained at atmospheric pressure and pressures of 30, 45, 65 psi. Figs.(74 to 77). It can be observed that for the above figures the curvature remains high at higher pressures, and it may be concluded that this is because only a small number of potential cavities exist on the surface and therefore only a relatively small amount of heat energy can be removed.

Equation (5.6.7) applied in its purely theoretical form is also shown in Figs. (68),(70),(72)and (73). The agreement with the experimental data appears to diminish as the pressure increases as can be seen when Figs. (68) and (73) are compared. This may be because at higher pressure the value of δ , the thermal layer thickness, may increase, however this remains undetermined with the exception of the work of Grant and Patten (70) where the value of f at pressure 30 psi. was found to be approximately the same as that at atmospheric pressure, but the trend may change at higher pressures. The bubble departure size, which decreases as the pressure increases, Semeria (32), may affect the predicted flux.

Equation (5.6.7) was applied with the experimental value of N_f , an assumed value of δ = 0.035 in and a value of bubble departure radius obtained from Semeria Equation (5.4.14) multiplied by a factor to correct the

predicted value to the measured one at atmospheric pressure. The influence area was taken as πD^2 . The correction factor for interference, see Section (9.4.2), applied at atmospheric pressure was also used for pressures of 30 and 45 psi., at higher pressures however it was not necessary. This emphasises the suggestion that the correction arises from interference of bubbles since the bubble size diminishes at higher pressure and reduces the chance of interference. When, however, predicted values were compared with the experimental results it was necessary to include a factor of the form

$$C = \frac{(P - P_o)}{5}$$

where P_o in psi. is atmospheric pressure and P in psi. the experimental pressure. This may be due to a combination of causes but it is suggested that it may be a result of neglecting a property or a factor which is pressure dependent, for example, δ , or that the bubble departure radius pressure relationship is different from that suggested by Semeria (32). The inclusion of this factor gives excellent agreement for all test surfaces Figs.(68) (70)(72)and (73).

Equation (2.7.10) due to Rohsenow is also applied to the experimental data using the following constants:-

Press. psi.	r′	m′	C_{sf}
30	0.33	1	0.0160
45			0.0232
60			0.00957
75			0.01045

where the constant C_{sf} is calculated from one measured value of q/A at each pressure. Good agreement is obtained for pressures of 30 and 45 psi., at higher pressure the equation predicts a heat flux value high compared with the experimental data.

The application of Zuber's combined Equation (C3), with the number of active sites obtained from Equation (5.5.5) gave good agreement with the experimental data up to 10,000 Btu/ft^{2}hr. for pressures of 30 and 45 psi. At higher pressure the agreement diminishes and the equation predicts a lower value of heat flux than experimental results.

CHAPTER 10

CONCLUSION AND REMARKS

10. 1 Initiation of a Bubble from an Individual Cavity

Bubble initiation was studied from individual cavities with radii varying from 0.0002 in. to 0.025 in. Although great care was taken in every aspect of the experimental work, there was a large amount of scatter in the results, especially in the data for large cavities and the following two suggestions are forwarded in possible explanation.

(i) The existence is proposed of small sub-cavities inside the large cavities. Microscopic examination of the inner surface of large cavities after boiling indicated the existence of small cavities which was substantiated photographically. Also, the presence of a film of deposit inside the large cavities similar to that observed in the vicinity of superficial cavities after a prolonged period of boiling offered further support.

(ii) From simple experimental investigations it was concluded that liquid may partially fill a cavity. The effect was observed here for radii as small as 0.005 in. and was also reported by Wei and Preckshot (66) and Kosky (67). The use of cavity radius as the critical radius in Equation (5.2.8) may thus result in an underestimate of the required temperature difference for initiation.

The closest agreement between experimental and theoretical values of initiation temperature difference for cavities of radii up to 0.02 in. was obtained from Howell and Seigel's Equation (2.2.8), when a thermal layer thickness of 0.001 in. was used.

A limit to the cavity size capable of initiation and dependent on the thermal

layer thickness all as predicted by Han and Griffith Equation (2.2.5) was not found here, since even for a thermal layer thickness of 0.035 in. cavities with radii up to 0.025 in. appeared to be active.

The values for initiation superheat temperature difference as predicted by Gibb-Clapeyron equation were found to be smaller than experimental results. A factor which may contribute to the difference is the assumption made in obtaining the above equation, namely that the cavity cone angle is equal to twice the liquid-solid contact angle.

10. 2 Initiation from a Surface with a Large Number of Active Sites

For a particular cavity size the initiation superheat required for a surface with a large number of active sites was slightly less than that for a surface with a smaller number of cavities. The following reasons for the difference are forwarded.

(i) Fluctuations within the thermal layer caused by bubble departure may produce the optimum thermal layer thickness for the initiation of a neighbouring potential site.

(ii) The heat lost to the bulk liquid from the thermal layer around a growing bubble may create a localised superheat temperature and hence give rise to initiation from a neighbouring cavity.

(iii) Local fluctuations in pressure due to the departure or collapse of a bubble may encourage growth from the neighbouring sites.

The above actions all arise from localised variation and hence affect the initiation from a surface with closely spaced sites. Again it was found that

Howell and Seigel Equation (2.2.8) with a thermal layer thickness of 0.001 in. gave the closest agreement to the experimental data. For both types of test surface experimental values of initiation temperature difference were higher than predictions from the above equation.

10. 3 Initiation at Pressures Higher than Atmospheric

It was found experimentally that the initiation temperature difference decreases as pressure increases and that for all pressures considered, the initiation temperature difference for surfaces with individual cavities is larger than for those with a large number of cavities. This was so even when the individual cavities were larger than the average cavity size on the surface with many cavities.

The experimental initiation superheat was much higher than the predictions of either Equation (5.2.8) or those of Howell and Seigel for a thermal layer thickness of 0.001 in.

In applying Equation (5.2.8) at higher pressures it was found that the cavity mouth radius r_c must decrease as the pressure increases if a reasonable fit is to be obtained for the experimental data. This was expressed in the form

$$r_{new} = C \; p^{n - 0.78}$$

where p is expressed in psi. and r_{new} in inches.

The assumption implied is that the liquid penetrates the cavity deeper as the pressure increases. The penetration of liquid into the cavity seemed to increase with the increase of cavity radius.

10. 4 Development of Capacitance Detector Probe

A probe for the detection of bubbles from a single cavity was developed and was shown to be capable of measuring the frequency at a single site at pressures higher and lower than atmospheric. The system is not dependent on the properties of a particular medium and therefore may be suitable for a number of liquids. Signals were either recorded on a U.V recorder or counted. No amplification is required in general although in a few cases a gain of 10 may be necessary, as for example when measuring total bubble population.

Further developments in the type of probe allowed bubbles to be detected as they detached from any section of the test surface without movement of the probe and the total number of bubbles emitted from a surface to be counted. Correction factors for dead time, $\mathcal{F}$, introduced in the later probe types have been proposed.

The size of a bubble departing from an individual site can be determined from the probe pulse height either by direct theoretical calculations or from a calibration graph and predicted values were found to be in agreement with experimental data to within approximately 10%.

The rising velocity of a bubble may also be determined directly from the duration of the pulse obtained, in conjunction with the bubble size. Potential applications of the frequency probe in chemical plants, where other detection methods are impractical, and in medicine are foreseen.

10. 5 Bubble Emission Frequency

The frequency of bubble emission was defined as $f = \frac{1}{tg + tw}$ where

tg and tw are the growth and waiting times respectively. An Equation (5.4.8) based on the amount of energy removed by an individual bubble and on the simple conduction equation was proposed for the evaluation of tw. Calculation of the waiting time from Equation (5.4.8) and of the growth time from the equation of Plesset and Zwick (5.4.12), showed the ratio tg/tw to be most significant at low heat flux, where tg is relatively large, and at very high fluxes where tw is small. In the regime of bubble interference the above definition of frequency is no longer applicable.

The variation of frequency from a single cavity with applied heat flux was investigated experimentally. It was found that the frequency increases with flux up to a certain flux value, depending on the surface condition and liquid properties, after which it tends to become independent of further flux increase. This trend was explained from the general definition of frequency and by separate consideration of the limits of tw obtained from Equation (5.4.8), and of tg obtained from Plesset and Zwick Equation (5.4.12), as the applied heat flux increased.

Calculations of the relative values of growth time tg, from the equations of Zuber (1), Golovin et al (5 7) and Plesset and Zwick, and of waiting time, tw, from Equation (5.4.8) indicated that the frequency could be justifiably defined as 1/tw.* This definition is substantiated by the experimental work of Hsu and Graham (7) and Han and Griffith (9). Using the experimental values of heat flux, Q/A , and temperature difference ΔT_{sup}, in Equation (5.4.8) predicted a frequency/heat flux relationship similar to the experimental one. Discrepancies in the results were related to the choice of the value of the ratio $\pi D_x^2/A$

* see page 75.

The equation for waiting time derived by Hsu (5.4.1) from the transient conduction equation predicted a different trend from the experimental data when heat flux, Q/A, and initiation temperature difference, ΔT_{int}, were used, when, however, experimental values of temperature difference corresponding to each applied heat flux value were substituted a trend similar to experimental results was obtained.

At a constant heat flux and at atmospheric pressure the frequency of bubble emission decreases gradually as the cavity radius increases. Experimental results were correctly predicted by Equation (5.4.15) and seemed to substantiate Han and Griffith Equation (App.B) which predicts a larger waiting time for an increase of cavity size.

There does not seem to be any net variation of the frequency at a particular heat flux for different pressures. There is however, a decrease in the waiting time obtained from Equation (5.4.8) and an increase in the growth time from Plesset and Zwick Equation (5.4.12). The combination of Equations (5.4.8) and (5.4.12) predicts a frequency of similar magnitude to the experimental data up to a certain pressure dependent heat flux, beyond which the frequency tends to a constant value, that is becomes independent of heat flux. The value of this heat flux limit is found to decrease as the pressure increases which emphasises the fact that the heat flux becomes independent of temperature difference at higher pressures and that the value of frequency from the combined equation will therefore be constant at a particular pressure.

The total frequency, defined as the total number of bubbles forming on a multi-cavity surface per second seemed to increase with applied heat flux up to a peak value and then to decline gradually. This was explained qualitatively

by postulating that an initial increase of applied heat flux causes the number of active sites to increase after which further increases result not only in an increase in the number of active sites but also in the frequency of each individual site and that at higher fluxes the bubbles coalesce on the surface so that the net frequency declines. This coalescence has been confirmed photographically.

The frequency of an individual cavity on a surface with a large number of sites, $f = \frac{f_{tot}}{N}$, was found to be smaller than that of an individual cavity on a surface with a small number of sites and also smaller than the frequency values predicted by Equations (5.4.15) and (5.4.11). It is claimed that this is a result of the more efficient circulation of liquid on the first type of surface due to bubble departure. It may be that a different value of dead time is needed to correct the measured value of total frequency.

The trend of the frequency ν heat flux curve for low fluxes was found to be the same as at atmospheric pressure but at higher fluxes, rather than declining, the measured values of frequency continued to increase gradually. The apparent frequency decrease for high fluxes at atmospheric pressure was thought to be caused by the overlapping of signals from the frequency probe. At high pressures the smaller bubble size reduces the interference so that the measured value continues to increase. In general the value of $\frac{f_{tot}}{N}$ was much smaller than the frequency from an individual site on a test surface with only a few cavities.

Although the general surfaces tested covered only a small range of average cavity sizes it was found that at constant heat flux the frequency decreases as the average cavity radius increases, which agrees with findings for an

individual cavity.

10. 6 Number of Active Sites

The number of active sites, N, was found to increase with the applied heat flux at atmospheric pressure. The variation found between the slopes of the number of active sites $\vee$ heat flux curves for different surfaces could be related to the cavity size distribution and to the geometry of individual cavities. For those surfaces where the standard deviation of the cavity size distribution was small the slope of the curve remained constant while for broader distributions the slope was found to vary.

The cavity size distribution was approximated to a sine function and used in conjunction with the initiation Equation (5.2.8) to give a relation between the number of active sites and the applied temperature difference for a given surface. In applying this relation to different surfaces in order to improve the fit to experimental data it was found necessary to introduce different constants into Equation (5.2.8).

The value of the constant was found to decrease as the average cavity radius decreased.

10. 7 Heat Flux Correlation

An equation based on the heat energy in that section of the superheated liquid removed by each bubble as it leaves the surface was introduced, which in its final form is in terms of the temperature difference and liquid properties only.

To predict the energy removed the number of active sites and the bubble frequency were obtained from Equations (5.5.5) and (5.4.15) respectively while Patten

Equation (5.6.2) was used to evaluate the bubble departure radius and Jakob Equation (5.6.1) gave the thermal layer thickness. The net heat flux is then obtained by applying the resulting equation to the area influenced by bubble departure and the natural convection equation as proposed by Jakob to the remainder of the surface.

When the theoretical predictions were compared with experimental data it was found that the equation predicted much higher values than the experimental results, especially at heat fluxes above 15,000 Btu/ft^{2}hr. When, however, the experimental values of the product of number of active sites and frequency were used rather than the theoretical ones there was better agreement, especially in the low heat flux region. Excellent agreement was obtained when the experimental values of number of active sites, frequency and bubble departure radius were used and when the thermal layer thickness was assumed to be 0.035 in. Again the best agreement was obtained at fluxes up to 15,000 Btu/ft^{2}hr. Above this value it was necessary to introduce an empirical factor in the form ($\frac{0.5\,q/A}{10,000} + 0.25$) to account for the affects of horizontal bubble interference.

The above approach may be applied only in the regime of isolated bubbles where good agreement is found. In the regime of interference the bubble departure size, frequency and number of active sites are not clearly defined and their absolute values are not obvious.

The same approach applied at pressures above atmospheric predicted heat flux values much lower than experimental data. This was so even when experimental values of the product of number of active sites and frequency were used with a value of bubble departure radius obtained from Semeria Equation (5.4.14). However excellent agreement was obtained for all test surfaces studied when a

factor of the form $\frac{P - P_o}{5}$ was incorporated in Equation (5.6.7).

Rohsenow Equation (2.7.10) was first applied to experimental data with $m' = 1$, $r' = 1.7$ and a value of C_{sf} calculated from one experimental value of applied heat flux. It was found to give good agreement with experimental results at all fluxes considered at atmospheric pressure and at pressures of 30 psi. and 45 psi. At higher pressures the equation predicted flux values higher than experimental data. The experimental determination of applied heat flux and thus of C_{sf} may be difficult in some industrial applications. The equation was also applied with the same values of m' and r' as above but with an averaged value of C_{sf} for a polished metal surface as proposed in the literature and similar agreement was obtained.

Heat flux predictions from Zuber Equation (2.7.18), which is based on the natural convection process were found to be in approximate agreement with experimental data up to fluxes of 10,000 Btu/ft^{2}hr at atmospheric pressure. The number of active sites which is required in the heat flux evaluation may prove difficult to determine experimentally, however the theoretical value of the number of active sites obtained from Equation (5.5.5) used in conjunction with Zuber Equation (2.7.18) gave reasonable agreement for fluxes up to 15,000 Btu/ft^{2}hr. at pressures from atmospheric to 75 psi.

APPENDIX A

Calculation of the number of Active Sites

If the range of cavity sizes is approximated by a linear distribution, see Fig. (a) below, rather than by a sine function, Section (5.5), the distribution of cavities with mean radius rm and of size range (rm - 2ϵ) to (rm + 2ϵ) may be expressed as

$$Y = \frac{dN}{dr} = a\,r - c \qquad \text{(A1)}$$

for the cavity size range (rm - 2ϵ) to rm, and as

$$Y = a\,r + c'$$

for the range rm to rm + 2ϵ

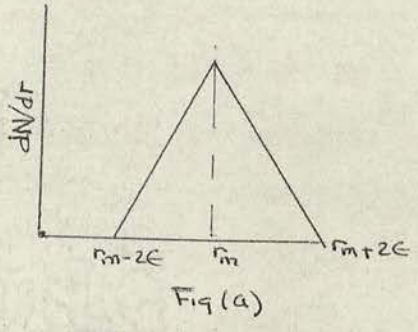

Fig (a)

If h' is the height of the distribution, then

$$\frac{No}{2} = \epsilon\, h' \qquad \text{(A2)}$$

and the constants, a, c and c' are given by,

$$a = \frac{h'}{2\epsilon} = \frac{No}{2\epsilon^2} \qquad \text{(A3)}$$

$$C = (rm - 2\epsilon)\ \frac{No}{2\epsilon 2} \qquad \text{(A4)}$$

$$c' = (rm + 2)\ \frac{No}{2\epsilon} \qquad \text{(A5)}$$

Equation (A1) may thus be written as

$$Y = \frac{No}{2\epsilon^2}\, r - (rm - 2\epsilon)\ \frac{No}{2\epsilon} \qquad \text{(A6)}$$

for the cavity size range (rm - 2 ϵ) to rm , and as

$$Y = \frac{No}{2\epsilon^2} + \frac{NO}{2\epsilon} (rm + 2\epsilon) \qquad (A7)$$

for the range rm to (rm + 2 ϵ)

The initiation equation obtained from the Gibb and Clapeyron equations can be written as

$$dr = \frac{-B}{\Delta T^2} d(\Delta T) \qquad (A8)$$

If the superheat temperature difference increases from ΔT_1 , to ΔT_2 there is a corresponding increase in the number of active sites from N_1 to N_2 . By combining Equations (A8) and (Ab) the change in the number of active sites may be expressed as

$$N_2 - N_1 = -\int_{\Delta T_1}^{\Delta T_2} \left\{ \frac{N_o B}{2\epsilon^2 \Delta T} - (r_m - 2\epsilon) \frac{N_o}{2\epsilon} \right\} \frac{B}{\Delta T^2} d(\Delta T)$$

$$= \frac{N_o B}{2\epsilon^2} \left\{ \frac{B}{2} \left(\frac{1}{\Delta T_2^2} - \frac{1}{\Delta T_1^2} \right) - (r_m - 2\epsilon) \left(\frac{1}{\Delta T_2} - \frac{1}{\Delta T_1} \right) \right\}$$

or from Equations (A8) and (A7) as

$$N_2 - N_1 = \frac{N_o B}{2\epsilon^2} \left\{ -\frac{B}{2} \left(\frac{1}{\Delta T_2^2} - \frac{1}{\Delta T_1^2} \right) + (r_m + 2\epsilon) \left(\frac{1}{\Delta T_2} - \frac{1}{\Delta T_1} \right) \right\}$$

APPENDIX B

Han and Griffith Equation for the Waiting Time tw (9).

The conduction equation was used to determine the temperature distribution in the thermal layer.

They obtained a solution of the form

$$\frac{dT}{dx} = - \frac{T_w - T_\infty}{\sqrt{\pi \alpha t}} e^{-\frac{x^2}{4\alpha t}} \qquad (B1)$$

and at $x = 0$. i.e. at the surface

$$\left.\frac{dT}{dx}\right)_{x=0} = - \frac{T_w - T_\infty}{\sqrt{\pi \alpha t}} \qquad (B2)$$

If the temperature distribution is assumed to be linear then from Equation (B2) the thermal layer may be put as

$$\delta = \sqrt{\pi \alpha t} \qquad (B3)$$

By equating the temperature of the vapour used by the bubble nucleus to that at a height of $3/2\, r_c$ from the surface an expression for the thermal layer thickness may be obtained in the form

$$\delta = 3/2 \quad \frac{(T_w - T_\infty)\, r_c}{T_w - T_{sat}\left(1 - \frac{2\sigma}{r_c \rho_v h_{fg}}\right)} \qquad (B4)$$

By combining Equations (B3) and (B4) the waiting time is given as,

$$t_w = \frac{\delta^2}{\pi\alpha} = \frac{9}{4\pi\alpha}\left\{\frac{(T_w - T_\infty) r_c}{T_w - T_{sat}\left(1 - \frac{2\sigma}{r_c \rho_v h_{fg}}\right)}\right\}^2 \qquad (B5)$$

Appendix C

Combination of Zubers Equation and the theoretical prediction of number of active sites

Zuber proposed a heat flux correlation for the region of isolated bubbles of the form (2.7.18)

$$\frac{hd}{K} = Const\left[\frac{gd^3}{V^2\alpha}\left(\beta'\Delta T + \frac{N\pi D^2}{A\,6}\,\frac{\Delta\rho}{\rho_{L\infty}}\right)\right] \qquad (C1)$$

The number of active sites required in the above relation may be obtained from Equation (5.5.5)

$$N_2 - N_1 = \frac{N_0}{2}\left\{\cos\left(\frac{\pi}{4\epsilon}\,\frac{B}{\Delta T_2} - \frac{\pi}{4\epsilon}(r_m - 2\epsilon)\right) - \cos\left(\frac{\pi}{4\epsilon}\,\frac{B}{\Delta T_1} - \frac{\pi}{4\epsilon}(r_m - 2\epsilon)\right)\right\} \qquad (C2)$$

Equation (C1) may thus be written in the form

$$\frac{hd}{K} = Const\left[\frac{gd^3}{V^2\alpha}\left(\beta'\Delta T + \frac{\pi D^2\Delta\rho}{6\,\rho_{L\infty}}\left\{\frac{N_0}{2}\left(\cos\left(\frac{\pi}{4\epsilon}\,\frac{B}{\Delta T_2} - \frac{\pi}{4\epsilon}(r_m - 2\epsilon)\right)\right.\right.\right.$$

$$\left.\left.\left. - \cos\left(\frac{\pi}{4\epsilon}\,\frac{B}{\Delta T} - \frac{\pi}{4\epsilon}(r_m - 2\epsilon)\right)\right)\right\}\right] \qquad (C3)$$

NOMENCLATURE

Symbol	Definition	Units
A	Heating surface area	ft^2
a	Amplitude of the sine function	
a_1	Distance from centre of dipole	ft
B	Defined as $\frac{2\sigma T_{sat}}{J h_{fg} \rho_v}$	$ft.F^0$
B_1	Defined by Equation 2.7.11	
b	Distance	ft
C, C_d, C_g, C_1, C_2, C_3	Constants	
C_{sf}	Coefficient used in Rohsenow Equation dependent upon the nature of the heating surface-fluid combination.	
C_p	Specific heat under constant pressure	Btu/lbm F°
D	Bubble diameter	ft
$\pi D^2 x$	Area of thermal layer removed by individual bubble	
Dmax	Maximum bubble diameter	ft
D_d	Bubble departure diameter	ft
d	Distance	ft
2d	Length of the capacitor probe	ft
E	Constant = $(\frac{0.5\Phi/A}{10,000} + 0.25)$	
E_o	External electric field	Volts/ft
f	Bubble emission frequency	$1/hr.$
g	Acceleration due to gravity	ft/hr^2
g_c	Dimensional constant	$\frac{lbm\ ft}{lb\ hr^2}$
G_b	Mass velocity of bubbles at departure from the heating surface	lbm/ft^2
h_{fg}	Specific Latent heat	Btu/lbm

h_e	Evaporation coefficient for heat transfer to bubble nucleus.	
h_c	Condensing heat transfer coefficient to the bubble nucleus.	
h	Heat transfer coefficient	$Btu/ft^2hr.F^o$
H	Signal height	ft
J	Joules Equivalent	ft.lb/Btu
K	Thermal conductivity	$Btu/ft.hr.F^o$
l	Characteristic of dimension	ft
2L	Length of the capacitor plate	ft
m	Exponent of Prandtl number	
N/A	Number of active sites	$1/ft^2$
n	Number of bubbles formed at a specific site	
p	Pressure	lb/ft^2
$\triangle p$	Pressure difference ($Pv - P_L$)	lb/ft^2
p^1	Dipole moment	
Q/A	Heat flux rate from heating surface area	$Btu/ft^2hr.$
$(Q/A)_{NC}$	Natural convection heat transfer rate per unit heating surface area	$Btu/ft^2hr.$
Q in	Heat transfer rate from thermal layer to bubble nucleus.	Btu/hr.
Q out	Heat transfer rate from heating surface to bulk liquid	Btu/hr.
Qw	Heat transfer rate from heating surface to bulk liquid	Btu/hr.
Qs	Surface factor	
Qb	Base factor	
Qc	Curvature factor	
Qv	Volume factor	

$\pm q$	Positive and negative charge	
r	Radius of nucleus	ft
rc	Cavity mouth radius	ft
r	New cavity radius	ft
rm	Average cavity radius	ft
R	Bubble radius	ft
r'	Exponent of Reynolds number	
R'	Perfect gas constant	$\frac{\text{ft. lb.}}{\text{lbm. F°}}$
T	Temperature	F^0
ΔT	Temperature difference	F^0
$\Delta T'$	Temperature difference corresponding to the first active cavity.	F°
t	time	hr.
tg	Bubble growth time	hr.
tw	Bubble waiting time	hr.
	Frequency of temperature fluctuation	
Ut	Terminal rise velocity of bubble	
Uv	Velocity of rising bubble defined as $\frac{\text{Volumetric Flow of Vapour}}{\text{Surface area X vapour void coefficent}}$	
V	Voltage	Volt
V	Applied voltage across capacitor probe	Volt
Vv	Specific volume of vapour	ft^3/lb
Vl	Specific volume of liquid	ft^3/lb
X	Distance	ft.
Y	Distance	ft.

Greek letters

α	Thermal diffusivity	$\frac{ft^2}{hr}$
α_w	Vapour void coefficient near the heating surface	
β	Solid-liquid contact angle	
β	Volumetric coefficient of expansion	$1/F^0$
β	Defined by equation (2.7.12)	
δ	Thermal layer thickness	ft
δ_{NC}	Thermal layer thickness in the natural convection condition	ft
ϵ	Standard deviation of cavity population	ft
ϵ_1	Dielectric constant of the bubble medium	
ϵ_2	Dielectric constant of the field medium	
θ	The cavity cone angle	
η	Arithmetic mean of cavity sizes	ft
ρ_L	Liquid density	$\frac{lb}{ft^3}$
ρ_v	Vapour density	$\frac{lb}{ft^3}$
$\rho_{L\infty}$	Density of liquid at the bulk liquid temperature	$\frac{lb}{ft^3}$
ρ_{Lw}	Density of liquid near the heating surface	$\frac{lb}{ft^3}$
σ	Surface tension	lb/ft
τ	Probe dead time	hr
μ	viscosity	

Dimensionless Groups

N_j	Jakob number =	$\frac{c_L \rho_L \Delta T}{h_{fg} \rho_v}$
N_{Nu}	Nusselt number =	$\frac{hD}{k}$
N_{Re}	Reynolds Number	$= \frac{G_b D}{\mu}$

N_{Gr}	Grashof number =	$\frac{g d^3 \beta \Delta T}{\nu^2}$
N_{Pr}	Prandtl number =	$\frac{\nu}{\alpha}$

Subscripts

W	Heating surface
sat	Saturation condition
∞	Bulk liquid
min	Minimum
max	Maximum
int	Initiation
sup	Superheat
LH	Latent heat
Tot	Total
L	Liquid

BIBLIOGRAPHY

1. Zuber, N., "Hydrodynamic aspects of boiling heat transfer", Ph.D Thesis, University of California, June 1959.

2. Corty, C. and Foust, A. S., "Surface variable in nucleate boiling", Chem. Eng. Prog. Symp. Series, No. 17, 151, 1955. pp. 1 - 12.

3. Grant, I., "Studies in nucleate boiling", Ph.D Thesis, University of Edinburgh, 1963.

4. Jakob, M., "Heat transfer", Vol. 1, Wiley New York, 1949.

5. Gaertner, R. F., "Distribution of active sites in the nucleate boiling of liquids", Chem. Eng. Prog. Symp. Series, No. 41, 59, 1963. pp. 52 - 61.

6. Bushell, A. L., "Comments on nucleate boiling heat transfer correlations and suggestion for evaluating the number of active sites", R.A.E., Tech. Note Mech. Eng. 391, 1963.

7. Hsu, Y. Y. and Graham, R. W., "An artificial and experimental study of the thermal boundary layer on ebullition cycle in nucleate boiling ", N.A.S.A., Tech. Note D-594, 1961.

8. Yatabe, J. M. and Westwater, J. W., "Bubble growth rate for ethanol-water and ethanol isopropanol mixture", Chem. Eng. Prog. Symp. Series, No. 64, 62, 1966. pp. 17 - 23.

9. Han, C. Y. and Griffith, P., "The mechanism of heat transfer in nucleate pool boiling", Tech. Rept. No. 7673-14, M.I.T., 1962.

10. Ivey, H. J., "Relationship between bubble frequency departure diameter and rise velocity in nucleate boiling", Int. J. of Heat and Mass transfer, 101 1967. pp. 1023 - 1040.

11. McAdams, W. H., Kennel, W. B., Minden, C. S., Rudolf, C., Picornell, C., and Dew, J., "Heat transfer at high rates with surface boiling", Industrial and Eng. chemistry, 41, 1949.

12. Gaertner, R. F., and Westwater, J. W., "Population of active sites in nucleate boiling heat transfer", Chem. Eng. Prog. Symp. Series, No. 30, 46, 1960. pp. 39 - 48.

13. Gaertner, R. F., "Photographic study of nucleate pool boiling from horizontal surface", J. of Heat transfer, A.S.M.E. 1965.

14. Yamagata, K., Hirano, F., Nishikawa, K. and Matsuoka, H., "Nucleate boiling of water on the horizantal heating surface", Kyushu University, No. 1, 15, 1955.

15. Rohsenow, W. M., "Heat transfer with boiling", Developments in heat transfer, Edward Arnold Ltd., pp. 169 - 260, 1964.

16. Zuber, N., "Nucleate boiling : The region of isolated bubbles and the similarity with natural convection", Int. J. of Heat and Mass transfer, 6, 1963. P.57.

17. Fisher, J. C., "The fracture of liquids", J. App. phys., 19, 1948. pp.1062 - 1067.

18. Bankoff, S. G., "Ebullition from solid surfaces in the absence of pre-existing gaseous phase", Trans. A.S.M.E., 1967. pp. 735 - 740.

19. Clark, H.B., Strenge, P.S., and Westwater, J.W., "Active sites for nucleate boiling", Chem. Eng. Prog. Symp. Series, No. 29, 55, 1969. pp. 103 - 110.

20. Westwater, J. W., "Boiling heat transfer", American Scientist, 47, 1959. pp. 427 - 446

21. Griffith, P. and Wallis, J. D., "The role of surface conditions in nucleate boiling", report No. 14, M.I.T., 1968.

22. Hsu, Y. Y., "On the size of active nucleation cavities of heating surface", J. of Heat transfer and Basic Eng., A.S.M.E., 84, 1962. pp. 207 - 216.

23. Hatton, A. P. and Hall, I. S., "Photographic study of boiling on prepared surfaces", Proc. of the 3rd Int. Heat transfer conf., Chicago, 1966. I.Mech.E. pp. 24 - 37.

24. Howell, J. R., and Siegel, R., "Incipience, growth and detachment of boiling bubbles in saturated water from artificial nucleation sites of known geometry and size", Proc. of the 3rd Int. Heat transfer Conf., Chicago, 1966. A.I.Ch.E., pp. 12 - 23.

25. Bosnjakavic, F., "Verdampfung und Flussigheitsubehitzung", Tech. Mech. und Therm., Bd. 1, 1930.

26. Fritz, W. and Ende, W., "Verdampfungsvorgang noch Kinemalogrhisheu Aufnahmen dampsfblasen", Phys. Zt., 37 1936.

27. Plesset, M. S. and Zwick, S. A., "The growth of vapour bubble in superheated liquids", J. App. phys., No. 4, 25, 1954.

28. Forster, H. K. and Zuber, N., "Growth of vapour bubbles in superheated liquid", J. App. phys., No. 4, 25, 1954.

29. Chang, Y. P., "Some possible critical conditions in nucleate boiling", J. of Heat transfer, A.S.M.E., Series, C, No. 2, 85, 1963.

30. Fritz, W., "Berechnung des maximal volumin von dampfblasen", phys. Zt. 37, 1936.

31. Staniszewski, B.E., "Nucleate boiling bubble growth and departure", report No. 16, M.I.T., 1959.

32. Semeria, R. L., "An experimental study of the characteristic of vapour bubbles", Symp. two-phase fluid flow, I.Mech.E. 1962.

33. Nishikawa, K. and Urakawa, K., "An experiment of nucleate boiling under reduced pressure", Fac.of Eng. University of Kyushu, 19, 139, 1960.

34. Patten, T. D., "Some characteristic of nucleate boiling of water at sub-atmospheric pressures", Paper 9, Thermodynamics and fluid mechanics convention, Proc., I.Mech.E., 1964.

35. Cole, R. and Shulman, L., "Bubble departure diameter at sub-atmospheric pressure", Chem. Eng. Prog. Symp. Series, 64, 62, 1966.

36. Cole, R., "Bubble frequency and departure volume at sub-atmospheric pressure", J. A.I.Ch.E., No. 4, 13, 1965. pp. 779 - 783.

37. Strenge, P. H., Orell, A. and Westwater, J. W., "Microscopic study of bubble growth during nucleate boiling", J. A.I.Ch.E., 7, 1961. P. 578.

38. Marcus, B.D., "Experiments on the mechanism of saturation nucleate pool boiling heat transfer", Ph.D Thesis, Cornell University, 1963.

39. Eckert, E.R.G., "Introduction to transfer of heat and mass", 1st Edn., P. 53, McGraw-Hill, New York 1950.

40. Carrie, G. M. and Patten, T. D., "Active sites and the initiation of nucleate boiling", research report, Heriot-Watt University 1967.

41. Van Stralen, S. T. D., "Heat transfer to boiling binary mixture at atmospheric and sub-atmospheric pressures", Chem. Eng. Society, 5, 290, 1956.

42. Lienhard, J. H. and Schrock,V. E., "The effect of pressure, geometry, and the equations of state upon the peak and minimum boiling heat flux", J. Heat transfer A.S.M.E., 85, 1963 P.261.

43. McFadden, P. W. and Grossman, P., "The relation between bubble frequency and diameter during nucleate pool boiling", Int. J. of Heat and Mass Transfer, 5, 1962. pp. 169 - 173.

44. Perkins, K. S. and Westwater, J. W., "Measurements of bubble formed in boiling methonal", J. A.I.Ch.E., 2, 1965. pp. 471 - 476.

45. Grant, I. D., Patten, T. D., and Carrie, G. M., "Inception of nucleate boiling of water at pressures above atmospheric : characteristics of a horizontal surface bearing a normal distribution of cavities", Paper 17, Thermodynamics and fluid mechanics convention, Proc. I.Mech.E., 1968.

46. Han, C. Y., "Mechanism of haat transfer in nucleate pool boiling", D.Sc. Thesis, M.I.T., 1962
*Referred to in "Development in heat transfer", Rohsenow, Edward-Arnold, London. 1964.

47. Rohsenow, W. M. and Clark, J. A., "Heat transfer and pressure drop data for high heat flux densities to water at high sub-critical pressure", Heat transfer and fluid Mechanics Inst. 1951.

48. Cichelli, M. T. and Bonilla, C. F., Heat transfer to liquid boiling under pressure", J. A.I.Ch.E., 41, 1945. P. 755.

49. Vachon, R. I., Nix, G. H., and Tong, G.E., "Evaluation of constant for the Rohsenow pool-boiling correlation", J. of Heat Transfer, A.S.M.E., 1968. pp. 239 - 246.

50. Malkas, W. R., "Discrete transition in turbulent convection", Proc. Roy.Soc.A., 225, 1954. P.185.

51. Peebles, F. N. and Garber, H. J., "Studies on the motion of gas bubbles in liquids", Chem. Eng. Prog., 49, 1953. P.88.

52. Moore, F. D. and Mesler, R. B., "The measurement of rapid surface temperature fluctuation during nucleate boiling of water", A.I.Ch.E.J., P 620-624, 1961.

53. Rallis, C. J. and Jawurek, H. H., "Latent heat transport in saturated nucleate boiling", Int. J. Heat and Mass transfer, 7, 1964. pp. 1051 - 1068.

54. Howie, R.C., Private communication. Department of Chemistry, Heriot-Watt University.

55. Elrod, W. C., Clark, J. A., Lady, E. R. and Merte, H., "Boiling heat-transfer data at low heat flux", J. of Heat transfer, A.S.M.E., 1967, pp. 235 - 242.

56. Even, U. R., "The corrosion and oxidation of metals", Edward Arnold, London, 1960.

57. Golovin, U. S., Kolchugin, B. A. and Zakharova, E. A., "Measurement of the rate of growth of vapour bubbles during the boiling of different liquids", Teplofizika Vysokish Temp., No. 1, 4, 1966. pp. 147 - 148.

58. Lackme, C., "Some statistical properties of two-phase flow in vertical tubes", proc. symp. of two phase flow, 2, 1965. pp. D201 - D213.

59. Shalton, J., "Electro-magnetic theory", McGraw-Hill, 1941, P.206.

60. Kip. A. F., "Fundamentals of electricity and magnetism", McGraw-Hill, 1962. P.55

61. Hole, N., obtained from:- "Radio active Isotopes", Whitehouse and Putman, Oxford, 1953.

62. Hatton, A. P., James, D.D., and Liew, T. L., "Photographic study of bubble formation from prepared cavities in nucleate pool-boiling", Research Report - private communication 1969.

63. Zuber, N., "Recent trends in boiling heat transfer research, part 1, nucleate pool-boiling", App. Mech. Rev., No. 9, 17, 1964.

64. Johnson, M. A., Pena, J. and Mesler, R.B., "Bubble shapes in nucleate boiling", Chem. Eng. Prog. symp. series, No. 64, 62. 1966. pp. 1 - 5.

65. Marcus, B. D. and Dropkin, D., "Measured temperature profiles within the superheated boundary layer above a horizontal surface in saturated nucleate pool-boiling of water", J. Heat transfer, A.S.M.E. No. 3, 87, 1965.

66. Wei, C.C. and Breckshot, G.W., "Photographic evidence of bubble departure from capillaries during boiling", Chem. Eng. Sci., 19, 839, 1964.

67. Kosky, P.G., "Nucleation site instability in nucleate boiling", Int. J. Heat Mass Transfer, 11, 1968. pp. 929 - 932.

68. Kirby, D.B. and Westwater, J.W., "Bubbles and vapour behaviour on a heating horizontal plate during pool-boiling near burnout", Chem. Eng. Prog. Symp. Series, No. 57, 61. 1965.

69. McNeill, J., "Thickness of the thermal layer during free-convection, non-boiling heat transfer from a horizontal surface", Project for Honours degree, Mech. Eng. Dept. University of Edinburgh, 1966.

70. Grant, I. D. R. and Patten, T.D., "Thickness of the thermal layer at the initiation of nucleate pool boiling ", Paper 16, Boiling heat transfer in steam-generating units and heat exchangers, Proc. Intn. Mech. Engrs. 1965. P.124.

71. Siegel, R. and Keshock, E.G., "Effects of reduced gravity on nucleate boiling bubble dynamics in saturated water", A.I.Ch.E.J. 10( ), 509, 1964.

Cavity Number	Surface A	Surface A^1	Surface B	Surface B^1	Surface C	Surface D	Surface F	Cavity Size inch.
1	0.001144	0.00356	0.00316	0.00368	0.0076	0.01505	0.02201	
2	0.002538	0.00310	0.00348	0.00324	0.00765	0.01485	0.01625	
3	0.00022	0.00324	0.00247	0.00294	0.0085	0.0096	0.01884	
4	0.00192	0.00226	0.00405	0.00488	0.0090	0.0092	0.0250	
5	0.000350	0.0030	0.00275	0.00444	0.0004	0.0172	0.0143	
6	0.002393	0.00268	0.00213	0.00450	0.010	0.01695	0.02202	
7	0.002315	0.00280	0.00298	0.00518	0.01005	0.00962	0.00916	
8	0.00210	0.00190	0.00226	0.0068	0.0103	0.00903	0.01796	
9	0.000817	0.000868	0.00160	0.00564	0.0138	0.0136	0.01142	
10	0.00036	0.00076	0.00282	0.0001	0.0135	0.0129		
11	0.00226	0.00088	0.000465	0.00210	0.0075	0.0115		
12	0.00232	0.00368		0.00372	0.0092	0.00995		
13	0.00194	0.00164		0.00310	0.01453	0.00282		
14	0.00216	0.00158		0.00530	0.0150			
15		0.00052						

Table (a)

Surface characteristics

Table (1b)
Surface Characteristics.

Test Surface	Average cavity radius in	Standard deviation in	Largest cavity radius in	Smallest cavity radius in	Number of cavities
NG1	0.003809	0.000423	0.00498	.00310	120
NG2	0.00176	0.0002342	0.002514	0.00108	124
NG3	0.002805	0.001069	0.00578	0.0005	124

Table (2a)
Sample of frequency correction.

Test Surface	Frequency Measured	Corrected frequency	Heat flux Btu/ft^2hr.
NG1	54	74	5,000
	62	90	10,000
	61	88	15,000
	58	80.5	20,000
	54	74	25,000
	53	72.2	30,000

Test Surface	Frequency Measured	Corrected Frequency	Heat flux Btu/ft^{2}hr.
NG2	20	23.2	5,000
	50	66.8	10,000
	58	81.5	15,000
	54	74.0	20,000
	53	72.2	25,000
	50	66.6	30,000

Table (2b)

Test Surface	Frequency Measured	Corrected Frequency	Heat flux Btu/ft^{2}hr.
NG3	35	42.3	5,000
	50	66.8	10,000
	53	72.2	15,000
	53	72.2	20,000
	50	66.8	25,000
	46	59.9	30,000

Table (2C)

Heat flux Btu/ft.hr.	Atm. Pressure			30 psi			45 psi			65 psi		
	T °F	t_g sec	t_w sec	T °F	t_g sec	t_w sec	T °F	t_g sec	t_w sec	T °F	t_g sec	t_w sec
2000	5.3	0383	300	5.2	0593	292	6.4	097	207	4.8	134	246
5000	10.2	00825	178	10.0	016	172	9.2	028	133	8.5	0428	0715
10000	13.4	0048	0775	13.3	009	0766	11.4	017	056	10.2	0295	0435
15000	14.9	00385	0425	15.0	0071	043	12.8	0136	0314	11	0247	0226
20000	15.9	0034	0271	16.0	0062	0275	13.2	0128	0187	11.3	0217	0135
25000	16.6	00302	0189	16.4	0059	0185	13.6	012	0127	11.4	0214	0086

TABLE (3a)

Calculations growth and waiting times for surface D

Heat flux Btu/ft.hr.	Atm. Pressure			45 psi			60 psi			75 psi		
	T °F	t_g sec	t_w sec	T °F	t_g sec	t_w sec	T °F	t_g sec	t_w sec	T °F	t_g sec	t_w sec
2000	4.0	0535	1715	2.8	268	084	2.0	703	0427	1.6	1.3	0272
5000	8.2	0130	116	4.2	127	031	3.6	2165	0222	3.6	258	0209
10000	12.9	0098	0715	7.2	0433	0222	6.0	077	0154	6.0	0915	0153
15000	16.4	0032	0512	10.0	0224	0189	9.5	0304	0170	9.0	0404	0152
20000	19.0	0023	0377	13.0	0133	01815	11.8	0203	01488	11.6	0248	0143
25000	20.7	00199	0295	14.9	0103	0151	14.0	0143	0134	14.8	0151	0149
30000	22.2	00175	0236	16.0	00865	0121	17.2	0094	014	17.0	0113	0137

TABLE (3a)

Calculations growth and waiting times for surface NG3

Measured Q/A $Btu/ft^2hr.$	Predicted Q/A from Equ. (5.6.7) with experimental values of N, P. R.	Predicted Q/A from Equ. (5.6.7) with experimental values and a constant E	Test Surface	Pressure lb/in^2
5,000	6250	6250	NG1	atm.
10,000	12930	12930	"	"
15,000	15790	15790	"	"
20,000	16050	19770	"	"
25,000	15805	23753	"	"
30,000	15112	26212	"	"

Table (4a)

Heat flux predictions from Equation (5.6.7)

Measured Q/A Btu/ft^{2}hr.	Predicted Q/A from Equ. (5.6.7) with experimental value of N.P.R	Predicted Q/A value with constant E included	Test Surface	Pressure lb/in^2
5,000	3446	3446	NG2	atm.
10,000	9895	9895	"	"
15,000	15160	15160	"	"
20,000	16350	20050	"	"
25,000	16978	25028	"	"
30,000	15070	25365	"	"
35,000				

Table (46)

Heat flux predictions from Equation (5.6.7)

Measured Q/A Btu/ft^{2}hr.	Predicted Q/A from Equ. (5.6.7)with N,f,R exp.	PredictedQ/A value with E constant included	Test Surface	Pressure lb/in^2
5,000	5155	5155	NG3	atm.
10,000	11645	11645	"	"
15,000	15555	15555	"	"
20,000	17655	21698	"	"
25,000	19052	27652	"	"
30,000	17000	28600	"	"
35,000				

Table (4C)

Heat flux predictions from Equation (6 · 6.7)

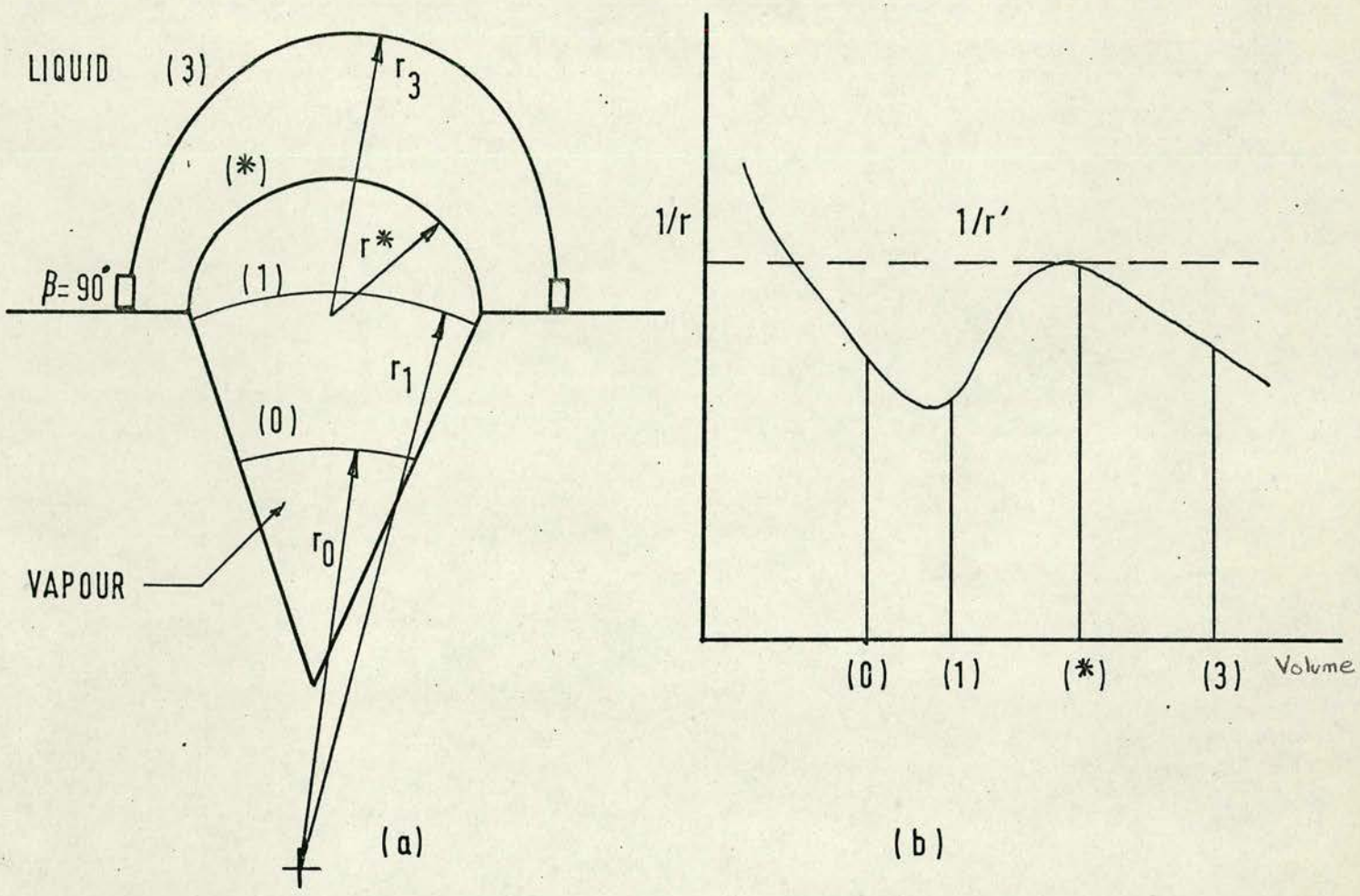

FIG.(1) THE PROPOSED MODEL ON WHICH GRIFFITH & WALLIS INTRODUCED THEIR INITIATION CRITERION

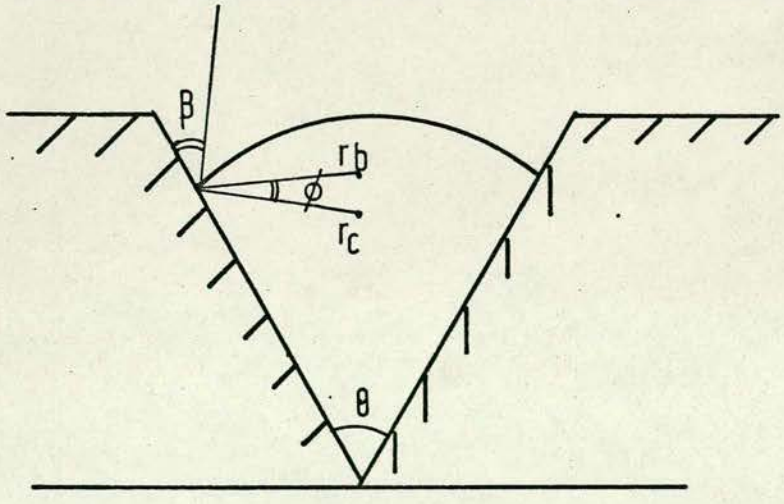

FIG.(2) IDEAL CONICAL CAVITY

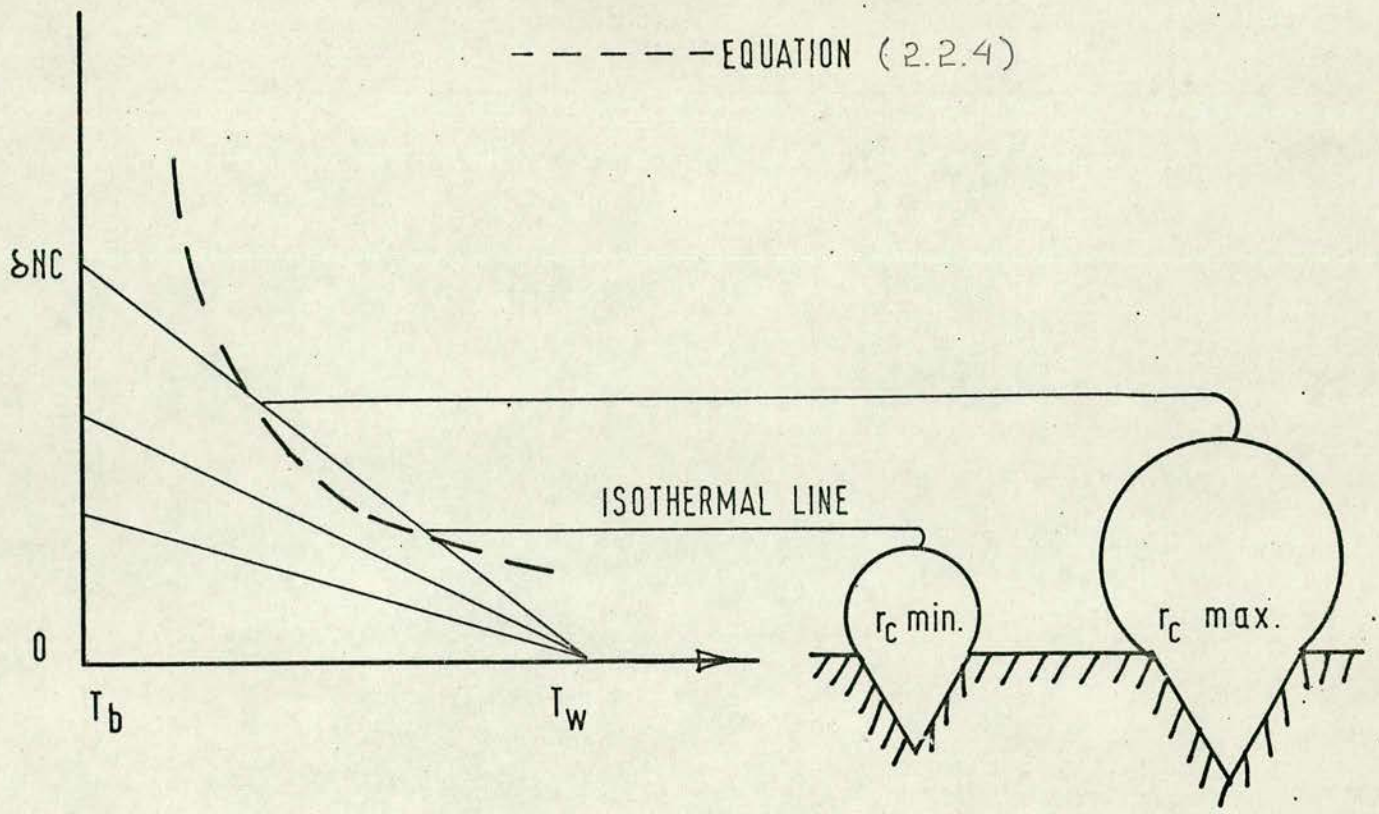

FIG.(3) MODEL FOR BUBBLE INITIATION AS PROPOSED BY HAN & GRIFFITH (9)

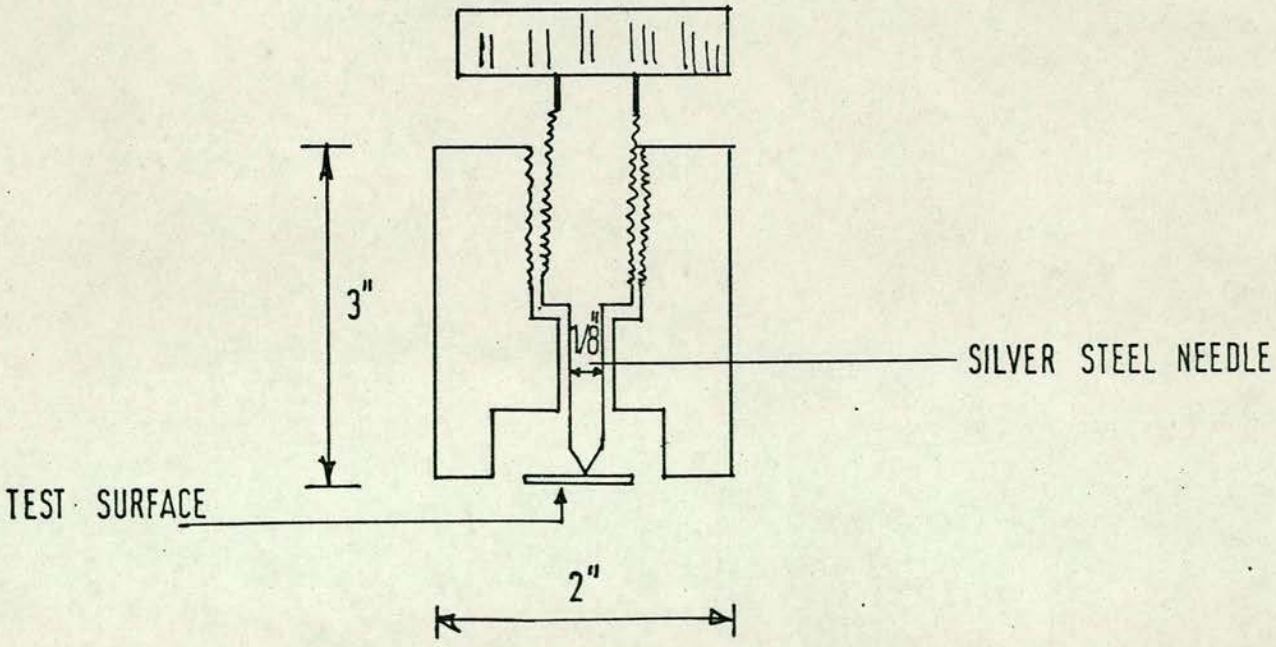

FIG.(4) THE DEVICE USED IN CREATING CAVITIES WITH RADII $\leqslant 7 \times 10^{-3}$ IN

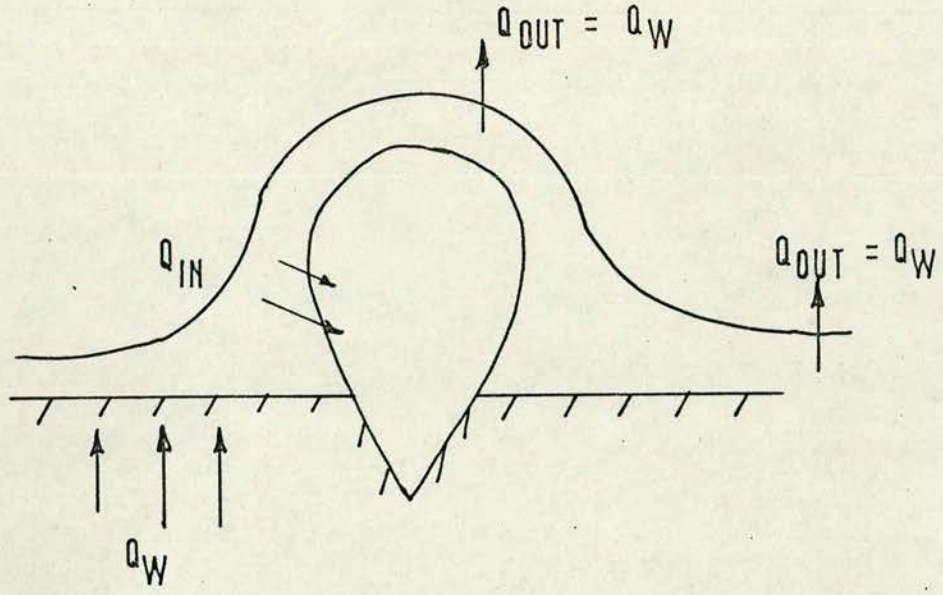

FIG.(5) BUBBLE GROWTH MODEL ZUBER (1)

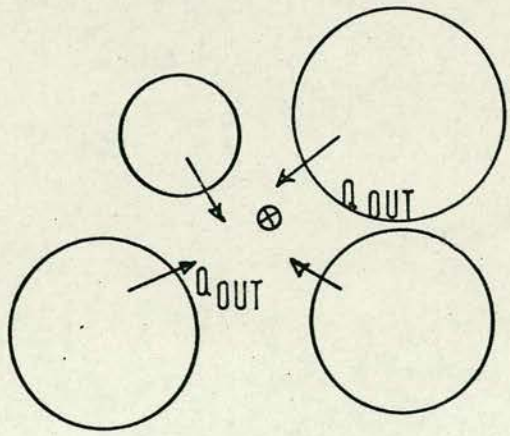

FIG.(6) HEAT LOST FROM NEIGHBOURING BUBBLES TO THE VICINITY OF POTENTIAL SITE

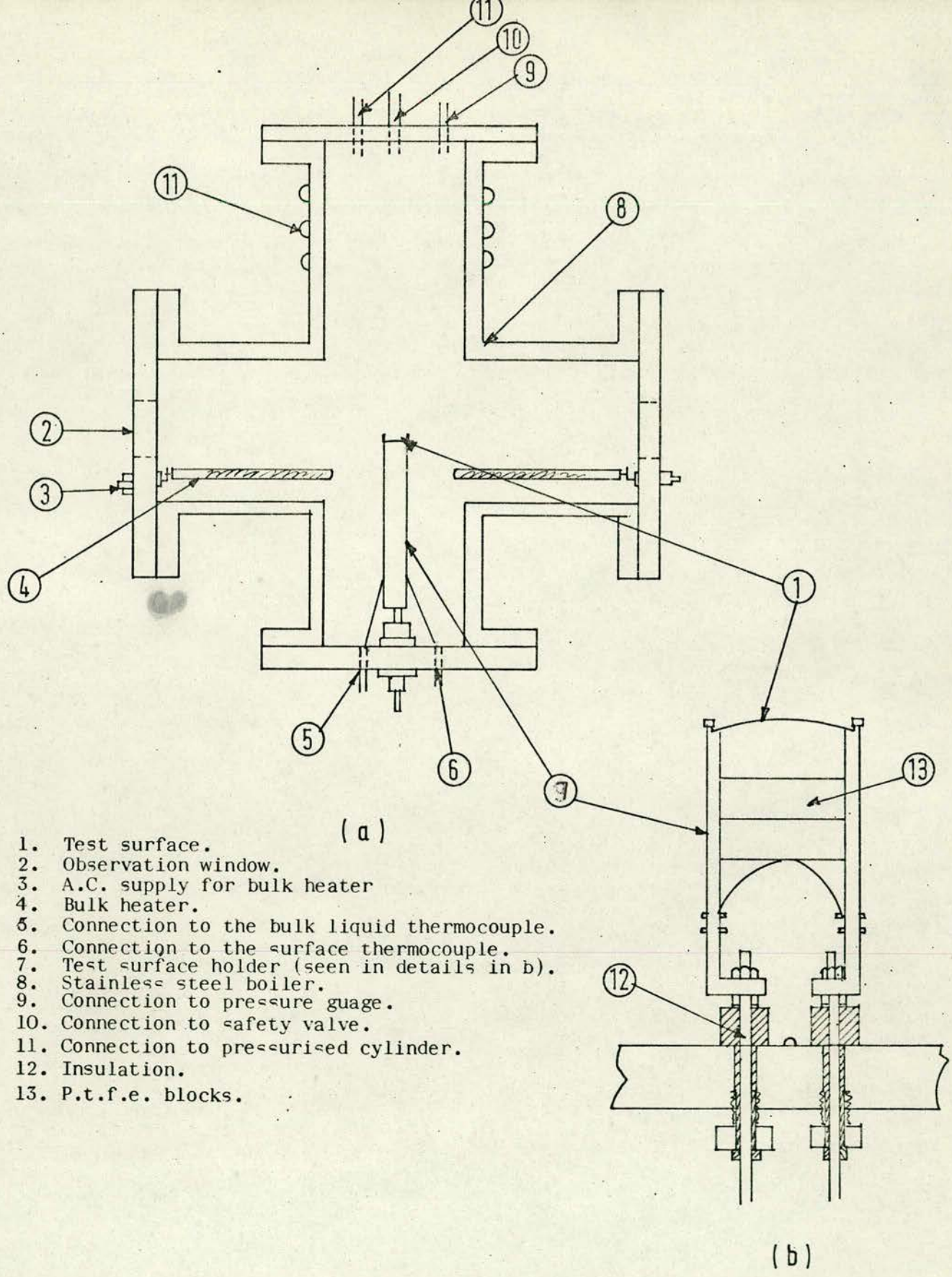

1. Test surface.
2. Observation window.
3. A.C. supply for bulk heater
4. Bulk heater.
5. Connection to the bulk liquid thermocouple.
6. Connection to the surface thermocouple.
7. Test surface holder (seen in details in b).
8. Stainless steel boiler.
9. Connection to pressure guage.
10. Connection to safety valve.
11. Connection to pressurised cylinder.
12. Insulation.
13. P.t.f.e. blocks.

FIG. (7) SECTION THROUGH THE BOILING VESSEL AND THE TEST SURFACE HOLDER

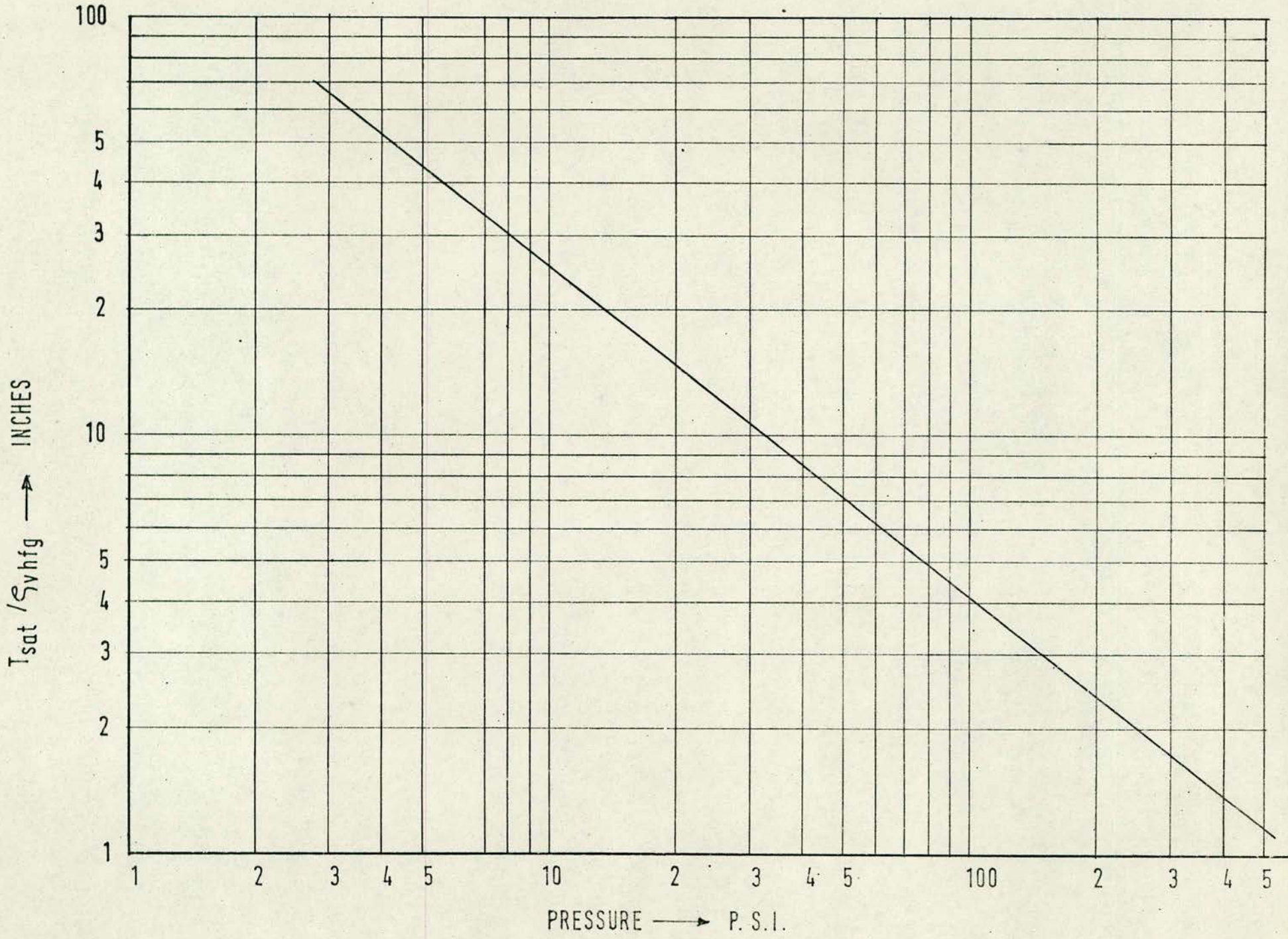

FIG. (8) VARIATION OF $T_{sat}/\rho_v h_{fg}$ WITH PRESSURE.

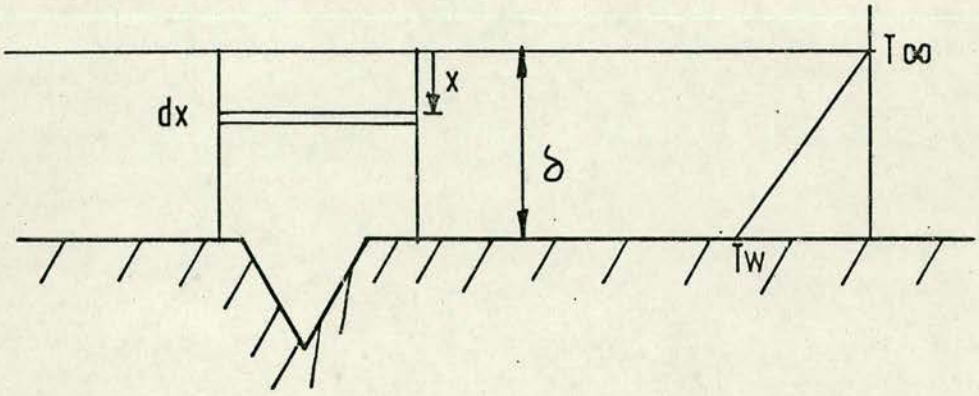

FIG.(9) A MODEL FOR CALCULATING THE WAITING TIME , tw , AND THE TEMPERATURE PROFILE

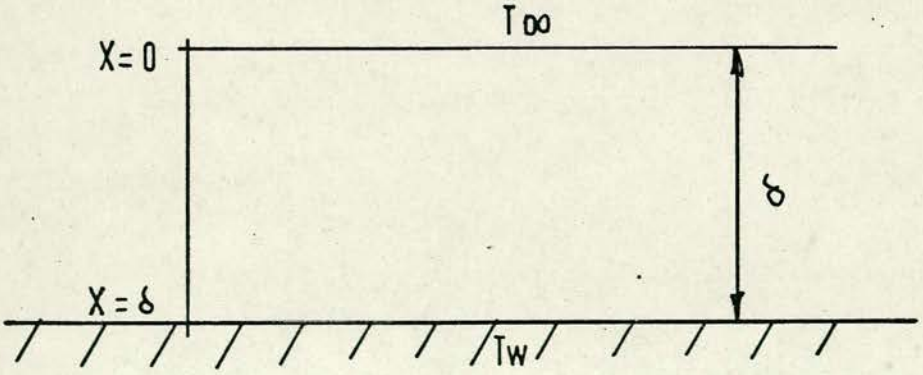

FIG.(10) BOUNDARY CONDITIONS USED BY Hsu(22) IN CALCULATING THE HEAT CONDUCTED THROUGH THE THERMAL LAYER

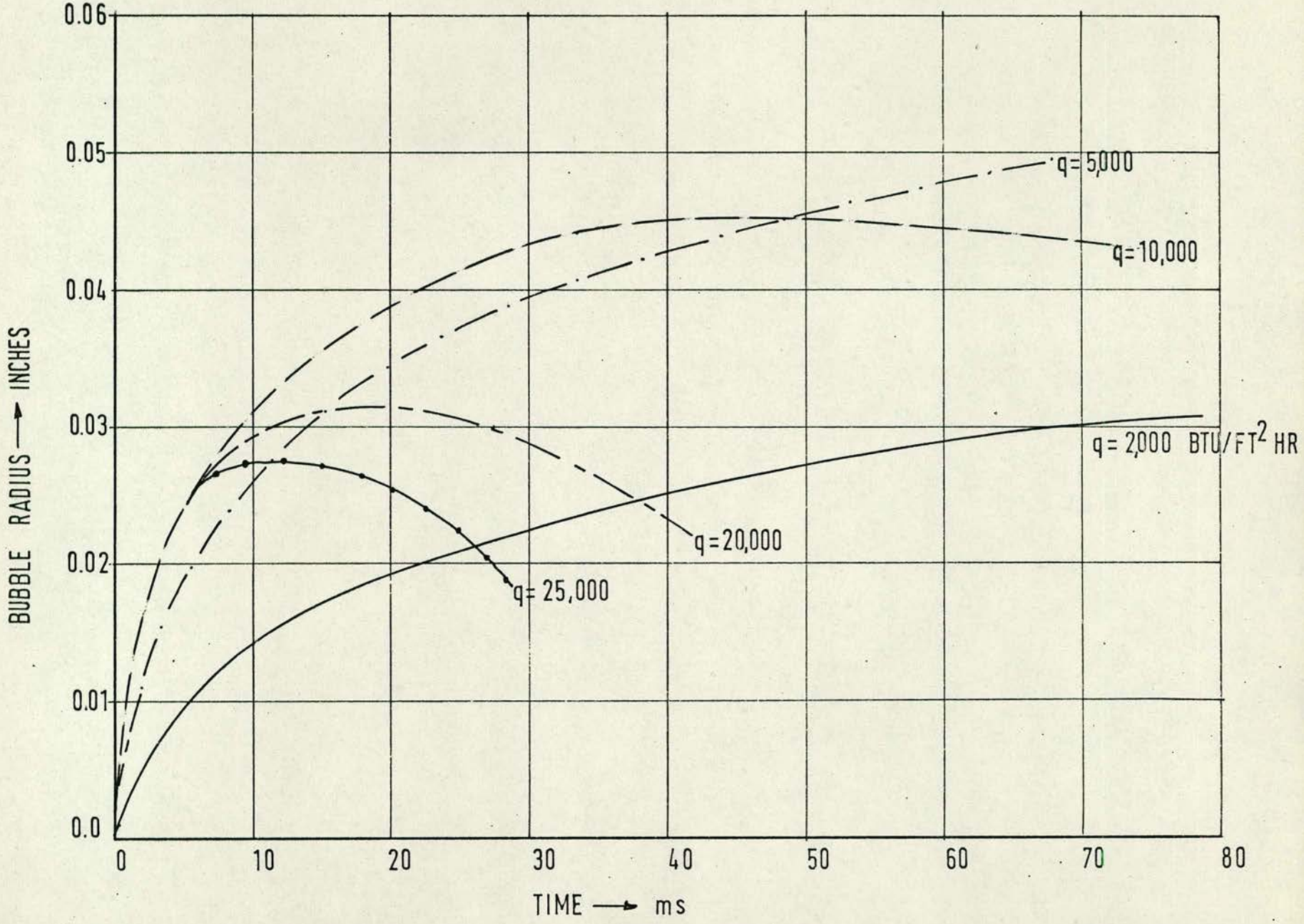

FIG.(11) BUBBLE GROWTH RATE PREDICTED BY ZUBER EQUATION (2.34)

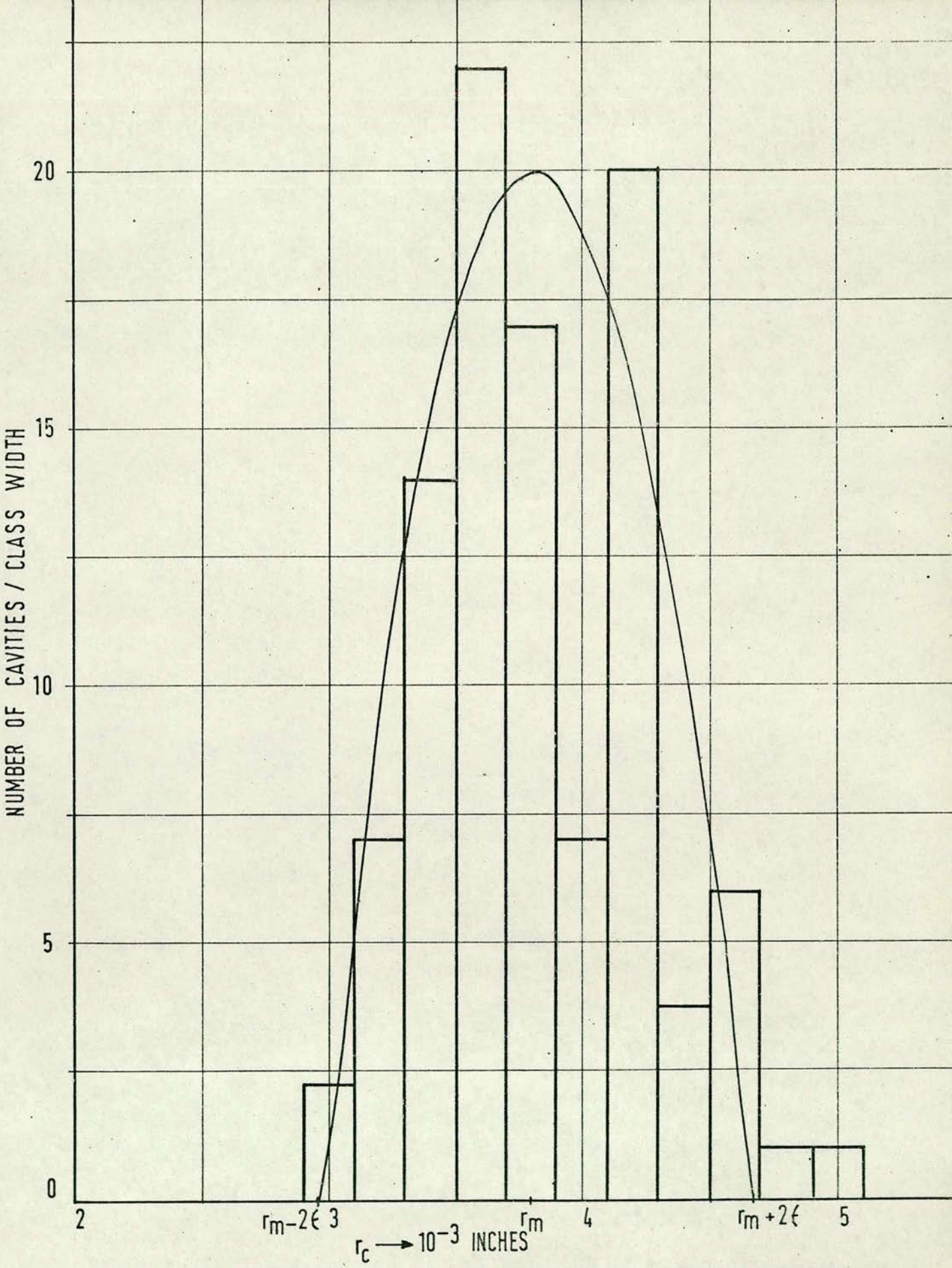

FIG. (12) HISTOGRAM OF CAVITY SIZE DISTRIBUTION FOR SURFACE NG 1

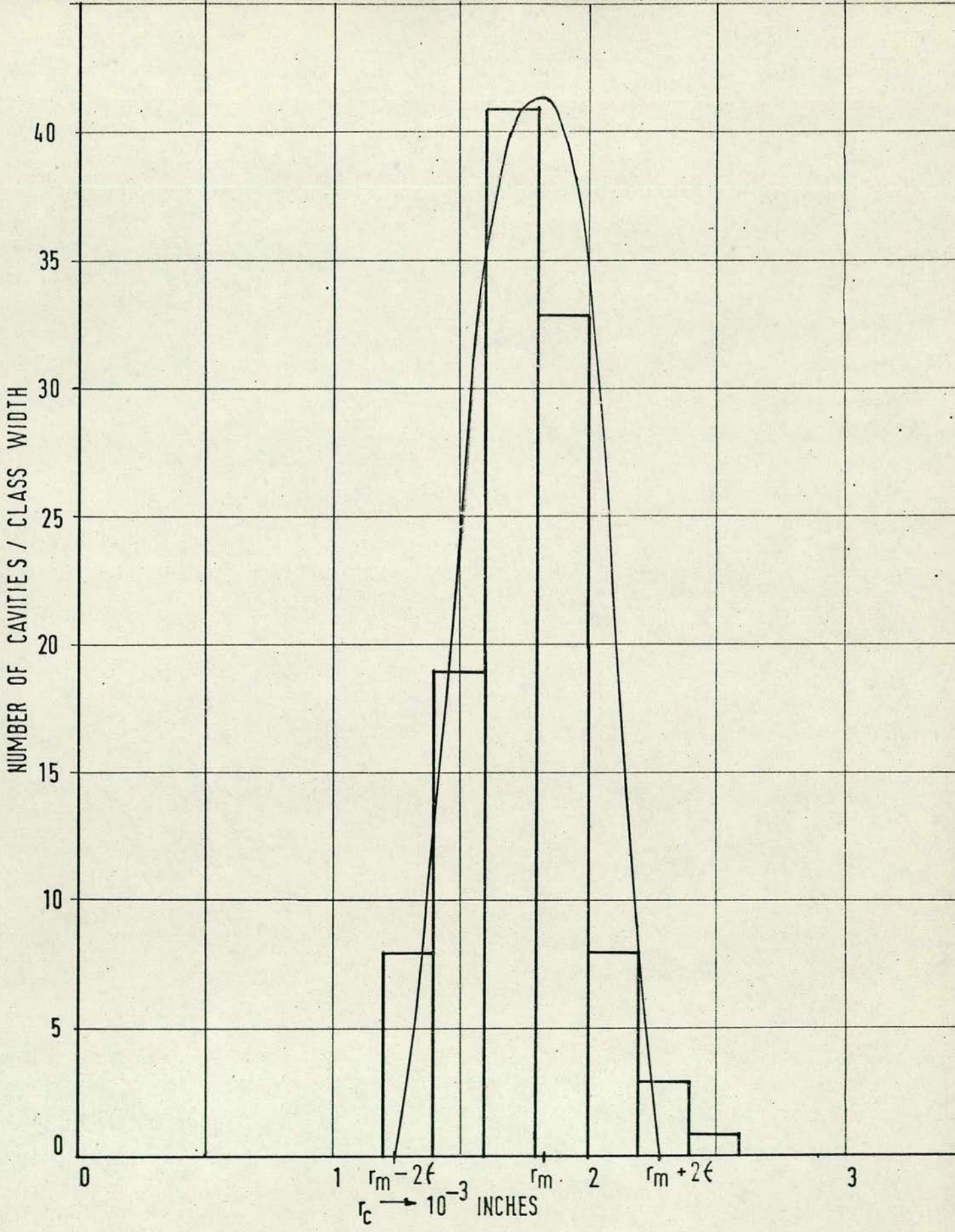

FIG. (13) HISTOGRAM OF CAVITY SIZE DISTRIBUTION FOR SURFACE NG 2

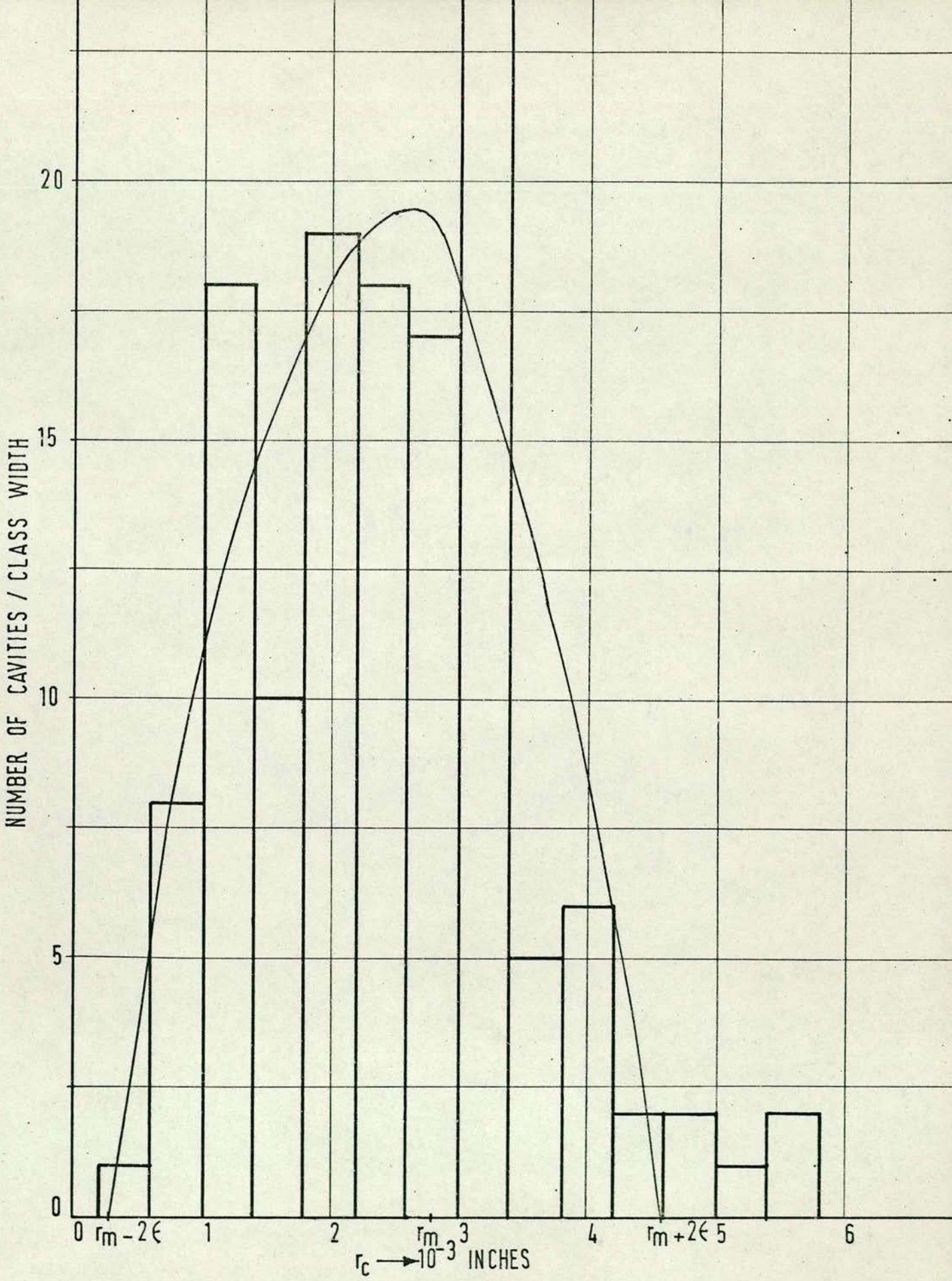

FIG. (14) HISTOGRAM OF CAVITY SIZE DISTRIBUTION FOR SURFACE NO 3

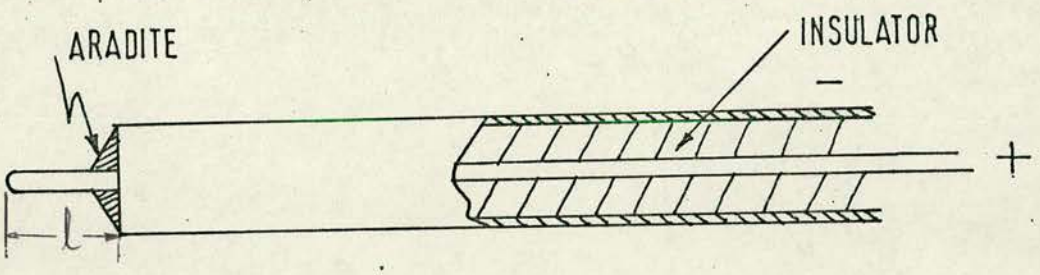

FIG.(15) SECTION THROUGH SINGLE BUBBLE FREQUENCY PROBE

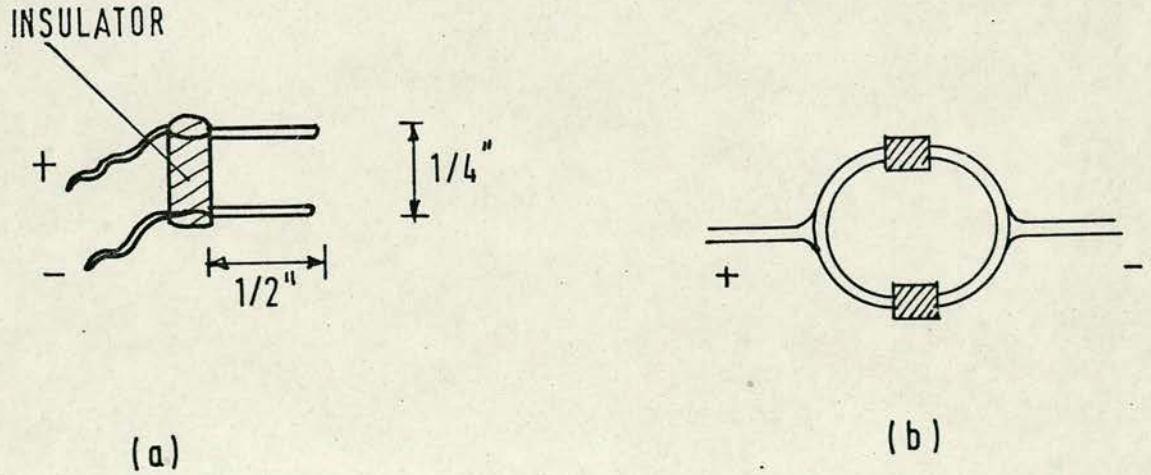

FIG.(16) MODIFICATION OF THE FREQUENCY PROBE

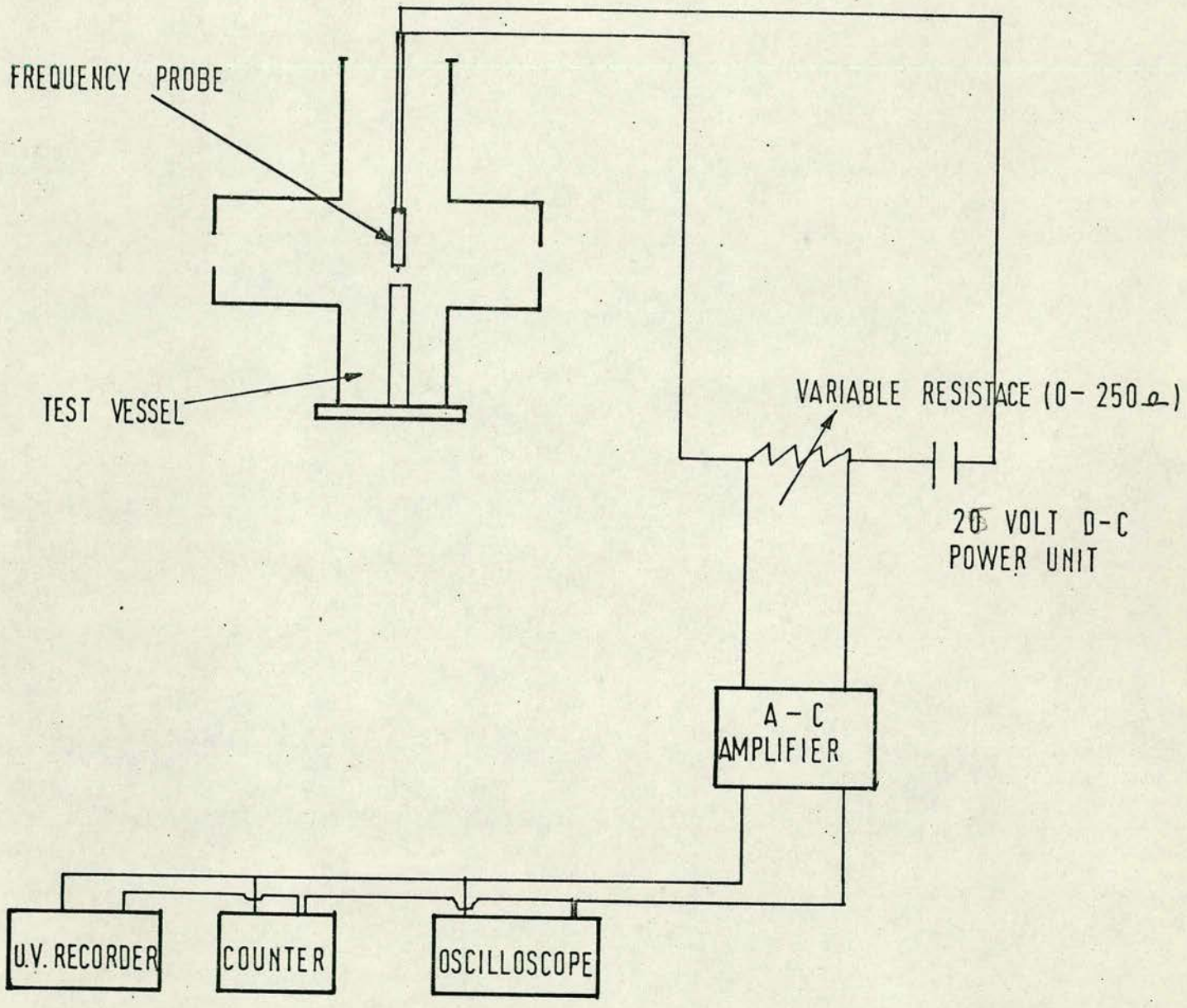

FIG. (17) SYSTEMATIC LAYOUT OF FREQUENCY MEASUREMENTS

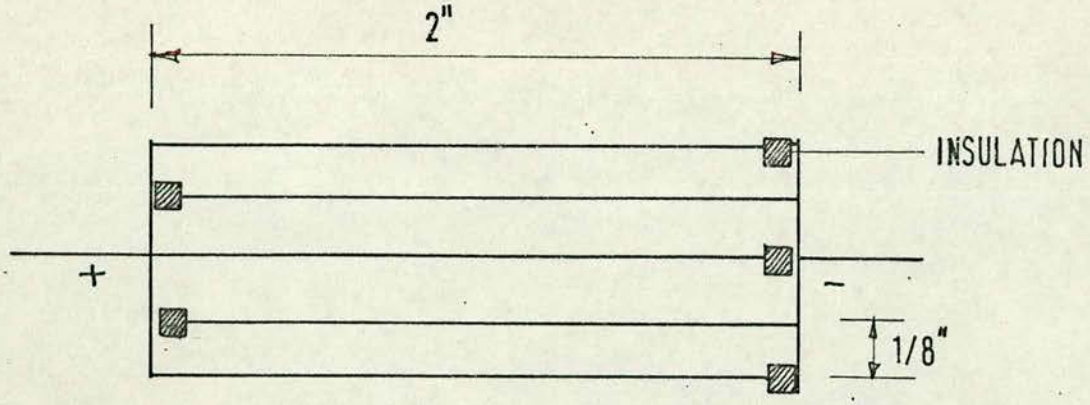

FIG.(18) FREQUENCY PROBE FOR DETERMINATION OF TOTAL BUBBLE POPULATION

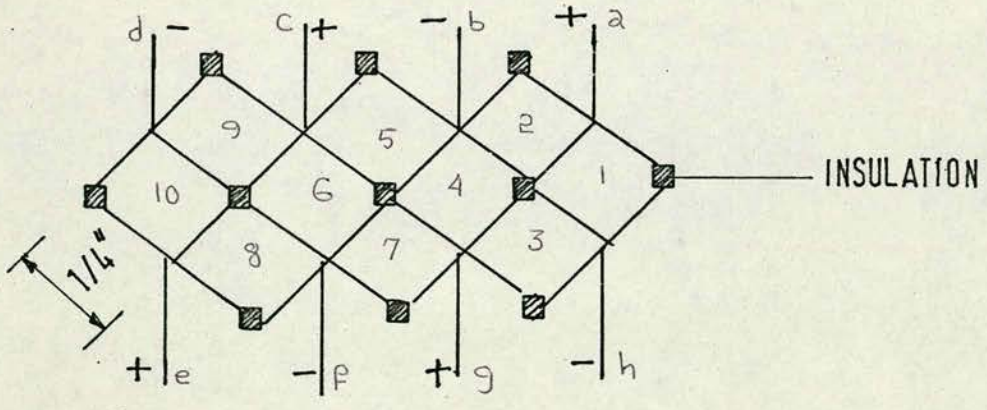

FIG.(19) FREQUENCY PROBE FOR DETERMINATION OF FREQUENCY ON A SPECIFIED SECTION OF THE TEST SURFACE

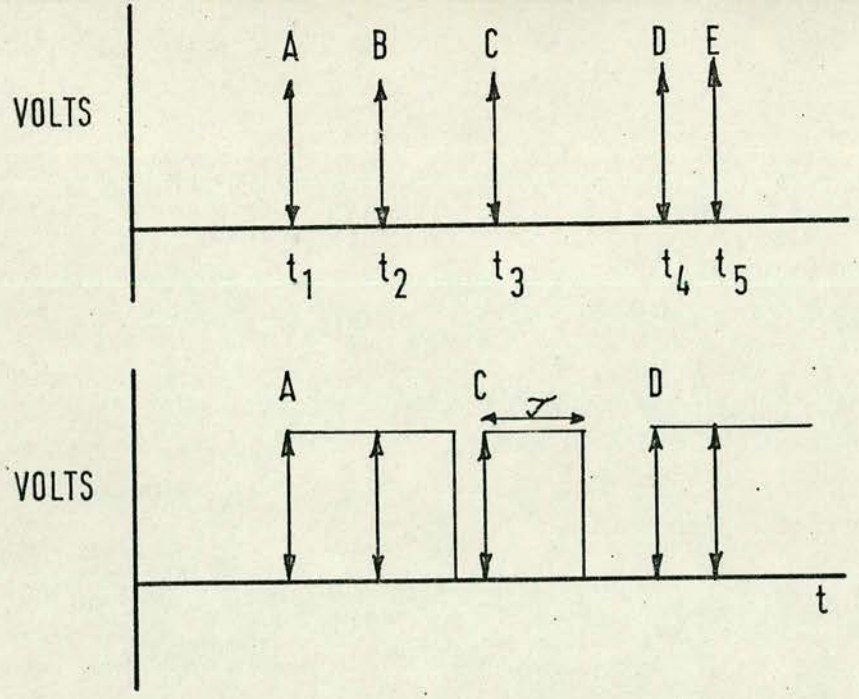

FIG.(20) THE EFFECT OF THE DEAD TIME, τ, ON BUBBLE COUNTING. ONLY A, C & D CAN BE DETECTED

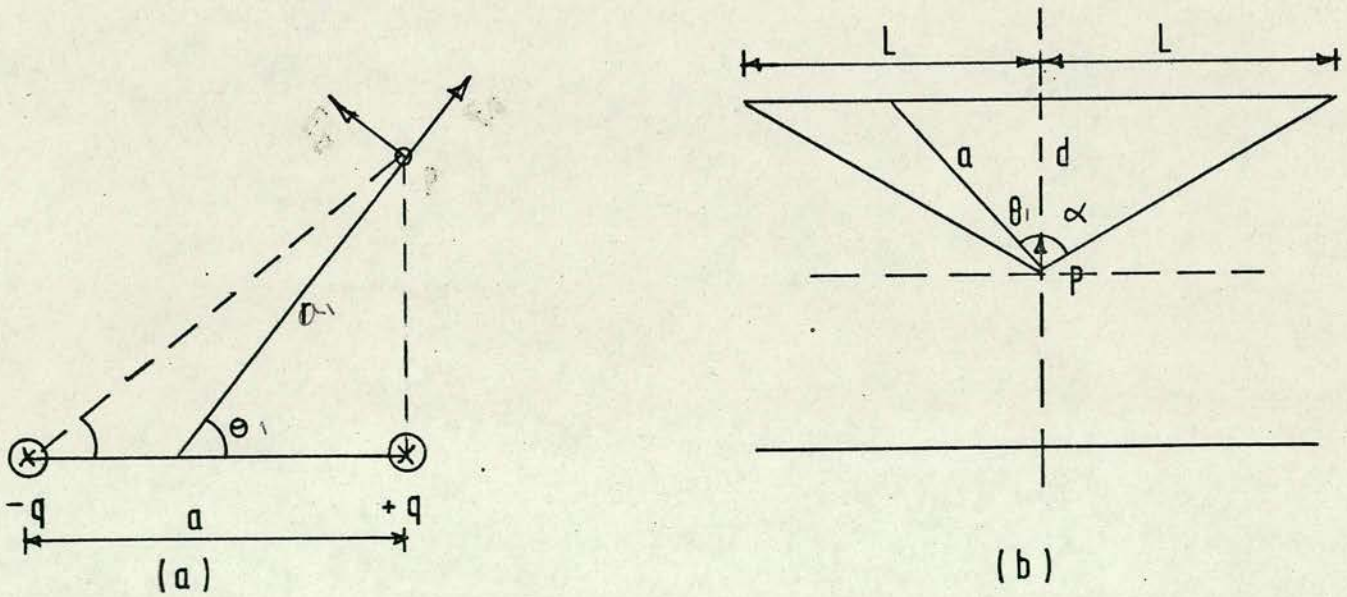

FIG.(21) ILLUSTRATING DIAGRAMS USED IN OBTAINING EQUATION (6.4.7)

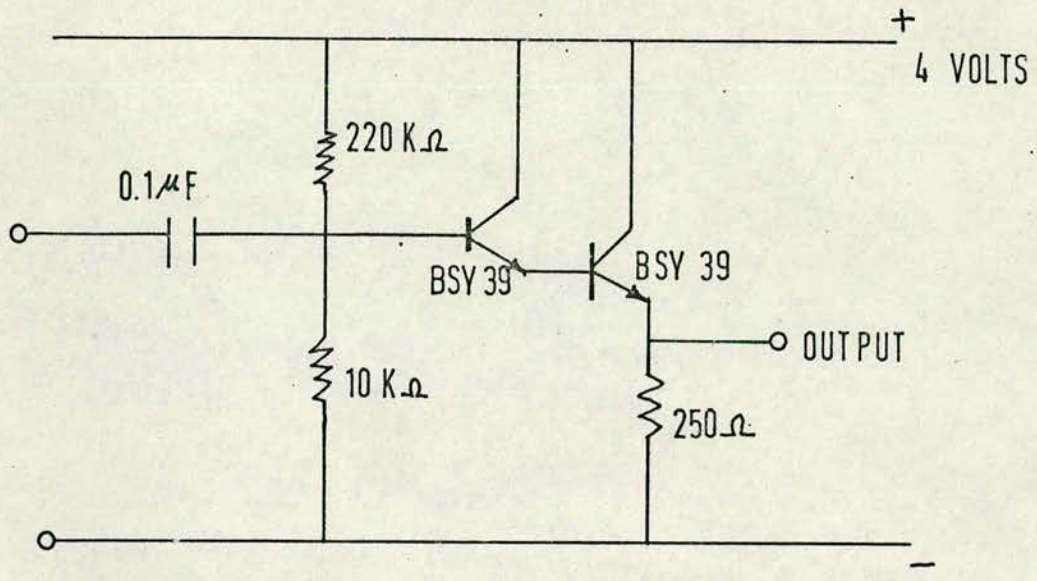

FIG. (22) DIFFERENTIAL CIRCUIT USED IN CONJUNCTION WITH FREQUENCY PROBE

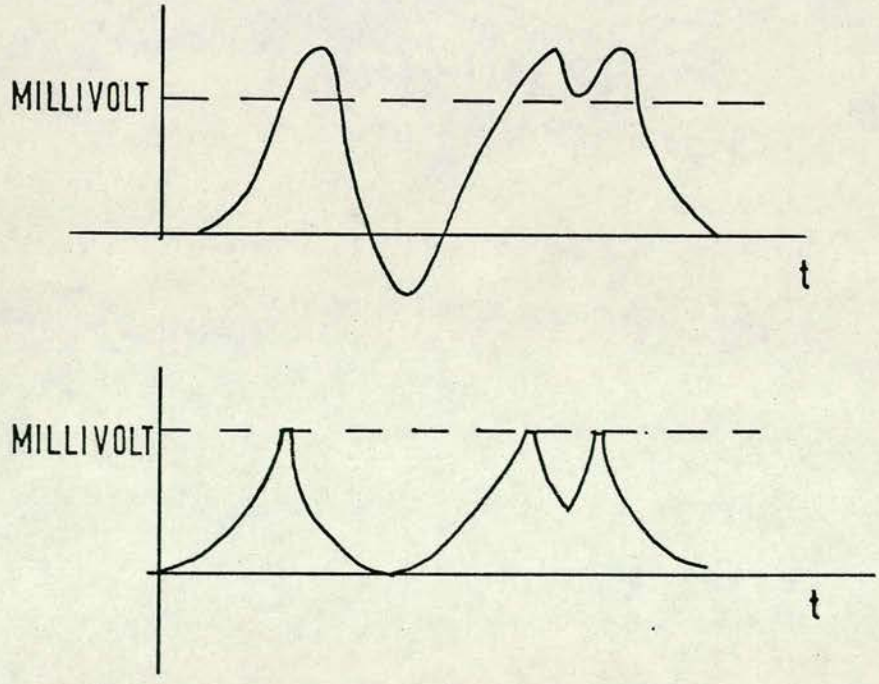

FIG. (23) THE EFFECT OF DIFFERENTIAL CIRCUIT ON A SAMPLE OF FREQUENCY PROBE SIGNAL

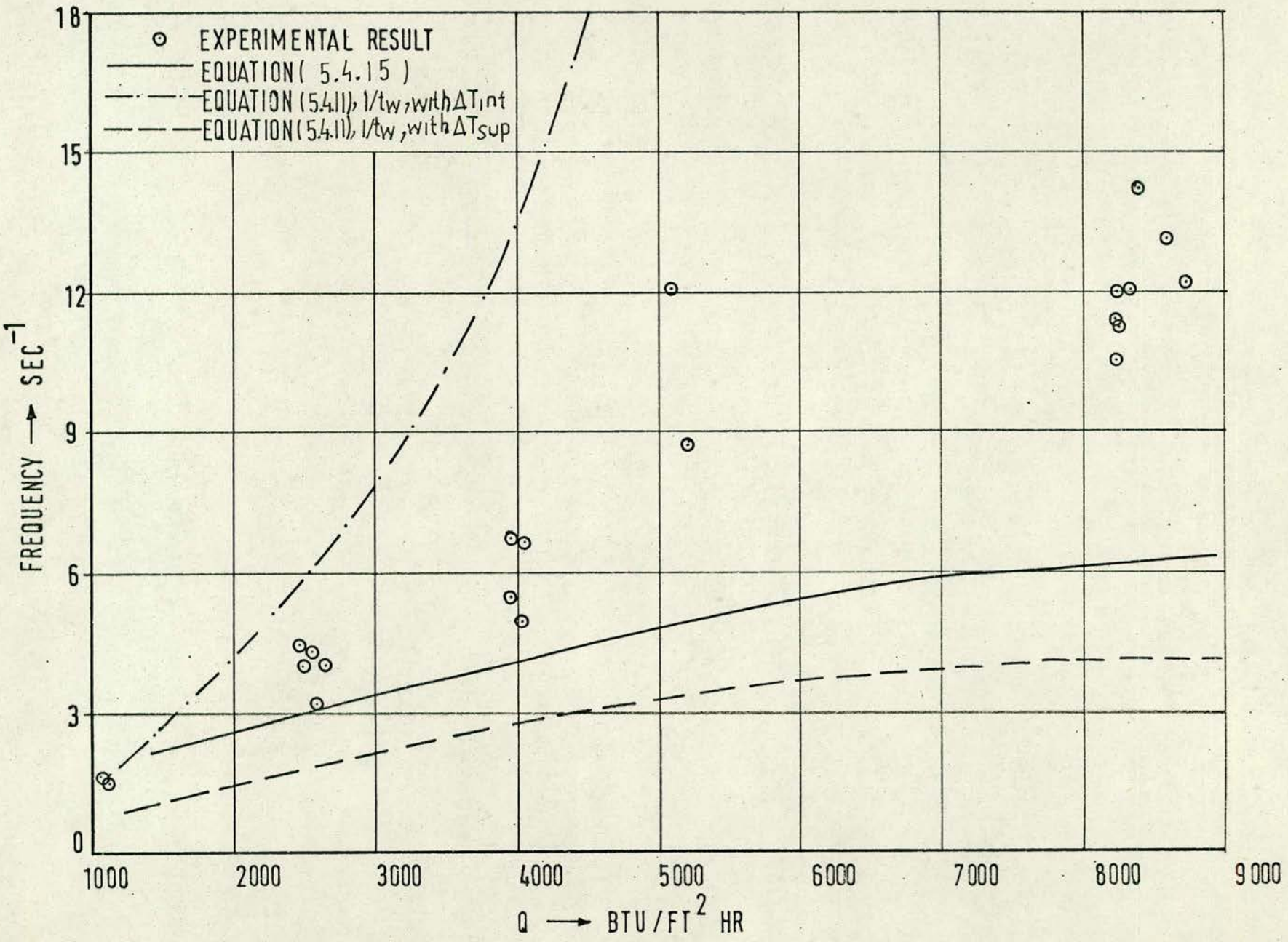

FIG.(24) FREQUENCY VARIATION WITH HEAT FLUX FOR CAVITY 5, SURFACE E, AT ATMOSPHERIC PRESSURE, RADIUS .0145 in.

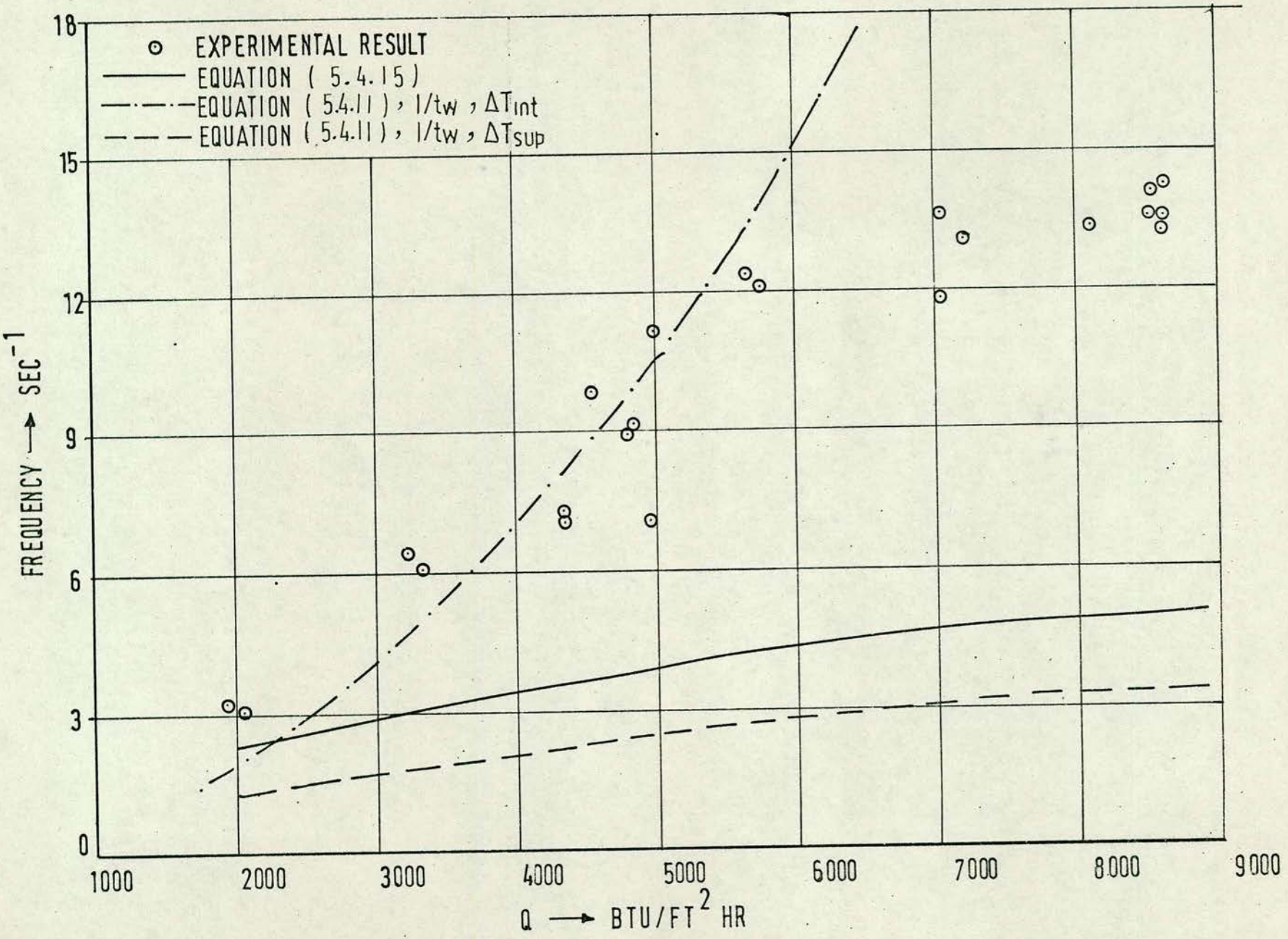

FIG.(25) FREQUENCY VARIATION WITH HEAT FLUX FOR CAVITY 9 SURFACE E, AT ATMOSPHERIC PRESSURE, RADIUS 0.0114 in

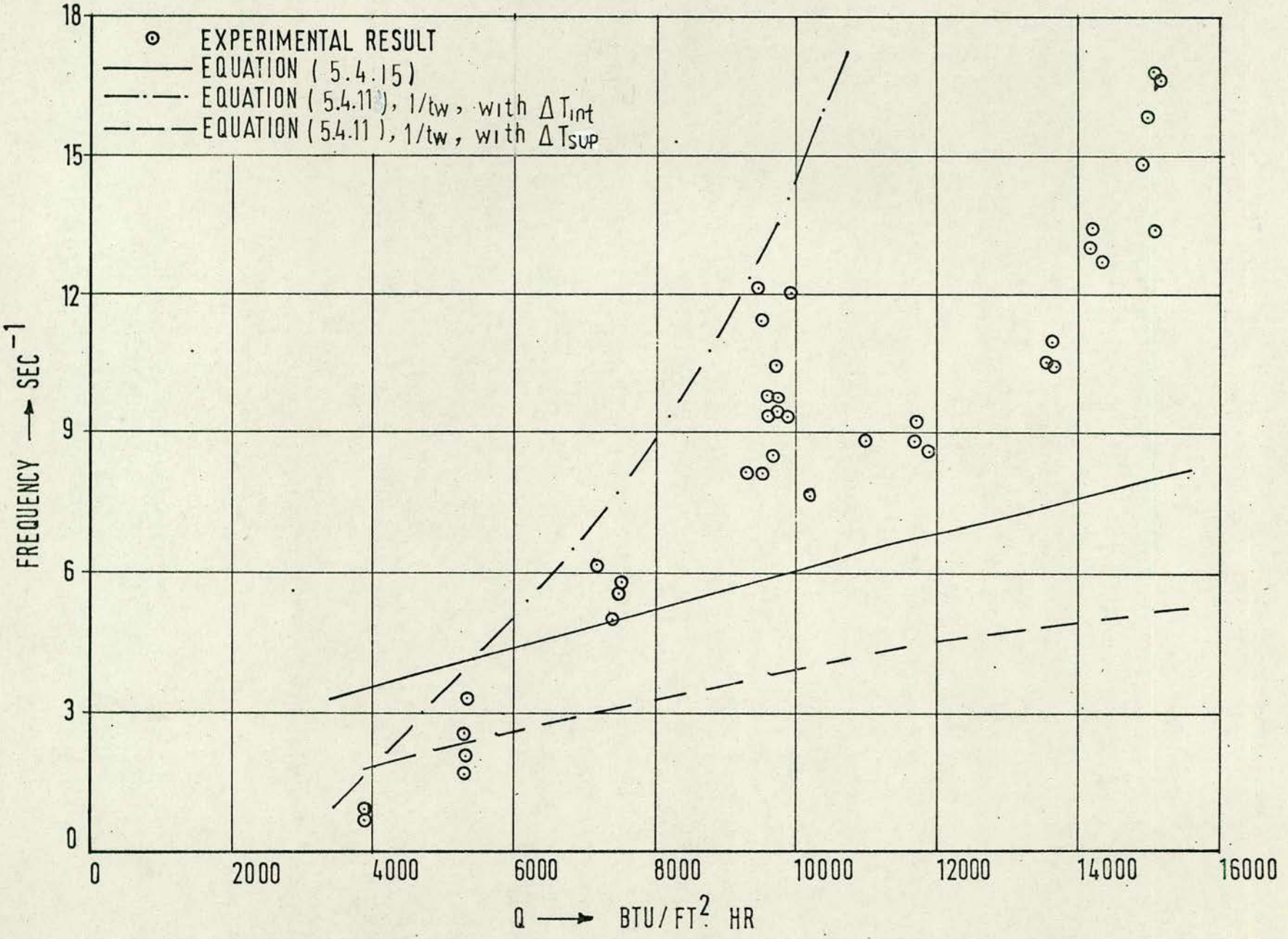

FIG.(26) FREQUENCY VARIATION WITH HEAT FLUX FOR CAVITY 4, SURFACE D, AT ATMOSPHERIC PRESSURE, RADIUS 0.0092 in.

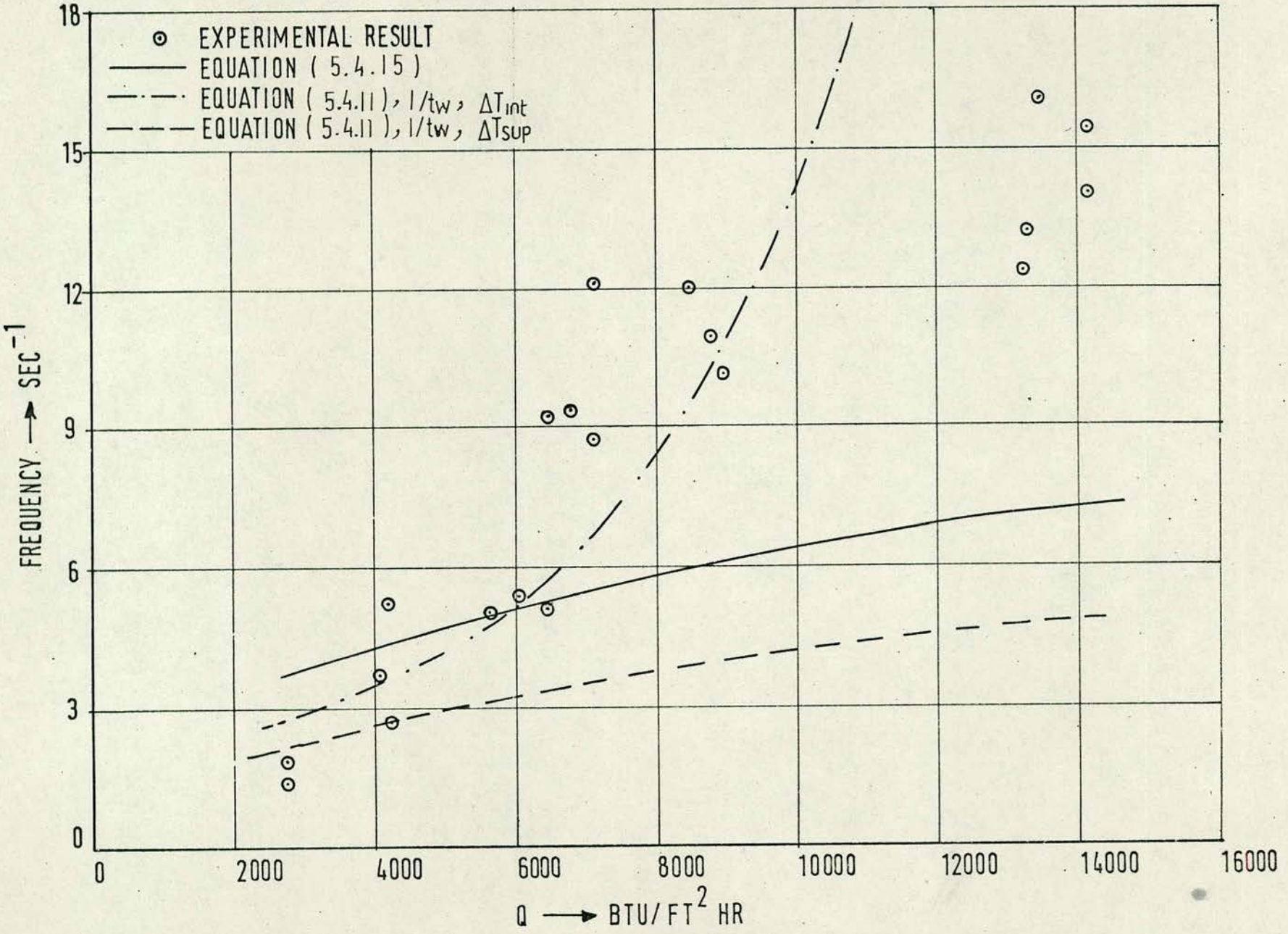

FIG.(27) FREQUENCY VARIATION WITH HEAT FLUX FOR CAVITY 10, SURFACE D, AT ATMOSPHERIC PRESSURE, RADIUS 0.0129 in.

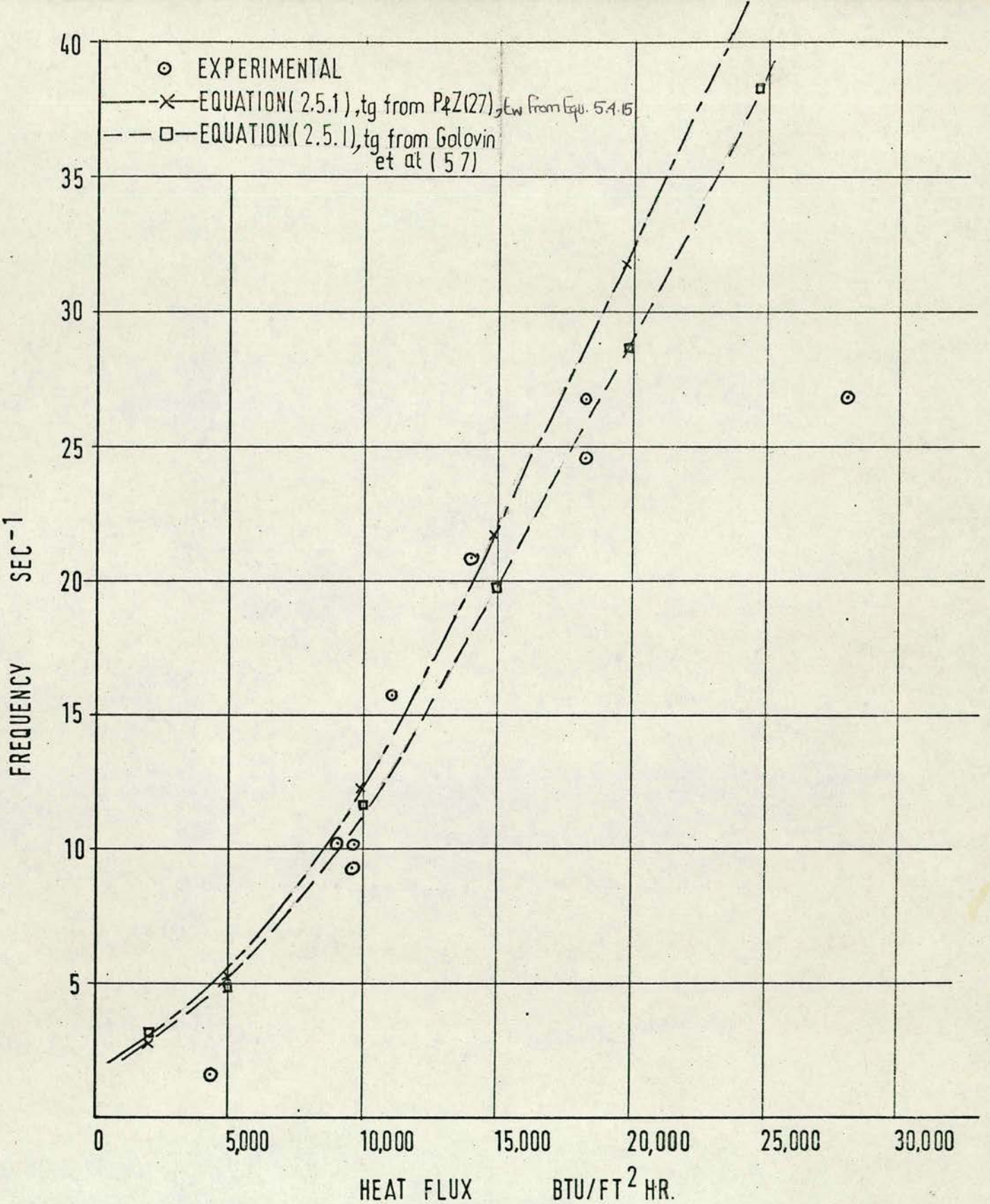

FIG. (28) BUBBLE FREQUENCY VARIATION WITH HEAT FLUX FOR CAVITY NO. 6, SURFACE D, AT 14.8 p.s.i, RADIUS 0.0169 in.

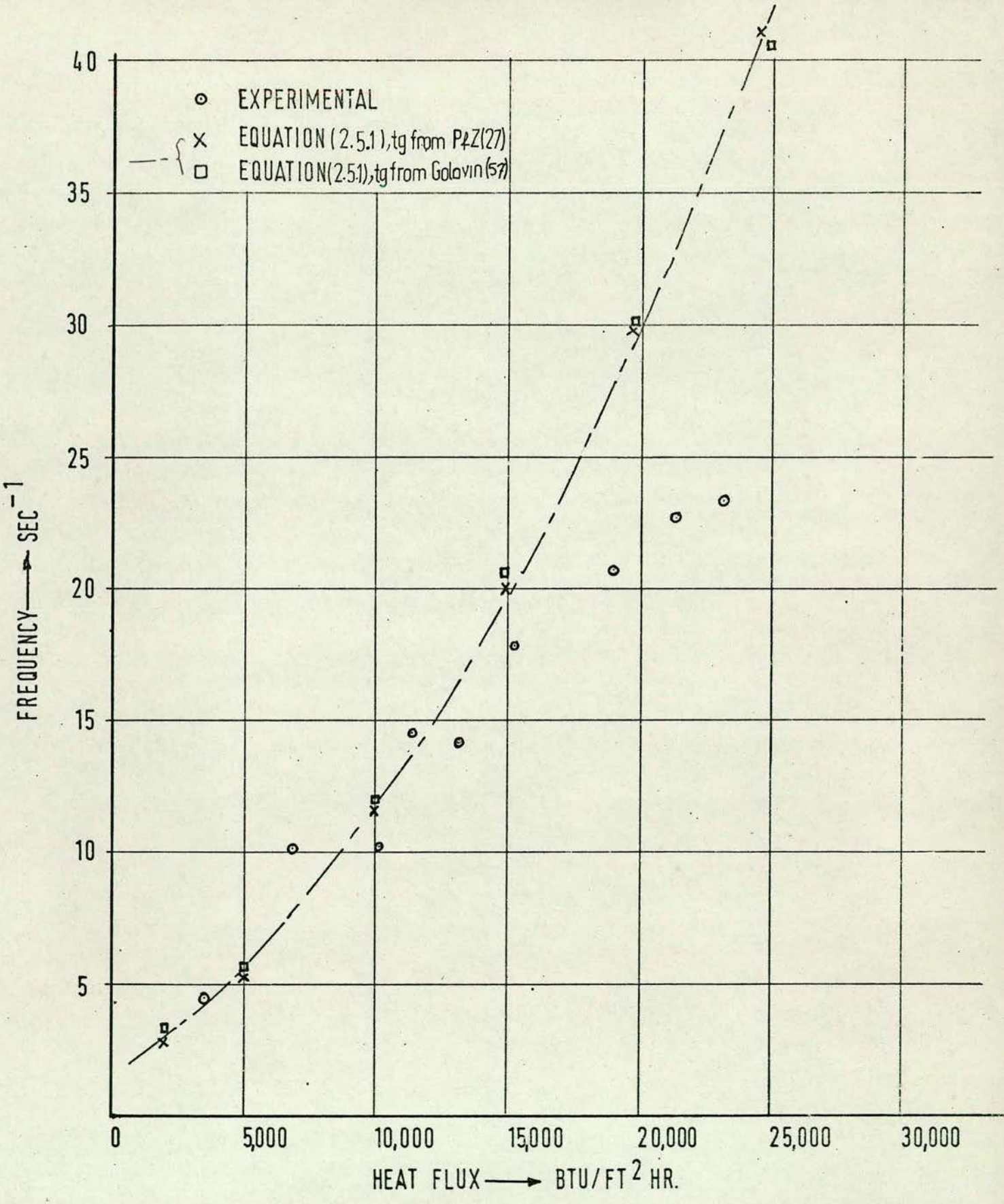

FIG. (29) BUBBLE FREQUENCY VARIATION WITH HEAT FLUX FOR CAVITY NO. 6, SURFACE D, AT 29.8 p.s.i.

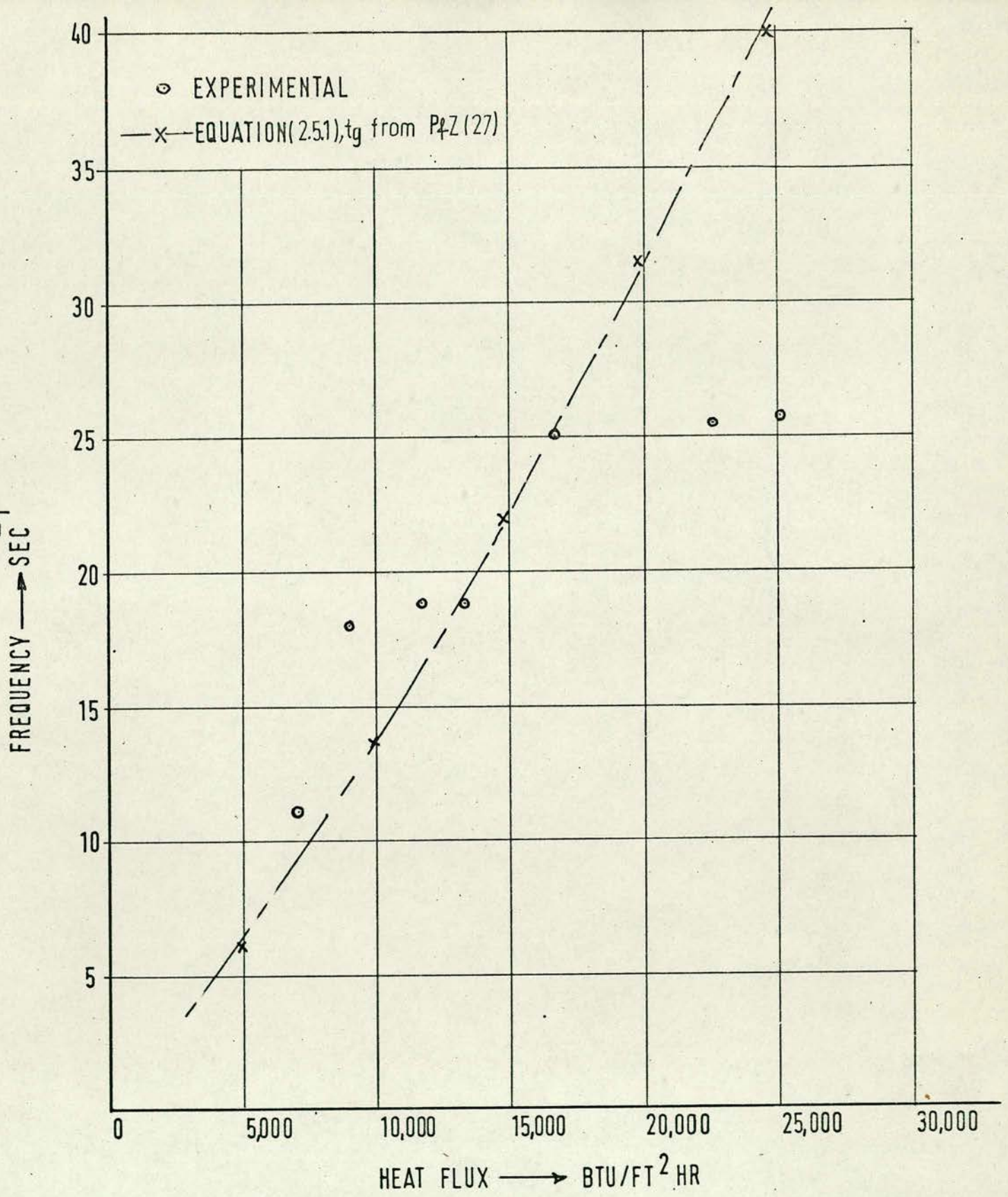

FIG (30) BUBBLE FREQUENCY VARIATION WITH HEAT FLUX FOR CAVITY NO. 6, SURFACE D, AT 44.8 p.s.i.

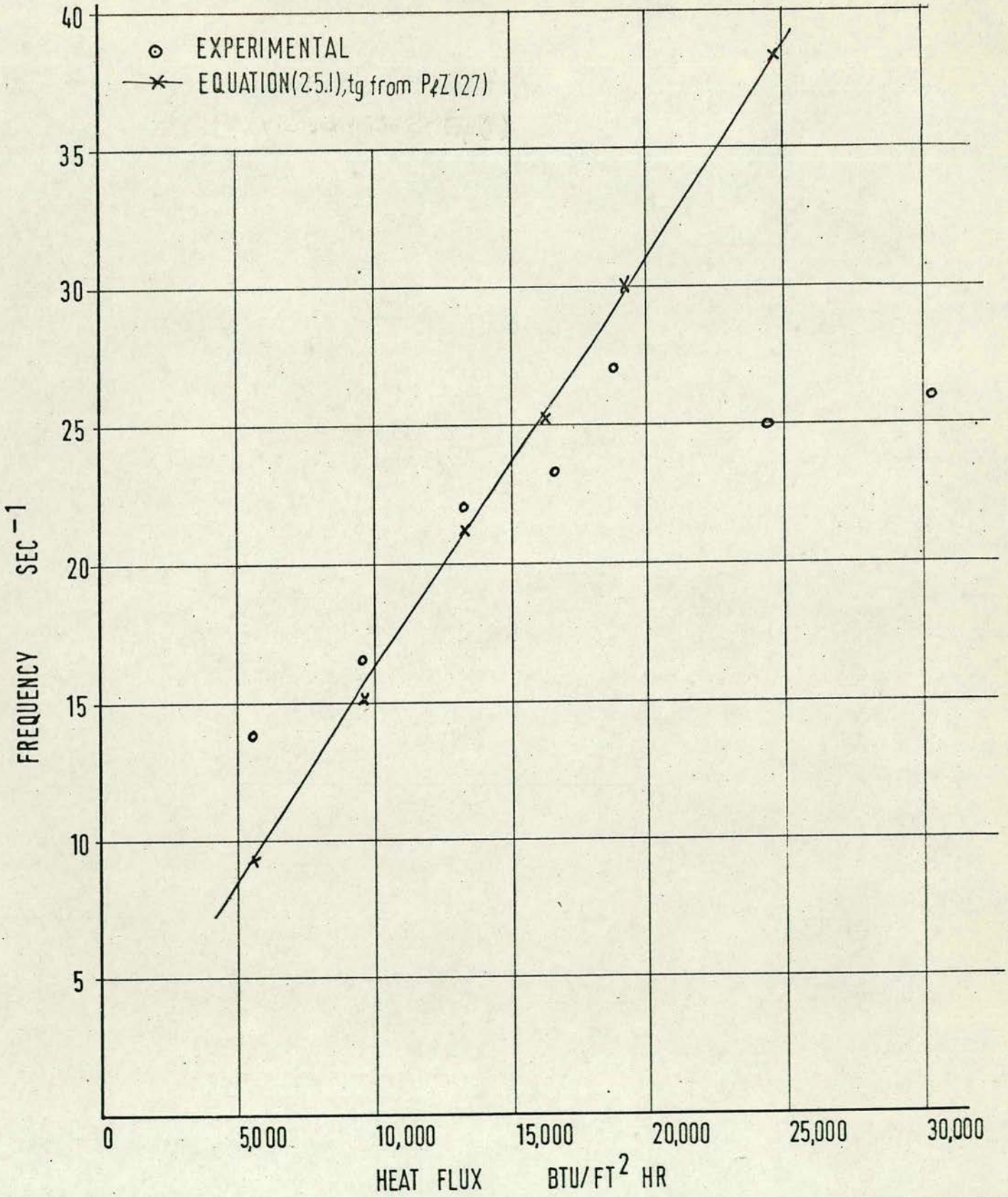

FIG. (31) BUBBLE FREQUENCY VARIATION WITH HEAT FLUX FOR CAVITY NO. 6, SURFACE D, AT 59.8 p.s.i

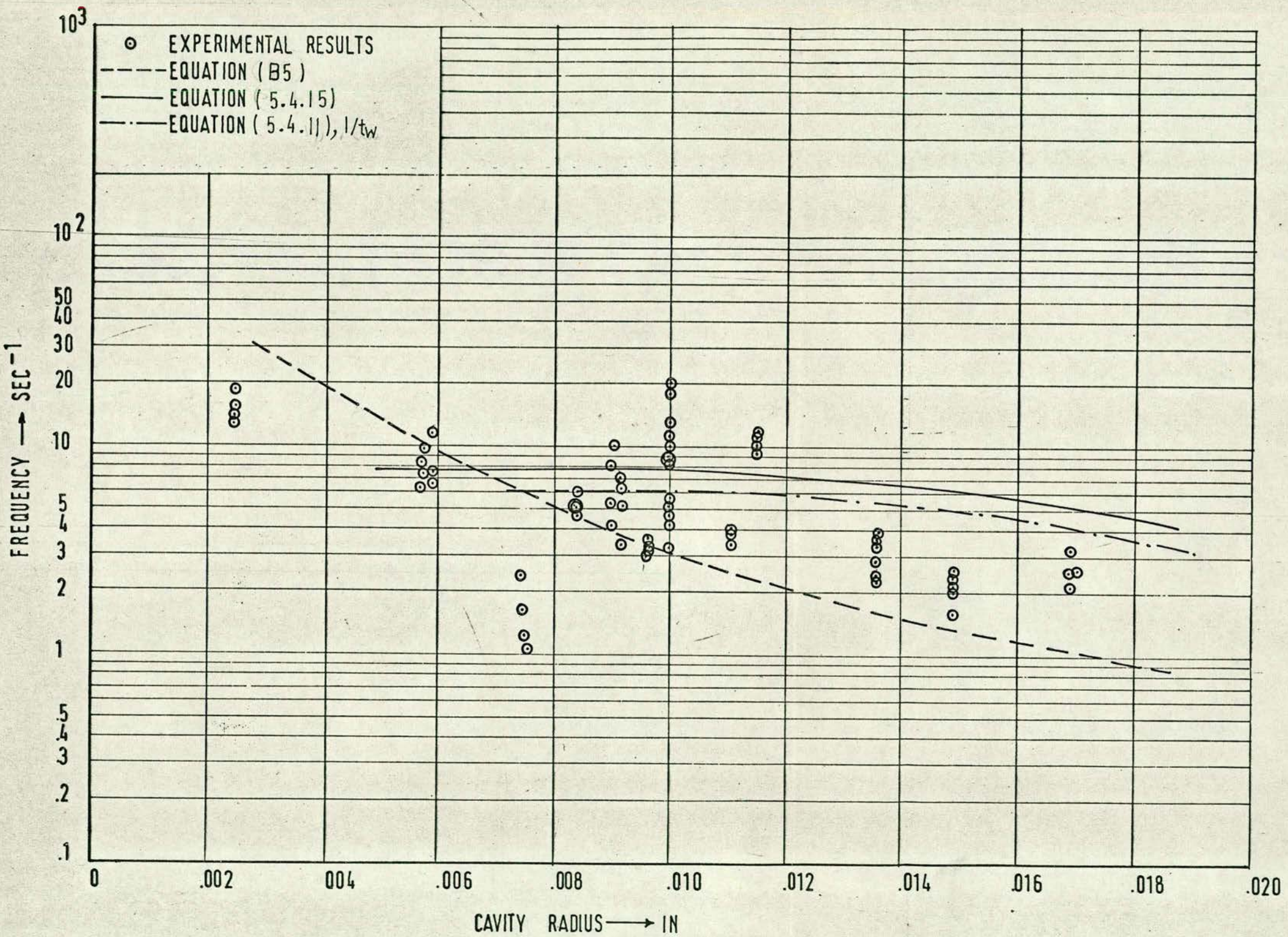

FIG.(32) FREQUENCY VARIATION WITH CAVITY RADIUS AT ATMOSPHERIC PRESSURE AND CONSTANT HEAT FLUX OF 7000 BTU/FT^2 HR

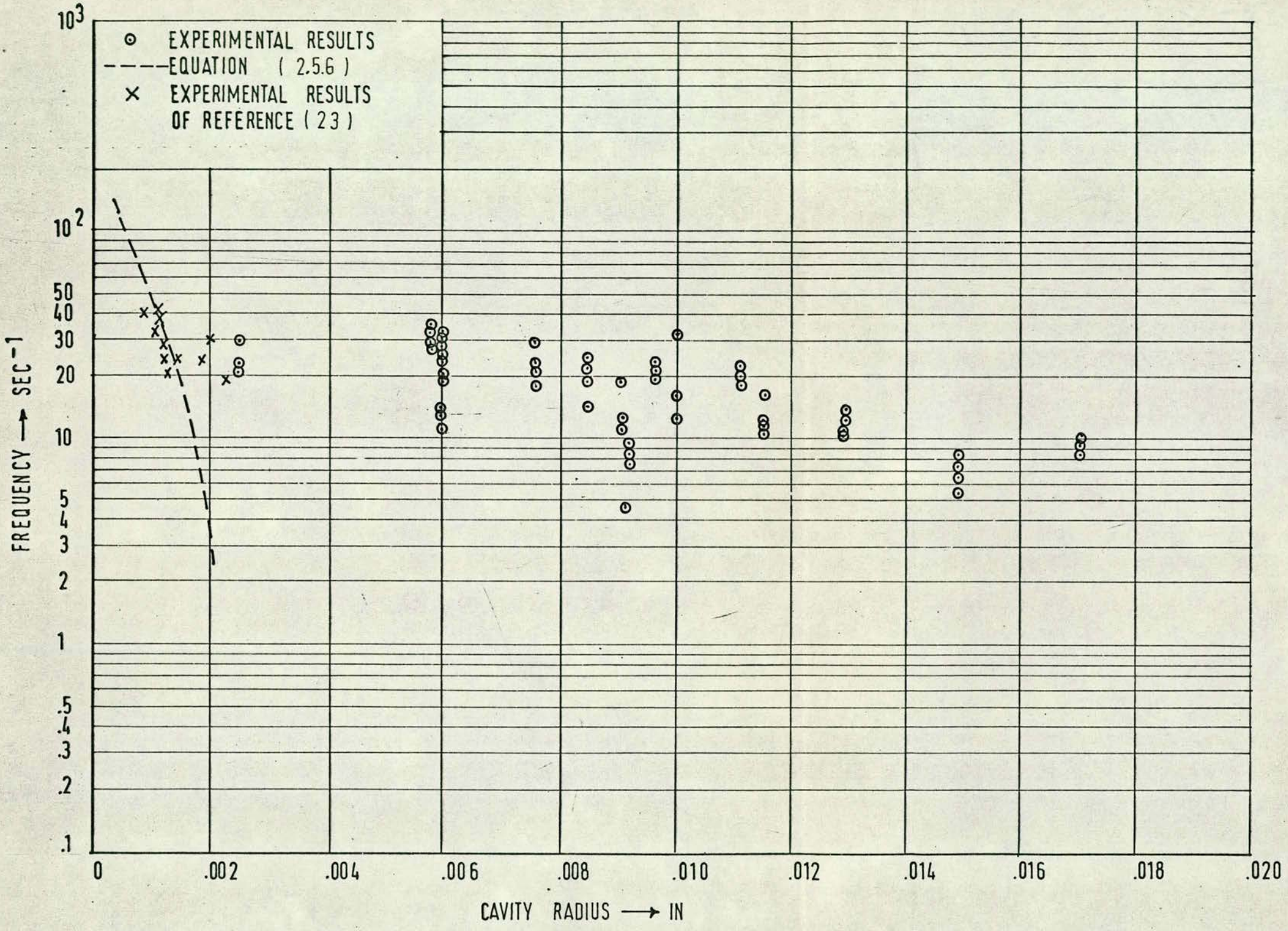

FIG.(33) FREQUENCY VARIATION WITH CAVITY RADIUS AT ATMOSPHERIC PRESSURE AND CONSTANT HEAT FLUX OF 10000 BTU/FT^2 HR

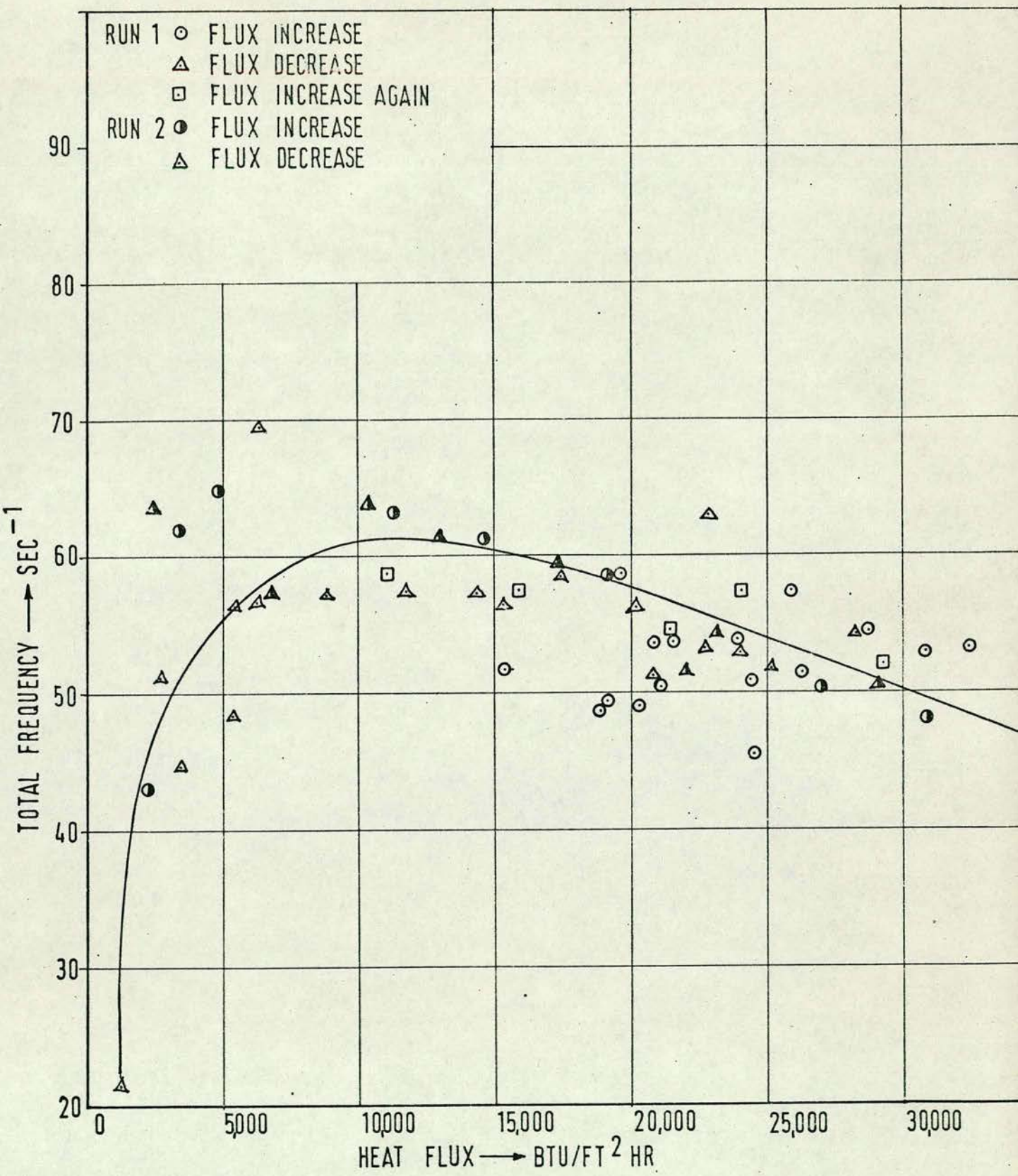

FIG. (34) TOTAL FREQUENCY VARIATION WITH APPLIED HEAT FLUX FOR SURFACE NG1 AT 15 p.s.i.

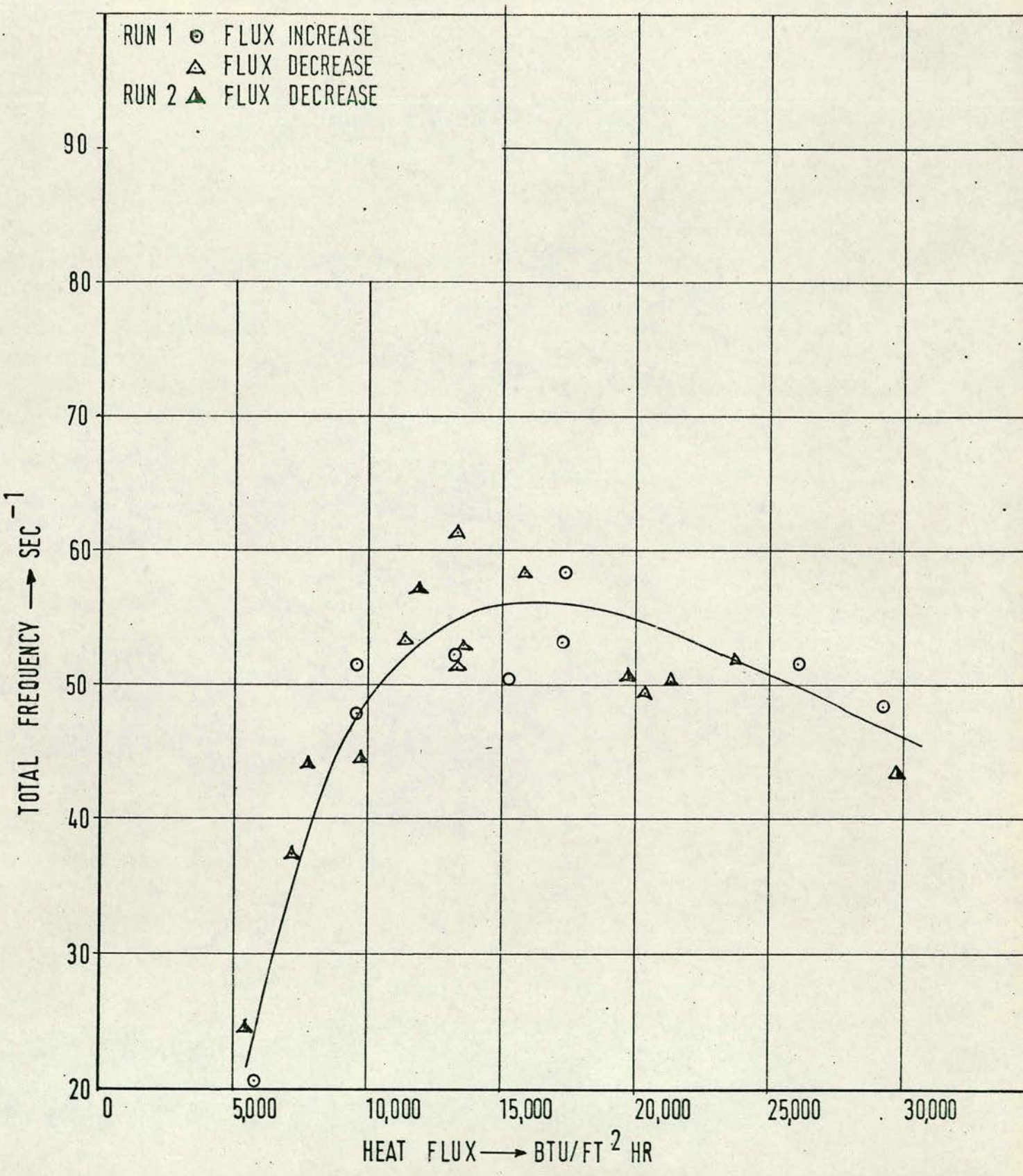

FIG.(35) TOTAL FREQUENCY VARIATION WITH APPLIED HEAT FLUX FOR SURFACE NG 2 AT 15 p.s.i.

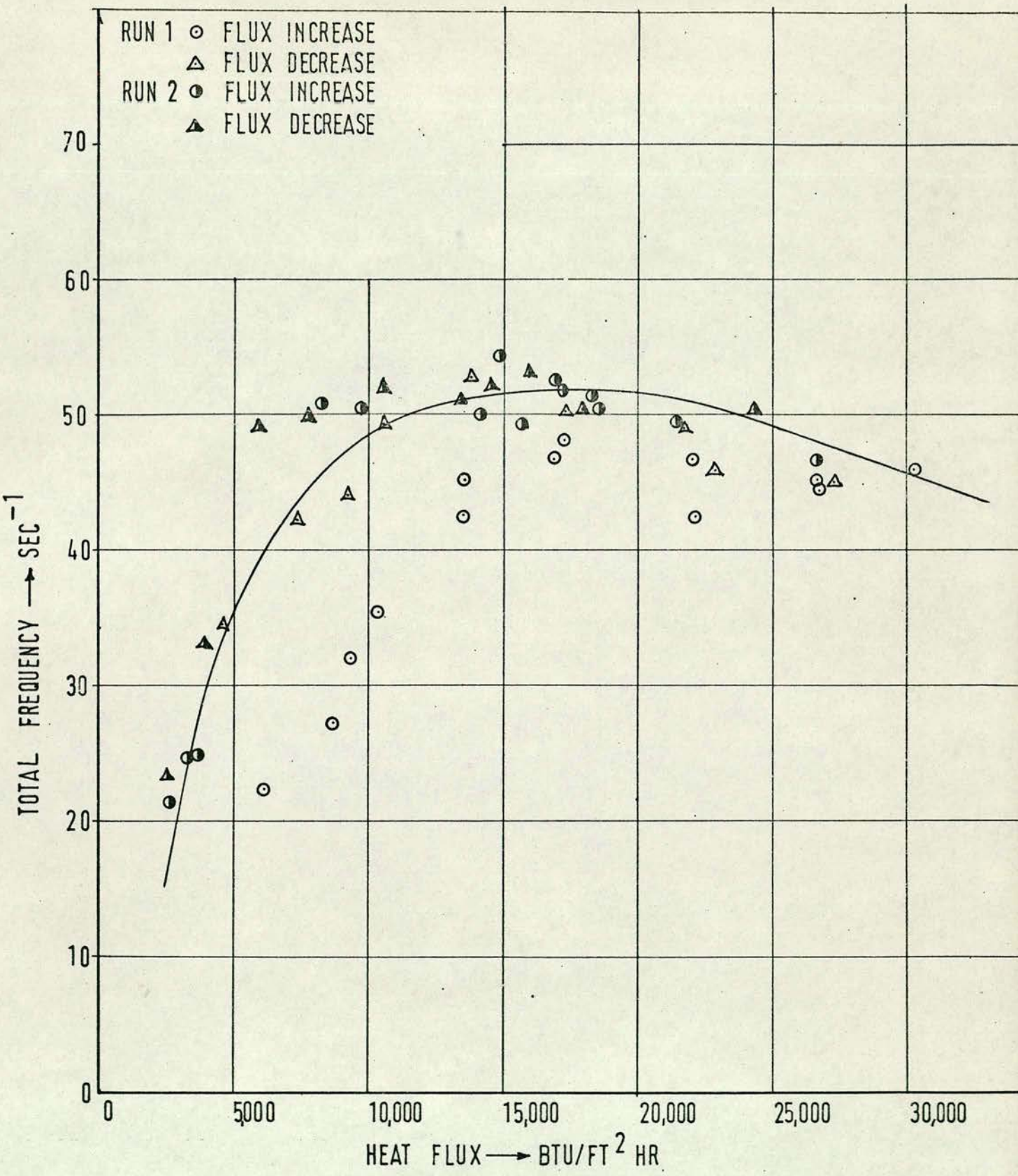

FIG. (36) TOTAL FREQUENCY VARIATION WITH APPLIED HEAT FLUX FOR SURFACE NG 3 AT 15 p.s.i.

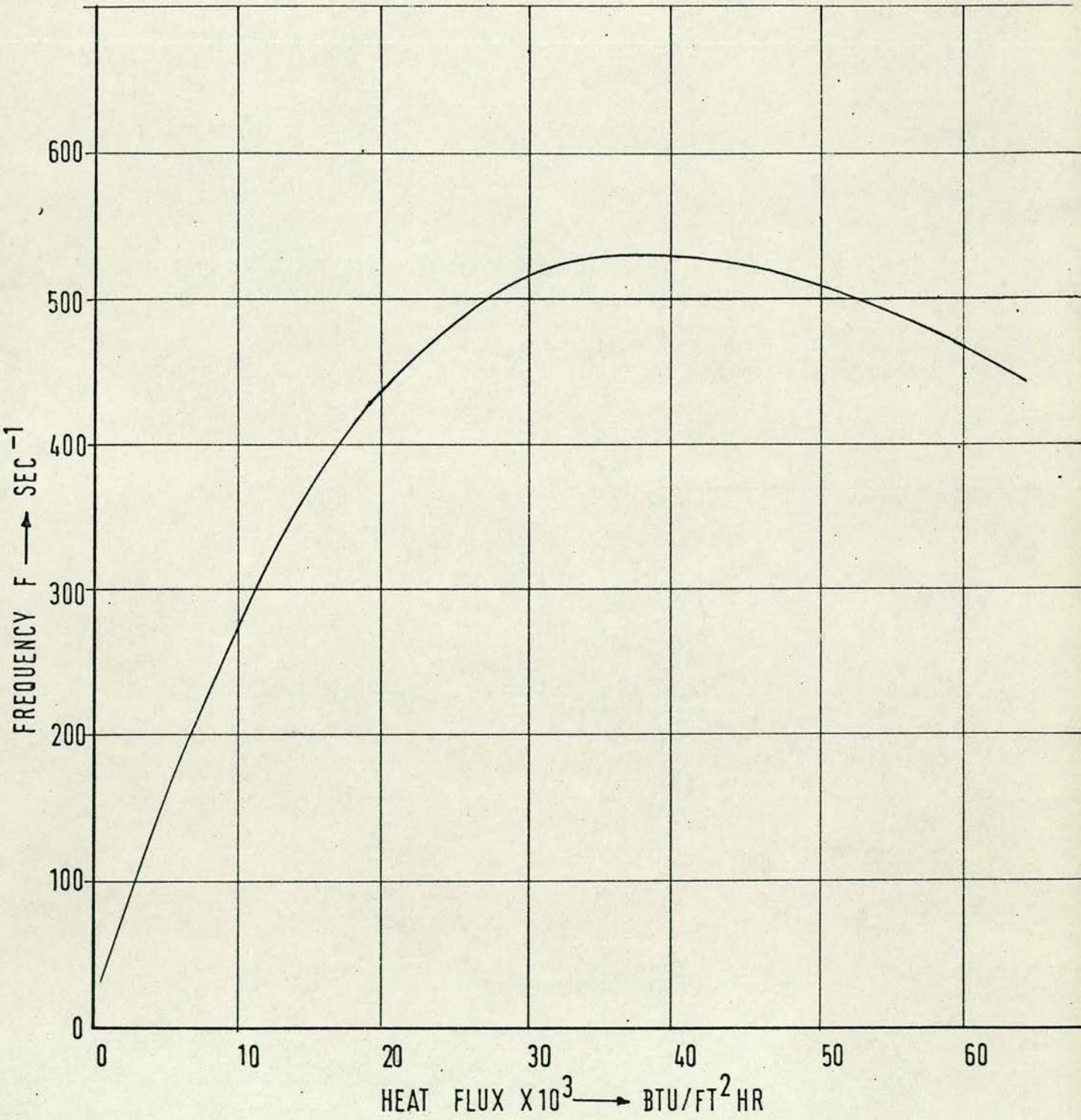

FIG.(37) TOTAL FREQUENCY VARIATION WITH APPLIED HEAT FLUX. KIRBY & WESTWATER [68]

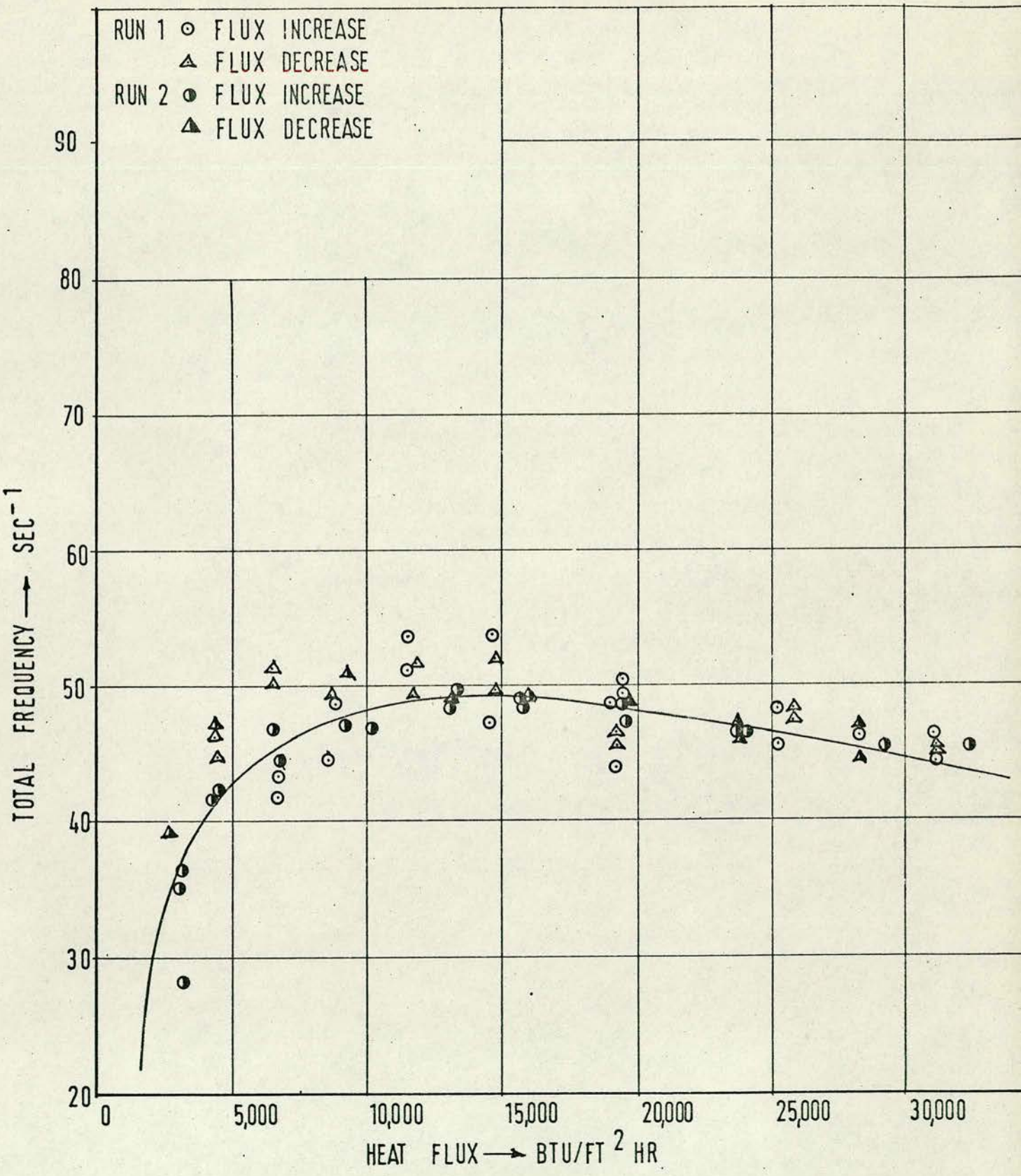

FIG.(38) TOTAL FREQUENCY VARIATION WITH APPLIED HEAT FLUX FOR SURFACE NG 3 AT 30 p.s.i.

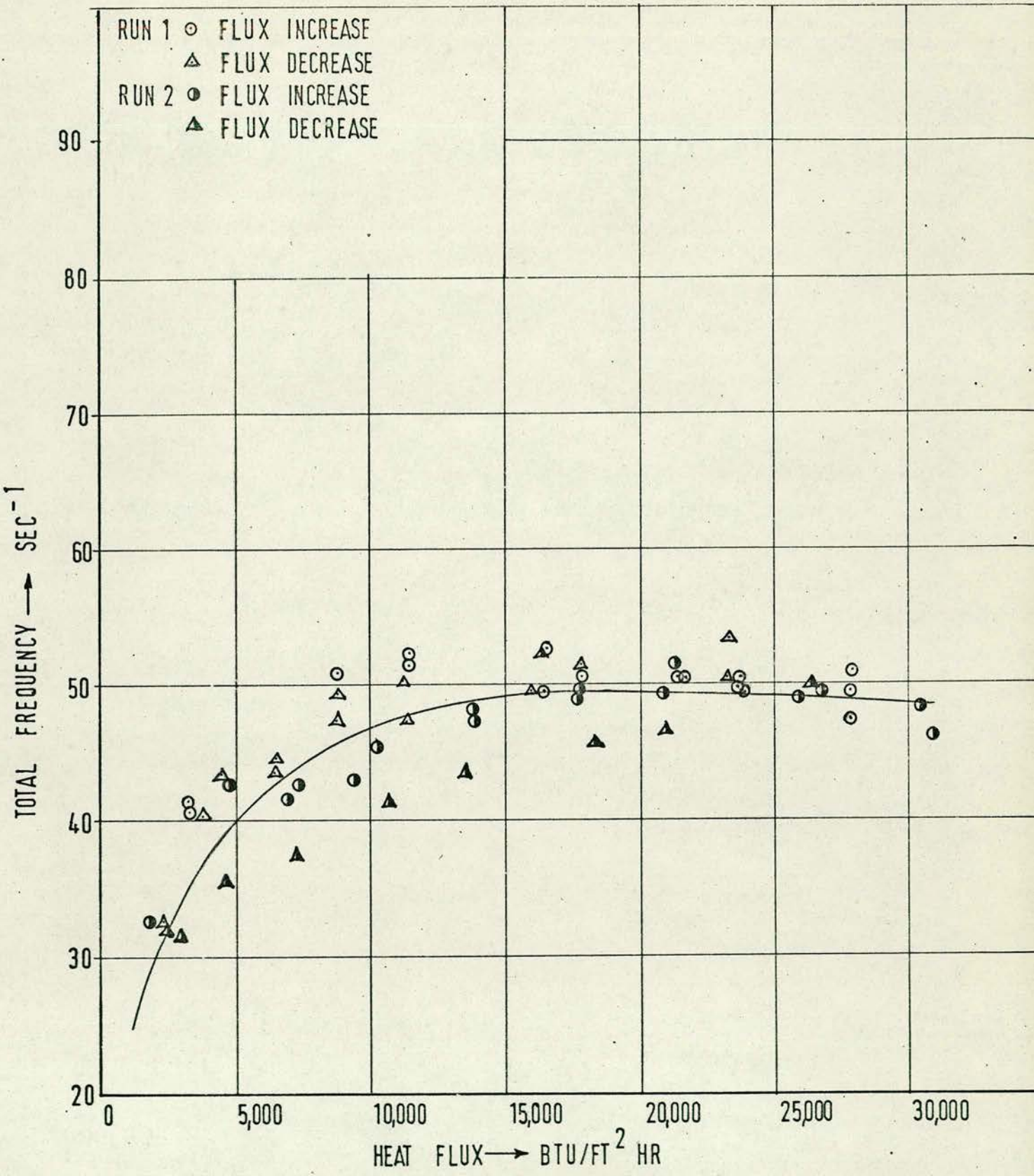

FIG.(39) TOTAL FREQUENCY VARIATION WITH APPLIED HEAT FLUX FOR SURFACE NG 3 AT 45p.s.i.

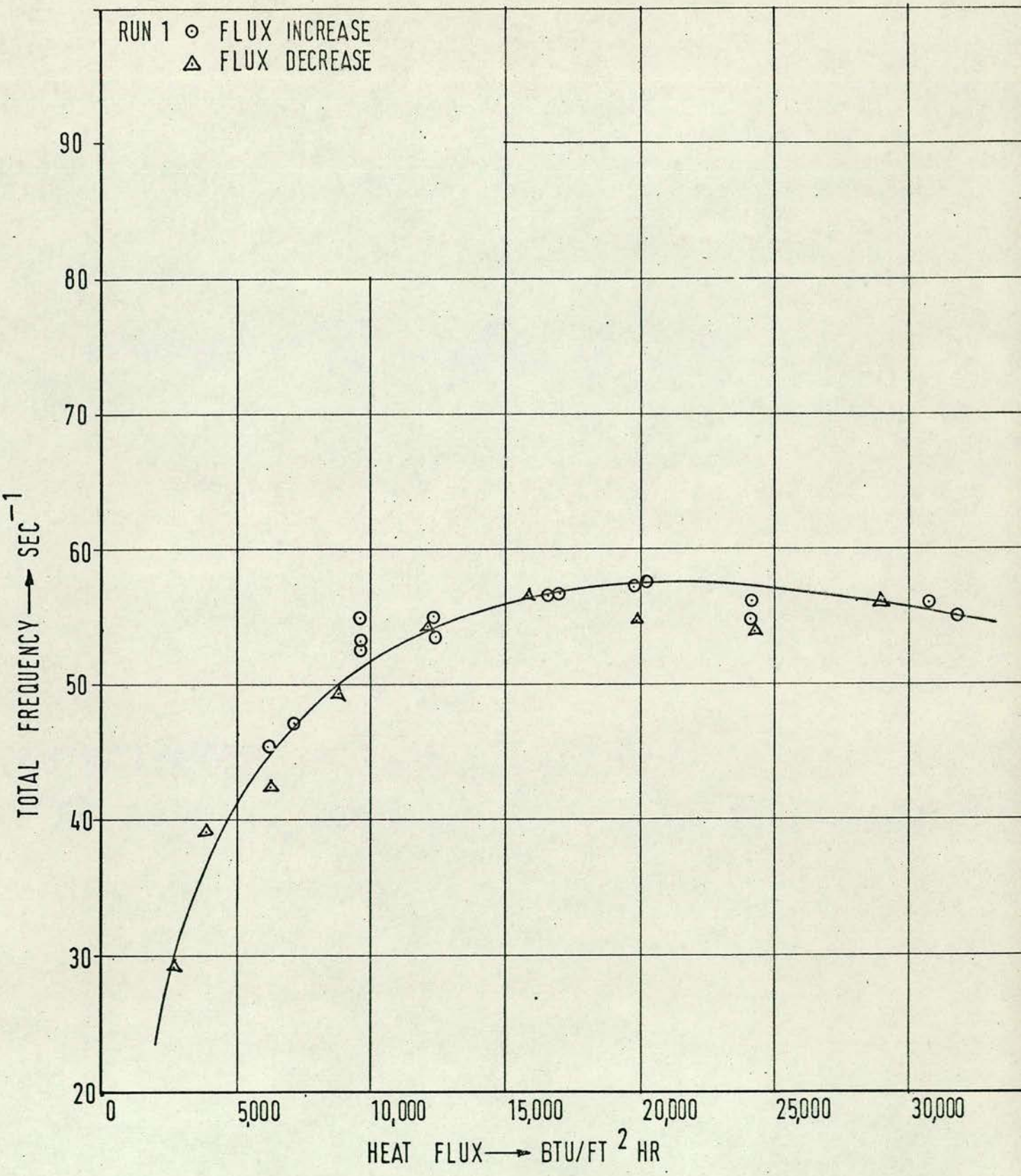

FIG.(40) TOTAL FREQUENCY VARIATION WITH APPLIED HEAT FLUX FOR SURFACE NG 3 AT 60 p.s.i.

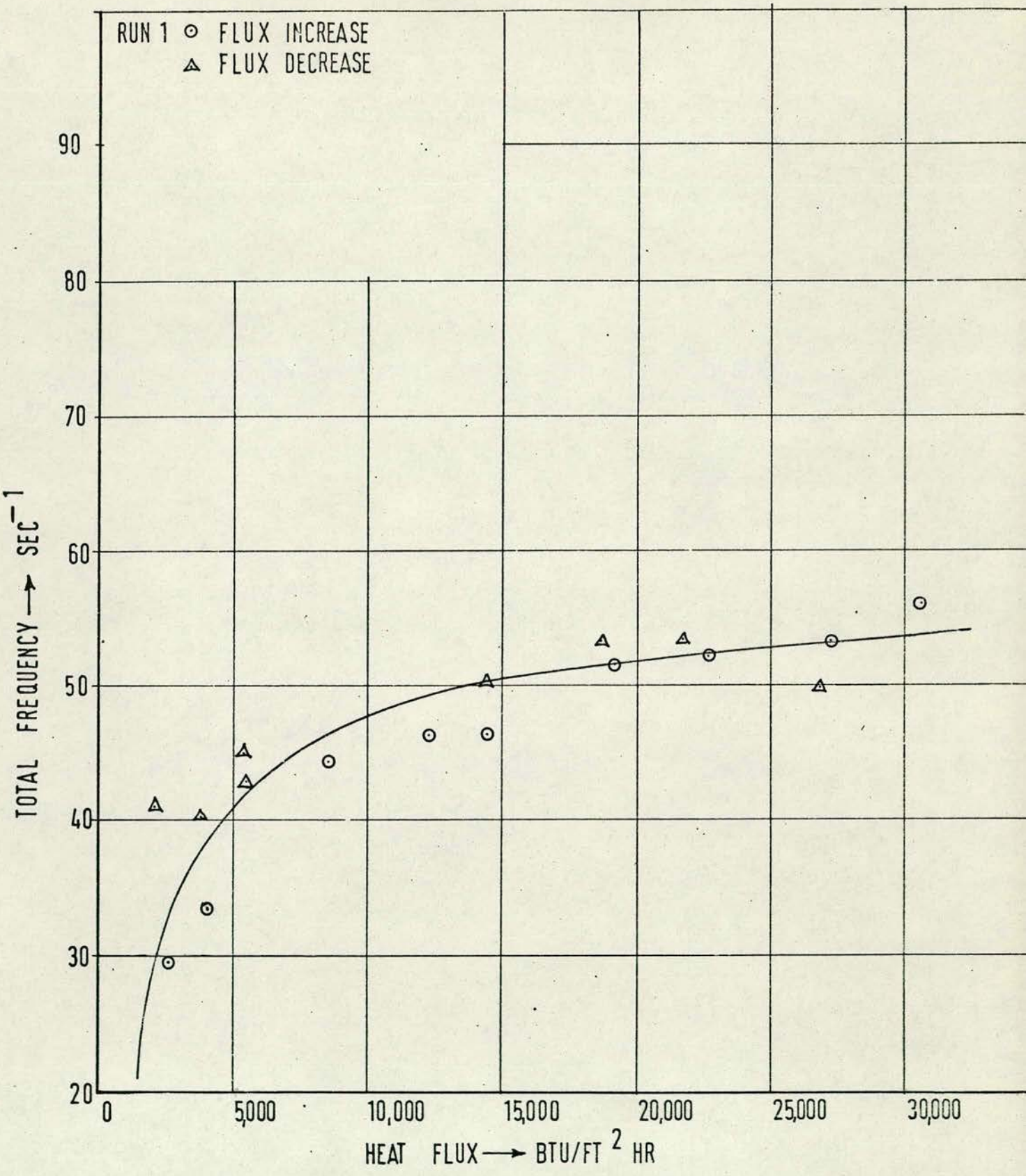

FIG.(41) TOTAL FREQUENCY VARIATION WITH APPLIED HEAT FLUX FOR SURFACE NG 3 AT 75 p.s.i.

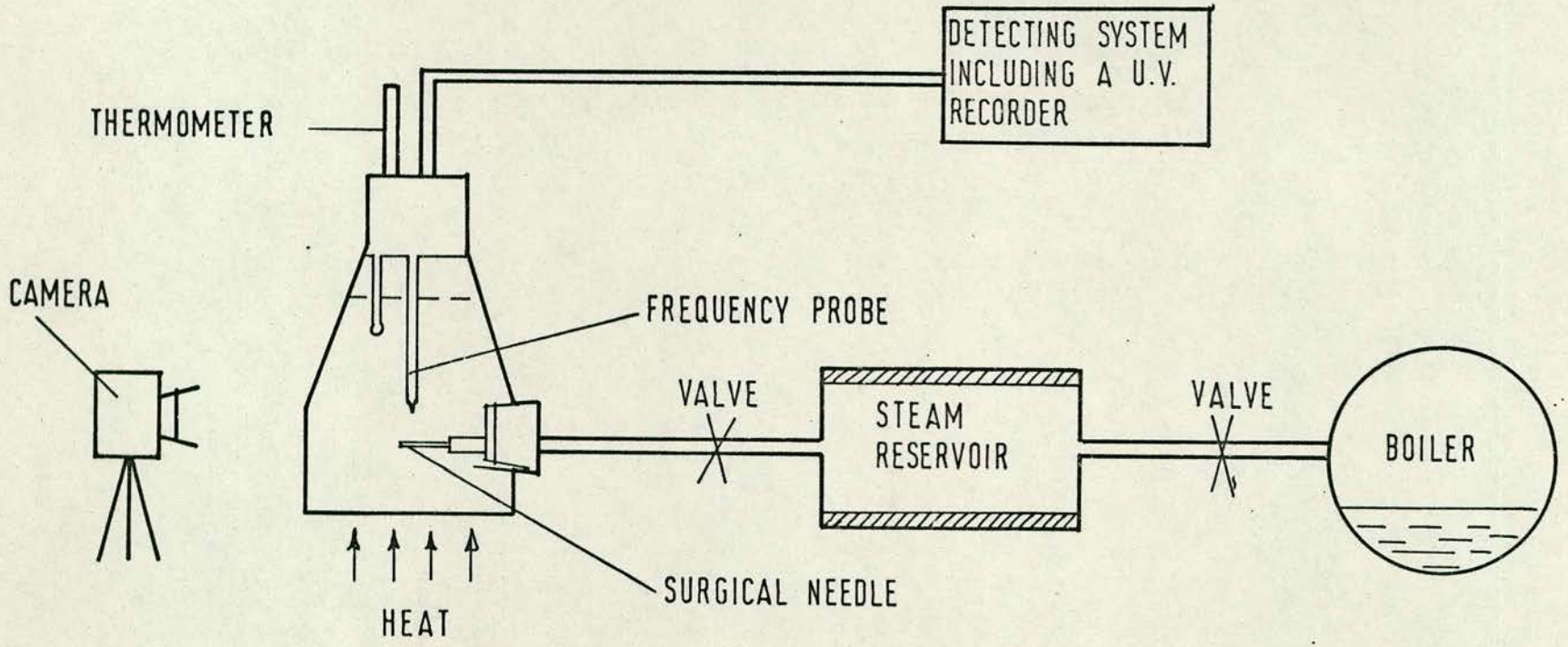

FIG.(42) ARRANGEMENT USED IN CALIBRATING THE FREQUENCY PROBE

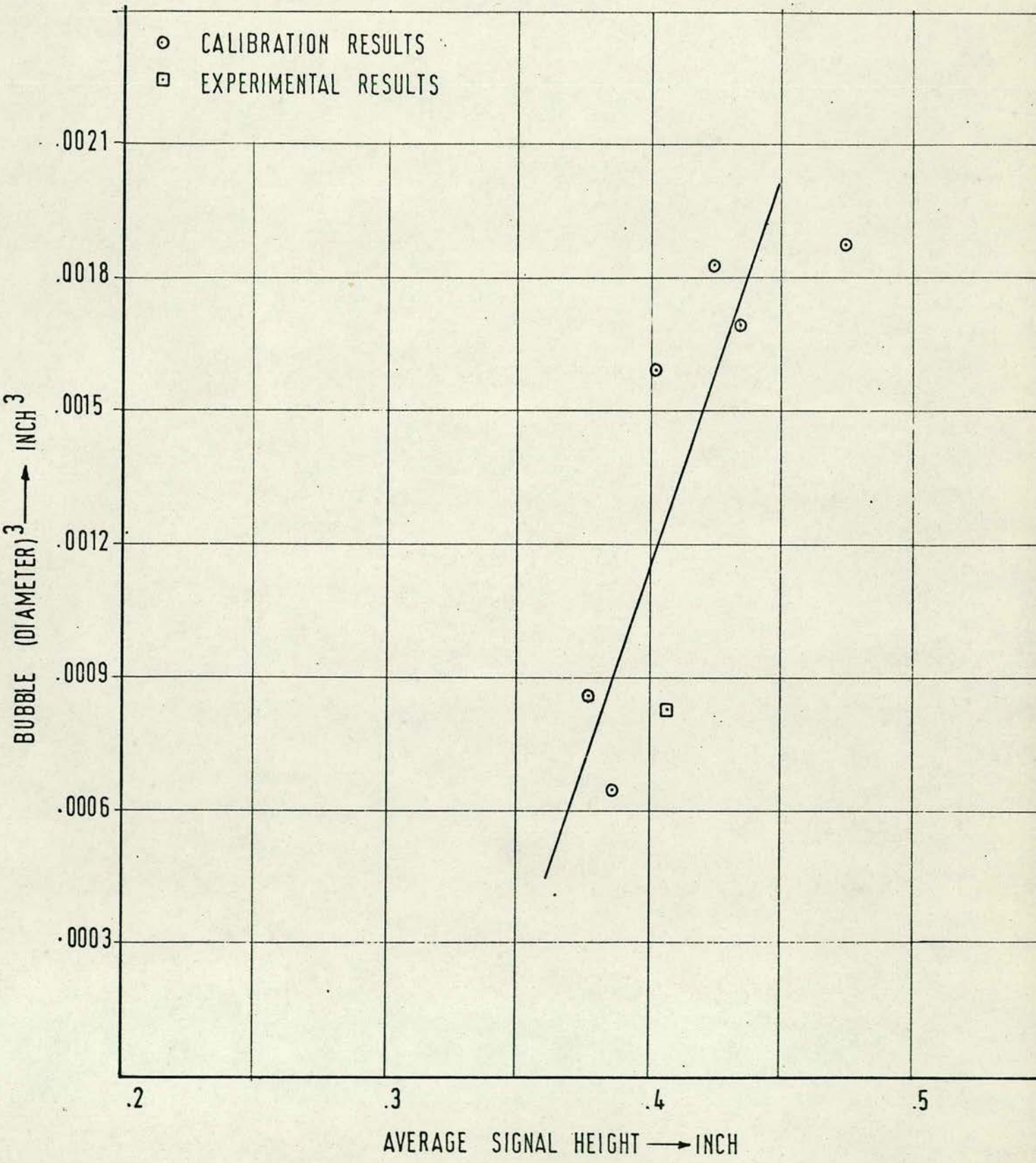

FIG.(43) CALIBRATION OF FREQUENCY PROBE

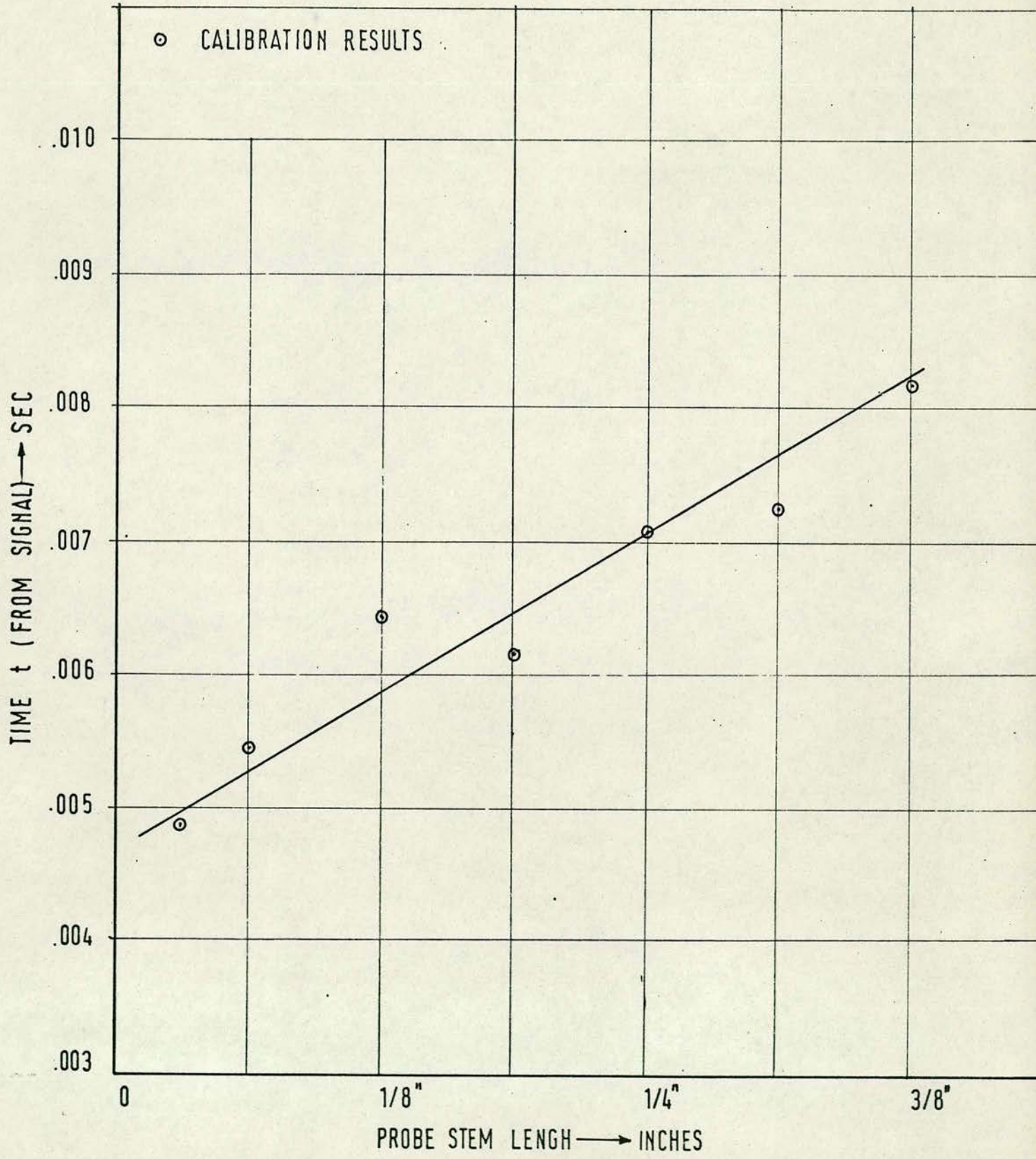

FIG. (44) VARIATION OF TIME OBTAINED FROM SIGNAL WITH PROBE LENGTH

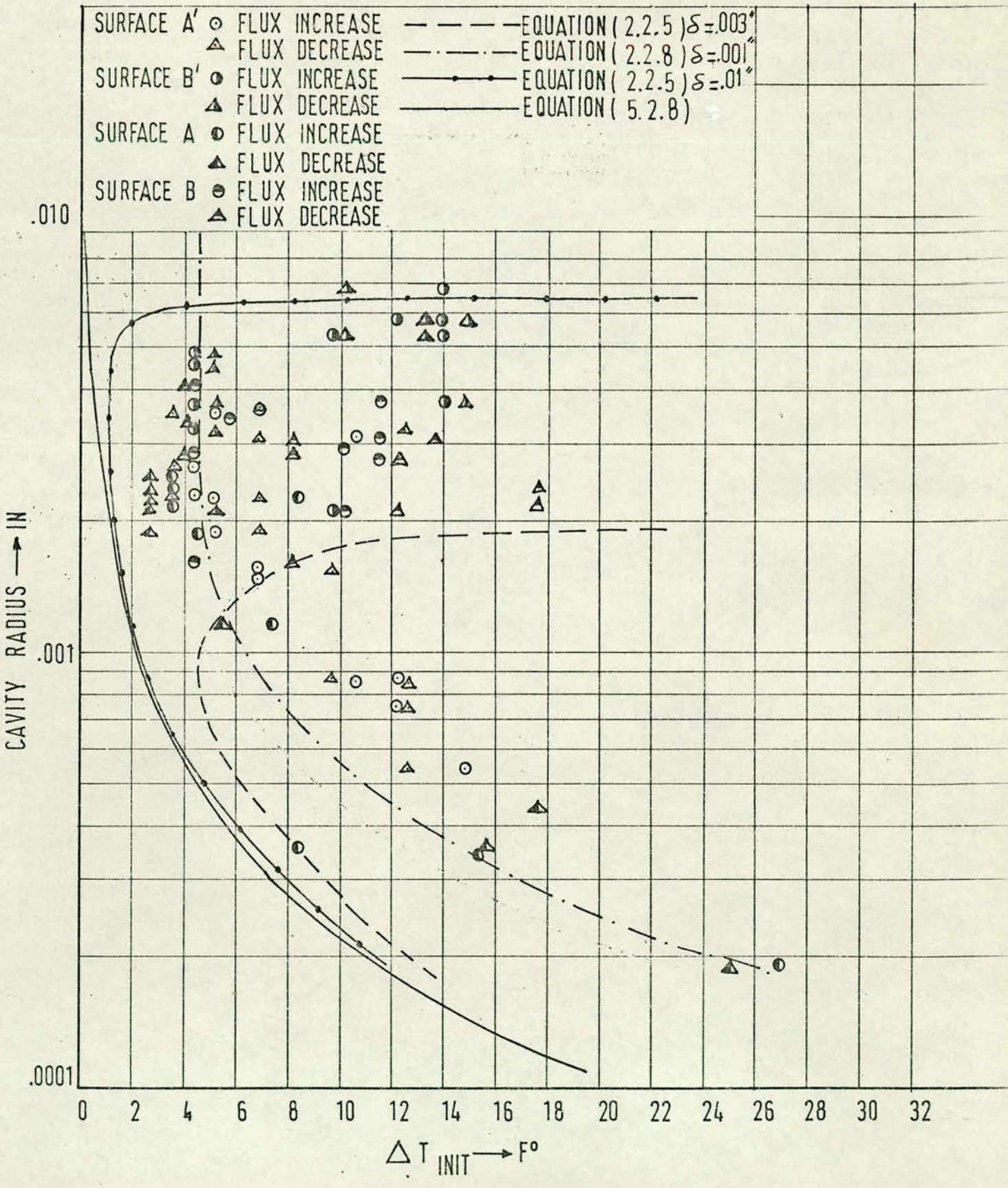

FIG.(45) VARIATION OF CAVITY RADIUS WITH INITIATION SUPERHEAT TEMPERATURE DIFFERENCE FOR SURFACES A', B', A&B AT ATMOSPHERIC PRESSURE

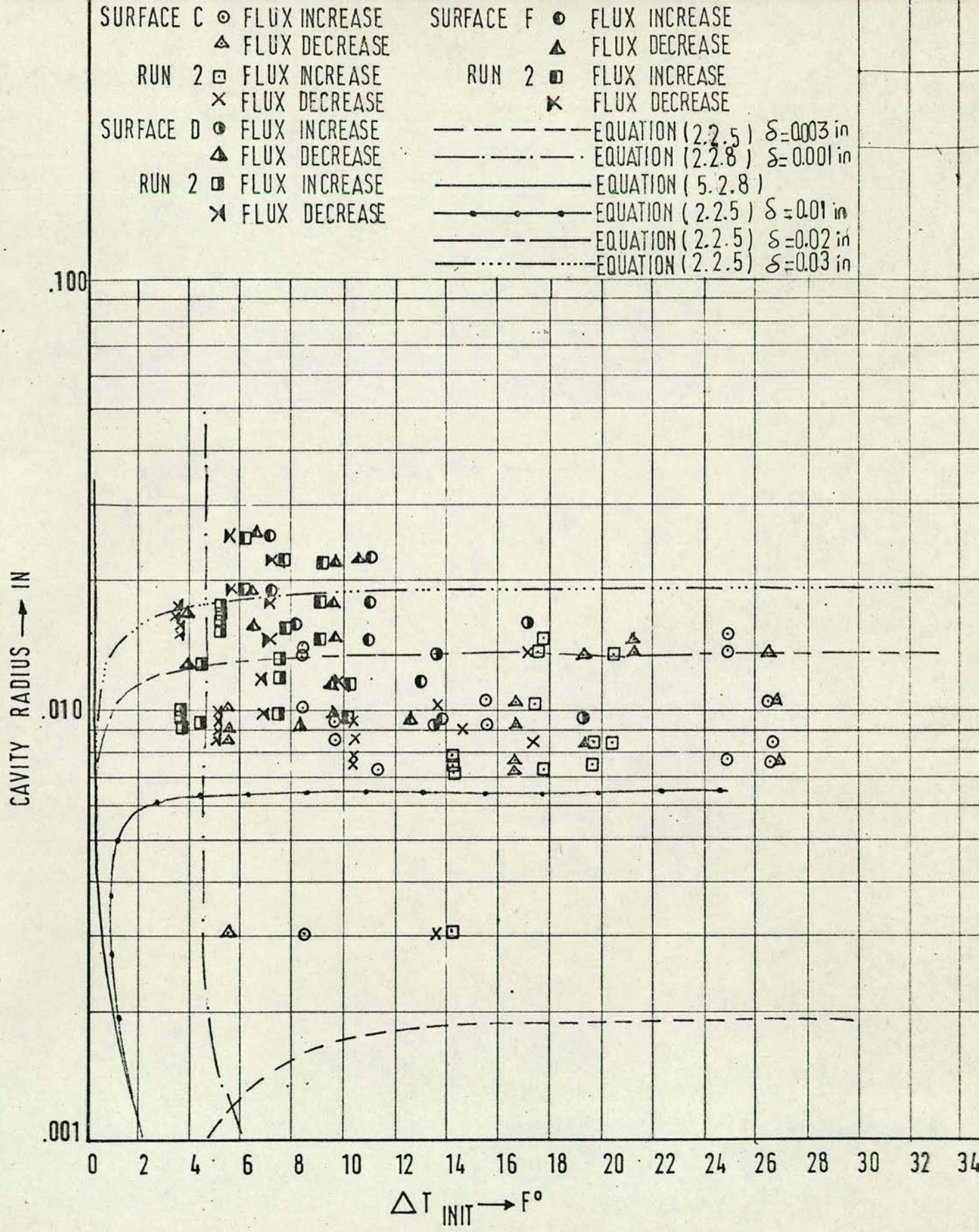

FIG.(46) VARIATION OF CAVITY RADIUS WITH INITIATION SUPERHEAT TEMPERATURE DIFFERENCE FOR SURFACES C, D & F AT ATMOSPHERIC PRESSURE

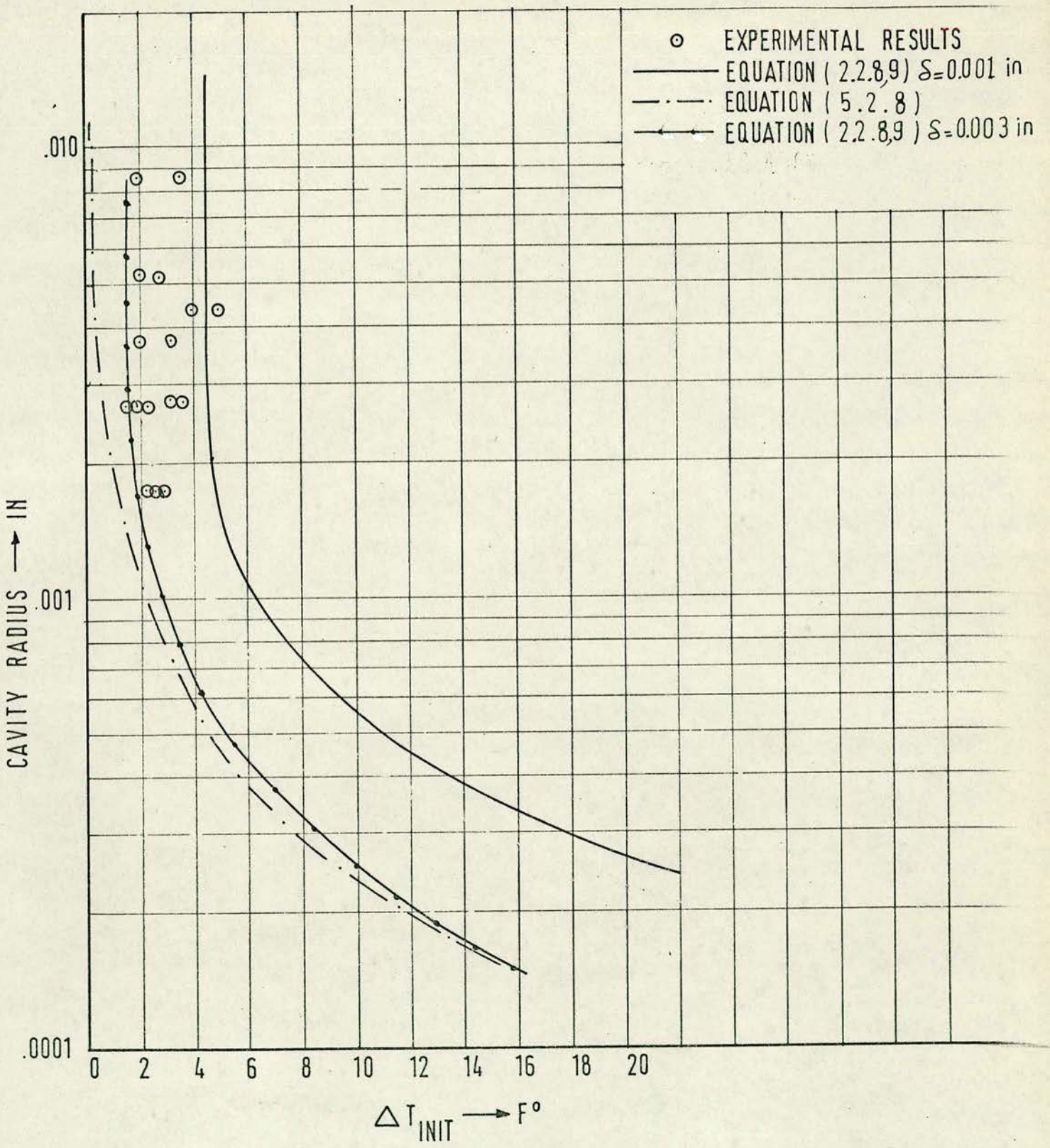

FIG.(47) VARIATION OF CAVITY RADIUS WITH INITIATION SUPERHEAT TEMPERATURE DIFFERENCE FOR GENERAL SURFACES AT ATMOSPHERIC PRESSURE.

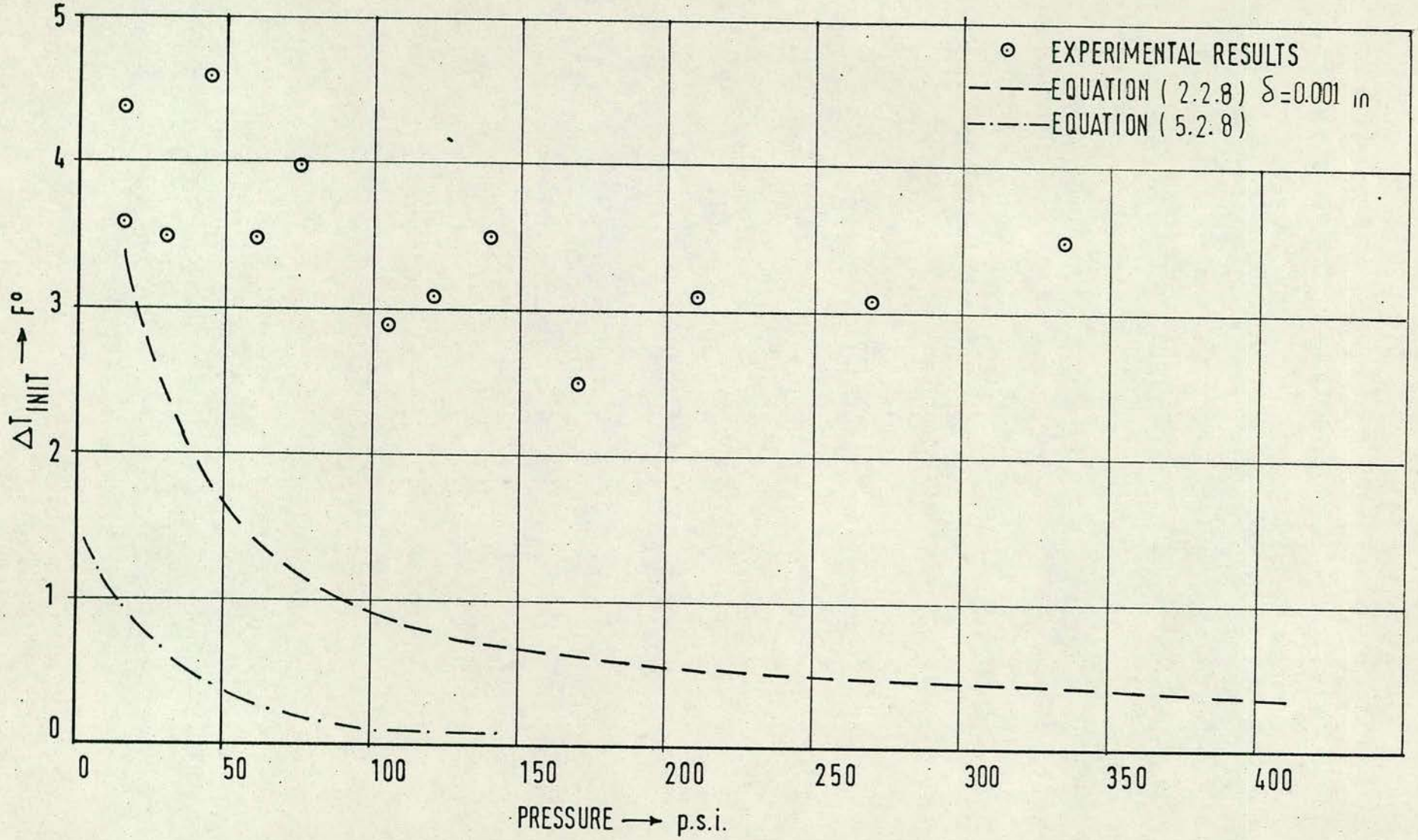

FIG.(48) VARIATION OF INITIATION SUPERHEAT TEMPERATURE DIFFERENCE WITH PRESSURE, SURFACE A'

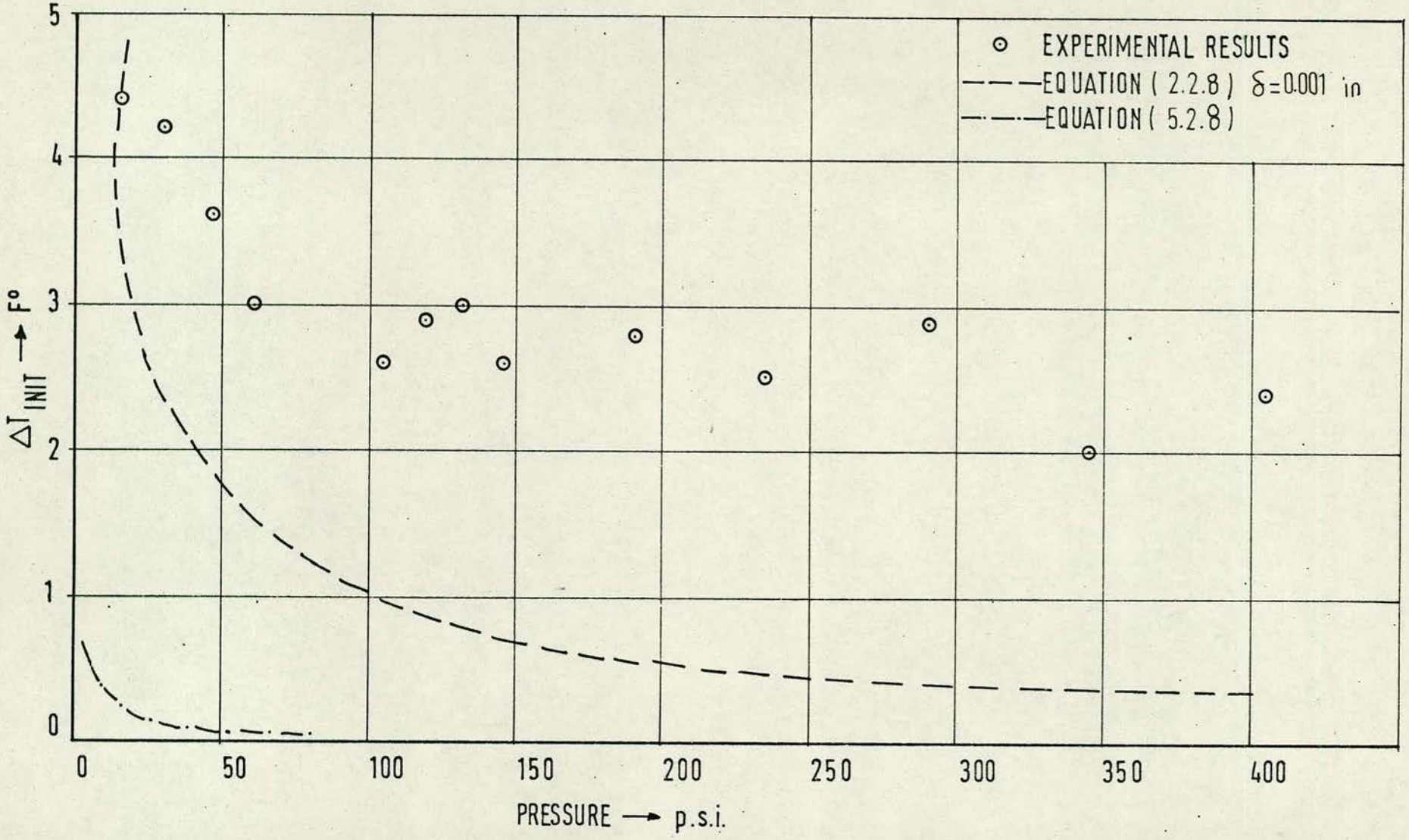

FIG.(49) VARIATION OF INITIATION SUPERHEAT TEMPERATURE DIFFERENCE WITH PRESSURE, SURFACE B'

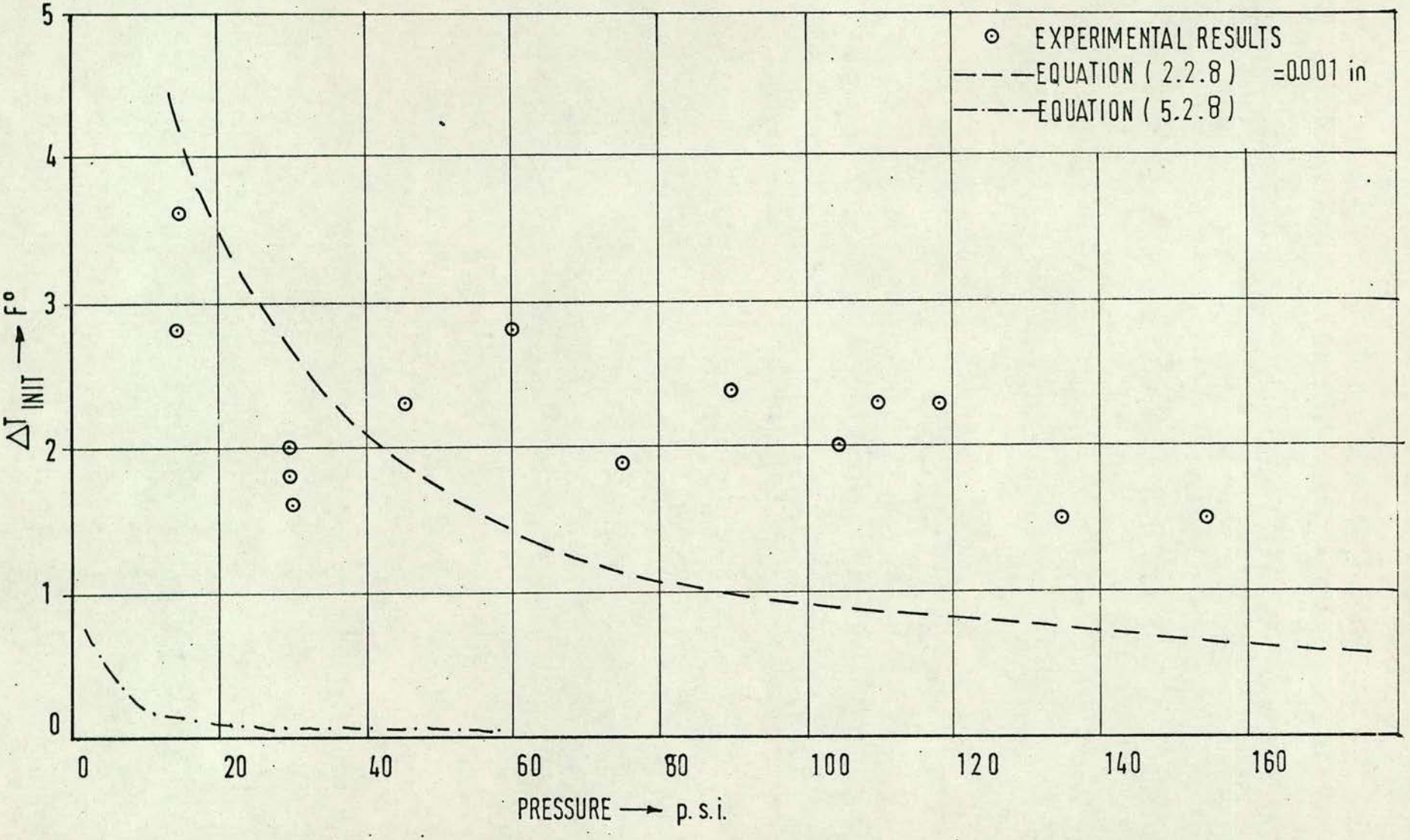

FIG.(50) VARIATION OF INITIATION SUPERHEAT TEMPERATURE DIFFERENCE WITH PRESSURE, SURFACE D.

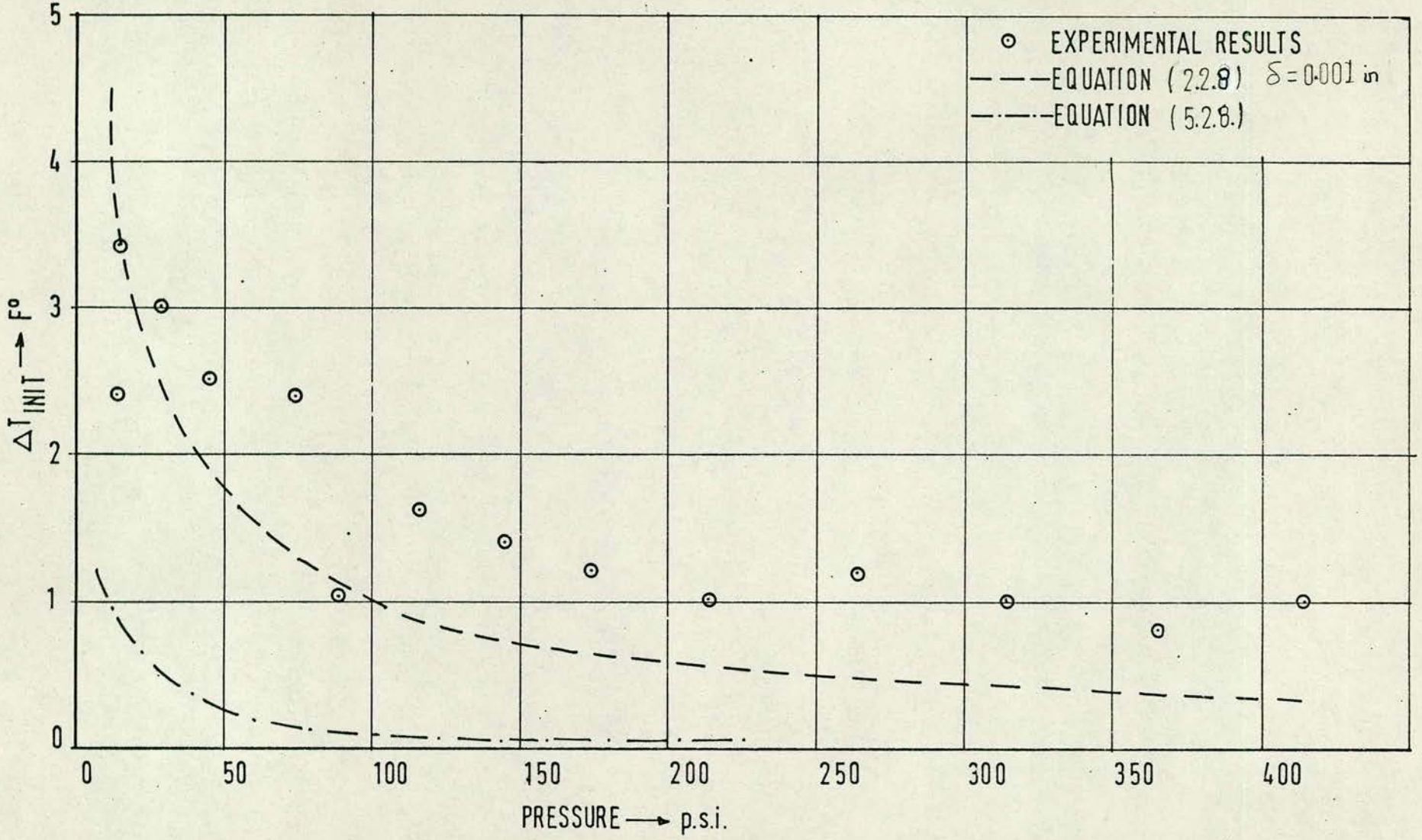

FIG.(51) VARIATION OF INITIATION SUPERHEAT TEMPERATURE DIFFERENCE WITH PRESSURE, SURFACE NG.2

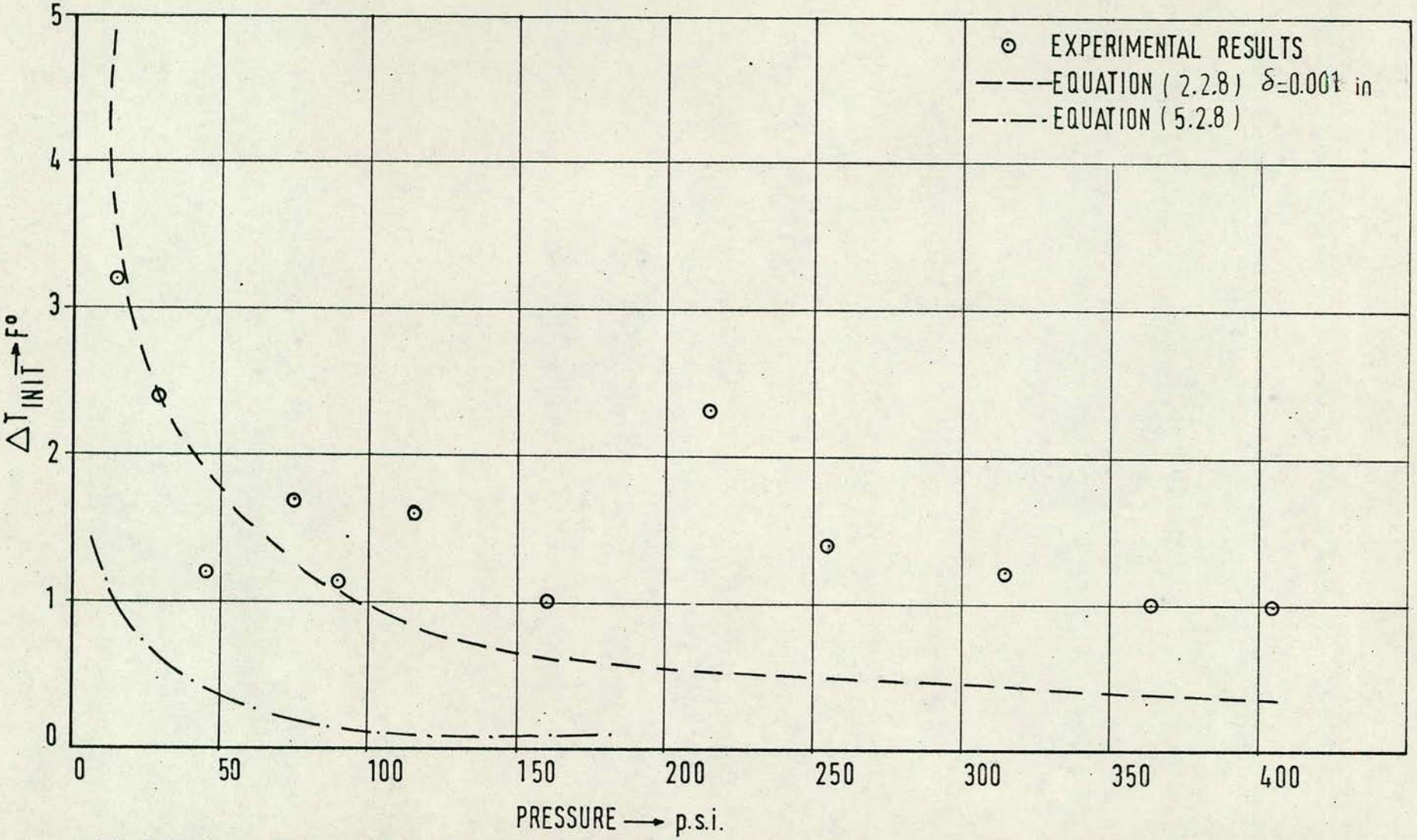

FIG. (52) VARIATION OF INITIATION SUPERHEAT TEMPERATURE DIFFERENCE WITH PRESSURE, SURFACE NG3.

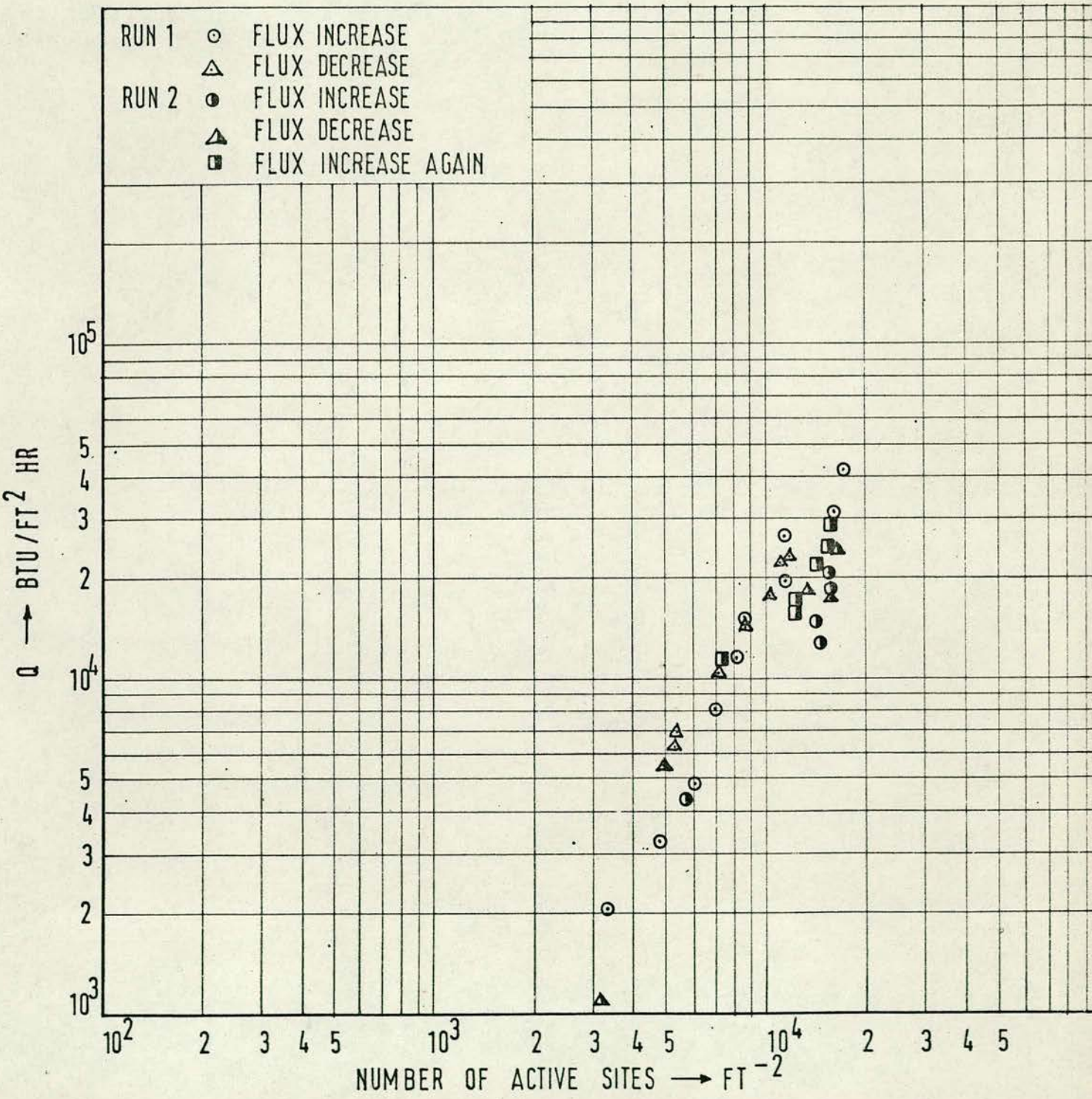

FIG. (53) VARIATION OF NUMBER OF ACTIVE SITES WITH HEAT FLUX FOR SURFACE NG 1 AT ATMOSPHERIC PRESSURE

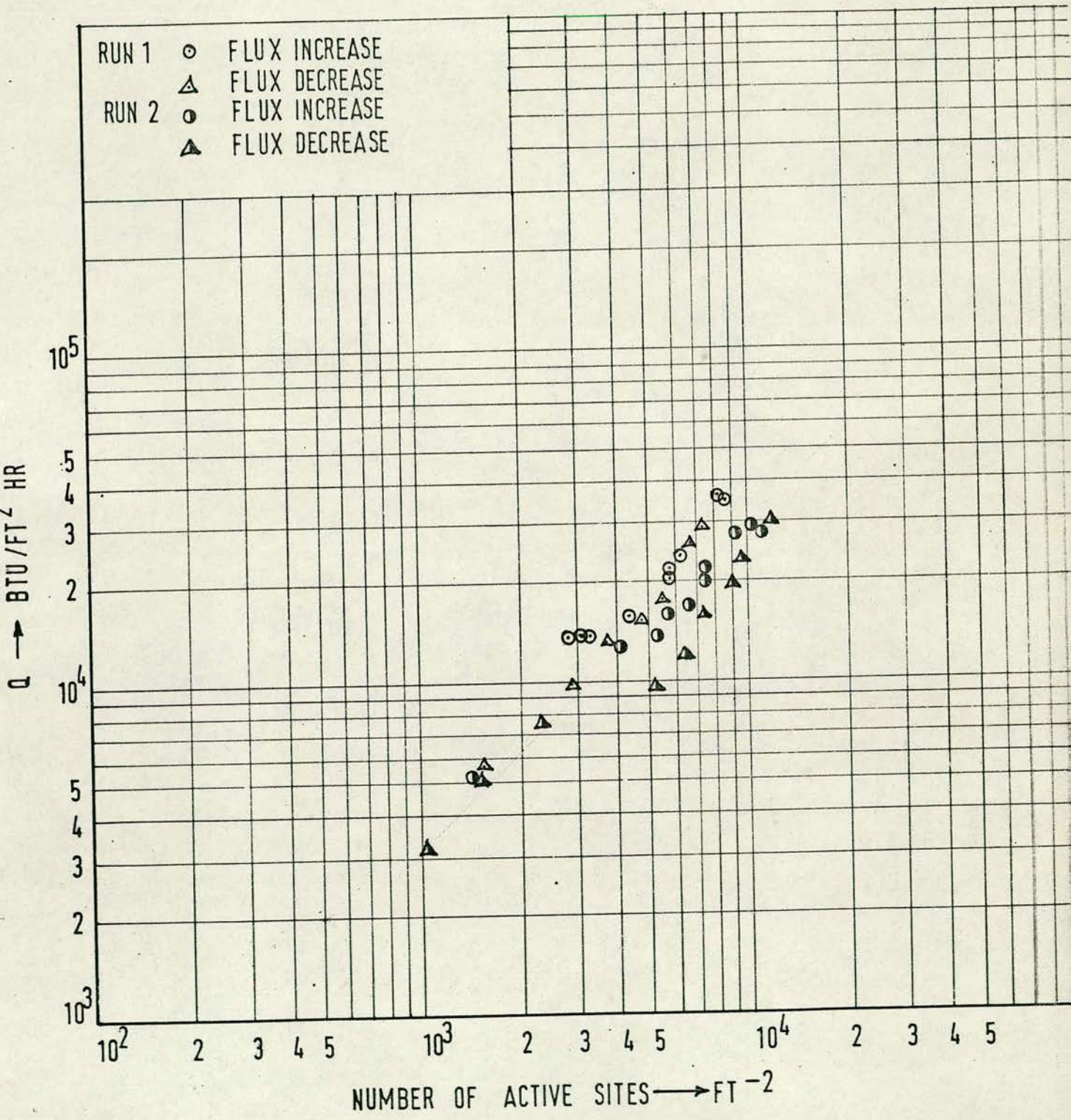

FIG. (54) VARIATION OF NUMBER OF ACTIVE SITES WITH HEAT FLUX FOR SURFACE NG 2 AT ATMOSPHERIC PRESSURE

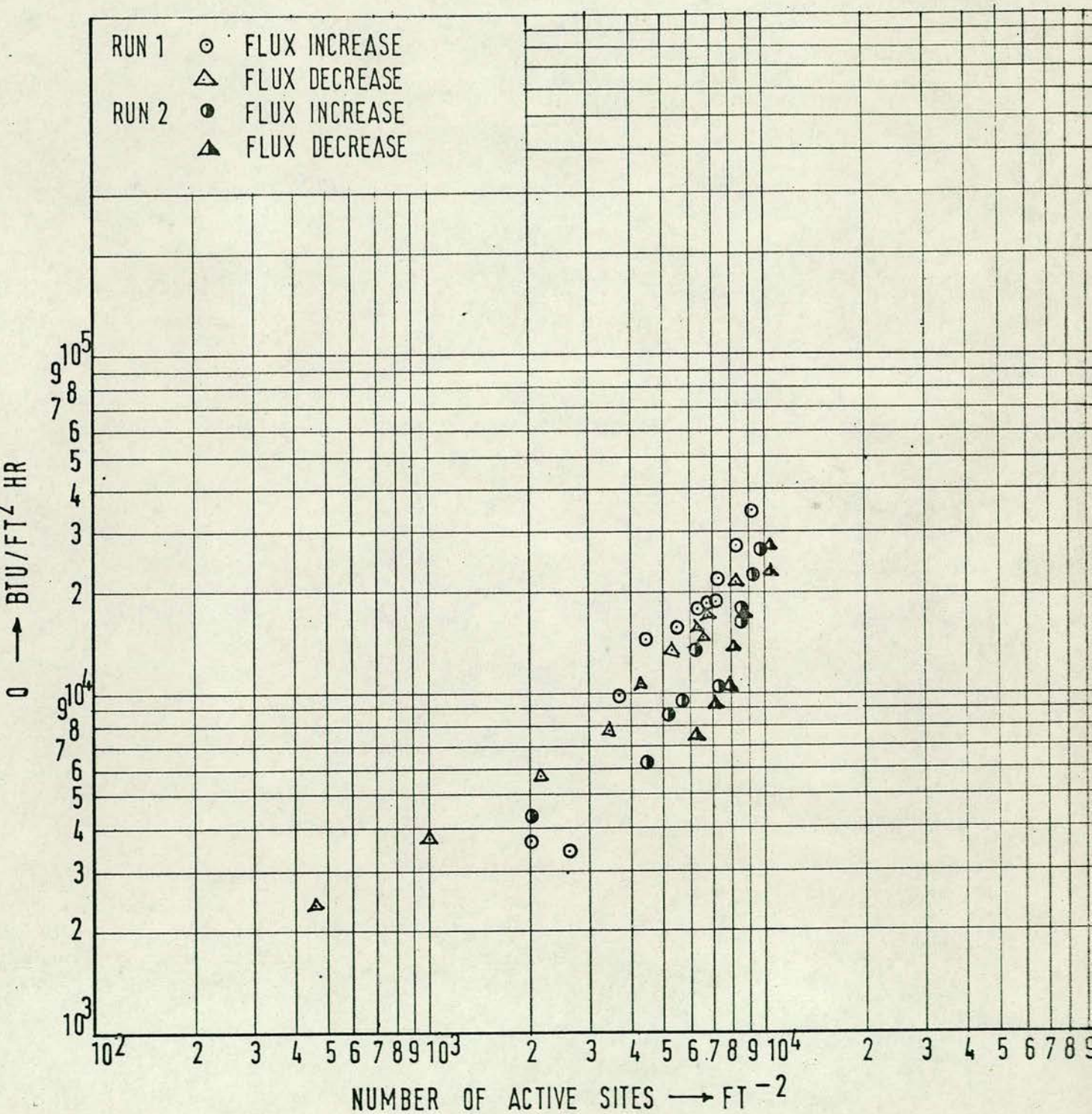

FIG. (55) VARIATION OF NUMBER OF ACTIVE SITES WITH HEAT FLUX FOR SURFACE NG 3 AT ATMOSPHERIC PRESSURE.

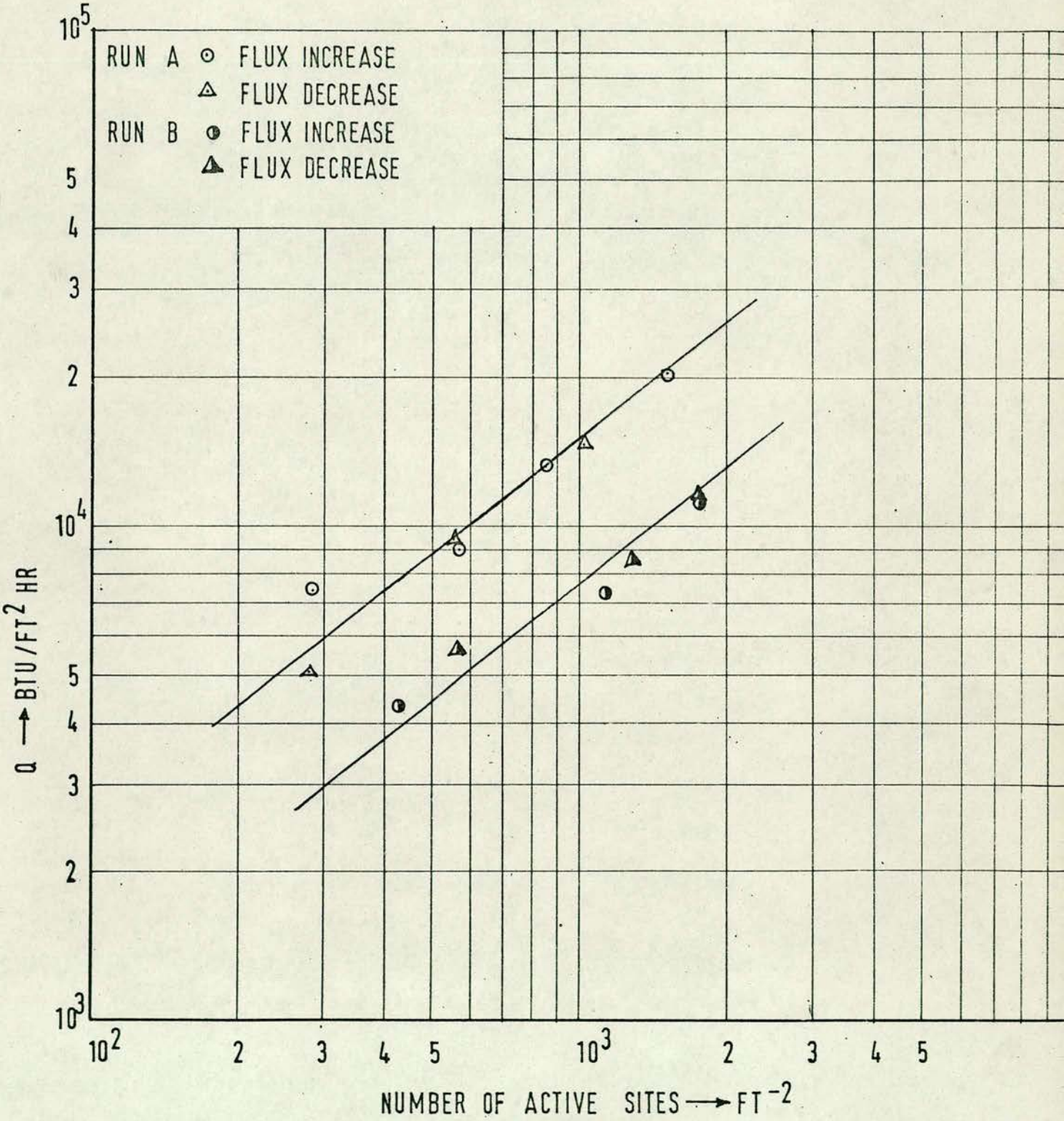

FIG.(56) VARIATION OF NUMBER OF ACTIVE SITES WITH HEAT FLUX FOR SURFACE A&B AT ATMOSPHERIC PRESSURE.

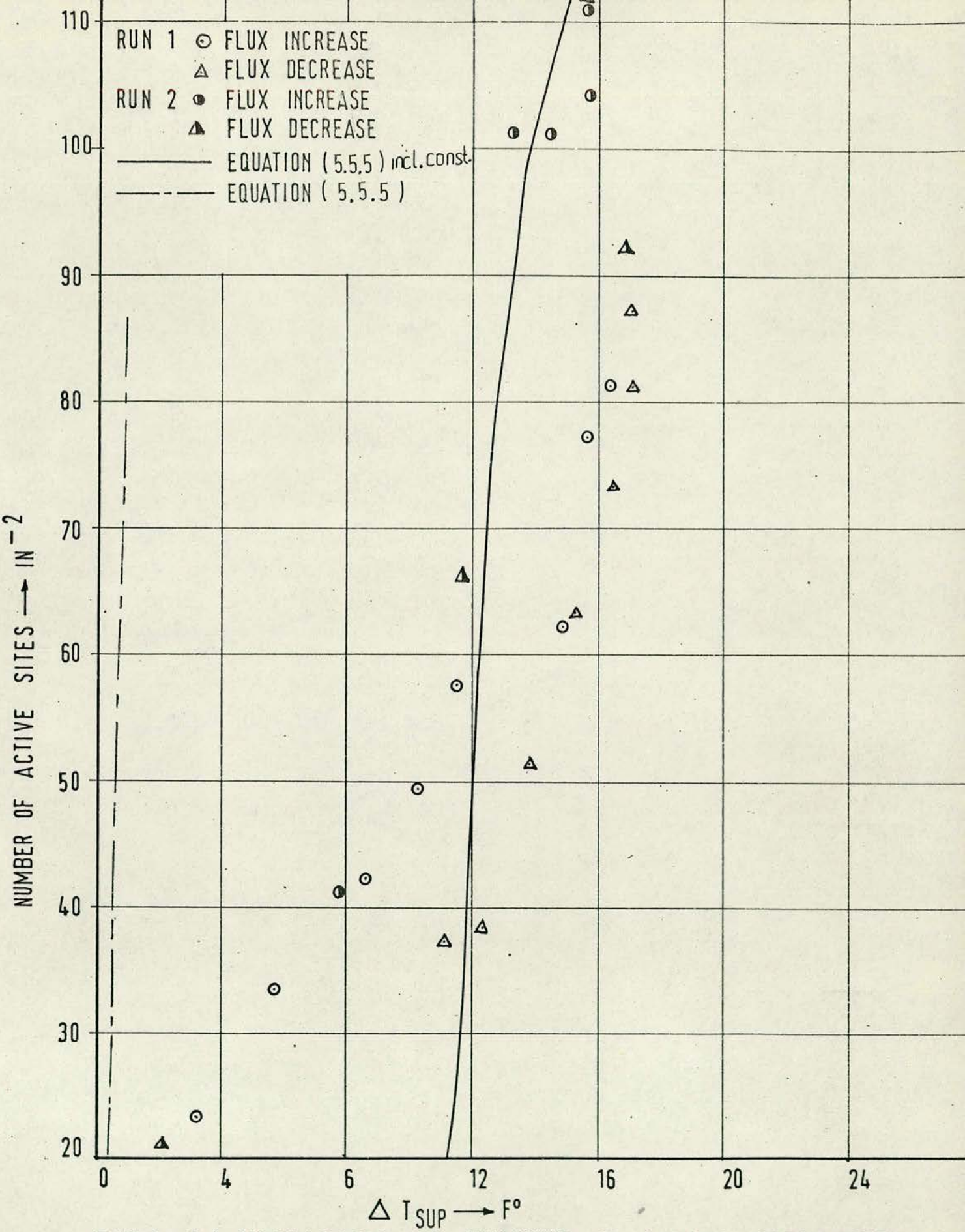

FIG.(57) VARIATION OF NUMBER OF ACTIVE SITES WITH SUPERHEAT TEMPERATURE DIFFERENCE FOR SURFACE NO 1 AT ATMOSPHERIC PRESSURE

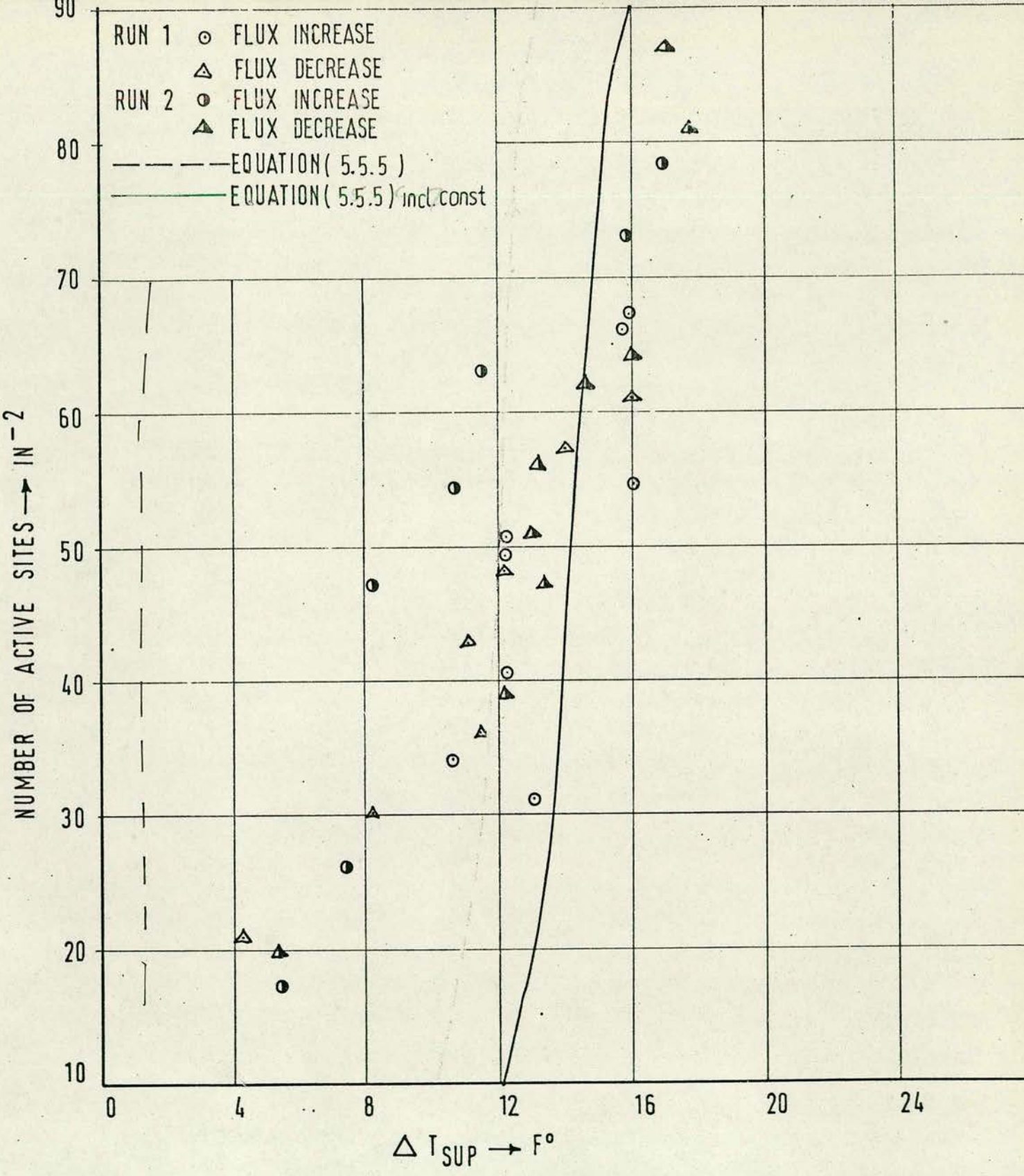

FIG(58) VARIATION OF NUMBER OF ACTIVE SITES WITH SUPERHEAT TEMPERATURE DIFFERENCE FOR SURFACE NG 2 AT ATMOSPHERIC PRESSURE

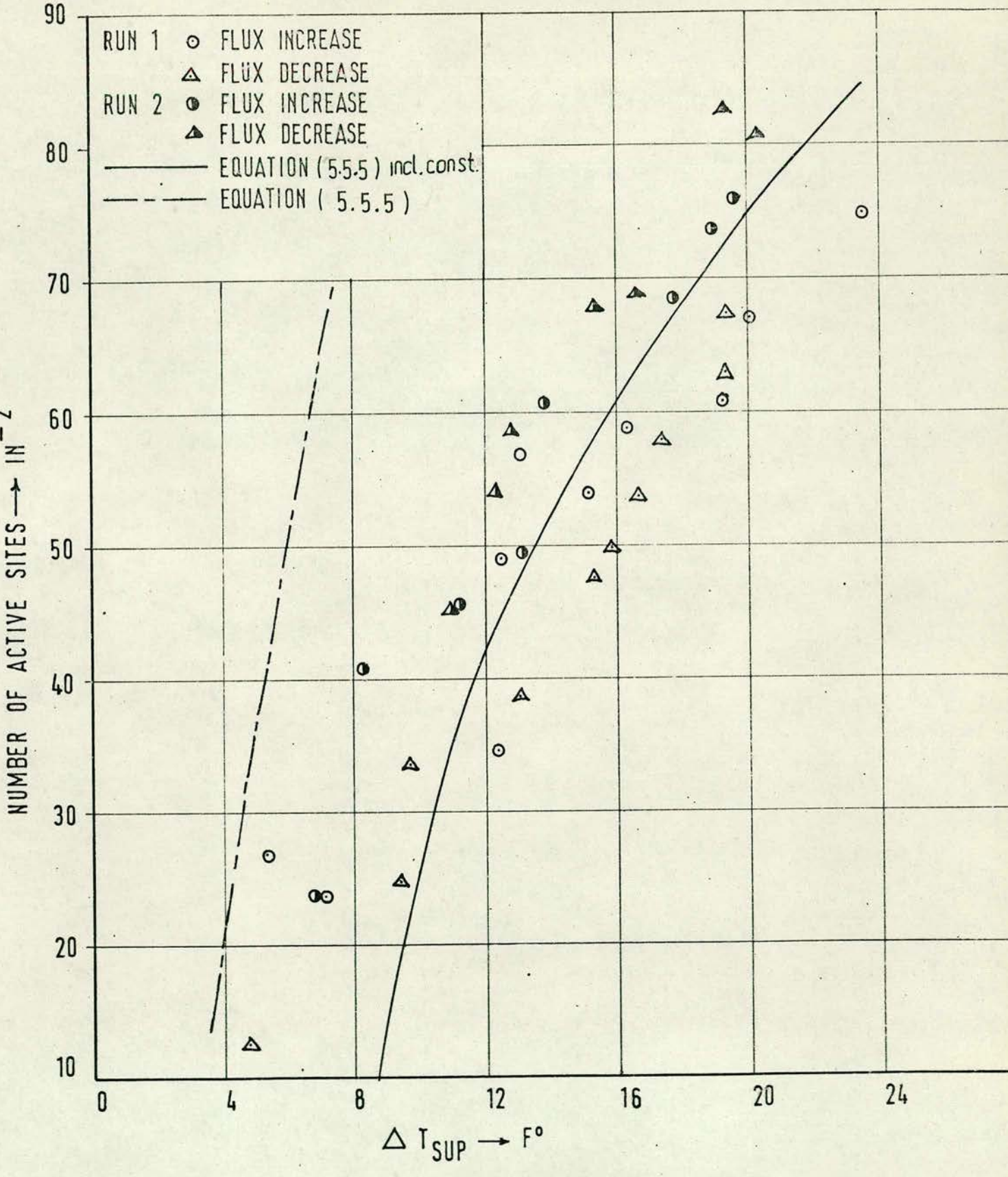

FIG.(59) VARIATION OF NUMBER OF ACTIVE SITES WITH SUPERHEAT TEMPERATURE DIFFERENCE FOR SURFACE NG 3 AT ATMOSPHERIC PRESSURE

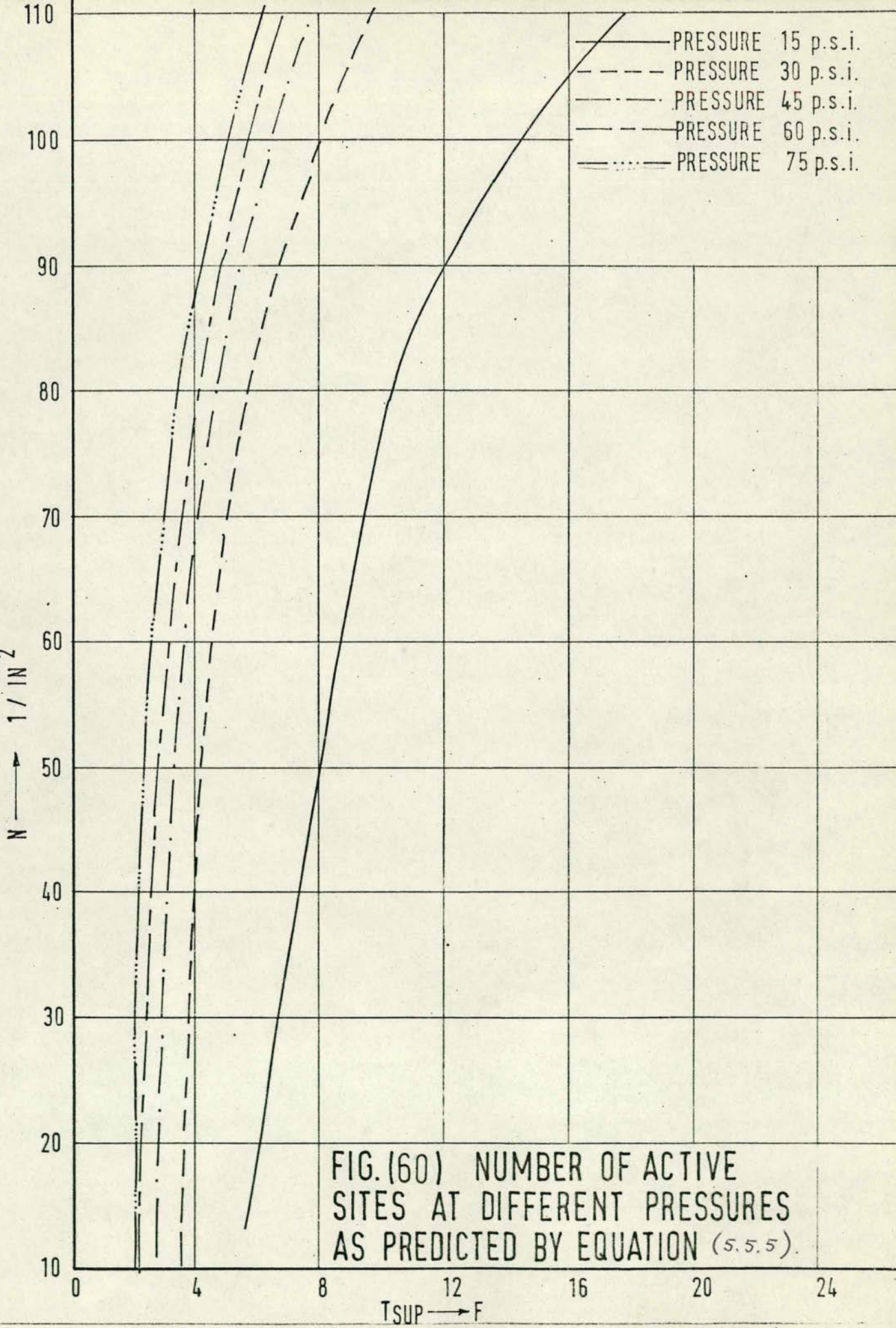

FIG. (60) NUMBER OF ACTIVE SITES AT DIFFERENT PRESSURES AS PREDICTED BY EQUATION (5.5.5).

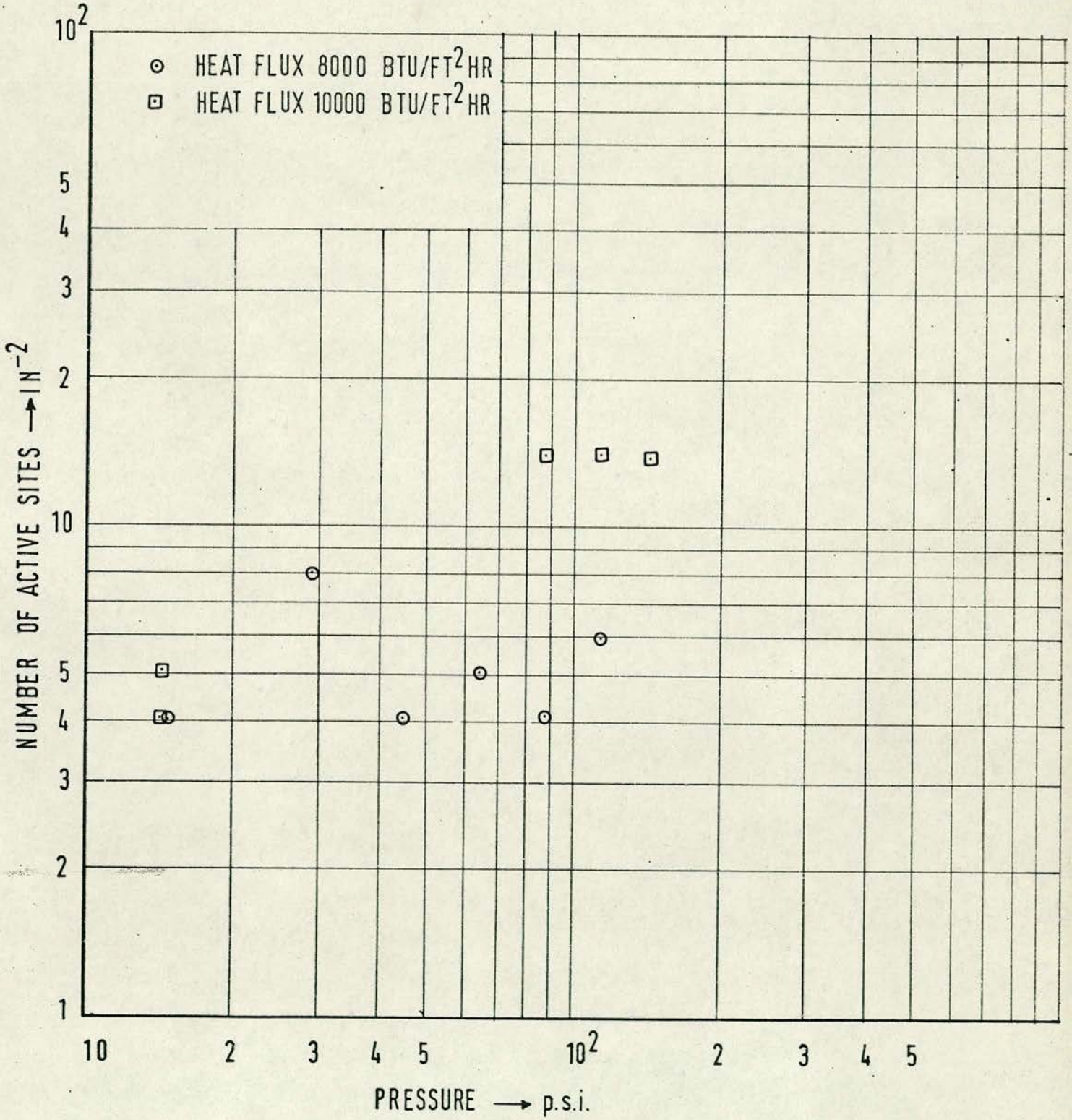

FIG.(61) VARIATION OF NUMBER OF ACTIVE SITES WITH PRESSURE FOR SURFACE C AT A CONSTANT HEAT FLUX.

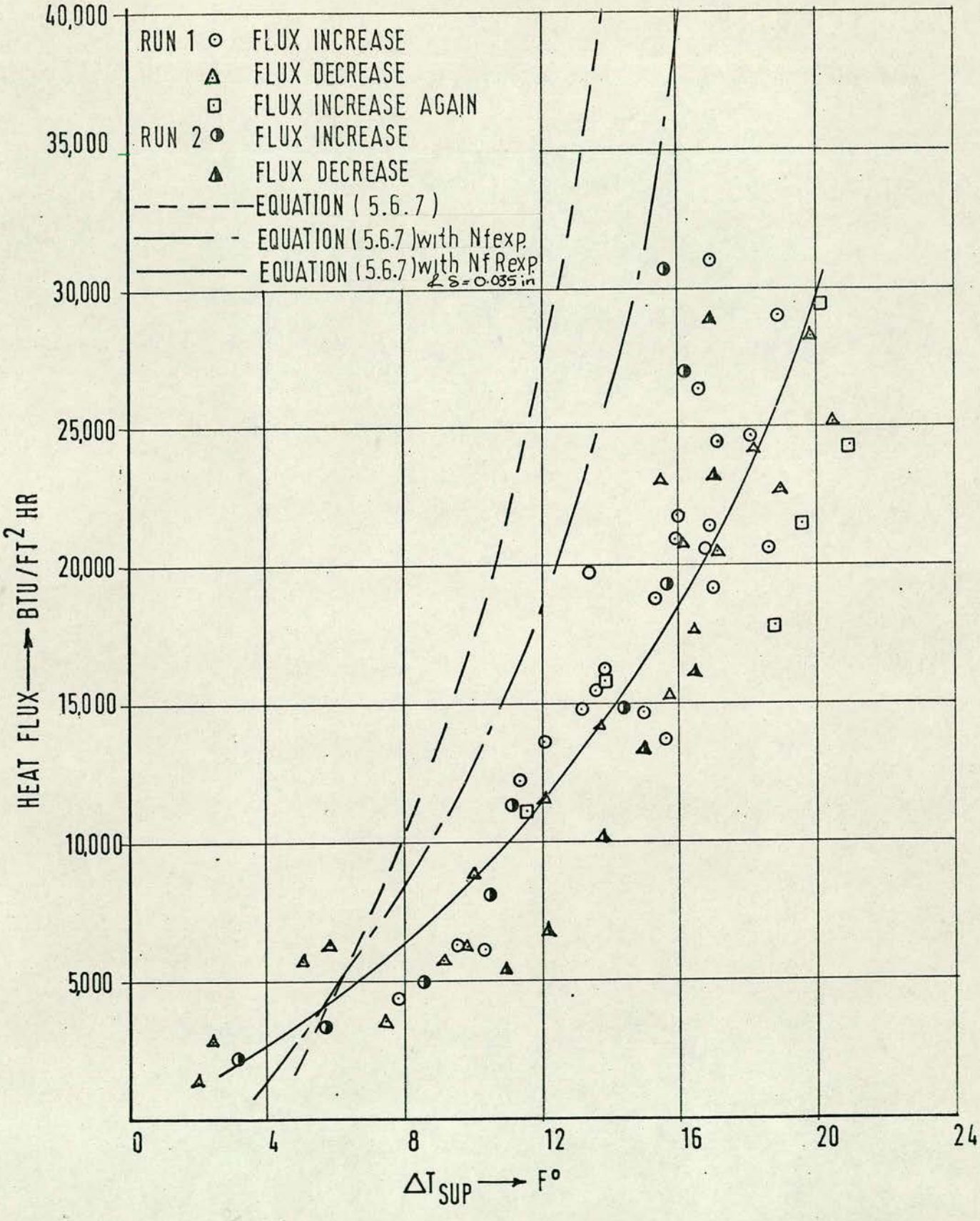

FIG. (62) HEAT FLUX VARIATION WITH SUPERHEAT TEMPERATURE DIFFERENCE FOR SURFACE NG1 AT 15 p.s.i.

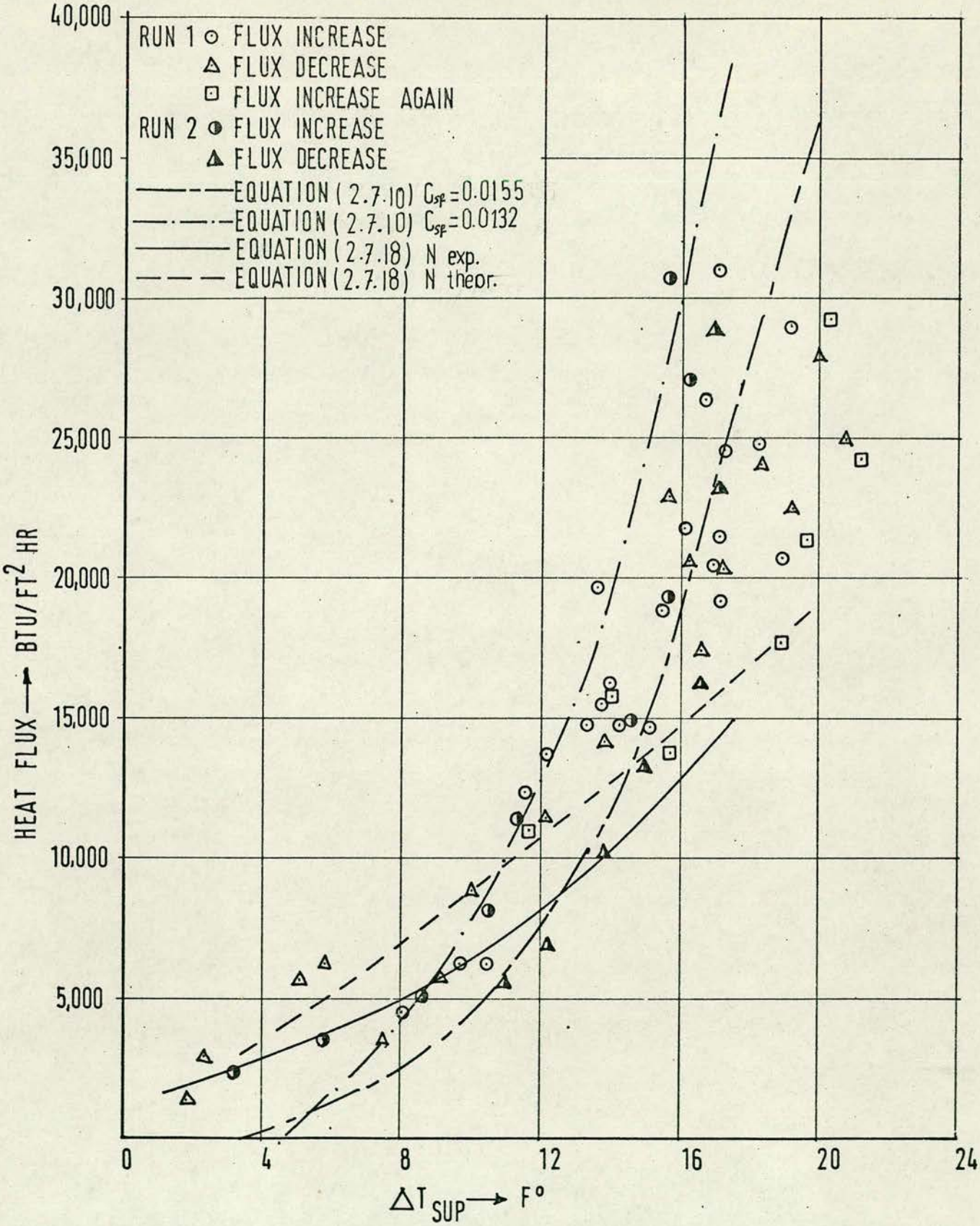

FIG.(63) HEAT FLUX VARIATION WITH SUPERHEAT TEMPERATURE DIFFERENCE FOR SURFACE NG1 AT 15p.s.i.

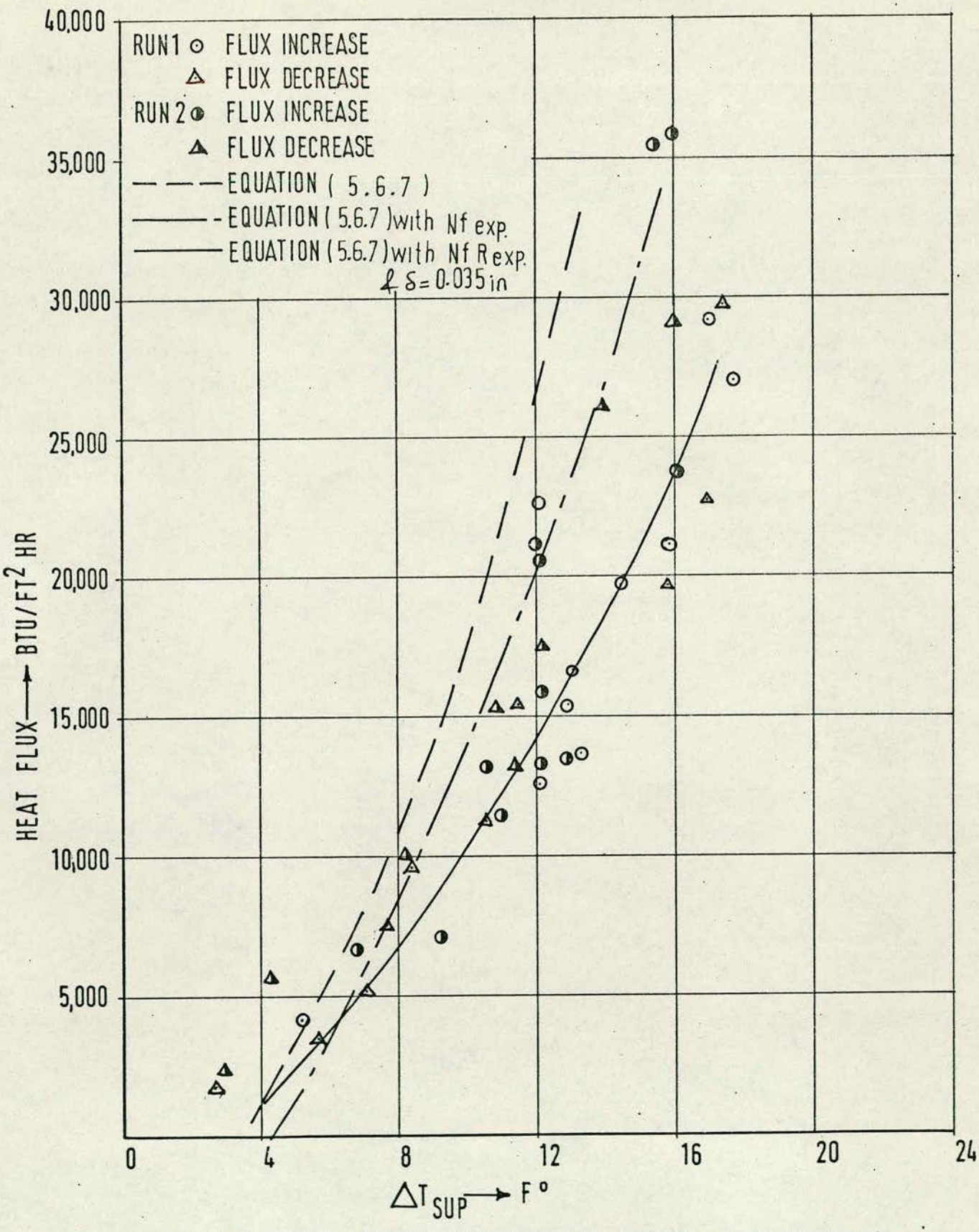

FIG.(64) HEAT FLUX VARIATION WITH SUPERHEAT TEMPERATURE DIFFERENCE FOR SURFACE NG2 AT 15 p.s.i.

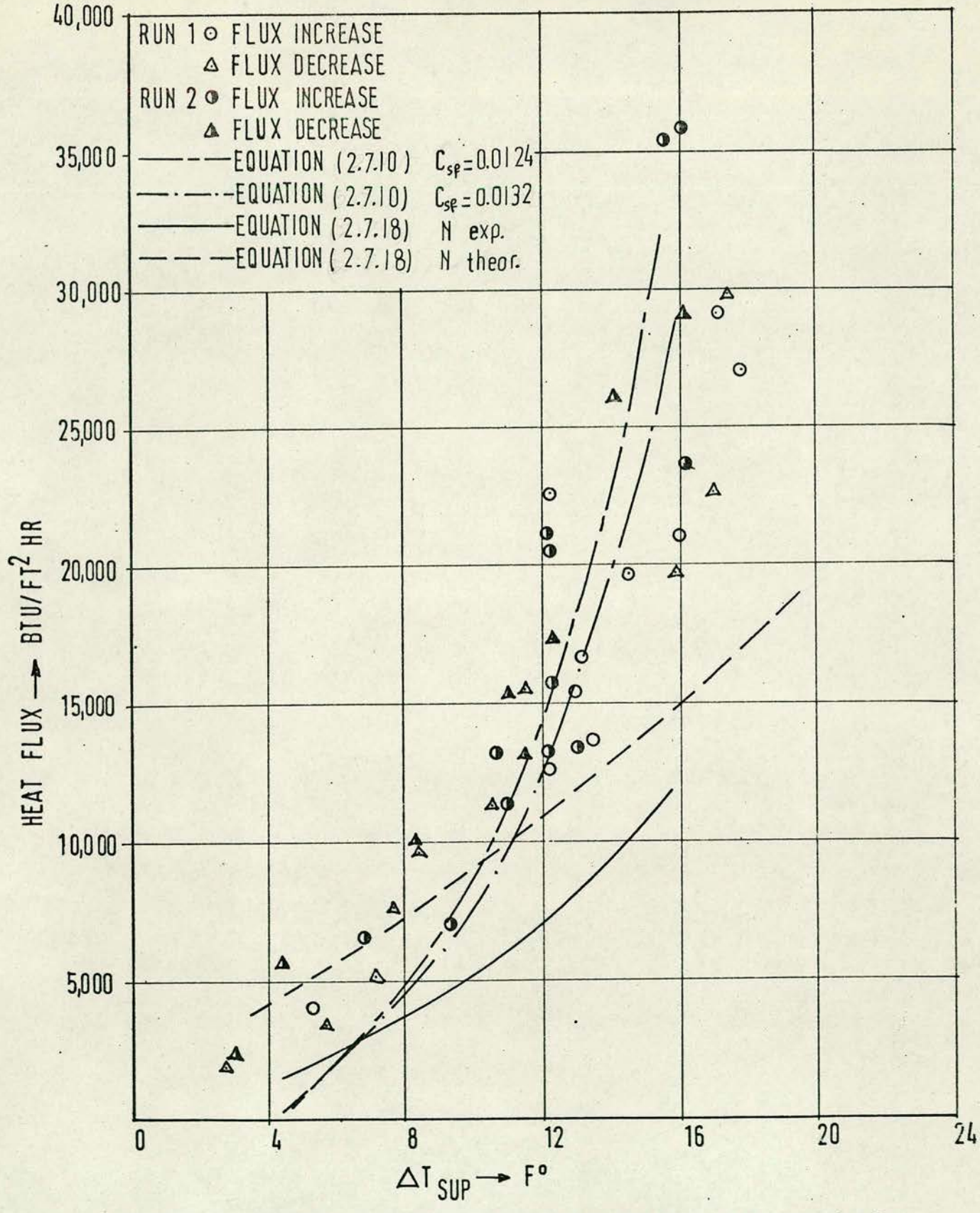

FIG.(65) HEAT FLUX VARIATION WITH SUPERHEAT TEMPERATURE DIFFERENCE FOR SURFACE NG2 AT 15 p.s.i.

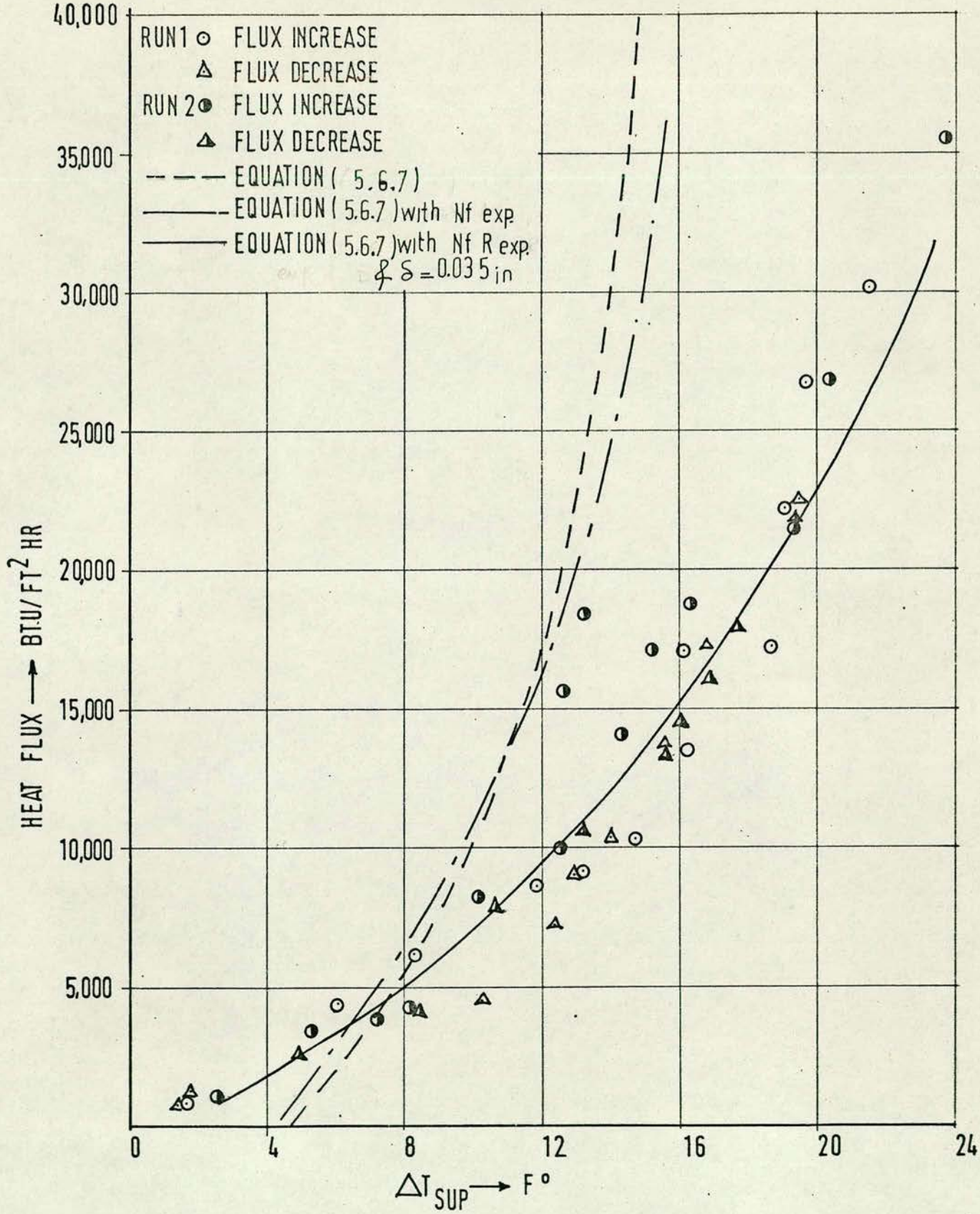

FIG(66) HEAT FLUX VARIATION WITH SUPERHEAT TEMPERATURE DIFFERENCE FOR SURFACE NG3 AT 15 p.s.i.

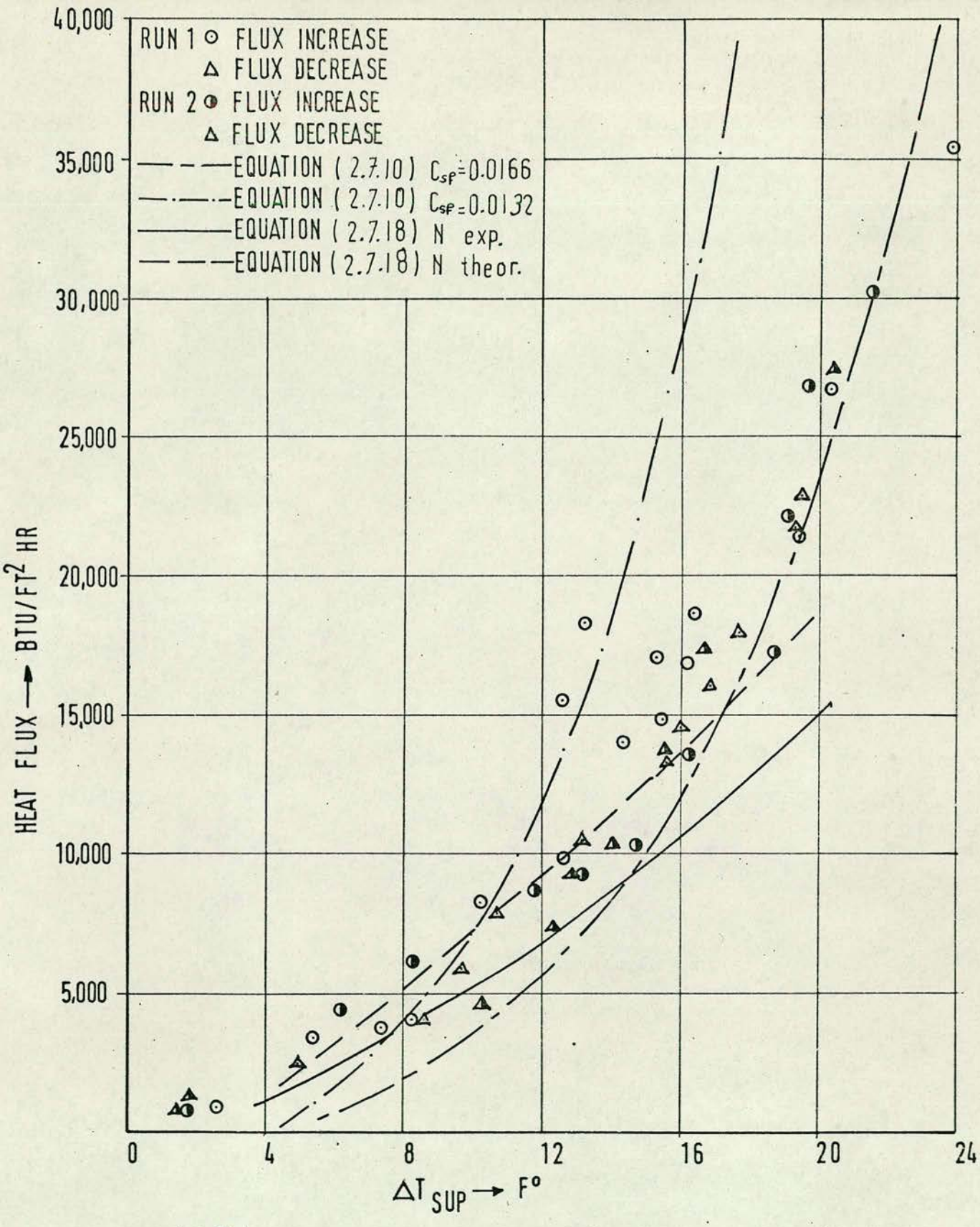

FIG.(67) HEAT FLUX VARIATION WITH SUPERHEAT TEMPERATURE DIFFERENCE FOR SURFACE NG3 AT 15 p.s.i.

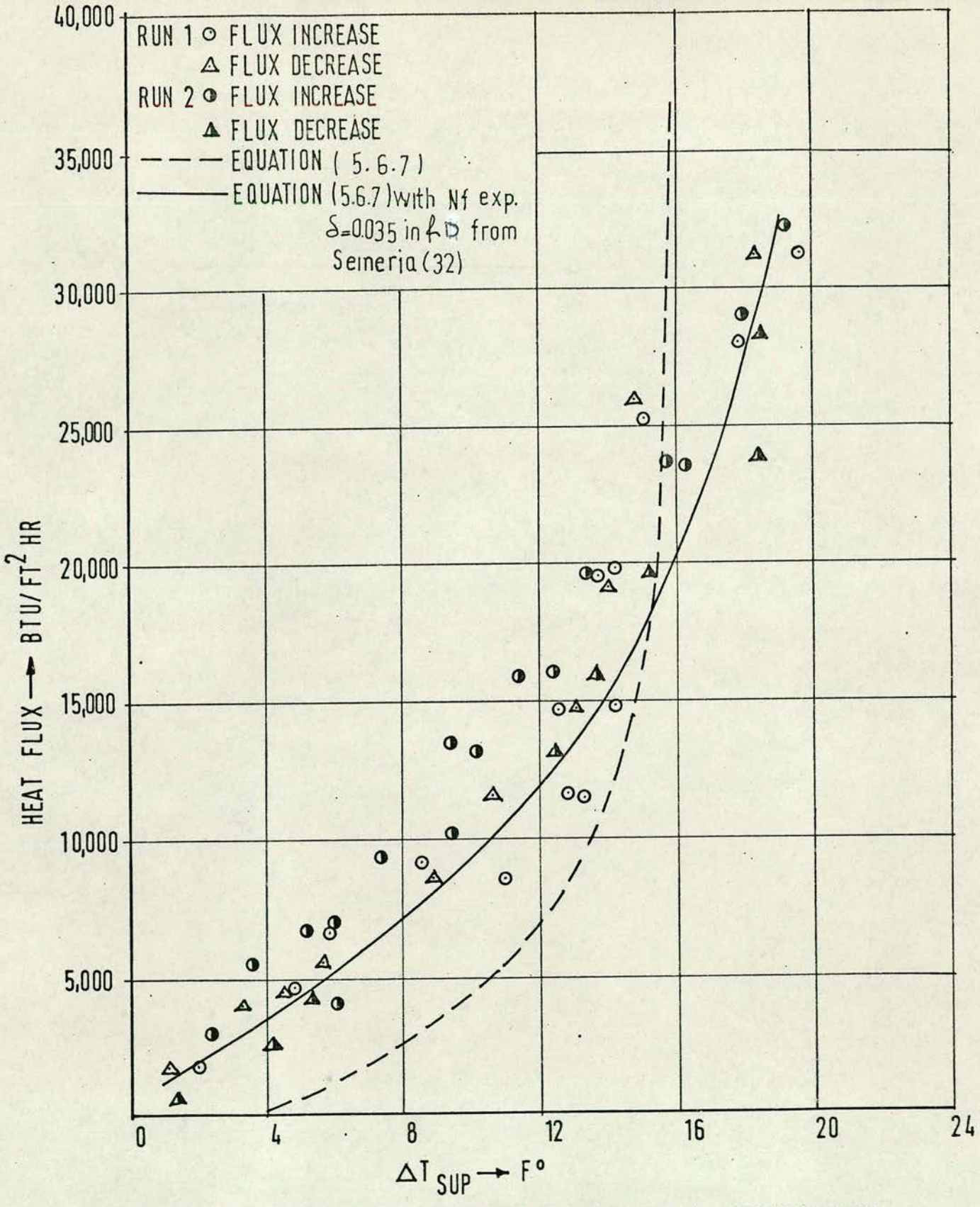

FIG. (68) HEAT FLUX VARIATION WITH SUPERHEAT TEMPERATURE DIFFERENCE FOR SURFACE NG3 AT 30 p.s.i.

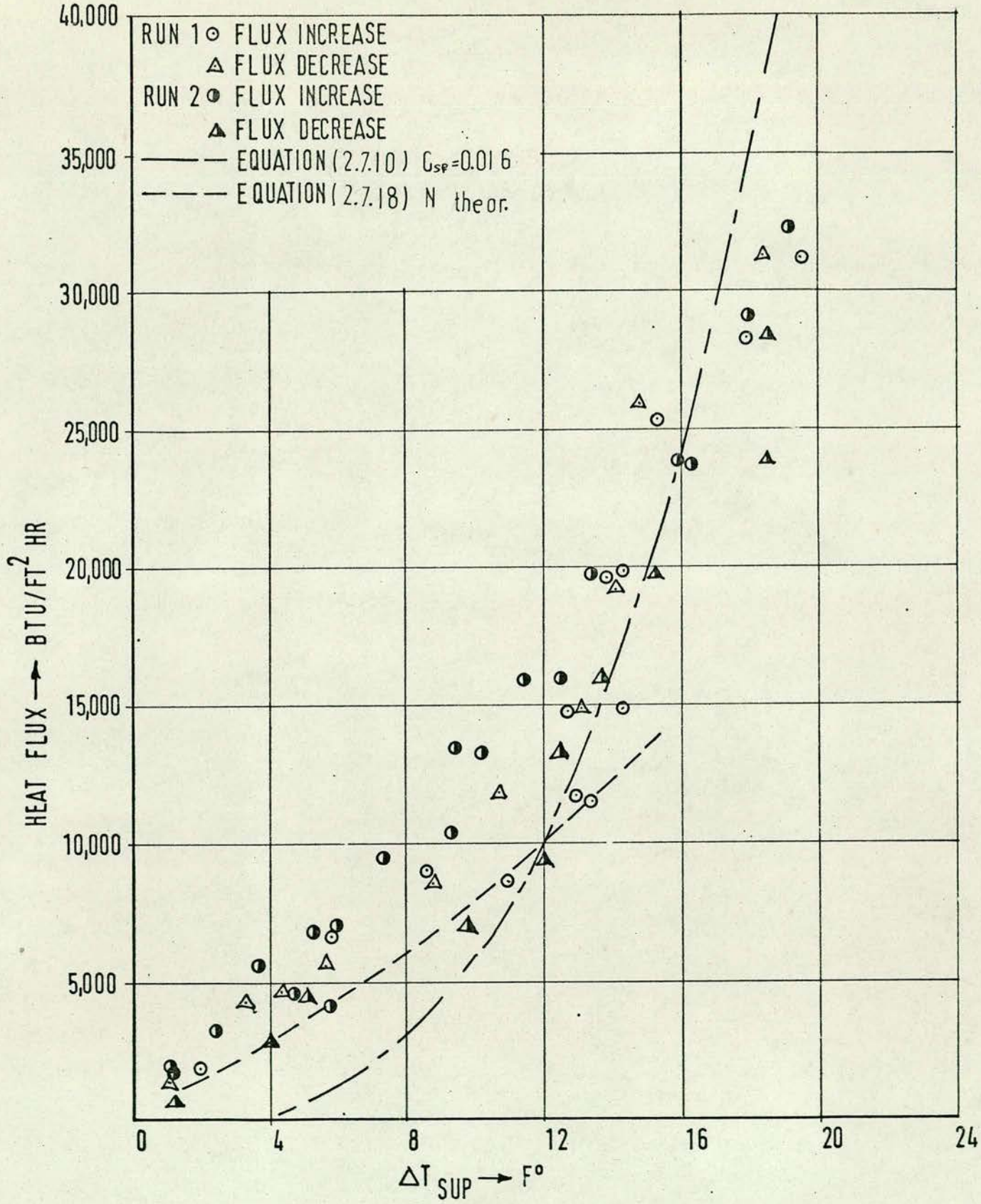

FIG.(69) HEAT FLUX VARIATION WITH SUPERHEAT TEMPERATURE DIFFERENCE FOR SURFACE NG3 AT 30 p.s.i.

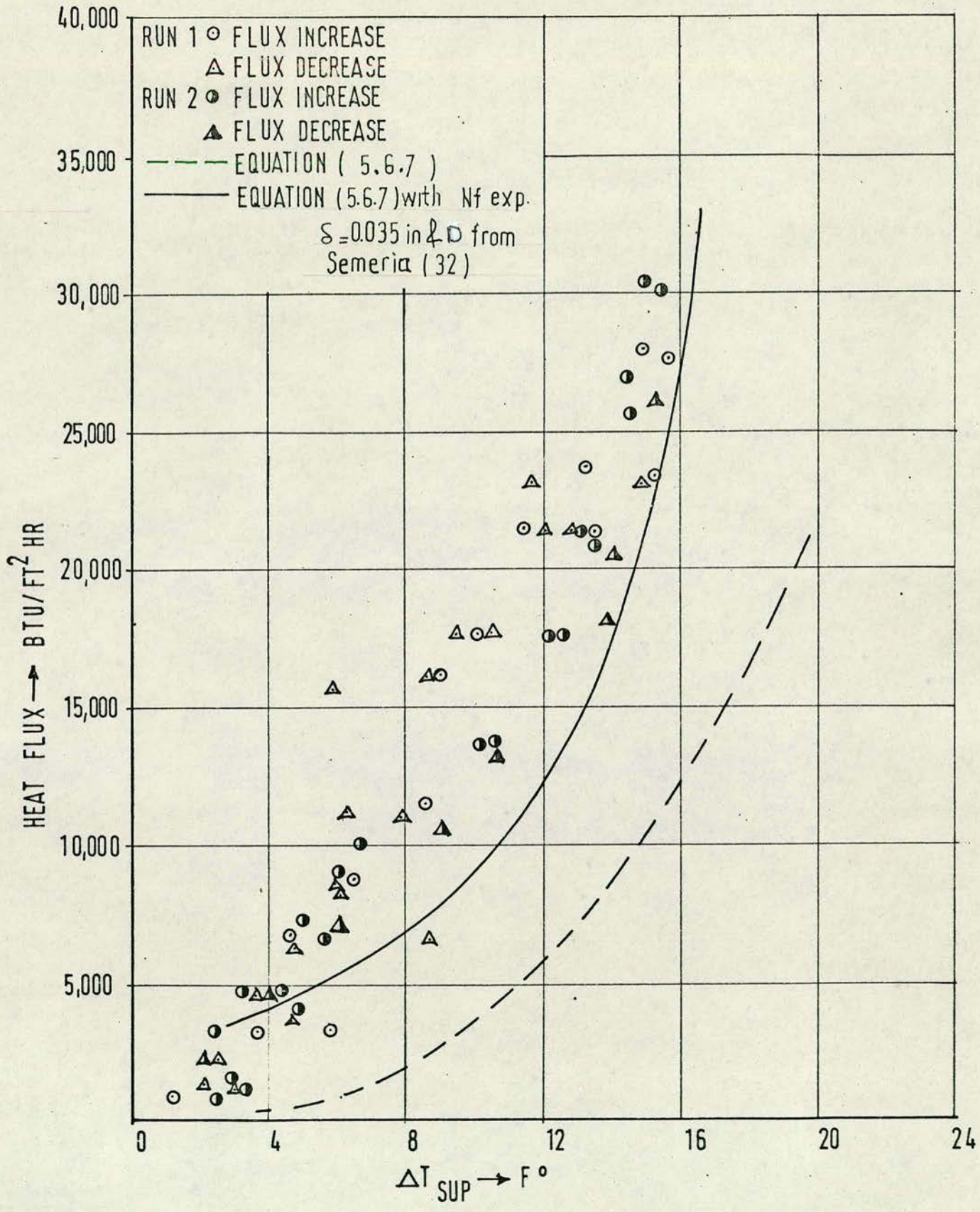

FIG. (70) HEAT FLUX VARIATION WITH SUPERHEAT TEMPERATURE DIFFERENCE FOR SURFACE NG 3 AT 45 p.s.i.

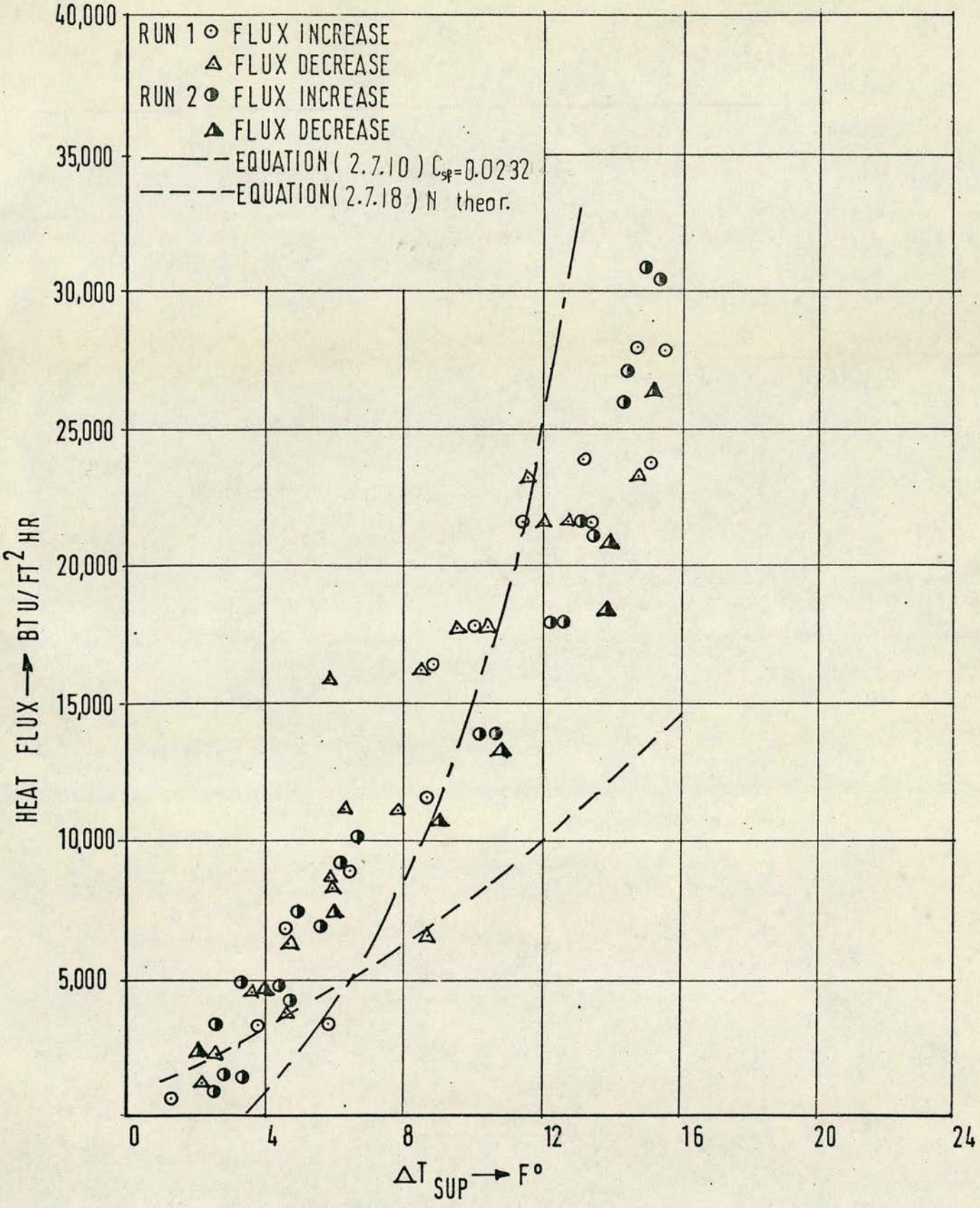

FIG. (71) HEAT FLUX VARIATION WITH SUPERHEAT TEMPERATURE DIFFERENCE FOR SURFACE NG3 AT 45p.s.i.

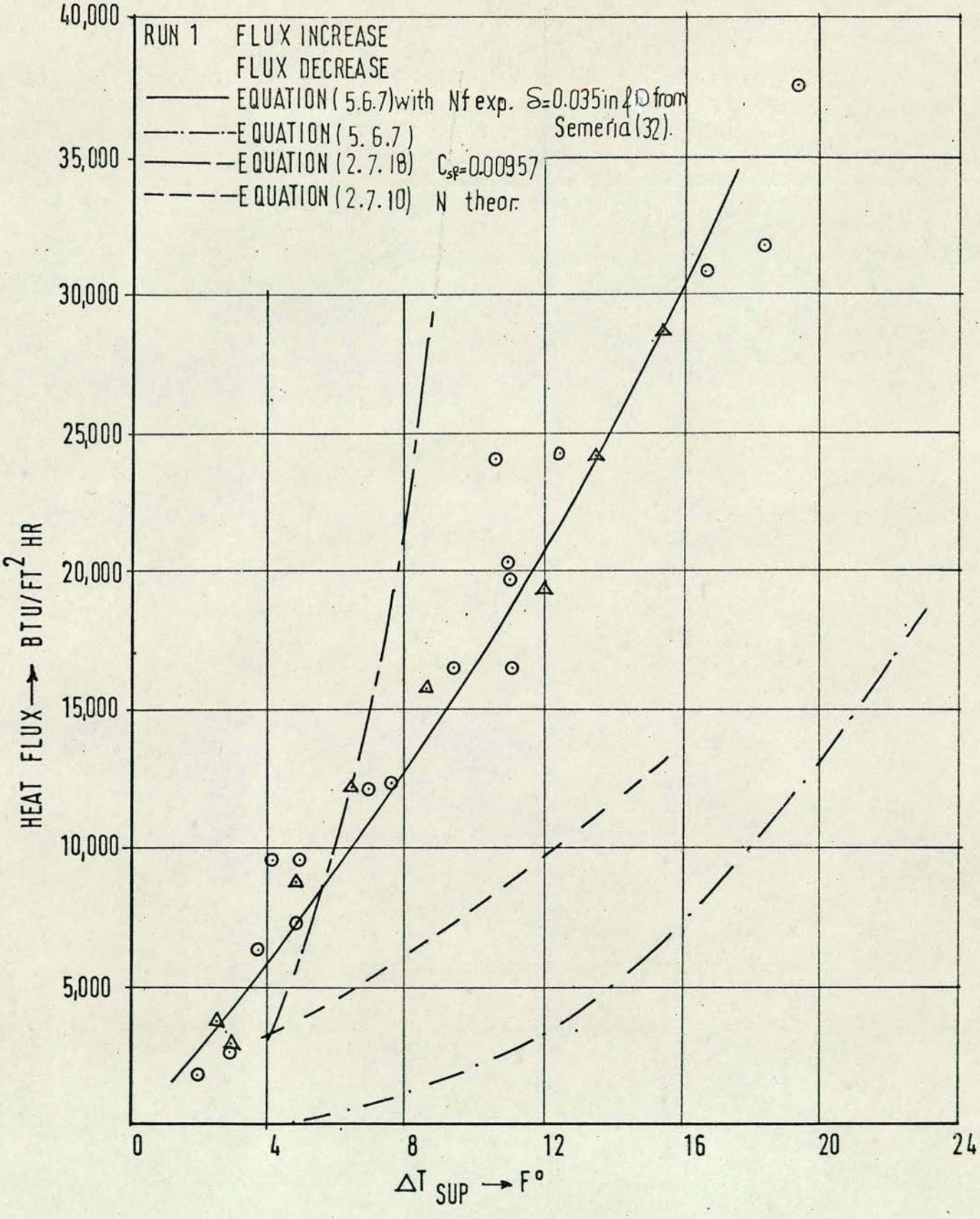

FIG. (72) HEAT FLUX VARIATION WITH SUPERHEAT TEMPERATURE DIFFERENCE FOR SURFACE NG3 AT 60 p.s.i.

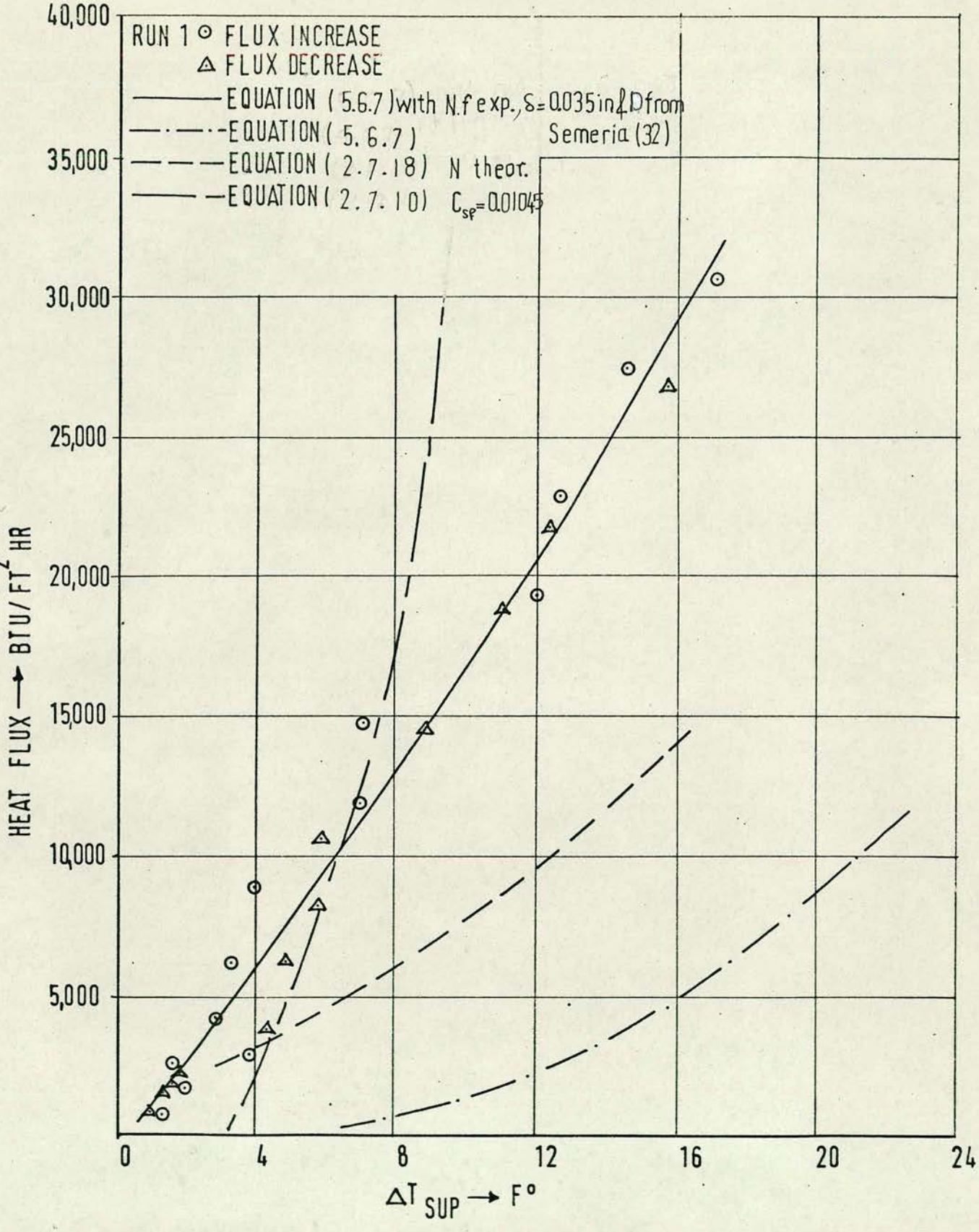

FIG.(73) HEAT FLUX VARIATION WITH SUPERHEAT . TEMPERATURE DIFFERENCE FOR SURFACE NG3 AT 75 p.s.i.

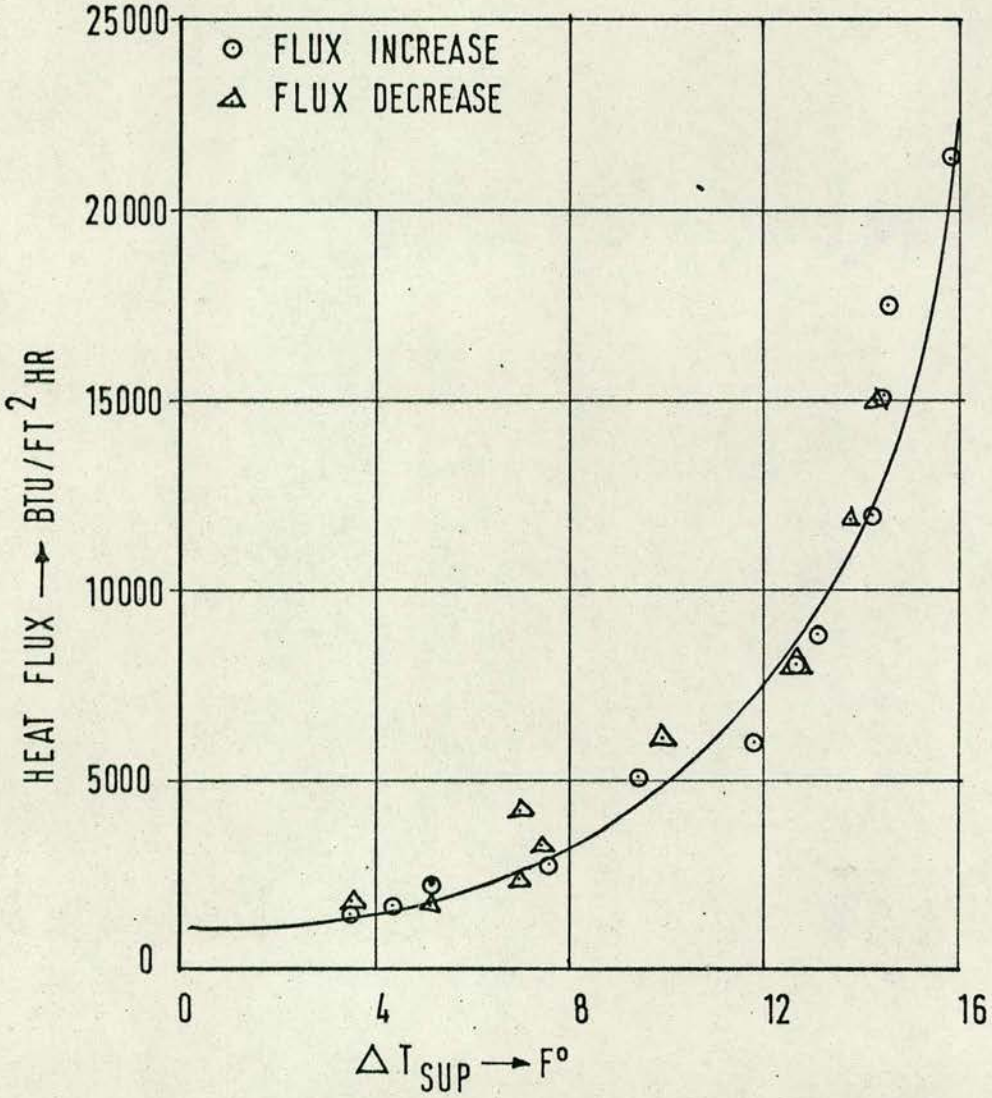

FIG.(74) HEAT FLUX VARIATION WITH SUPERHEAT TEMPERATURE DIFFERENCE FOR SURFACE D AT 15 p.s.i.

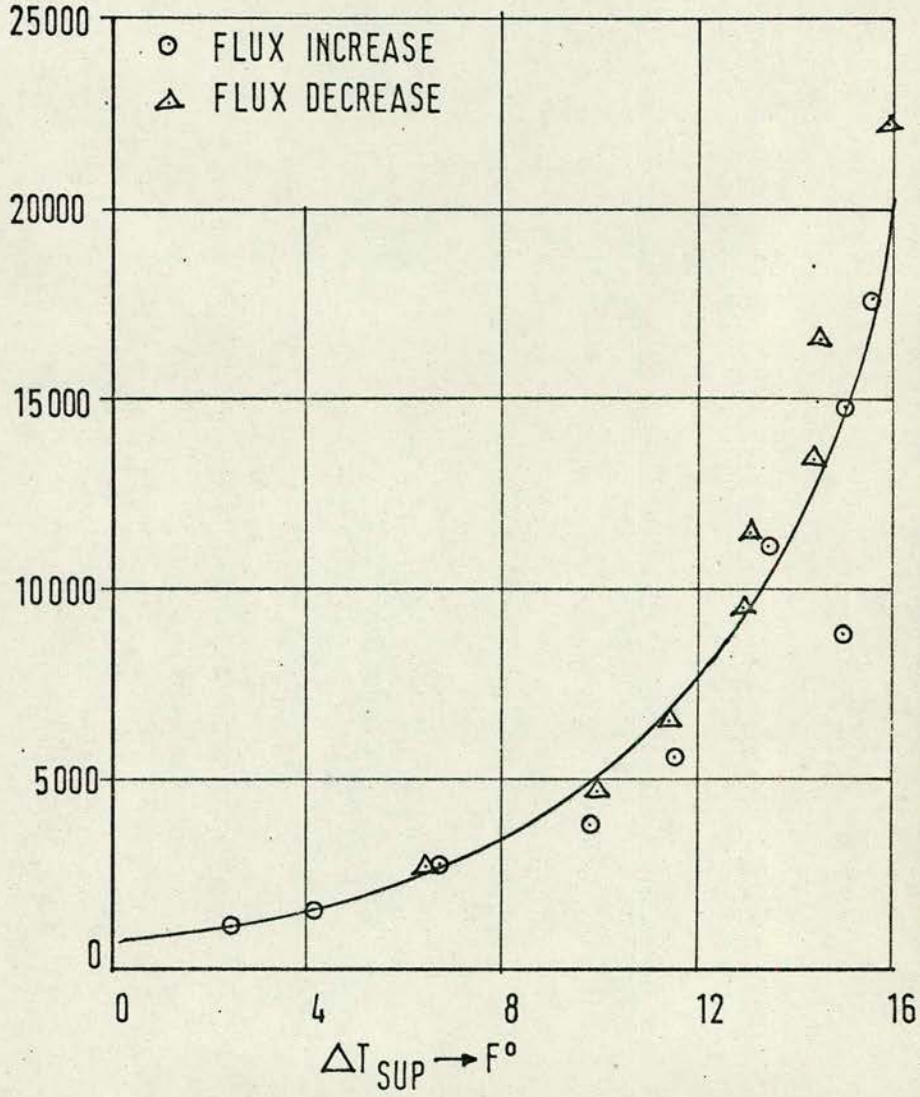

FIG.(75) HEAT FLUX VARIATION WITH SUPERHEAT TEMPERATURE DIFFERENCE FOR SURFACE D AT 30 p.s.i.

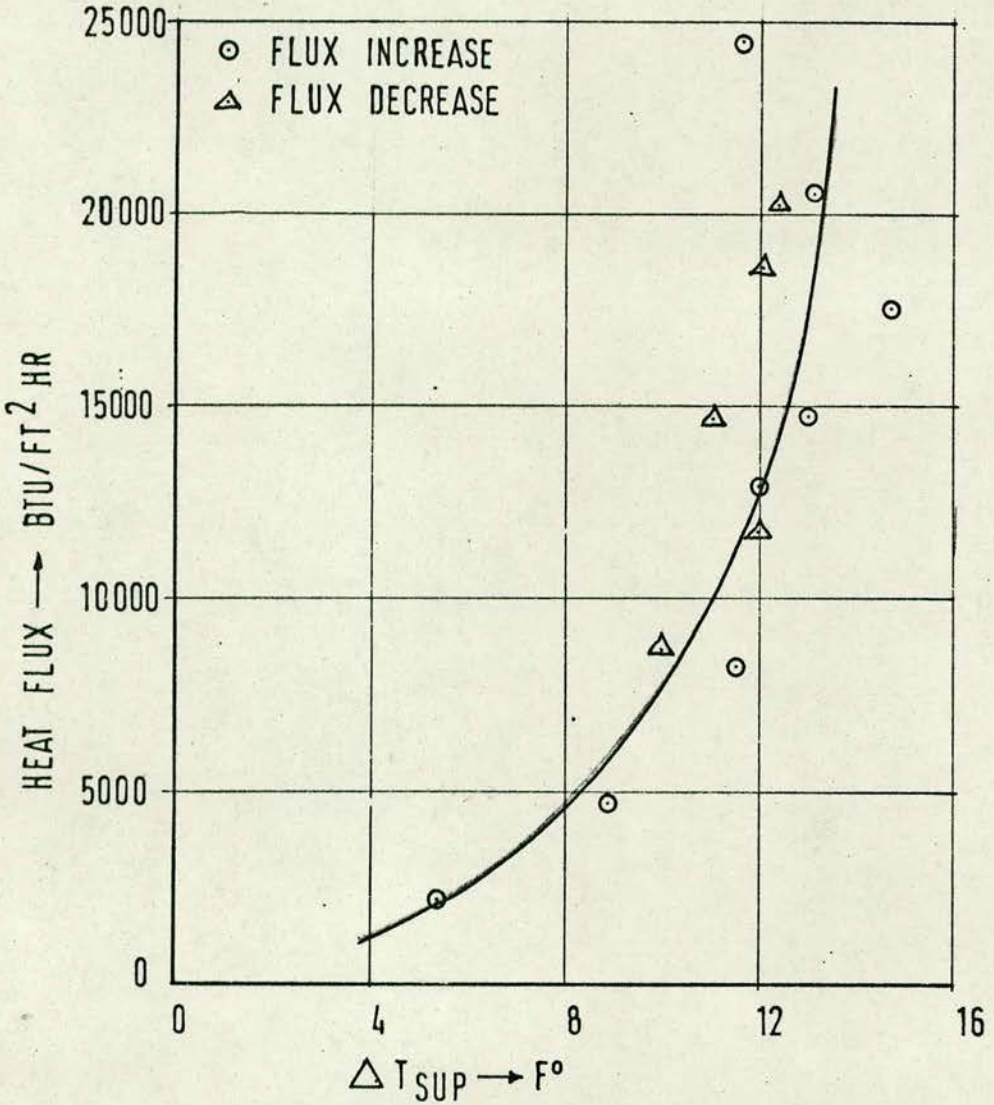

FIG.(76) HEAT FLUX VARIATION WITH SUPERHEAT TEMPERATURE DIFFERENCE FOR SURFACE D AT 45 p.s.i.

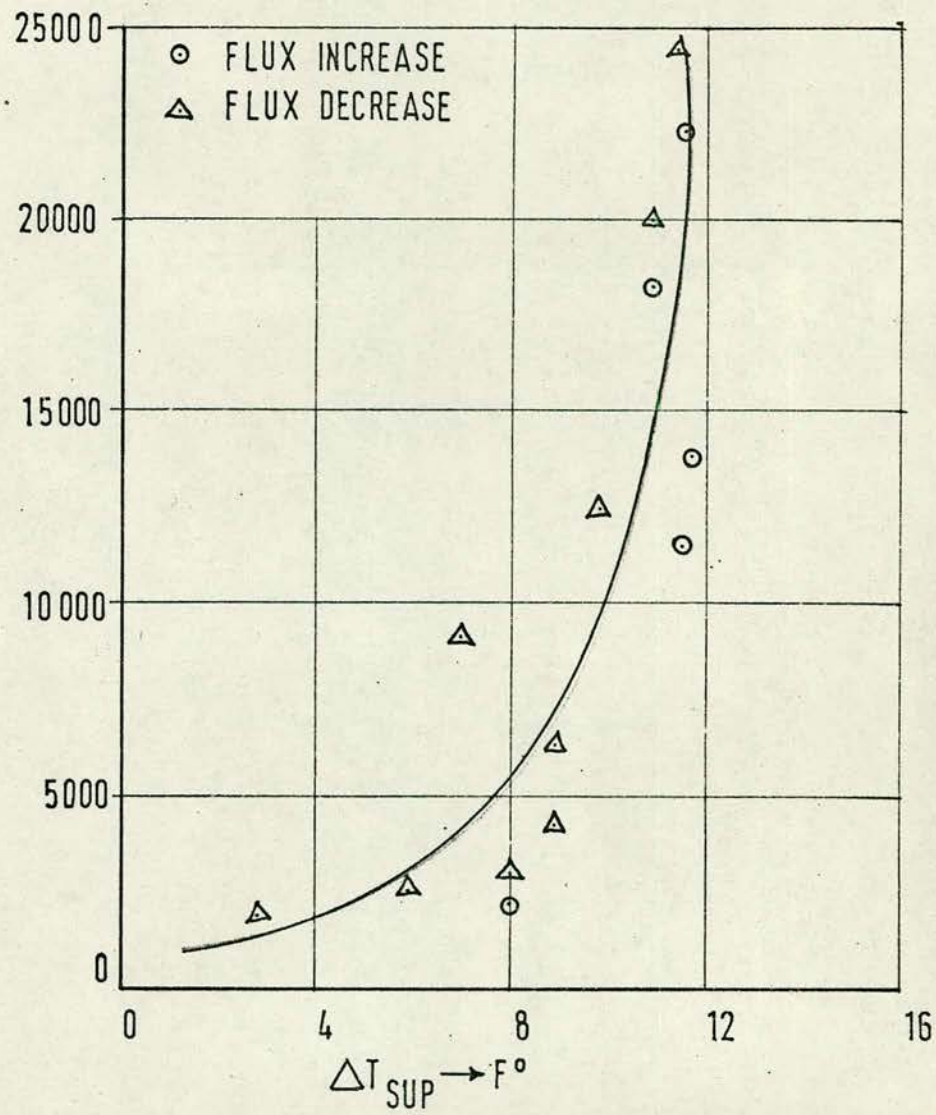

FIG.(77) HEAT FLUX VARIATION WITH SUPERHEAT TEMPERATURE DIFFERENCE FOR SURFACE D AT 65 p.s.i.

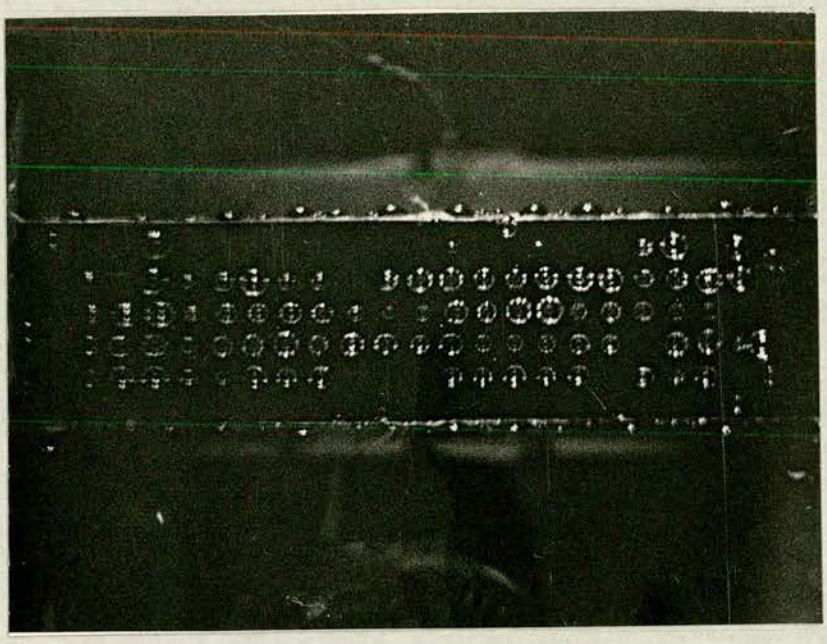

Fig. (78) Bubbles forming on surface NG1 at pressure 14.68 psi.

Q/A = 2660 Btu/ft^{2}hr, Tw = 215.6^{o}F Tb = 209.6^{o}F

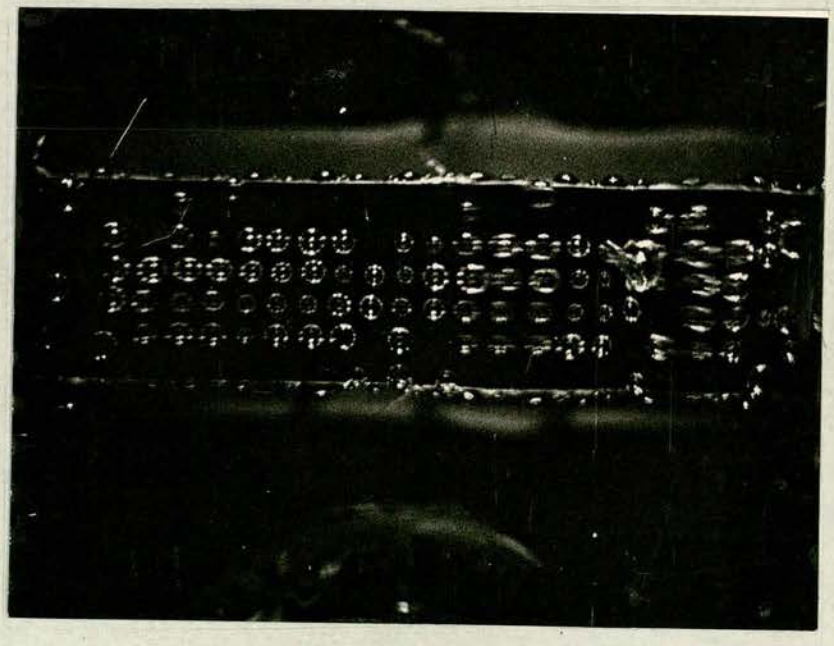

Fig. (79) Bubbles forming on surface NG1 at pressure 14.68 psi.

Q/A = 6180 Btu/ft^{2}hr., Tw - 221^{o}F, Tb = 209.2^{o}F

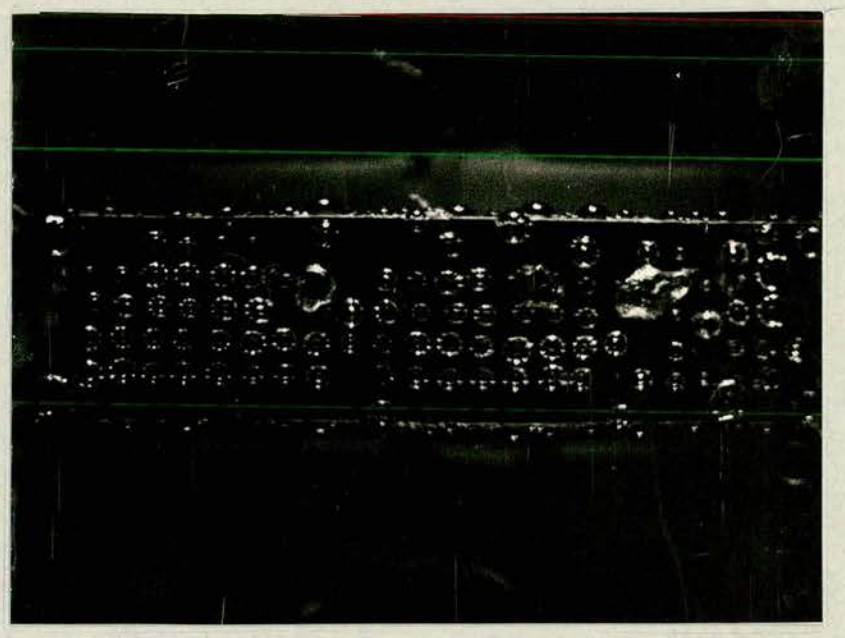

Fig. (80) Bubble forming on surface NG1 at pressure 14.68 psi.

Q/A = 8080 Btu/ft^{2}Hr. Tw = 221.8F^o, Tb = 209.6F^o

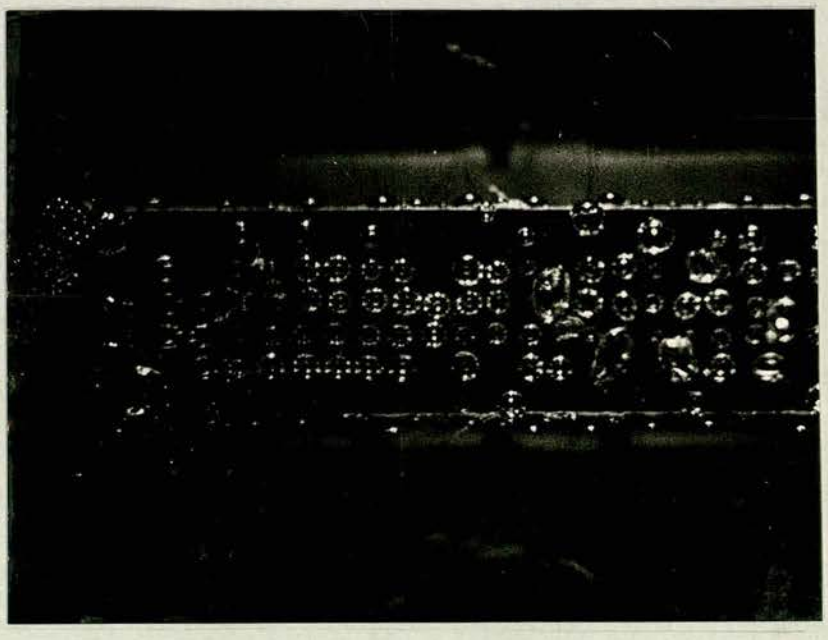

Fig. (81) Bubble forming on surface NG1 at pressure 14.68psi.

Q/A = 9810 Btu/ft^{2}hr., Tw = 223^{o}F, Tb = 209.2^{o}F

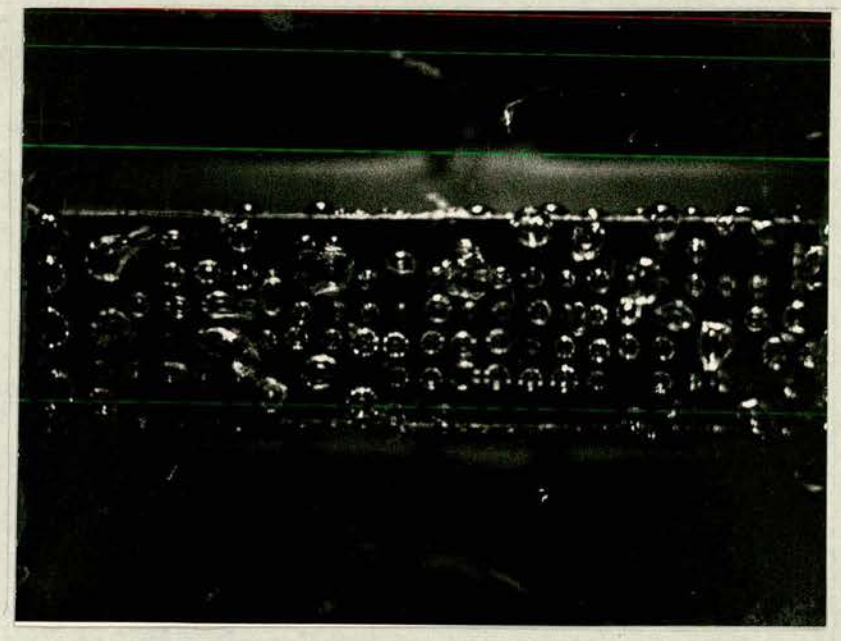

Fig. (82) Bubbles forming on surface NG1 at pressure 14.68psi.

Q/A = 16900 Btu/ft^{2}hr., Tw = 226.5^{0}F, Tb = 209.2F^0

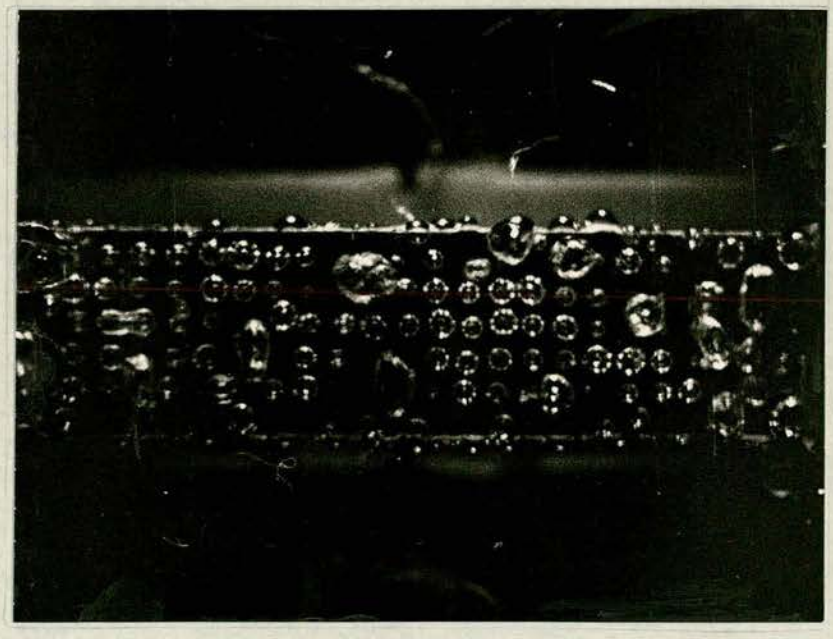

Fig. (83) Bubble forming on surface NG1 at pressure 14.68 psi.

Q/A = 20700 Btu/ft^{2}hr., Tw = 230F^0 Tb = 209.6F^0

Fig. (84) Bubble forming on surface NG1 at pressure 14.68 psi.,
Q/A = 19390 Btu/ft^{2}hr, Tw = 228F^o, Tb = 210F^o

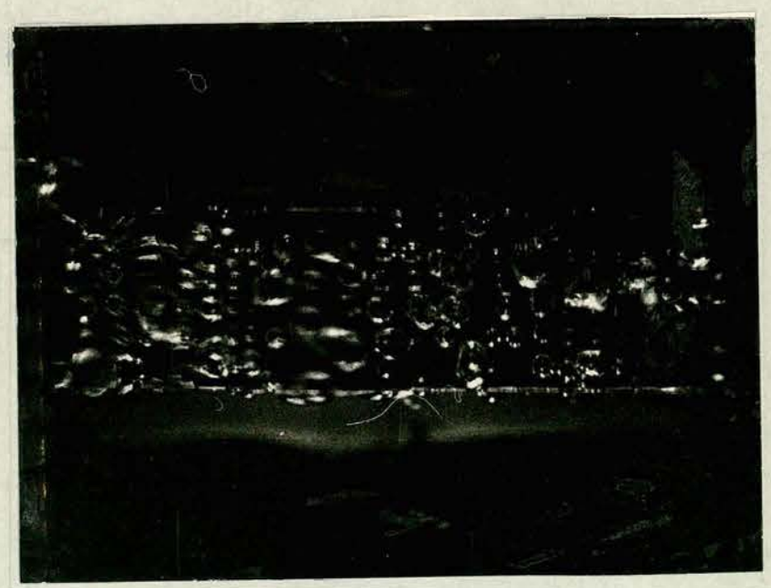

Fig. (85) Bubble forming on surface NG3 at pressure 14.68 psi.
Q/A = 24450 Tw = 233.4^{o}F Tb = 209.6^{o}F

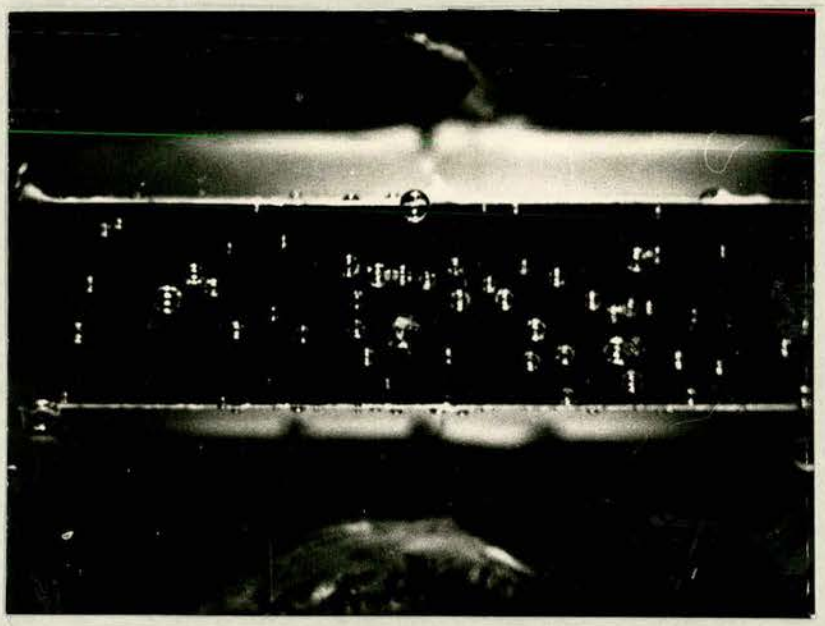

Fig. (86) Bubbles forming on surface NG3 at pressure 14.6 psi.,

Q/A = 3710 Btu/ft^{2}hr. Tw = 216, Tb = 208.8 F^o

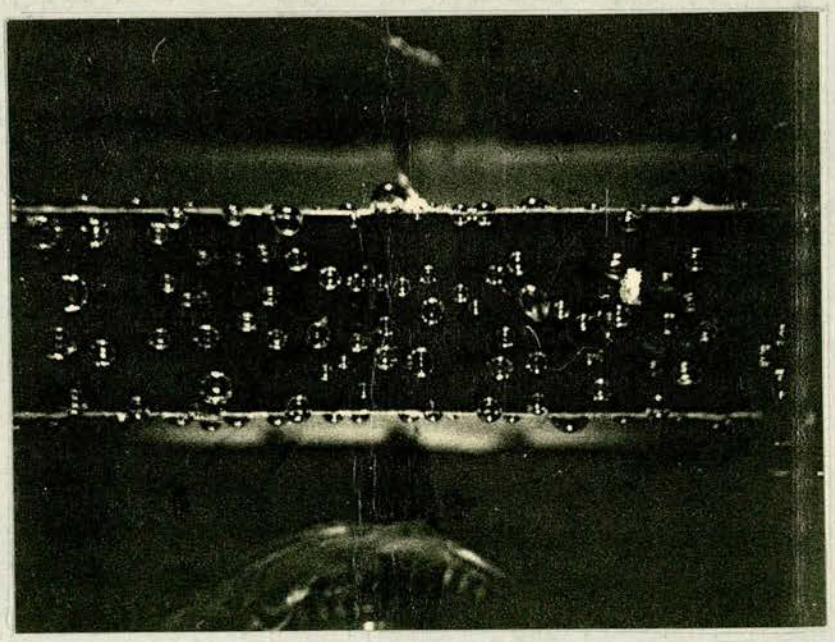

Fig. (87) Bubbles forming on surface NG3 at pressure 14.6 psi.,

Q/A = 4409 Btu/ft^{2}hr. Tw = 2185F^o, Tb = 209.6 F^o

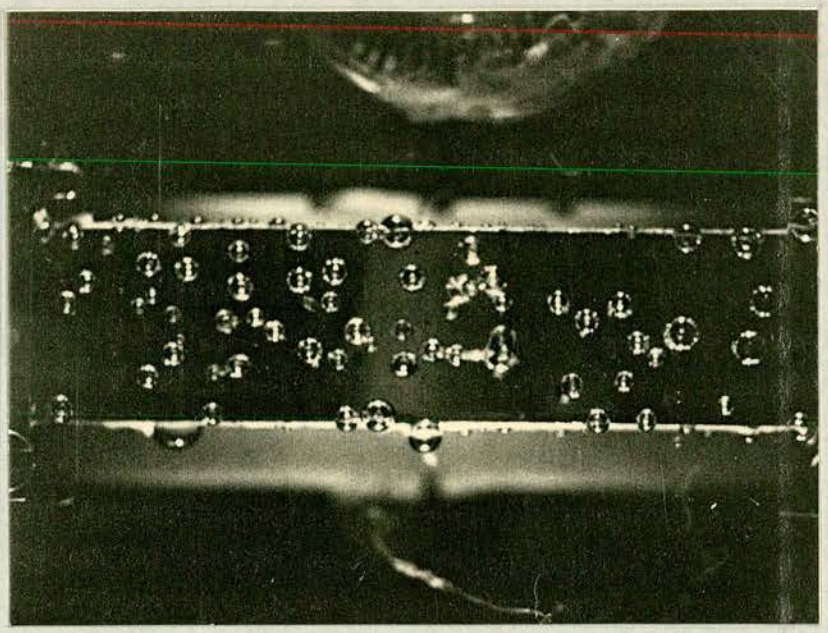

Fig. (88) Bubbles forming on surface NG3 at pressure 14.6 psi.,

Q/A = 8320 Btu/ft^{2}hr., Tw = 221.8^{0}F Tb = 210F^0

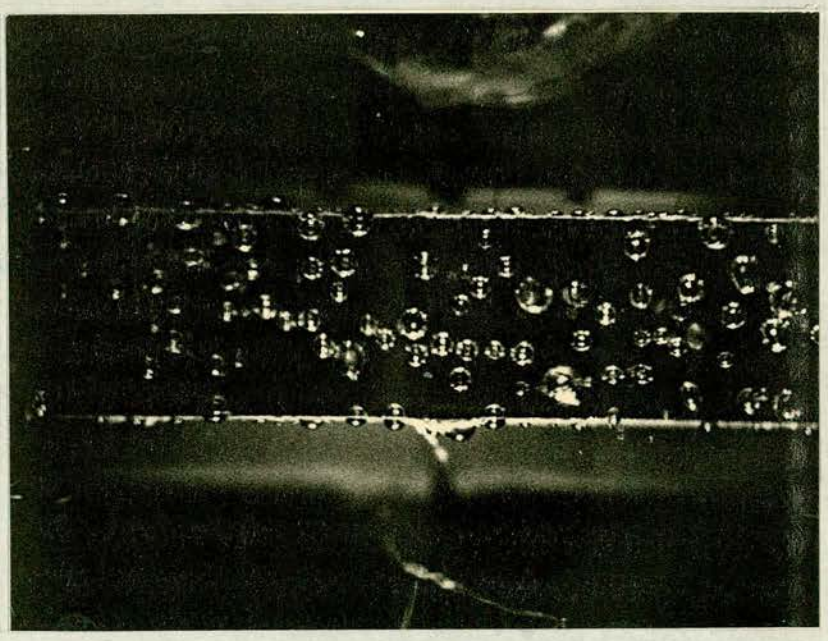

Fig. (89) Bubbles forming on surface NG3 at pressure 14.6psi.

Q/A = 12000 Btu/ft^{2}hr., Tw = 225^{0}F Tb = 208.2F^0

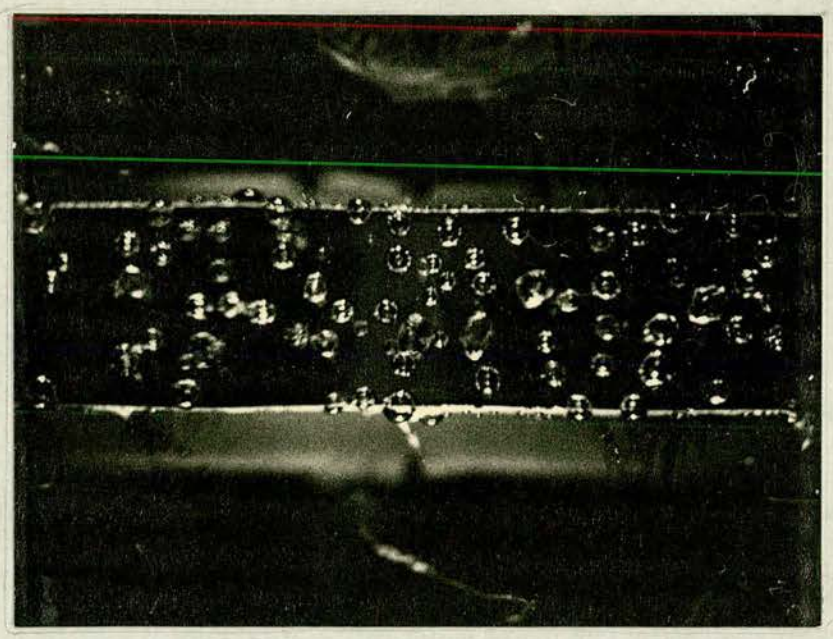

Fig. (90) Bubbles forming on surface NG3 at pressure 14.6 psi.,

Q/A = 15,620 Btu/ft^{2}hr Tw - 227.5F^o Tb = 209.6^{o}F

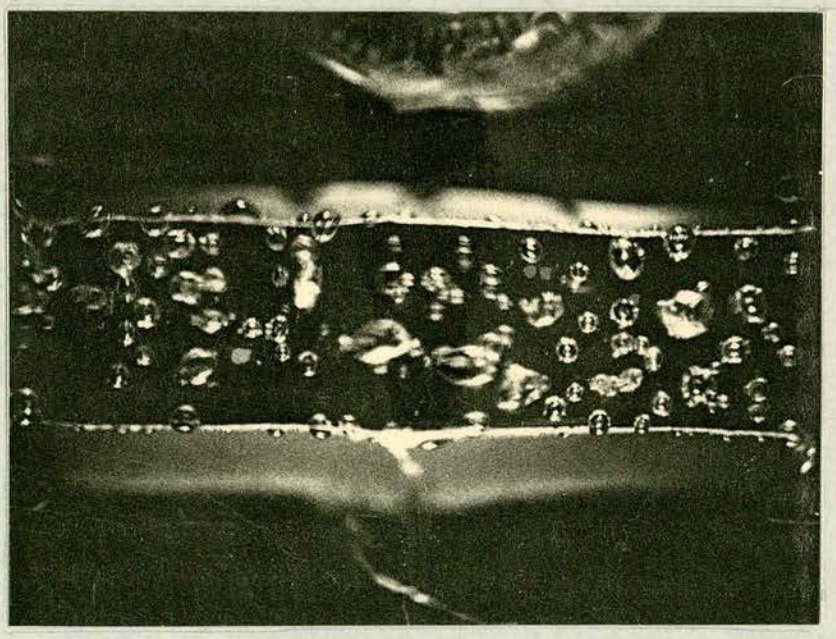

Fig. (91) Bubbles forming on surface NG3 at pressure 14.6 psi.

Q/A = 19000 Btu/ft^{2}hr, Tw = 230.F^o Tb = 209.2F^o

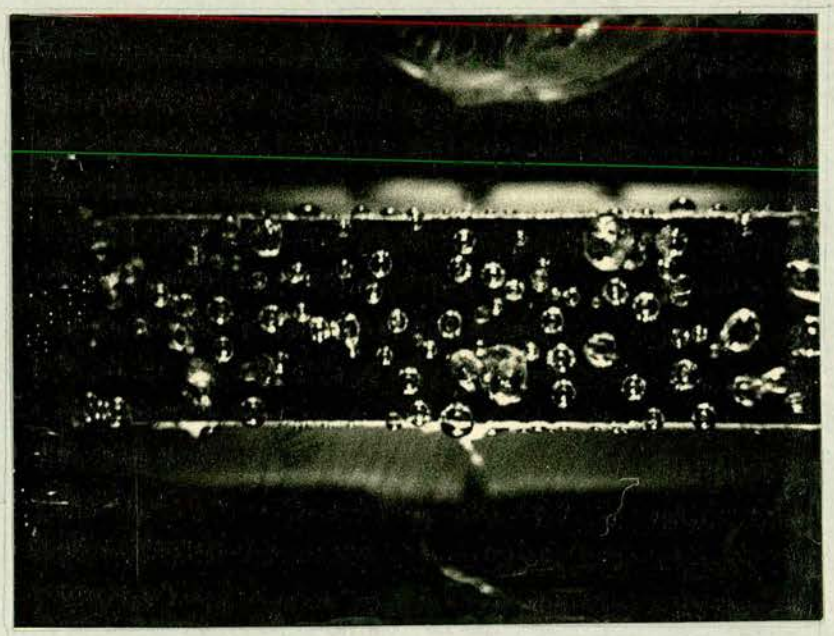

Fig. (92) Bubbles forming on surface NG3 at pressure 14.6,psi.

Q/A = 23600 Btu/ft^{2}hr, Tw = 232^{o}F, Tb = 209.2F^o

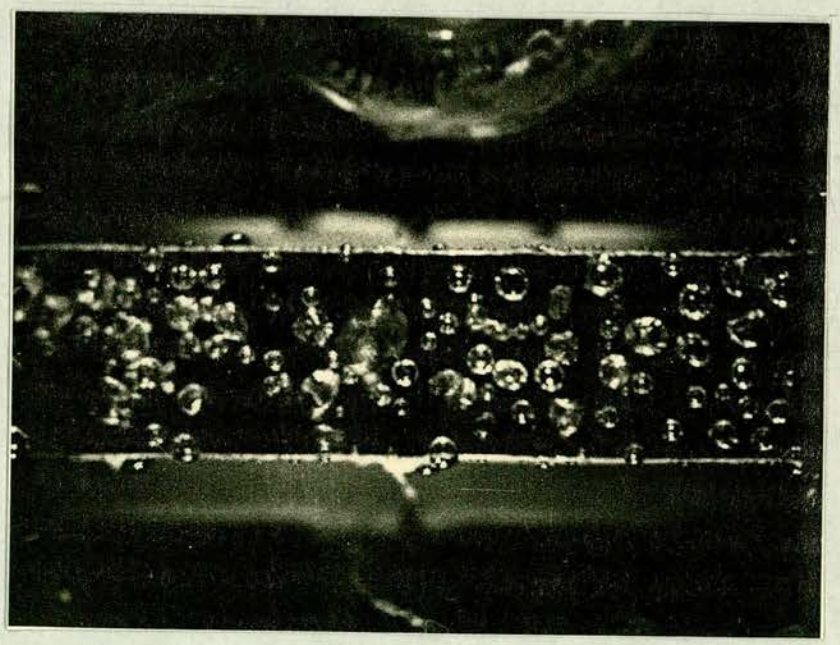

Fig. (93) Bubbles forming on surface NG3 at pressure 14.6psi.

Q/A = 26550 Btu/ft^{2}hr, Tw - 233.2F^o, Tb = 208.8 F^o

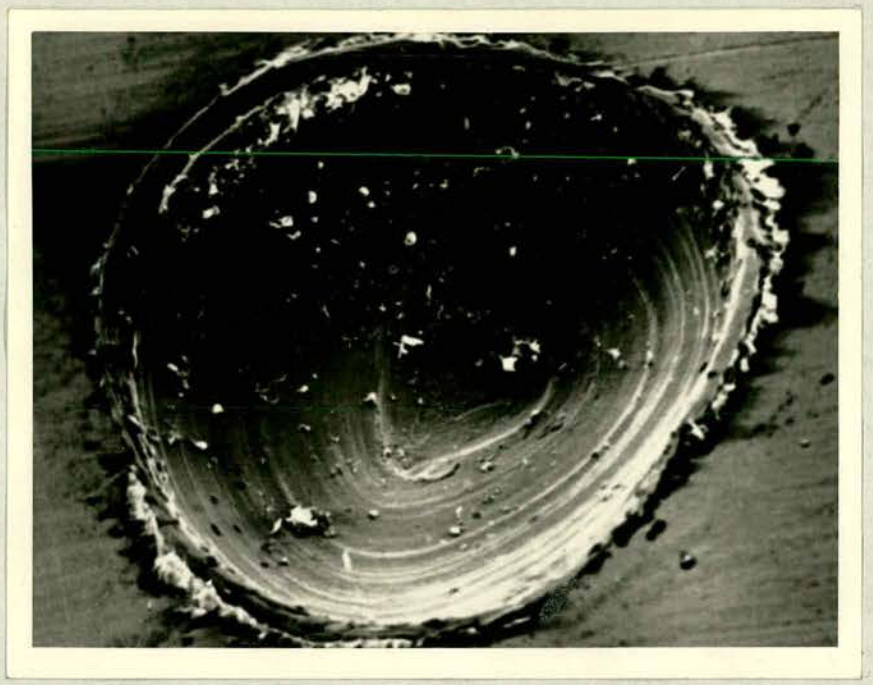

Fig. (94) Cavity mouth on surface F. Cavity Size = .025 in Magnification X65

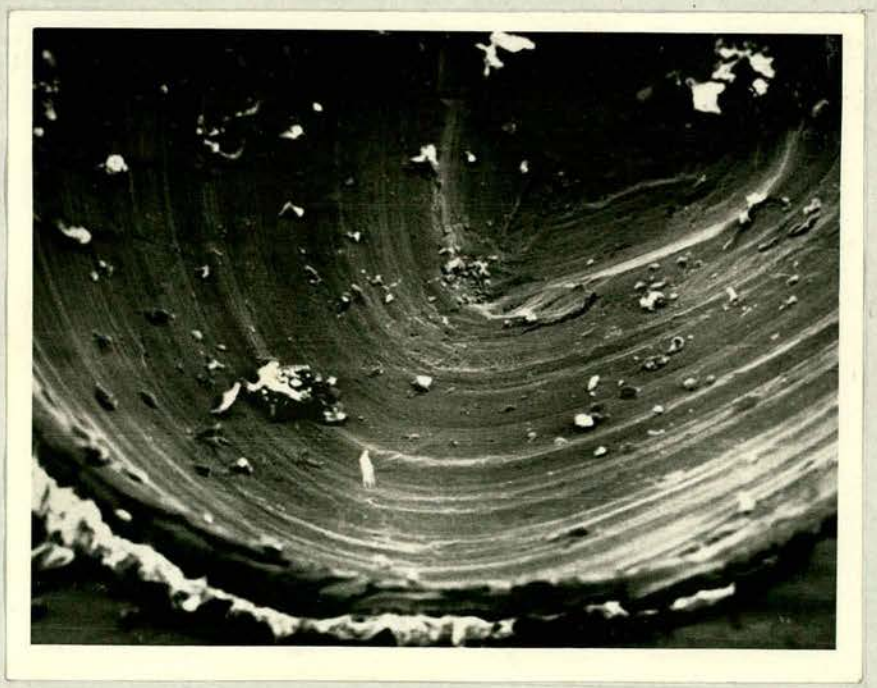

Fig. (95) The above cavity, showing the conditions of the inner surface

Magnification X260

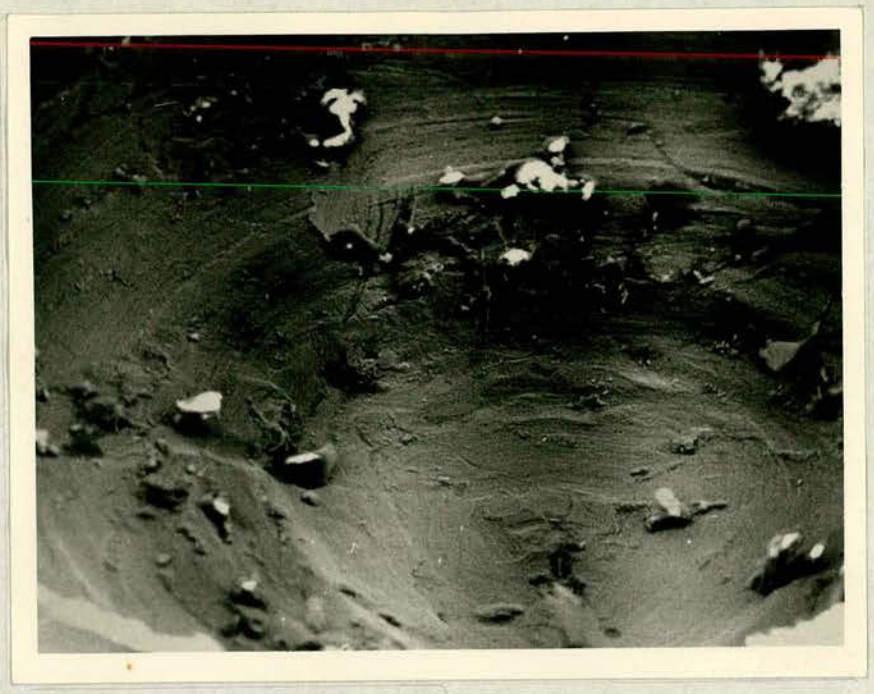

Fig. (96) the condition of the cavity base

Magnification X260

Fig. (97) The cavity base condition in more detail

Magnification X600

Fig. (98) condition of the cavity inner walls

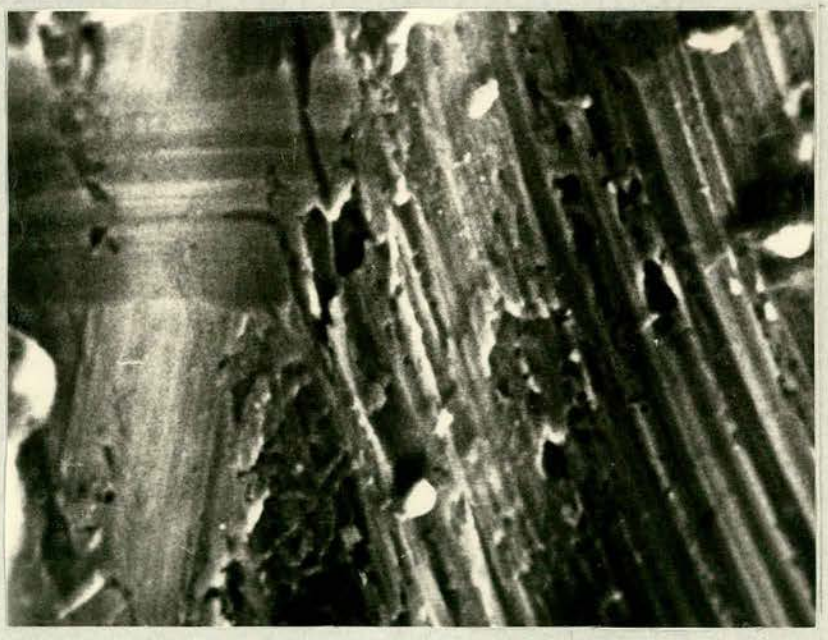

Fig. (99) condition of the cavity inner walls, different side

Magnification X2600

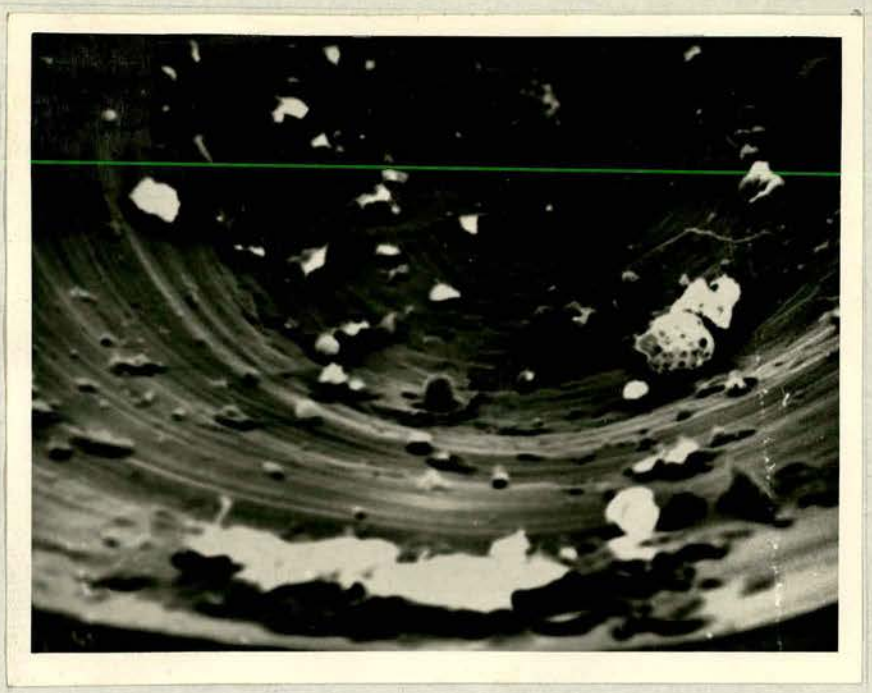

Fig. (100) The second cavity wall

Size = 0.0138 in Magnification X260

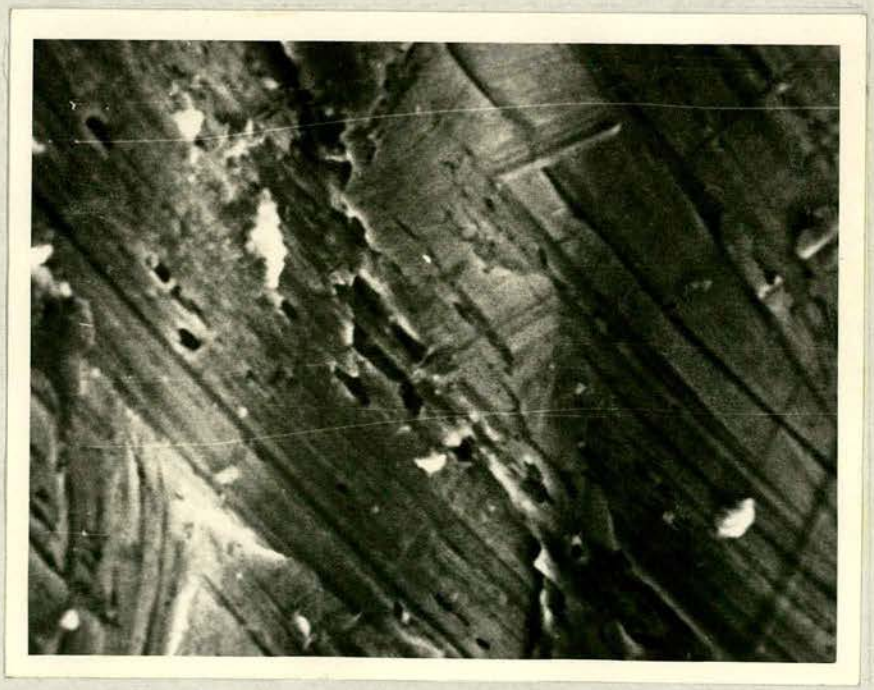

Fig. (101) conditions of cavity inner wall

Magnification X2600

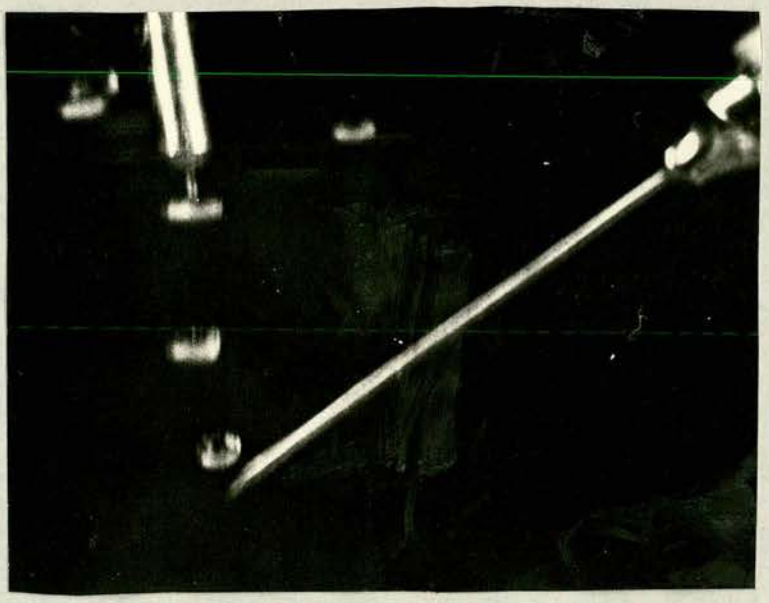

Fig. (102) Probe calibration using bubbles from a surgical needle.

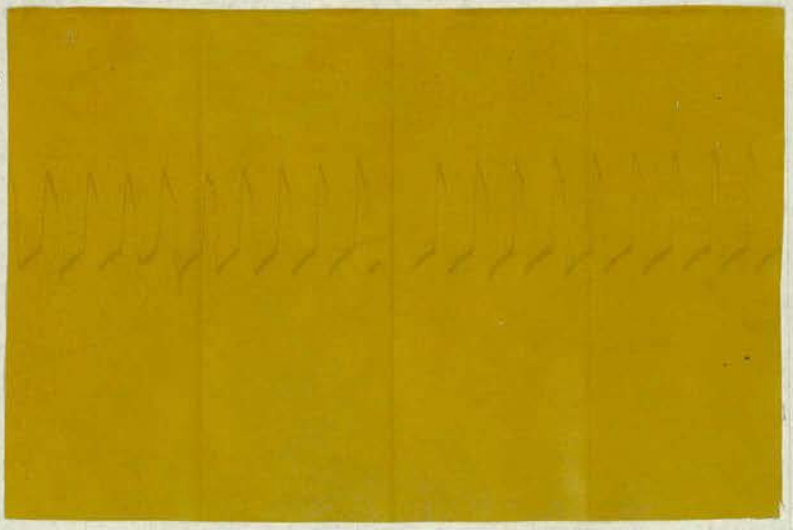

Fig. (103) Sample of signal on a U.V recorder

Fig. (104) Typical signal from the capacitance probe obtained on an oscilloscope.

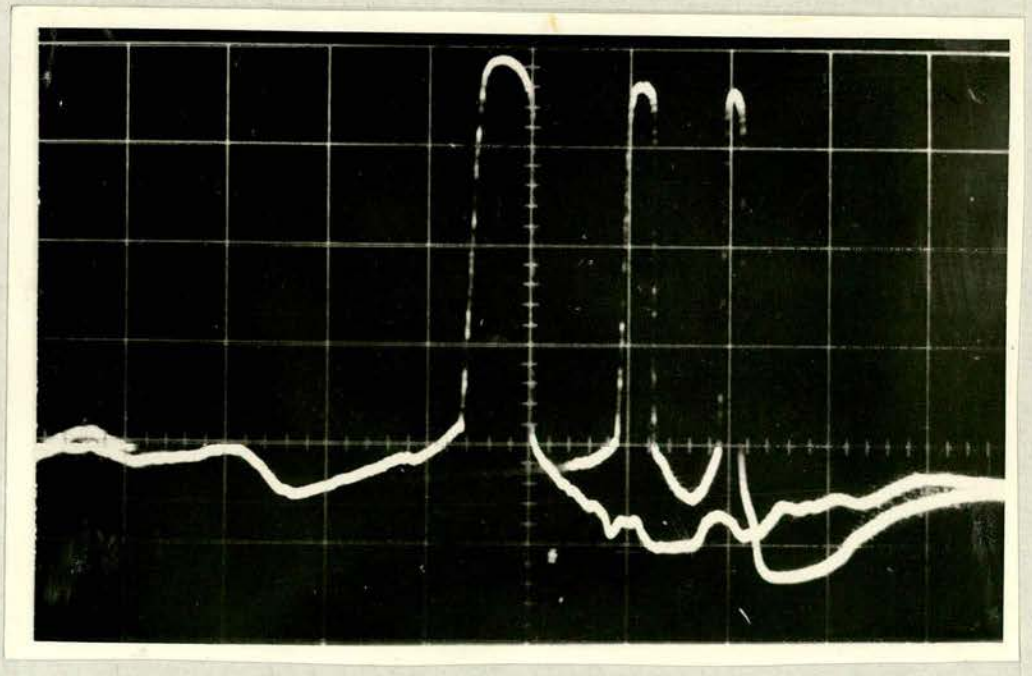

Fig. (105). Signal obtained from a large bubble formed from the coalescence of two or more bubbles

Fig. (106) Two bubbles passing through the probe almost simultaneously giving rise to a combined pulse

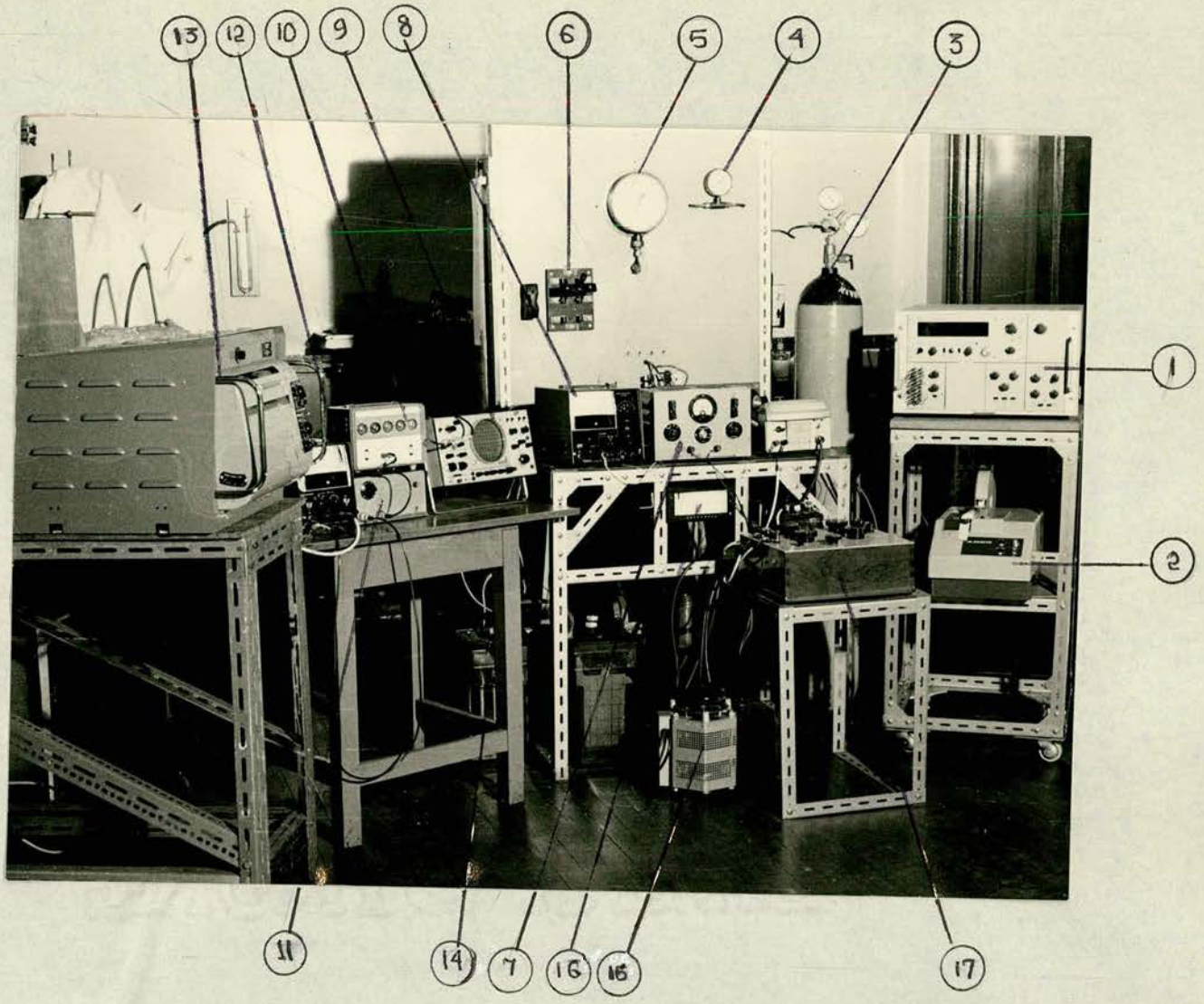

Fig. (107) Layout of recording equipment

1. Data logger
2. Paper tape punch
3. Nitrogen cylinder
4. Vacuum Gauge
5. High pressure gauge
6. Knife switch and fuse
7. Battery charger
8. D.C power unit
9. Oscilloscope
10. Counter
11. Amplifier
12. D.C power unit
13. U.V recorder
14. Cell for D.C supply
15. Variac
16. Wall temperature controller
17. Auxiliary equipment to check temperature measurement.